# Conceptual Thermodynamic Cycle and Aerodynamic Gas Turbine Design - on an Oxy-fuel Combined Cycle

NILSSON DAHLQVIST, ADRIAN

2016

*Document Version:*
Publisher's PDF, also known as Version of record

# Conceptual Thermodynamic Cycle and Aerodynamic Gas Turbine Design

## on an Oxy-fuel Combined Cycle

*Adrian Dahlquist*

LUND
UNIVERSITY

May 10th 2016
Doctoral Thesis
Division of Thermal Power Engineering
Department of Energy Sciences
Faculty of Engineering
Lund University
Sweden

Division of Thermal Power Engineering
Department of Energy Sciences
Faculty of Engineering
Lund University
Sweden

ISSN 0282-1990
ISBN 978-91-7623-770-0 (tryck)
ISBN 978-91-7623-771-7 (pdf)
ISRN LUTMDN/TMHP-16/1116-SE

Typeset in LaTeX
Lund 2016

*To my family*

# Populärvetenskaplig sammanfattning

Vi står idag inför ett stort problem med en världsomspännande globala uppvärmningen av jordens medel temperatur. Även om vi saknar en fullständig förståelse för klimatsystemet, så är majoriteten av klimatforskarna idag eniga om att den accelererande klimatförändringen huvudsakligen beror på mänskliga aktiviteter. Växthuseffekten är dock i grunden är ett naturligt fenomen, som höjer temperaturen på jorden till den behagliga temperaturnivå som vi är vana vid. Faktum är att utan den ”naturliga” växthuseffekten så skulle medeltemperaturen vara ca -19 °C, i stället för de jordens nuvarande medeltemperatur på +14 °C. Den globala medeltemperaturen på jorden har varit relativt stabil sen senaste istiden för ca 10,000 år sen, men vad som nu sker är att växthuseffektens energibalans förskjuts. Detta resulterar i att medeltemperaturen öka, och det är denna pågående temperaturökning som man kallar för den globala uppvärmningen.

Följderna av en ökad global medeltemperatur kommer visa sig lite olika beroende på var på jorden man tittar, men generellt så kommer klimatet att bli allt mer extremt. Detta kan t.ex. yttra sig genom att öken och torka sprider ut sig över redan torra områden, stormar, översvämningar och orkaner blir mer frekvent förekomande samt att glaciärerna smälter och havsnivån höjs. På andra platser, så som i norden, kan vi förvänta oss varmare, snöfattigare och fuktigare vintrar, samt att vår, sommar och höstvädret blir kallare, blåsigare och blötare.

Den största bidragande orsaken till den globala uppvärmningen är utsläpp av växthusgaser i atmosfären och då primärt i form av koldioxid ($CO_2$). Ett nettoutsläpp av koldioxid bildas när man förbränner fossila bränslen såsom olja, kol och naturgas. Jordens totala energiförsörjning, för elektricitet- och värme produktion, transport, industri processer, etc., täcktes år 2013 till 82% genom förbränning av fossila bränslen, och spås fortsätta att göra så i ytterligare minst 20 år. Elektricitet- och värme produktionen är den enskilt största sektorn utav koldioxidutsläpp från fossila bränslen, och stod för ca 42% av de totala $CO_2$ utsläppen år 2011. Samtidigt lever ca 1.3 miljarder människor utan elektricitet idag, och produktionen av elektricitet spås därför att öka med 70% fram till år 2035. Allt detta kommer leda till en ohållbar utveckling om vi inte agerar nu. Vid det globala klimatmötet (COP 21) i Paris december 2015 enades man om att den globala uppvärmningen inte får överstiga + 2.0 °C, samt om att sträva efter att hålla tempertur ökningen under + 1.5 °C.

Att begränsa den globala uppvärmningen till denna nivå kommer kräva omfattande insattser inom många olika områden, men troligen kommer dels de ekonomiska kostnaderna och inte minst lidandet bli betydligt större om vi inte agerar i tid. Det kommer krävas effektivare energianvändning, mer förnybar energi produktion (t.ex. sol, vind och vatten) samt inte minst att vi undviker koldioxidutsläpp från våra fossileldade kraftverk för att begränsa den globala uppvärmningen.

Det är just denna sista punkt, om hur man undviker koldioxidutsläpp från fossileldade kraftverk vid elektricitet- och värme produktion som studerats i denna vetenskapliga avhandling. Denna teknologi brukar kallas ”carbon capture and sequestration” och förkortas CCS, vilket står för koldioxidavskiljning och omhändertagande. Det finns några olika CCS teknologier för hur man kan åstadkomma koldioxidavskiljning i ett kraftverk. Den metod som undersökts specifikt i denna doktorsavhandling är en metod som kallas ”oxy-fuel combined cycle” och förkortas OCC. Det specifika med denna teknologi är att man utför förbränningen med ren syrgas ($O_2$) i stället för med luft, vilket görs konventionellt. Då luft till största del (75 vikt-%) består av kväve ($N_2$) så får man, vid förbränning i luft, en stor rökgasvolym med en låg koncentration av koldioxid. Den låga koldioxidkoncentrationen gör det energikrävande

att rena rökgasen från koldioxid efteråt. När man istället utför förbränningen med ren syrgas så bildas en förbrännings produkt av enbart vattenånga ($H_2O$) och koldioxid ($CO_2$). Denna rökgas är mycket lättare att rena från koldioxid, vilket kan ske genom att man kyler ner rökgasen så att vattenångan övergår till sin flytande vattenfas (kondenserar) medan koldioxiden förblir i sin gasfas. Vattnet kan då avskiljas, och kvar har man ren koldioxid. Koldioxiden komprimeras sen tills ett tryck där även koldioxiden övergår i sin flytande fas, vilket sker vid tryck över $74\,\mathrm{bar}$ (atmosfärstryck). Därefter kan koldioxiden lagras djupt nere i marken, i antingen geologiska bergrum eller uttömda oljefält.

En vanligt förekommande typ av konventionella kraftverk är så kallade naturgaseldade kombi-kraftverk, vilka har en gasturbin som sin huvudsakliga energigenererande enhet.

I kraftverk som bygger på oxy-fuel teknologin används förbränningsgasen av koldioxid och vattenånga som arbetsmedium i gasturbinen, i stället för luft så som i konventionella kombi-kraftverk. Denna gas består av ca 85 -vikt.$\%$ $CO_2$, 10 -vikt.$\%$ $H_2O$ och ett få procentenheter $N_2$ och Ar. Användandet av denna $CO_2$-rika gas som arbets medium ställer helt nya krav på designen av kraftverket i stort och specifikt på gasturbinens design. Dessa frågeställningar om hur man designar ett kraftverk och den ingående gasturbinen för drift med ren syrgas eldning har undersökts i denna avhandling. Avhandlingen presenterar en design som täcker dels den övergripande termodynamiska processdesignen av kraftverket, så väl som en detaljerad aerodynamisk design av gasturbinen med avseende på dess kompressor och två turbiner.

Det är författarens uppfattning att det med “oxy-fuel combined cycle” teknologin är tekniskt möjligt att producera elektricitet och värme utan något koldioxidutsläpp, om bara de politiska incitamenten skapas.

# Acknowledgements

This doctoral thesis was carried out in the form of an industrial doctoral work between Siemens Industrial Turbomachinery AB and the Faculty of Engineering at Lund University. The thesis was founded by Siemens Industrial Turbomachinery AB, where the present author also was employed at the department of Performance and Thermodynamic Engineering under the management of Lennart Näs. The work was supervised by professor Magnus Genrup at Lund University and senior specialist Mats Sjödin at Siemens Industrial Turbomachinery AB. Which I am very grateful for!

*I like to express my gratitude especially to:*

*Lennart Näs* - For giving me the opportunity to conduct my doctoral thesis at the department of gas turbine performance, through enabling this collaborative project between Siemens Industrial Turbomachinery AB and Lund University. I know it required some effort and I really appreciate it and that you believe in me.

*Magnus Genrup* - As you first introduced me to thermodynamic cycle and aerodynamic gas turbine engineering, then to Siemens, and finally providing me the opportunity to become an industrial PhD student at Lund university. Thank you for so openly and enthusiastically have shared your knowledge to me.

*Mats Sjödin* - For you gladly and openly have shared your knowledge with me and guided me throughout my journey. I have learned so much from you!

*Klas Jonshagen* - Because you genuine and kindly has participated, supported, and guided me. I really appreciate it, thanks!

*Sven Gunnar Sundkvist* - To have organized and reviewed my PhD-project, and always wanted my very best, thanks!

*Åke Klang* - I have so very much to thank you for. You have always believed in me, taking you the time to explain when I do not understand and motivated me to keep a high ambition. I have a LOT to thank yoUr kindneSs for!

*Colleagues at Siemens* - As you all are so good friend, which I have a lot of fun with. You have cleared my thoughts at the coffee table many times, with a lot of both nonsense discussions. You have also inspired and assisted me along the way.

*Jens Klingmann* - Thanks for offering me a place as a PhD student at the Faculty of Engineering at Lund University.

*Marcus Thern* - For helping me along the way with very valuable comments and advices, not the least in LaTeX.

*Majed Sammak* - Thanks for the fruitful collaboration and discussions we have had.

*Sven Axelsson* - Thanks for the kind support and that you openly have shared your knowledge with me.

*Colleagues at Lund University and Chalmers University* - For the collaboration and all the fun discussion we have had.

*My grandparents, parents, brother and sisters* - Because you support and encourage me in everything I take on, and always want me my very best. I love you all, and you know it!

# Abstract

The world is today facing a serious problem with global warming, which is heading towards an appallingly high temperature level. The greater part of the overall climate science community agree that global warming is caused by the greenhouse effect, which depends largely on emitted $CO_2$ emissions from the combustion of fossil fuel. The agreement at the COP 21 climate meeting in Paris (December 2015) was that global warming must be limited to no more than + 2.0 °C, with the aim of keeping it below + 1.5 °C. Accomplishing this requires a concerted effort in several different areas, for example through increased energy efficiency, more renewable energy sources and the utilization of carbon capture and sequestration (CCS) technology.

The oxy-fuel combined cycle (OCC), which is the topic of this thesis, is a subcategory of oxy-fuel combustion which, in turn is one of the three main technologies for CCS today. The key idea with oxy-fuel combustion is to avoid mixing the $CO_2$ formed in the combustion with the non-condensable nitrogen, as occurs at the combustion in a conventional combined cycle power plant (CCPP). This is achieved by combusting the gas fuel with pure oxygen ($O_2$) and thereby forming a combustion product consisting of only steam ($H_2O$) and carbon dioxide ($CO_2$). The $CO_2$ can then be separated downstream of the HRSG by condensing out the $H_2O$ and thereby leaving a pure stream of $CO_2$ for sequestration.

The OCC consists of a topping Brayton cycle and a bottoming Rankine cycle and has many similarities with a conventional CCPP. In the OCC, however, the flue gas leaving the HRSG is recirculated back to the gas turbine units compressor inlet, instead of being emitted to the atmosphere as in a CCPP. Thereby, the combustion products also act as the working medium in the topping (gas turbine) cycle. The working medium has a composition of about 85 wt.-% $CO_2$, 10 wt.-% $H_2O$ and a few percentage points of enriched nitrogen and argon, which follows with the oxygen stream as impurities.

The $CO_2$-rich working medium has significantly different gas properties, compared to air and conventional flue gas. This affect the design of the topping cycle, the exhaust heat utilization in the HRSG, the design requirements for the gas turbine unit and the aerodynamic design of its compressor and turbines. One of the major effects on the design, is the requirement for a higher gas turbine pressure ratio than for a conventional CCPP, as a result of the lower isentropic exponent ($\gamma$) for the $CO_2$-rich working medium.

This thesis takes the OCC concept to the next technical readiness level not just by identifying, optimizing and proposing a cycle design for a 115 $MW_{el}$ OCC. It also addresses the conceptual design of a gas turbine unit suitable for an OCC and a quite detailed conceptual aerodynamic design for the gas turbines unit's turbomachineries, i.e. one compressor and two turbines. The work investigated the performance levels to be expected from both the entire OCC, the embedded gas turbine unit and its turbomachineries. The proposed gas turbine unit was a single-shaft gas generator with a free direct-driven power turbine. The conceptual turbomachinery design of the compressor, the compressor turbine and the power turbine covered the conceptual design loop of the 1D mid-span, the 2D through-flow, and the 3D steady-state calculations. The compressor design was a 16-stage design, with a mass flow of 220 kg/s and a pressure ratio of 31.0. The turbine design was a two-stage compressor turbine and a four-stage power turbine.

The oxy-fuel combined cycle was calculated to have an overall net efficiency of 48.2%, which includes the energy cost for the $CO_2$ compression to 140 bar and the external $O_2$ production in an air separation unit (ASU).

## Publications

**Publication I** Sammak, M., Jonshagen, K., Thern, M., Genrup, M., Thornbergsson, E., Gronstedt, T., **Dahlquist, A.**,
*Conceptual Design of a Mid-sized Semi-closed Oxy-fuel Combustion Combined Cycle*,
ASME Turbo Expo 2011, GT2011-46299

**Publication II** **Dahlquist, A.**, Genrup, M., Sjoedin, M., Jonshagen, K.,
*Optimization of an Oxy-fuel Combined Cycle Regarding Performance and Complexity Level*,
ASME Turbo Expo 2013, GT2013-94755

**Publication III** Sundkvist, S.G., **Dahlquist, A.**, Janczewski, J., Sjoedin, M., Bysveen, M., Ditaranto, M., Langørgen, Ø., Seljeskog, M., Siljan, M.,
*Concept for a Combustion System in Oxy-fuel Gas Turbine Combined Cycles*,
ASME Turbo Expo 2013, GT2013-94180

**Publication IV** **Dahlquist, A.**, Thern, M., Genrup, M.,
*The Influence from the Working Medium on the Profile Loss in Compressor and Turbine Airfoils*,
ASME Turbo Expo 2014, GT2014-25069

**Publication V** **Dahlquist, A.**, Genrup, M.,
*Aerodynamic Gas Turbine Compressor Design for an Oxy-fuel Combined Cycle*,
ASME Turbo Expo 2015, GT2015-42028

**Publication VI** **Dahlquist, A.**, Genrup, M.,
*Aerodynamic Turbine Design for an Oxy-fuel Combined Cycle*,
ASME Turbo Expo 2016, GT2016-56439

# Contents


**1 Introduction** **1**
- 1.1 Global warming and energy trends . . . 1
- 1.2 Carbon capture and sequestration . . . 3
  - 1.2.1 Pre-combustion capture . . . 3
  - 1.2.2 Post-combustion capture . . . 4
  - 1.2.3 Oxy-fuel combustion capture . . . 5
  - 1.2.4 Transport, utilization and storage . . . 6
- 1.3 Motive for the doctoral thesis . . . 7
- 1.4 Objective . . . 8
- 1.5 Method . . . 9
- 1.6 Limitation . . . 10
- 1.7 Thesis outline . . . 10

**2 The oxy-fuel combined cycle** **11**
- 2.1 The oxy-fuel combined cycle . . . 11
  - 2.1.1 Compressor . . . 14
  - 2.1.2 Combustion chamber . . . 14
  - 2.1.3 Air separation unit . . . 15
  - 2.1.4 Turbine . . . 16
  - 2.1.5 Heat recovery steam generator and steam cycle . . . 16
  - 2.1.6 Flue gas condenser . . . 17
  - 2.1.7 Recirculation, pre-heating and $CO_2$ separation . . . 17
- 2.2 Working medium . . . 20
- 2.3 Cycle optimization . . . 24
  - 2.3.1 Gas turbine pressure ratio and exhaust gas temperature . . . 24
  - 2.3.2 Turbine cooling and disc sealing flow . . . 29
  - 2.3.3 Influences on the steam cycle . . . 31
  - 2.3.4 Cooling and pre-heating of the recirculated working medium . . . 34
  - 2.3.5 Preferred cycle design . . . 35

**3 The impact on the gas turbine design** **37**

**4 Compressor design** **41**
- 4.1 Scope of the compressor design . . . 41
- 4.2 Compressor design process . . . 41
- 4.3 Design parameters . . . 43
  - 4.3.1 Dimensionless stage parameters and stage characteristic . . . 44
- 4.4 Design philosophy . . . 47

**5 Turbine design** **55**
5.1 Scope of the turbine design . . . . . 55
5.2 Turbine design process . . . . . 56
5.3 Design parameters . . . . . 64

**6 Concluding remarks** **69**
6.1 The oxy-fuel combined cycle . . . . . 69
6.2 Compressor design for the gas turbine . . . . . 69
6.3 Turbine design for the gas turbine . . . . . 70
6.4 Overall . . . . . 70

**7 Summary of papers** **71**
7.1 Conceptual Design of a Mid-sized Semi-closed Oxy-fuel Combustion Combined Cycle . . . . . 71
7.2 Optimization of an Oxyfuel Combined Cycle Regarding Performance and Complexity Level . . . . . 72
7.3 Concept for a Combustion System in Oxyfuel Gas Turbine Combined Cycles 73
7.4 The Influence from the Working Medium on the Profile Loss in Compressor and Turbine Airfoils . . . . . 74
7.5 Aerodynamic Gas Turbine Compressor Design for an Oxy-fuel Combined Cycle . . . . . 75
7.6 Aerodynamic Turbine Design for an Oxy-fuel Combined Cycle . . . . . 76

# List of Tables


2.1 Properties of the streams in the oxy-fuel combined cycle. . . . . 13
2.2 The composition and gas properties of the working medium in an oxy-fuel gas turbine, compared to the gas properties of air or flue gas, at the same gas state . . . . . 20
2.3 The composition and gas properties in the gas turbine for a typical natural gas-fired CCPP. . . . . 21

4.1 Design boundaries and performance requirements for the compressor design 42
4.2 Compressor cascade nomenclature . . . . . 43
4.3 Design parameters for the compressor . . . . . 52

5.1 Boundary condition and design criteria for the compressor turbine . . . . . 56
5.2 Boundary condition and design criteria for the power turbine . . . . . 56
5.3 Turbine nomenclature . . . . . 64
5.4 Stage parameters for the compressor turbine . . . . . 67
5.5 Stage parameters for the power turbine . . . . . 67

# List of Figures


1.1 Trends of emitted $CO_2$ emissions from fossil fuel combustion. . . . . 2
1.2 Energy-related $CO_2$ emissions by region (OECD and non-OECD countries). 3

2.1 A schematic process diagram over the oxy-fuel combined cycle. . . . . 13
2.2 Layout of the combined wet cooling tower and scrubber. . . . . 18
2.3 Specific heat at constant pressure vs. temperature, for air and $CO_2$. . . . . 21
2.4 Isentropic exponent vs. temperature, for air and $CO_2$. . . . . 22
2.5 Dynamic viscosity vs. temperature, for air and $CO_2$. . . . . 22
2.6 Compressibility factor, for $CO_2$ ($Z_{CO_2}$). . . . . 23
2.7 Compressibility factor, for air ($Z_{Air}$). . . . . 23
2.8 The isentropic relation between the temperature ratio (in Kelvin) and the pressure ratio, for $CO_2$ and air. . . . . 26
2.9 The effects on the exhaust gas temperature of the gas turbine's pressure ratio. 27
2.10 The effects on the SAS consumption of the gas turbine's pressure ratio. . . . 28
2.11 The effects on the temperature into the power turbine of the gas turbine's pressure ratio. . . . . 28
2.12 The effects on the total cycle efficiency of the gas turbine's pressure ratio. . . 29
2.13 Specific heat at constant pressure ($c_p$) for $CO_2$ and the flue gas in a conventional CCPP. . . . . 33
2.14 T-Q chart showing the variation in gas temperature (T) vs. extracted heat energy (Q), for $CO_2$ and air. . . . . 33
2.15 Energy utilization in the HRSG for the oxy-fuel combined cycle design. . . 34

4.1 A blade-to-blade cross section of a compressor row. . . . . 43
4.2 Diffusion of a part of the dynamic pressure into a static pressure rise. . . . . 44
4.3 Theoretical stage characteristics for a low- and a high-flow stage. . . . . 46
4.4 Compressor rotor 1. . . . . 47
4.5 Stage parameters: the stage load ($\psi$) and the flow coefficient ($\phi$), at the mid-span section. . . . . 50
4.6 Total stage pressure ratio ($PR_{st.}$) and the deHaller coefficient for the rotors and stators, at the mid-span section. . . . . 51
4.7 Normalized axial velocity component out of the stator rows. . . . . 52
4.8 Normalized axial velocity component out of the rotor rows. . . . . 52
4.9 Rotor loading for the compressor at the mid-span. . . . . 54
4.10 Enthalpy-based stage reaction for the compressor, at the hub-, mid-, and tip section. . . . . 54

5.1 Rotor 2 in the compressor turbine. . . . . 58
5.2 Mid-span cross-section and blade curvature for rotor 2, in the compressor turbine. . . . . 58

5.3 Mid-span cross-section and Mach number for rotor 2, in the compressor turbine. . . . . 59
5.4 Rotor 3 in the power turbine. . . . . 59
5.5 Mid-span cross-section and blade curvature. . . . . 60
5.6 Mid-span cross-section and Mach number. . . . . 60
5.7 Schematic view of the turbines and the turbine intermediate duct. . . . . 63
5.8 Flow- and geometrical parameters in a turbine cascade. . . . . 64
5.9 Flow field and velocity triangles in a turbine row (reaction stage). . . . . 65
5.10 The solidity and the aspect ratio for the turbines. . . . . 68

# Nomenclature

## Arabic Symbol

| | | |
|---|---|---|
| A | area | $[m^2]$ |
| AR | aspect ratio | [−] |
| C | velocity in stationary coordinate system | [m/s] |
| $c_p$ | specific heat at constant pressure | [kJ/(kg K)] |
| HTC | heat transfer coefficient | [W/(m K)] |
| k | disc gap | [m] |
| M | molecular mass | [kg/mol] |
| Ma | Mach number | [−] |
| m | mass flow | [kg/s] |
| PR | pressure ratio | [−] |
| R | Specific gas constant | [kJ/(kg K)] |
| r | radius | [m] |
| s | pitch | [m] |
| | seal efficiency | [−] |
| SM | stall margin | [−] |
| T | temperature | [°C, K] |
| TR | temperature ratio | [−] |
| U | blade velocity | [m/s] |
| W | velocity in relative coordinate system | [m/s] |

## Greek/ Latin Symbol

| | | |
|---|---|---|
| $\alpha$ | flow angle in the stationary coordinate system | [°] |
| $\beta$ | flow angle in the relative coordinate system | [°] |
| $\delta$ | flow deviation | [°] |
| $\eta$ | efficiency | [%] |
| $\gamma$ | isentropic exponent | [−] |
| $\Lambda$ | degree of reaction | [−] |
| $\omega$ | radians | [rad/s] |
| $\phi$ | flow coefficient | [−] |
| $\pi$ | pressure ratio | [−] |
| $\psi$ | stage load | [−] |
| $\rho$ | density | $[kg/m^3]$ |
| $\sigma$ | solidity | [−] |
| $\tau$ | throttle number | [−] |
| $\varepsilon$ | cooling effectiveness | [−] |

## Subscripts Symbols

| | |
|---|---|
| $a$ | axial |
| $c$ | coolant |
| $Des$ | design |
| $g$ | gas |
| $h$ | enthalpy |
| $in$ | inlet to an airfoil row |
| $m$ | metal |
| $out$ | outlet from an airfoil row |
| $p$ | pressure |
| | polytropic |
| $Ref$ | reference |
| $s$ | static |
| | isentropic |
| $st.$ | stage |
| $t$ | total |
| $\theta$ | swirl (tangential) |
| 0 | total |
| 1 | compressor rotor inlet |
| | turbine stator inlet |
| 2 | compressor stator inlet |
| | turbine rotor inlet |
| 3 | compressor stator outlet |
| | turbine rotor outlet |

## Abbreviations

| | |
|---|---|
| ASU | Air separation unit |
| CCPP | Combined cycle power plant |
| CCS | Carbon capture and sequestration |
| COP 21 | Conference of the Parties twenty-first session |
| COT | Combustion outlet temperature |
| CT | Compressor turbine |
| ECO | Economizer |
| EGR | Exhaust gas recirculation |
| EGT | Exhaust gas temperature |
| EOR | Enhanced oil recovery |
| ETS | Emissions trading schemes |
| EV | Evaporator |
| GG | Gas generator |
| GHG | Greenhouse gases |
| GT | Gas turbine |
| HP | High-pressure |
| HRSG | Heat recovery steam generator |
| IGCC | Integrated gasification combined cycle |
| IP | Intermediate pressure |
| LNG | Liquefied natural gas |
| LP | Low-pressure |
| LPE | Liquid petroleum |
| OCC | Oxy-fuel combined cycle |
| OECD | Organisation for economic co-operation and development |
| pp. | Pinch-point |
| PS | Pressure side (of an airfoil) |
| PT | Power turbine |
| R | Rotor |
| S | Stator |
| SC-OCCC | Semi-closed oxy-fuel combustion combined cycle |
| SH | Super heater |
| SS | Suction side (of an airfoil) |
| TID | Turbine intermediate duct |
| UNCCC | United Nations Climate Change Conference |

# 1 Introduction

*This chapter introduces the doctoral thesis and give the motivation for the work trough providing an overview of how the work fits into the broader context. The motive, objective, method, limitations and the thesis outline are also provided in this chapter.*

## 1.1 Global warming and energy trends

The world is today facing a serious problem with global warming, which is heading towards an appallingly high temperature level. The greater part of the overall climate science community agree that global warming is caused by a reinforced greenhouse effect, which the United Nations Climate Change Conference (UNCCC) environmental agreement at the Conference of the Parties twenty-first session (COP 21) in Paris demonstrated [3]. The greenhouse effect is a prerequisite phenomena for the life we are accustomed to on Earth today, as its effect traditionally increases the average temperature on Earth by approximately 33 °C, to a mean temperature level of 14 °C [1].

The current issue is that the greenhouse effect's energy balance has been amplified, because of an increased concentration of greenhouse gases (GHGs) in the atmosphere. The effect of greenhouse gases is that they absorb the infrared radiation radiating out from Earth and re-emit it back towards Earth, instead of allowing the heat to pass out from the atmosphere. Carbon dioxide ($CO_2$) is the main greenhouse gas and what has occurred, and continue to do so, is that the $CO_2$ concentration in the atmosphere has increased significantly from a fairly stable level of 280 ppm in the mid-nineteenth century to the current levels of above 400 ppm in December 2015 [32].

The main reason for the rising $CO_2$ level is the ever-growing demand for energy, which has increased continuously since the mid-nineteenth century and is anticipated to continue to do so for the foreseeable future. This energy demand has historically mainly been met by combustion of fossil fuels, which today covers over 80% of the total energy demand [12]. The forecast is that fossil fuels will continue to be the main energy source for at least the next 20 years. Fossil fuel combustion comprised 82% of the worlds energy consumption in 2013 [5], which led to major $CO_2$ emissions. The $CO_2$ emissions emitted from fossil fuel combustion increased from nearly zero before the middle of the nineteenth century to a level of over 30 $GtCO_2$ $yr^{-1}$ in 2012 [47], with a significant increase after World War II (Figure 1.1) [14]. $CO_2$ emissions comprises today about 90% of the total $CO_2$ equivalent GHG emissions, while methane ($CH_4$) comprises about 10% and nitrous oxide ($N_2O$) a small fraction [13]. The single sector responsible for by far the largest $CO_2$ emissions is electricity and heat production, which emitted 42% of the total $CO_2$ emission in 2011 [14]. Approximately 1.3 billion people are today living without electricity and "The World Energy Outlook 2013" [12] forecasts that the electricity demand will increase by 70% by 2035 and that the annual global GHG emissions will increase to about 37 $GtCO_2$ $yr^{-1}$ by 2035. At the UNCCC COP 21 meeting in Paris 2015 [3], 195 nations agreed through the Paris Agreement that global warm-

ing must be limited to no more than plus 2.0°C compared to the pre-industrialization level and they also agreed on the goal of limiting the global warming to plus 1.5°C.

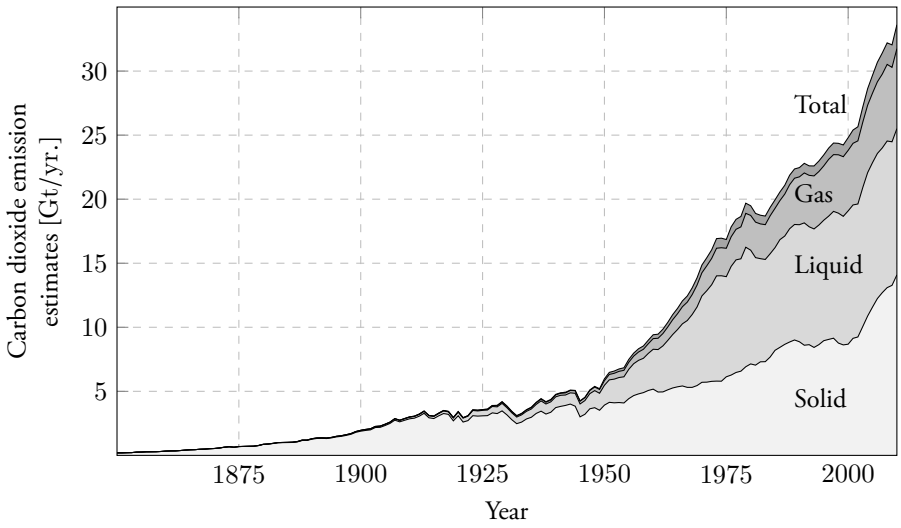


Figure 1.1: Trends of emitted $CO_2$ emissions from fossil fuel combustion, based on data from Boden et.al. [14]. (Gas flaring and cement production are included in the total)

Power generation represents a significant proportion of the increase in emitted $CO_2$ emissions since 1990. The increase comes mainly from non-OECD countries, whose emissions rate increased markedly in the early millennium and their total $CO_2$ emissions increased from 10 $GtCO_2$ $yr^{-1}$ in 1990 to above 22 $GtCO_2$ $yr^{-1}$ in 2014. The OECD countries show a more stable, but occasionally higher level per capita (of about 11.5 $tCO_2$ per capita vs. non-OECD of about 2.5 $tCO_2$ per capita in 2004 [20]), and the OECD countries increased their $CO_2$ emissions from 12 $GtCO_2$ $yr^{-1}$ in 1990 to about 13 $GtCO_2$ $yr^{-1}$ in 2014 (Figure 1.2) [13].

Against this background, it is obvious that there is an urgent need for concerted efforts in several areas in order to achieve the goal of controlling and limiting global warming to a sustainable level.

No single sector or technology alone will be able to solve the issue of global warming. Instead, concerted efforts within several different areas are required, for example by increased energy efficiency, more renewable energy sources and the utilization of carbon capture and sequestration (CCS) technologies. One method suggested to enforce a reduction of GHG emissions is to change over substitutes from fossil fuel towards renewable energy sources and introduce emission trading schemes (ETS) that sets a price on $CO_2$ emissions. Emission trading schemes are in use in several countries around the world and are tested and evaluated further in a number of locations today, but a problem with ETS has been achieving global agreements and keeping the price at a sufficiently high level to get the market to adapt [47].

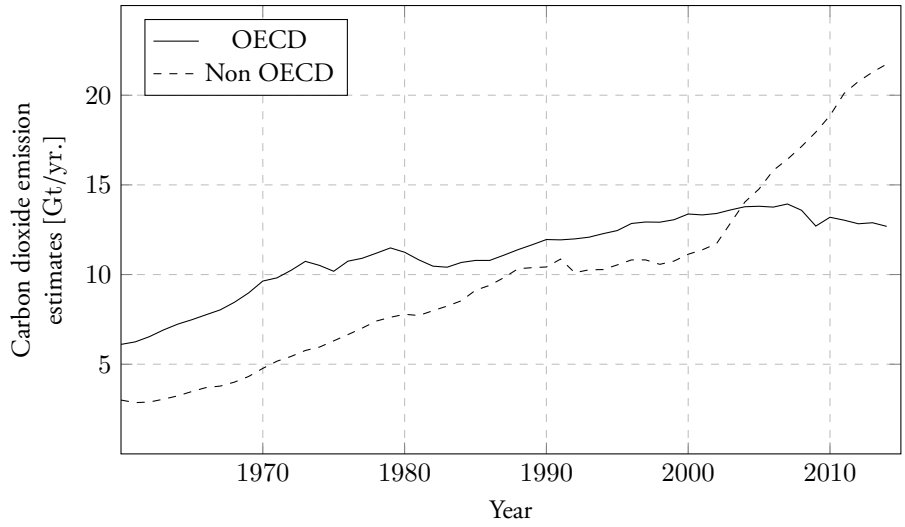


Figure 1.2: Energy-related $CO_2$ emissions by region (OECD and non-OECD countries), based on data from [20].

## 1.2 Carbon capture and sequestration

Carbon capture and sequestration (CCS) technology is a generic term that comprises technologies where the $CO_2$, formed through oxidation (combustion) of a carbon-containing (fossil) fuel at some stage in the process gets captured for sequestration. CCS technology can be applied to both fossil-fired power plants and suitable industry processes, such as cement production and steel production [53]. Depending on the method used for $CO_2$ capture, is the CCS technology divided into three main groups: pre-combustion, post-combustion and oxy-fuel combustion. There are also some additional CCS technologies which shows potential and might enter the CCS market in the future, for example CCS through chemical looping [62]. Common to all of these CCS technologies is the fact that $CO_2$ capture and sequestration comes with an increase in both the investment cost and the energy consumption, which thereby reduces the efficiency and the power density and increases the CAPEX (capital expenditures) of the facility. The different CCS technologies all have their different pros and cons in terms of the efficiency penalty, operability, capture rate, maturing level and adaptability for commercial operation. Next the three main CCS technologies are described briefly.

### 1.2.1 Pre-combustion capture

Pre-combustion refers to the technology where $CO_2$ is removed from the fuel prior to the combustion. This is achieved through treating the (fossil) fuel in order to avoid the $CO_2$ formed by oxidation to be mixed with the main working medium in the power plant. Depending on the fuel type (gas, liquid or solid) and its properties (composition and impurities), the fuel treatment process is performed with different methods. The Integrated Gasification Combined Cycle (IGCC) process is one type of pre-combustion technology that is applicable to thermal power plants.

A common pre-combustion method is to first partially oxidise (gasify) the fuel together

with pure oxygen to form a synthetic gas that consists mainly of $H_2$, CO, $CO_2$ and some traces of hydrocarbons [71, 46]. The carbon monoxide in the synthetic gas is then further oxidized with steam, which results in a final gas composition of $CO_2$ and $H_2$, from which the $CO_2$ is separated. The $H_2$ can then either be combusted as a conventional fuel or used in fuel cells.

A strength with the pre-combustion technology is that it is only the minor fuel stream that has to be processed, which enhances the process and size of the additional equipment. Two downsides are that pure oxygen has to be provided as the oxidizer from an air separation unit (ASU) and that combusting pure hydrogen fuel with conventional combustor technology is complicated. Therefore it may be necessary to blend the hydrogen with other fossil gas fuels to facilitate the combustion.

The net efficiency for a combined cycle power plant (CCPP) with pre-capture is typically about 45-47% [49, 17].

Today, there are some ten major pre-combustion projects planned or under construction worldwide to be put into operation between 2016 and 2022 [6]. The project planned to be commissioned first is the Kemper County Energy Facility in Mississippi USA, which is an IGCC planned to come into operation during 2016 in which lignite (brown coal) is to be used as the fuel [6].

### 1.2.2 Post-combustion capture

For thermal power plants, where the combustion occur through conventional combustion with air as the oxidizer, the post-combustion technology can be used to capture the $CO_2$ emissions from the flue gas. The separation of the $CO_2$ is done after (post) the combustion has occurred, i.e. the opposite to pre-combustion. As the combustion occurs with air, which has a large fraction of inert gases, mainly of $N_2$ (78 vol.-%) and some Ar, the $CO_2$ concentration in the flue gas is low, and hence also the partial $CO_2$ pressure. A low partial $CO_2$ pressure has a negative effect on the $CO_2$ capture rate, the required size of the $CO_2$ scrubber, and makes the capturing process more energy demanding. The $CO_2$ concentration is in turn dependent on the carbon/hydrogen (C/H) ratio in the fuel and the configuration of the power plant, e.g. if utilizing exhaust gas recirculation (EGR). A conventional CCPP without EGR typically has a $CO_2$ concentration in the flue gas in the range of 3 -vol.% for a natural gas-fired gas turbine [16, 53] to about 7 -vol.% for a liquid fuel-fired gas turbines [53]. The difference is because liquid fuel has a higher C/H ratio than natural gas, which mainly consists of methane ($CH_4$). Through using EGR can the $CO_2$ concentration be increased substantially, which enhances the $CO_2$ capturing process. The limiting factor for how much EGR that can be used is virtually set by the lowest acceptable $O_2$ concentration in the combustor, for achieving a complete and stable combustion (low CO emissions). This lower limit of the $O_2$ concentration is somewhat machine specific (i.e. depending on the combustion design and temperature), but as an indicative figure can an upper EGR limit of 60-70% be used, corresponding to a $CO_2$ concentration of about 10-12 -vol.% [15]. A more realistic EGR ratio is about 40%, which (depending on combustion temperature) correspond to a $O_2$ concentration into the combustor of about 16 vol-%, and result in a $CO_2$ concentration of about 6 -vol.% [15, 34]. The theoretical upper limit for the $CO_2$ concentration, in a pure steam power plant that operates with a close to stoichiometric combustion, is about 20-21 -vol.% ( 21 -vol.% $O_2$ in atmospheric air). The capturing process is commonly performed on the flue gas after it has passed through the heat recovery steam generator (HRSG) in either a CCPP

or in a steam power plant, where the pressure of the flue gas is just above atmospheric. An alternative approach is to carry out the capture at an intermediate state of the expansion in the gas turbine, to benefit from an increased partial $CO_2$ pressure [19]. The $CO_2$ capture rate is primarily a trade-off against the cost, as the physical size and energy consumption increases for a higher capture rate, but the $CO_2$ capture rate is commonly in the range between 80 and 95%, and typically about 90% [62]. The net efficiency for a CCPP with post-capture is typically about 48-50% [49, 17].

There are several demonstration and pilot plants either in operation or planned around the world to demonstrate the technology and prepare it for the commercialized market. For example, Boundary Dam is a 115 MW base load power plant in Canada that utilizes post-capture and has been in operation since autumn 2014. It has a $CO_2$ capture rate of upto 90% and the captured $CO_2$ is transported by pipeline and utilized for EOR [68, 63]. There are some five other post-combustion capture projects currently under development and planned to be in operation before 2020 [6], of which the Petra Nova Carbon Capture Project is next and will come into operation during 2016 [55].

### 1.2.3 Oxy-fuel combustion capture

Oxy-fuel combustion capture technology comprises technologies where the combustion (oxidization) occurs in the presence of virtually pure oxygen ($O_2$), instead of in the presence of air as conventional. The basic theory with this technology is that by performing the combustion of the fuel with virtually pure oxygen, form a combustion products that consist of solely steam ($H_2O$) and carbon dioxide ($CO_2$), from which the $H_2O$ can then be separated by condensation.

Oxy-fuel combustion technology is applicable to power plants consisting of either a simple cycle gas turbine, a steam power plant or a combined cycles power plant. Depending on the configuration of the power plan, the technology can be used with either an internal or an external combustion, using either a gas-, liquid- or solid fuel. By removing practically all the inert nitrogen ($N_2$) from the oxidizer stream the combustion would reach an adiabatic flame temperature of above 5,000 °C [57], which is far higher than the acceptable temperature. The oxygen and fuel streams are, thus, diluted prior to the combustion to reduce the temperature and to cool the combustor. The dilution can be performed with externally provided water/steam or, preferably, through recirculation of the working medium. Common to the oxy-fuel cycle concepts are, therefore, that they are semi-closed by partial recirculation of the working medium (i.e. the combustion products).

As previously mentioned, the working medium in the cycle mainly consists of $CO_2$ and $H_2O$. The ratio between the two varies depending on the cycle configuration and ranges from essentially consisting of $H_2O$ as in the Graz cycle [62], to the other end of the spectrum where it mainly consists of $CO_2$ as in a semi-closed oxy-fuel combustion combined-cycle (SC-OCCC) [60]. The focus for this thesis and the coming chapters is on the later cycle, namely, the SC-OCCC, which for simplicity hereafter is referred to as an oxy-fuel combined cycle (OCC).

The theoretical capture rate for the oxy-fuel combustion is virtually 100% [49], with only potential minor leakage flows to reduce this. A drawback with this technology is the need for virtually pure oxygen from an ASU, which is an energy-intensive process, a considerable investment and has a large footprint. The net plant efficiency for an OCC is expected to be in the range of 45-50% [62, 15, 81, 17, 49, 59], although there have been publications

indicating efficiencies as low as 36.7 [75] and 41.2% [16] and as high net efficiencies as 51.3% [8] and 53.9% [70].

The net plant efficiency reduction for an OCC is expected to be about 8-13 percentage points, compared to a conventional CCPP without $CO_2$ capture [62, 15, 8, 16, 17, 49, 59]. The range depends on the cycle configuration, the pressure of the delivered $CO_2$ stream and the ASUs energy cost. The figures just shown for the reduction of the net power plant efficiency is relative to a comparable reference CCPP. However, the efficiency penalty from the ASU and the $CO_2$ compression is actually about 2-3 percentage points higher. The explanation of this is that the cycle efficiency for the OCC without $CO_2$ compression and "free" $O_2$ actually is increased by another 2-3 percentage points, relative to a comparable reference CCPP [8, 17].

The efficiency reduction from the oxygen production in the ASU and the $CO_2$ compression to 140 bar for the oxy-fuel combined cycle was in this work calculated to be 12.2 percentage point (i.e. relative the OCC without $CO_2$ compression and "free" $O_2$), as presented in publication VI [24].

Today there are two large oxy-fuel combustion projects planned: the White Rose CCS Project in the UK [80] and the Shanxi International Energy Group CCUS Project in China, which are both scheduled to be in operation in 2020 [6]. They are both super-critical steam power plants and are to use oxy-fuel combustion of coal. Unfortunately, currently there is no oxy-fuel combined cycle planned or under construction that the present author is aware of.

### 1.2.4 Transport, utilization and storage

The last part in the CCS chain is the sequestration, which results in a need for appropriate transport and storage or utilization of the captured $CO_2$. It would be ideal if the entrapment and the storage or utilization were located geographically close to each other. That might be achievable on some occasions, but for most cases some transportation will be required. The two most conceivable alternative for the transport of $CO_2$ are through a pipeline or by ship. Which transport method is preferable depends, for example on the distance, the geological structure, the current infrastructure, the amount of $CO_2$ to be transported and the time horizon of the production. Utilizing pipelines for the transport of a $CO_2$ stream is already common today in applications for enhanced oil recovery (EOR). For EOR is today about 50 $MtCO_2\ yr^{-1}$ from mainly natural $CO_2$ sources transported through a 2,500 km pipeline network in the USA [62], of which several have been in operation for decades. $CO_2$ transport can also utilize a similar technology as used for the transport of LNG (liquefied natural gas) in an LNG carrier. For slightly longer transport distances the alternative of shipping the $CO_2$ tends to be more cost-effective than pipelines. The crossover depends on the site-specific conditions, but there are indications that the crossover is in the order of 1,000 km [62].

Trapped $CO_2$ occurs naturally in geological underground reservoirs, e.g. in the Colorado Plateau region and the Southern Rocky Mountains region [7], and is not a new and unique phenomenon. These $CO_2$ reservoirs are of a similar structure to the oil- and gas fields that are being explored and extracted today: consequently their structure is relatively well understood. In these geological formations the $CO_2$ is trapped in pores with a surrounding structure that seals it off. The knowledge that these formations have been around for hundreds of millions of years provides a certain confidence regarding its function and its stability and provides an opportunity to study the long-term process and aspects of how $CO_2$ binds to other elements. The use of $CO_2$ for EOR has been in operation since the mid-seventies and provides knowledge of the injection process.

Depending on the type of $CO_2$ storage or utilization, different qualities of the delivered $CO_2$ stream are required, for example its pressure, temperature, water content and to reduce the corrosiveness also impurities such as $H_2S$, $O_2$ and CO. The critical point for $CO_2$ is 73.7 bar and 31.1 °C [50] and, therefore $CO_2$ reaches its supercritical state (phase) when exposed to the pressure and temperature commonly present at over 800 m depth [53]. The trapping mechanisms for the $CO_2$ are through being sealed off by solid rock formations and through either being miscible with water and oil or through reacting with minerals and forming a carbonate structure [53].

CCS and EOR are two contradictory activities, but they could actually benefit from each other as they share a common interest. The former, (CCS), has a need to dispose and store $CO_2$ while the latter, (EOR), has an economic interest in utilizing $CO_2$ for an increased oil production. A conceivable path forward would, therefore, be if these two could act together to develop, demonstrate and mature the CCS technology. The need of $CO_2$ for EOR is nevertheless of the same magnitude as what is needed for CCS, if CCS is to be scaled up to its full required extent for reaching the environmental goal of a maximum temperature rise of no more than plus 2.0 °C [3]. The only long-term alternatives for storage, that are apparent today, are either to use depleted oil- and gas fields or deep saline formations. The oil- and gas fields are estimated to have a total storage capacity in the order of 675-900 $GtCO_2$ and are an attractive option as many of these fields have the infrastructure in place and are well explored. Geological formations for $CO_2$ storage are estimated to have a storage capacity in the order of 1,000 to 10,000 $GtCO_2$ [62] compared to the annual emissions of above 30 $GtCO_2\ yr^{-1}$ in 2011 [47].

The capacity to utilize or store $CO_2$ is demonstrated through several projects around the world today. For example, at Weyburn in Canada $CO_2$ is used commercially for EOR [79], and at In Salah in Algeria $CO_2$ was injected into geological sandstone between 2004 and 2011, which is now monitored [52]. Storage is also ongoing in a saline formation at Snöhvit, Norway [67] and in an aquifer at Sleipner, Norway [66, 72].

## 1.3 Motive for the doctoral thesis

In the previous sections (section 1.1 and 1.2) was it clarified that there is an urgent need for major reductions of $CO_2$ emissions, in which the CCS technology might have a key role to play. The International Energy Agency stated that CCS technology is vital for reducing the $CO_2$ emissions from the energy sector and industry, and in the "450 Scenario" they state that there is a requirement for a capture rate of 5.1 $GtCO_2\ yr^{-1}$ in 2040 [13].

When comparing different fossil-fired thermal power plants, CCPPs have the advantage of a superior total net efficiency compared to other thermal power plants, such as simple cycle gas turbine or steam power plants, and the net efficiency for conventional CCPPs is today reaching above 60% [4]. The potential for a high total efficiency was the motive for studying oxy-fuel combustion technology in a combined cycle application, instead of an oxy-fuel combusted steam power plant. The different CCS technologies (pre-combustion, post-combustion and oxy-fuel combustion) all show the potential for a similar net plant efficiency in the range of 45-50%, when applied to a natural gas-fired CCPP, [53, 17, 49].

The motive for choosing the oxy-fuel combustion instead of any of the other CCS technologies was that the oxy-fuel combustion technology has the potential for a $CO_2$ capture rate of virtually 97-100% without the risk of emitting other harmful pollutions, while the other CCS technologies' capture rate is about 85-90% at comparable power plant efficiencies

[53, 49]. With current technology the OCC is expected to obtain a total net plant efficiency that is certainly comparable with the other suggested CCS technologies [49, 17]. The OCC also has the potential for a substantial efficiency improvement, if any of the more novel and less energy-demanding ASU technologies become commercial [73, 53].

Previous investigations of OCC concepts have mainly been carried out through process simulations, where the focus has been on the overall cycle design. Such process simulations have a low technology detail level, where the turbomachinery (i.e. compressors and turbines) are represented by modules. These modules are basic and rely on predetermined performance figures, which (in general) are user specified and based on the assumption that these turbomachineries can be designed with performance levels comparable to conventional gas turbine engines. It was, for example, stated that the OCC concept seems to be an attractive CCS alternative because of its simplicity, but that the gas turbine technology for this concept does not exist today [17]. There is, therefore, a need to take the OCC concepts to the next technical readiness level, by carrying out quite detailed conceptual aerodynamic designs of the gas turbine unit's turbomachinery and investigate which performance levels are to be expected. The OCC design also needs to be revised to find out whether any design trade-offs can be made with either the cycle design, the design of the gas turbine unit or the individual turbomachineries, to facilitate the design of the total OCC.

To bring the technology forward it is also important to clarify whether conventional aerodynamic design methods can still be used or if any major modifications to the design process are required.

## 1.4 Objective

The main objective of this doctoral thesis was to extend the thermodynamic and aerodynamic research of the oxy-fuel combined cycle, to bring it to the next technical readiness level. The objective can be divided into three dependent subsets of different detail levels, namely designing and modelling the OCC's thermodynamic cycle design, performing a conceptual design of an oxy-fuel-fired gas turbine unit, and carry out the conceptual aerodynamic designs of the compressor and turbines for the gas turbine unit.

The objective of the thermodynamic cycle design was to identify, optimize and propose an oxy-fuel combined cycle, which would also serve to specify the design requirements for the gas turbine unit and provide the boundary conditions for its design. (The term "optimize" refers herein to finding a sound balance between performance, technical challenge and complexity, in order to propose a OCC design that is feasible in the near future, with mainly conventional state-of-the-art technology.)

The objective of the conceptual design of an oxy-fuel-fired gas turbine unit was to address questions such as: what the preferred shaft configuration and shaft speeds are, and to find a broad layout for the gas turbine unit.

Finally, the conceptual aerodynamic design of the compressor and the turbines for the gas turbine unit was to be performed up to the detail level of a steady-state 3D design. This was to investigate whether the aerodynamic design could be carried out, the influence the $CO_2$-rich working medium and different performance requirements had on the design and what performance figures could be expected. The aerodynamic designs were also supposed to address the question of whether conventional aerodynamic design methods could still be used in the concept phase, or not.

It is the author's belief that, through performing these conceptual design steps, major potential hurdles can be identified and solved before beginning the more extensive final design.

## 1.5 Method

The doctoral work followed a logical top-down sequence, by beginning from an overall conceptual thermodynamic cycle design at a low detail level and then proceeding with the design down to detailed aerodynamic 3D designs of the gas turbine unit's compressor and turbines. The work process was divided into several work packages, each of which is summarized in one of the present author's publications (publication I-VI) [61, 25, 69, 26, 23, 24].

Initially, a knowledge base for the proceeding work was established through reviewing published works and participating as a co-author in the first publication, see publication I [61].

In the next phase, the thermodynamic cycle design of the OCC was modelled in the process simulation tool Krawal Modular. Krawal Modular is a Siemens in-house program, but the choice of software is not crucial for the outcome and several other software of similar capacities could have been used. This general interchangeability of software programs is also true for the other in-house programs used in this work, i.e. they could all have been replaced by equivalent commercial software programs, with the same expected outcome.

Although the process simulation only takes into account the heat and mass balance, the model was made fairly detailed by subdividing crucial gas turbine components into smaller components. For example, each turbine stage was represented individually by a separate turbine module, with its oven turbine cooling and disc sealing flow calculation. This process simulation model of the OCC was used to investigate the influence of various cycle parameters, in order to obtain an optimum cycle design for the OCC, see publications II and III [25, 69]. With this optimization study, the OCC's cycle design was considered essentially completed. This cycle design formed, thereafter, the foundation for the proceeding investigations of the gas turbine unit's design and eventually also the foundation for the turbomachinery design of the compressor and the turbines.

The next phase was to carry out a conceptual design of the gas turbine unit to, for example decide the preferred shaft configuration, its shaft speed and to obtain a preliminary geometrical gas path shape. Different shaft configurations were examined and initially was a twin-spool gas generator (GG) with a free power turbine (PT) considered appropriate, as used in publications II and III [25, 69]. The gas turbine concept, that was finally considered to be the preferred balance between performance, technical challenges and complexity and, therefore, chosen to proceed with was a single-shaft GG with a free PT, as used in publications V and VI [23, 24].

Before proceeding with the aerodynamic design of the compressor and the two turbines, the influence of the $CO_2$-rich working medium on the flow physics in a compressor and turbine was investigated. This was to gain confidence in whether empirical correlation, on which traditional aerodynamic 1D and 2D design and analysis tools rely could still be used, or not, see publication IV [26].

Conceptual aerodynamic designs were carried out for both the compressor and the two turbines. The conceptual aerodynamic designs covered the 1D mid-span, the 2D through-flow and the 3D blade design and, mainly for validation, the steady-state 3D analysis calculations. The overall performance of the OCC design was finally revised based on the calculated performance figures for the compressor and the turbines, see publication V and VI [23, 24].

## 1.6 Limitation

No efforts were made to simulate any transients or part-load behaviours of either the overall oxy-fuel combined cycle design or for any of the turbomachinery designs of the compressor or the turbines. Neither were any of the procedures for start-up or shutdown or load control considered, nor potential operational hazards, such as for example $CO_2$ leakage.

The present author has neither studied the adjacent research areas of combustion system, materials nor chemical reactions due to the different working medium. To some extent, these adjacent research areas have instead been investigated in another related overreaching work package by the collaborative project OxyGT, between Siemens Industrial Turbomachinery AB, SINTEF Energi AS, Nebb Engineering AS and Lund University. The conclusions from this collaborative project can be found in the project's technical report [65] and publication III [69].

The thermodynamic cycle design was defined in such a manner that neither the external incoming oxygen stream for combustion nor the outgoing $CO_2$ stream was simulated thermodynamically in the process simulation. These streams were instead accounted for by adding specific energy costs to the cycle performance.

The alternative CCS technologies and the sequestration process of the captured $CO_2$ has not been investigated to any greater extent than through broad literature studies to provide a fundamental understanding.

## 1.7 Thesis outline

The thesis is based around six publications, which are appended at the end of the thesis. The thesis is divided into seven chapters. Chapter one gives an introduction to the thesis by putting the work into its broader context. The motive, objective, method and limitations are also given in Chapter one. Chapter two describes the oxy-fuel combined cycle and its subcomponents at a broad overall detail level. Chapter three discusses the influences that the performance requirements, set by the cycle design of the oxy-fuel combined cycle, have on the gas turbine unit. Chapter four discusses the aerodynamic design of the compressor. Chapter five discusses the aerodynamic design of the turbines. The thesis and the six publications are summarized in Chapter six by the concluding remarks. Chapter seven summarizes the six publications, appended at the end.

# 2 The oxy-fuel combined cycle

*This chapter describes the oxy-fuel combined cycle in general and provides a description of its different main subcomponents. The aerodynamic design details of the gas turbine unit and its turbomachinery components (compressor and turbines) are not addressed in this chapter as that is the subject of the subsequent chapters 3, 4 and 5.*

*The subject was investigated and discussed in the following publications:*
**Publication I:** *Conceptual Design of a Mid-sized Semi-closed Oxy-fuel Combustion Combined Cycle, GT2011-46299 [60]*
**Publication II:** *Optimization of an Oxy-fuel Combined Cycle Regarding Performance and Complexity Level, GT2013-94755 [25]*
**Publication III:** *Concept for a Combustion System in Oxy-fuel Gas Turbine Combined Cycles, GT2013-94180 [69]*

## 2.1 The oxy-fuel combined cycle

The OCC has many similarities with a conventional combined cycle power plant (CCPP) as they both consist of a Brayton topping cycle (a gas turbine) in which the heat input occurs through combustion. Both cycles also contains a Rankine bottoming cycle (a steam cycle) that is driven by the waste heat from the topping cycle (gas turbine exhaust heat). A schematic process diagram of the oxy-fuel combined cycle can be seen in Figure 2.1.

When initially focusing on the similarities between a conventional CCPP and an OCC, the bottoming steam cycle in both cycles works by the same principle and with virtually identical operation conditions. That implies that the working medium in the steam cycle is pure $H_2O$ in both and with similar gas states (i.e. pressure and temperature) throughout the bottoming cycle. For the specific OCC design in this work a steam cycle with two pressure levels was found to be preferable, with a design gas state of 565 °C and 100 bar at the high-pressure steam turbine inlet. That is a typical standard level for steam cycles of this size today (yr. 2016), as discussed further in section 2.1.5 and publication II [25]. These design parameters are not invariable for the OCC design and depending on the specific design requirements, either one-, two- or three pressure levels, other gas states and reheat might be preferred, in accordance with a conventional CCPP. Because of the similarity between the two bottoming cycles, traditional steam cycle equipment is to be used, with the reservation that the material in the HRSG and its heat exchanger, which is exposed to the $CO_2$-rich working medium in the topping cycle, need to be further investigated to ensure that there are no material restrictions.

The topping cycle in the OCC resembles a traditional topping cycle in a CCPP in the sense that the OCC includes both a gas turbine unit and an HRSG. However, the topping cycle in a CCPP is an open cycle design in that the gas turbine compressor breaths in atmospheric air and that the exhaust flue gas is emitted into the atmosphere after it has been passed through the HRSG and the exhaust stack. The OCC, on the other hand, is a recirculated semi-closed cycle

where the majority of the working medium (about 90 -wt.%) is recirculated from the HRSG exhaust back towards the gas turbine unit's compressor inlet. The working medium that is recirculated back from the HRSG is passed through several additional facility components before it reaches the compressor inlet, which for obvious reasons is not required in a traditional CCPP facility. That is to accomplish the $CO_2$ separation and to change the state of the working mediums to obtain desirable gas properties for the gas turbine unit's compressor inlet. The major additional facility components required between the HRSG outlet and the gas turbine unit's compressor inlet are in order from the HRSG as follows: a condenser, a scrubber, a bleed-off for the working medium ($CO_2$ and $H_2O$), a working medium preheater and a compressor inlet filter, as shown in Figure 2.1. The gas turbine combustion also requires a stream of substantially pure $O_2$ to be supplied in additional to the fuel flow, as the name oxy-fuel suggest.

A general description of the OCC process is given next, while more detailed descriptions of its subcomponents are given in the following subsections. The layout of the OCC is shown in Figure 2.1, with a summary of the gas state in Table 2.1. The numbers in brackets "( )" in the following section refer to the stream numbers in Figure 2.1 and Table 2.1. Starting at the gas turbine unit's compressor inlet (1), the working medium has a temperature of about 64 °C, a pressure slightly above atmospheric (1.015 bar), and a composition of about 85 -wt.% $CO_2$, 9 -wt.% $H_2O$ and a few percentage points of enriched Ar and $N_2$. The lowest pressure in the cycle is at the compressor inlet, which is kept just above the atmospheric pressure to avoid diluting leakages of atmospheric nitrogen-rich air into the cycle. Instead, it is preferable (from a performance perspective) if any potential small leakages are going out from the cycle instead of into it. That is with the reservation of the risk that leaking $CO_2$ might get accumulated on the ground, as it is heavier than air, and thereby cause a risk of choking. The pressure ratio (PR) across the gas turbine unit's compressor, for this specific OCC design, is 31.0, which is far higher than in a conventional CCPP. Pressure ratios suggested in the published literature for the OCC's topping cycle are generally in the range of 30-40 [37, 60, 62, 15, 17, 70, 59], although there are proposed PRs reaching up to about 60 [75, 81]. The underlying reason for this high PR is because of the different gas properties of the working medium in the OCC, as discussed in more detail in Chapter 3.

As there is no natural oxidizer ($O_2$) present in the working medium, the oxidizer has to be provided externally from an air separation unit (ASU). Both a fuel stream (5) and an oxygen stream (4) are, therefore, injected into the combustion chamber (3). The combustor outlet temperature (COT) (6) in CCPPs has traditionally an upper limit that is mainly set by the temperature limit of the material in the compressor turbine, available cooling technology and emissions control ($NO_x$ and CO), of which the emissions may be somewhat subsidiary in the OCC because of the semi-closed loop. Compared to a conventional CCPP has the OCC instead a considerably stronger need for balancing the COT against the gas turbine unit's PR and the upper temperature limit in the exhaust gas temperature (EGT) from the gas turbine into the HRSG. The trade-off between the COT, the gas turbine unit's PR and the EGT into the HRSG is discussed further in Chapter 3.

The working medium leaving the power turbine (8) has a temperature of about 610 °C and a pressure slightly above atmospheric (1.08 bar). As the working medium passes through the HRSG from (8) to (9), it transfers heat energy to the bottoming steam cycle. The working medium leaving the HRSG has a temperature of about 70 °C and is therefore cooled to a desirable recirculating temperature and cleaned of potential acids, deposits, and soot formations in a combined cooling tower and scrubber (10).

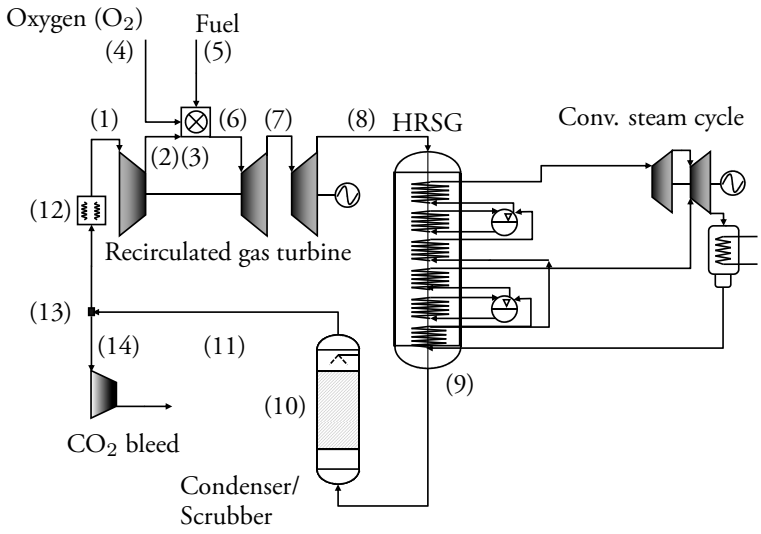


Figure 2.1: A schematic process diagram over the oxy-fuel combined cycle.

The steam that is condensed in the cooling tower is separated, before the rest of the working fluid is recirculated back (11) towards the compressor inlet. From the recirculated working medium (11) a minor stream is bled off (13). The bleed stream (14) is compressed in an inter-cooled compressor train with stepwise water separation, which finally provides a stream of nearly pure $CO_2$ for sequestration. The $CO_2$ bleed stream and the water separation in the cooling tower correspond to about 10 -wt.% of the total mass flow and the aim is to keep the mass balancing in the topping cycle stable, by balance the injected fuel flow, the oxygen supply and potential minor leakages.

The majority of the working medium (about 90 -wt.%) is pre-heated a few degrees (12) before the fluid is filtered and recirculated back to the compressor inlet (1).

Table 2.1: Properties of the streams in the oxy-fuel combined cycle, as shown in Figure 2.1

| Stream | Name | Temp. [°C] | Pressure [bar] | Mass flow [kg/s] | $CO_2$ [-wt.%] | $H_2O$ [-wt.%] | $N_2$ [-wt.%] | Ar [-wt.%] | $O_2$ [-wt.%] |
|---|---|---|---|---|---|---|---|---|---|
| 1 | Compressor inlet | 64.7 | 1.015 | 219.9 | 84.56 | 8.85 | 2.59 | 3.89 | 0.11 |
| 2 | Combustor inlet | 438.6 | 31.17 | 168.6 | 84.56 | 8.85 | 2.59 | 3.89 | 0.11 |
| 4 | Oxygen stream | 560.7 | 34.28 | 20.9 | 0.00 | 0.00 | 2.00 | 3.00 | 95.00 |
| 5 | Fuel stream | 15.0 | 32.65 | 4.96 | (100 -wt.% $CH_4$, LHV 50,013 kJ/kg) | | | | |
| 6 | HP Turbine inlet | 1340.0 | 30.31 | 194.4 | 80.34 | 13.40 | 2.46 | 3.69 | 0.10 |
| 7 | PT inlet | 932.9 | 7.29 | 236.5 | 81.09 | 12.59 | 2.48 | 3.72 | 0.10 |
| 8 | HRSG inlet | 612.8 | 1.080 | 245.7 | 81.22 | 12.45 | 2.48 | 3.73 | 0.10 |
| 9 | HRSG outlet | 69.9 | 1.058 | 245.7 | 81.22 | 12.45 | 2.48 | 3.73 | 0.10 |
| 11 | Condenser outlet | 60.0 | 1.058 | 236.0 | 84.56 | 8.85 | 2.59 | 3.89 | 0.11 |
| 14 | $CO_2$ bleed | 60.0 | 1.058 | 16.1 | 84.56 | 8.85 | 2.59 | 3.89 | 0.11 |

### 2.1.1 Compressor

The purpose of the OCC's gas turbine unit's compressor does not differs from the compressor in a conventional gas turbine unit, in that it should compress the working medium in an efficient and stable manner. The compressor design for the OCC's gas turbine unit is described in Chapter 4 and more information regarding the general basic aerodynamic compressor design was discussed in the present author's licentiate thesis [22].

### 2.1.2 Combustion chamber

The fundamental idea with the oxy-fuel combined cycle is to enhance the $CO_2$ separation process by avoid mixing the, combustion-formed, $CO_2$ with the inert non-condensable nitrogen ($N_2$) in the air. That is achieved through the use of virtually pure oxygen ($O_2$) as an oxidizer in the combustion process, instead of using air as the oxygen carrier, which contains about 75 -wt.% (78 -vol.%) inert $N_2$. Ideally the combustion products from the combustion of methane ($CH_4$) and oxygen ($O_2$) are pure steam ($H_2O$) and carbon dioxide ($CO_2$), from which the $CO_2$ can be separated by condensing the steam (Equation 2.1). Oxy-fuel combustion entails additional challenges for the combustion system design, which can not be designed straight off in the same manner as in a conventional gas turbine. The adiabatic flame temperature reaches above 5,000 °C for a stoichiometric combustion of pure oxygen and methane (at 25 °C) [57] and therefore recirculated carbon dioxide and steam are required for dilution to avoid too excessive temperatures far beyond the material integrity. The oxygen separation in an ASU consumes energy, which penalizes the cycle performance substantially. The combustion system must, therefore, be designed to operate at close to stoichiometric condition, with virtually pure oxygen as the oxidizer and recirculated $CO_2$-rich working medium for dilution.

$$CH_4 + 2\,O_2 \Rightarrow CO_2 + 2\,H_2O \tag{2.1}$$

The desire to operate the combustion at close to stoichiometric condition, to minimize the oxygen consumption, changes the properties for the combustion, e.g. the flame speed, flame stability and flammability, and entails a risk of unburned hydrocarbon or CO emissions [69]. A challenge for the design of the combustion system is to control the flame temperature and adjust the combustion properties through dilution of the recirculated working medium at different stages of the combustion. It is thought that this is done by mixing the three streams (oxygen, fuel and the diluent $CO_2$-rich working medium) precisely regarding location and quantity. The combustion-related issues and the operation with close to stoichiometric combustion were not included in the scope of this thesis work. Instead the basic methods were addressed in the collaborative project OxyGT [69, 65] and are a subject for further studies. The approach for this doctoral thesis was to presume that the combustion could be achieved with an oxygen excess of 1.0 -wt.% $O_2$ above the stoichiometric combustion ratio. The low oxygen excess might result in elevated CO emissions, which would not be acceptable for an open power plant cycle. This CO emission issue may be somewhat subsidiary in an OCC because of the semi-closed loop, as the CO emissions in the minor $CO_2$ bleed stream can be oxidized catalytically to $CO_2$ if required, with the reservation that the mixture of $H_2O$, $CO_2$ and CO does not cause any material or chemical issues (e.g stress-corrosion-crack [76]). That the combustion is feasible with only 1.0 -wt.% excess of oxygen is strengthened by the fact

that the oxygen stream is controllable and can be injected at the precise location needed for the combustion, instead of smoothly diluted with the surrounding working medium as in a conventional combustion chamber that utilizes air. The basis for the OCC to be an attractive alternative for CCS is not compromised considerably even if it turns out that the oxygen excess needs to be increased slightly. An increase to, for example, a stoichiometric ratio of 1.05 (i.e. an $O_2$ excess of 5.0 -wt.% in the combustor) "only" reduces the total net cycle efficiency by about 0.3-0.4 percentage point.

### 2.1.3 Air separation unit

The oxidizer stream of virtually pure oxygen required for oxy-fuel combustion is produced by separating air into its main components, i.e. nitrogen, oxygen, argon and water. The other rarer components in air can also be separated individually at an additional energy cost, but as that is not required for oxy-fuel combustion these trace components follows as impurities. The most common ASU technology today is through cryogenic air separation. Other available or upcoming ASU technologies at different levels of maturities are ITM (ion transport membrane), OTM (oxygen transport membrane), PSA (pressure swing adsorption) and VSA (vacuum swing adsorption), and were briefly described in [27, 53, 22].

The main application for cryogenic ASU today is supplying steel factories and coal gasification plants with oxygen, while nitrogen in some cases can be used for inert storage of, for example, petroleum. In a cryogenic ASU the air is separated by utilizing the different temperatures at which oxygen and nitrogen condense, which occurs at 77.2 K (-195.95 °C) for $N_2$, and at 90.1 K (-183.05 °C) for $O_2$ at standard atmospheric pressure [50].

As argon has a condensation temperature of 87.2 K (-185.95 °C) [50] which is fairly close to that of oxygen, most of the argon follows with the oxygen when the oxygen is separated from the nitrogen. The purity of the oxygen from a cryogenic ASU is generally in the range of 85.0-99.5 -wt.% $O_2$ [27, 8, 56] and depending on the required oxygen purity, the oxygen separation is carried out in one or several distillation columns in the ASU [8]. The production of $O_2$ is the single largest source for efficiency reduction in an OCC, compared to a conventional CCPP. A higher purity comes with an additional energy cost [8] and the cost is substantial increasing for a purity above 95 -wt.% $O_2$ [73]. An oxygen purity of 95 -wt.% $O_2$ was considered to be a justifiable trade-off between the energy cost and the purity, which is a purity commonly used when studying OCCs [81, 16] although there are example of studies using higher $O_2$ purities [17, 62]. A benefit with an increased $O_2$ purity is that it might lead to a reduced cost for the eventually needed after-treatment of the $CO_2$ bleed stream, and should therefore be balanced against the increased production costs for a $O_2$ stream with a higher purity.

The oxygen stream used in this investigation was presumed to be provided from a cryogenic ASU with a composition of 95.0 -wt.% $O_2$, 3.0 wt.-% Ar and 2.0 -wt.% $N_2$ and supplied with a pressure of 1.20 bar and a temperature of 30.0 °C. The energy cost for the oxidizer stream used was 735 kJ/kg (i.e. 204 kW h/t $O_2$) [27]. Compared to the figures used in previous published studies this is in the lower spectrum. The typical published energy cost stream with a $O_2$ purity of 95.0 -wt.% $O_2$ are 200-260 kW h/t $O_2$ [73, 27, 53, 8], and a variation in energy cost from 221.3-268.7 kW h/t $O_2$ for a oxygen purity in the range from 85.0 -wt.% to 97.0 -wt.% [8]. There is, however, expectations that the production cost can get as low as 140 kW h/t $O_2$, with heat integration [27]. Several of the published cost figures above were also for a pressurised oxygen stream and not for an atmospheric condition as the case for the herein used cost of 735 kJ/kg $O_2$. The further required compression to the combustor

delivery pressure was made with an isentropic efficiency of 80.0%, and if including the energy cost for the compression to 34.28 bar is the energy cost 1,280 kJ/kg (i.e. 356 kW h/t $O_2$). The total energy consumption for the production and compression was 26.8 MW, which reduces the total OCC efficiency by 10.8 percentage points.

### 2.1.4 Turbine

The purpose of the OCC's gas turbine unit's turbines does not differs from the turbine in a conventional gas turbine unit's, in that it should expand and extract work from the working medium as efficiently as possible. The turbine design for the OCC's gas turbine unit is described in Chapter 5 and more information regarding the general basic aerodynamic turbine design was discussed in the present author's licentiate thesis [22].

### 2.1.5 Heat recovery steam generator and steam cycle

The thermodynamic design of the heat recovery steam generator (HRSG) and the steam cycle for the OCC is similar to a conventional CCPP and they virtually do not differ from each other. A slight difference between the two is, however, that the design and the performance of the HRSG and steam cycle are actually slightly enhanced in the OCC. That is because of the gas properties of the $CO_2$-rich working medium in the topping cycle, as discussed in section 2.3.3.

The steam cycle for the OCC was designed as a two pressure level design with the admission data at the high-pressure (HP) steam turbine inlet of 100 bar and 565 °C, which gives a volume flow of 1.5 $m^3$/s into the HP steam turbine. The low-pressure (LP) steam cycle had an admission data of 4.5 bar and 195 °C, which gives a volume flow of 2.7 $m^3$/s at the injection valve into the LP steam turbine. A Siemens SST-700 steam turbine was identified as a suitable commercial off-the-shelf steam turbine module for the steam cycle. The design of the turbine blading for this module and the calculation of their efficiency were carried out with Siemens design program. The pressure level at the injection valve for the LP steam cycle (4.5 bar) was chosen to match the pressure level after stage 6 in the LP turbine. The low volume flow in the HP turbine results in the need for a smaller mean blade diameter to maintain the blade height. This means that the shaft speed needs to be increased to compensate for the otherwise reduced blade speed. The steam turbine was, therefore, a dual-casing design to allow for a higher shaft speed in the HP turbine, than in the IP- and LP turbines.

The pinch-points have a direct effect on the steam production and, thereby, on the total plant power and efficiency too. Realistic design values of the pinch-point in the economizers are typically between 8-15 °C [48], but can be as high as 25 °C to reduce the heat transfer area further. Varying the pinch-point in the OCC from 8 to 25 °C changes the efficiency and power of the total power plant by about 1.0 percentage point and 2.0 MW. A 10 °C pinch-point was used for the HP economizers and a pinch-point of 15 °C was used for the LP economizer. The first LP economizer was also used to preheat the HP feedwater, to improves the utilization of the exhaust heat in the flue gas. The approach-point is typically in the range from 5-12 °C [48], and a 12 °C approach-point were used for both the LP- and HP steam drum evaporators. The steam turbine condenser was seawater cooled with an incoming temperature of 15 °C, outgoing temperature of 25 °C and a temperature difference between the outgoing condensate and the outgoing cooling water of 3.5 °C, which correspond to a condenser pressure of 0.039 bar. The high-pressure steam was first expanded in the HP-turbine with a PR of 3.1 down to 31.7 bar, then in the IP-turbine with a PR of 7.3 down to 4.4 bar.

In the LP turbine the steam was finally expanded to the condenser pressure of 0.039 bar, into which the LP steam was also injected. The HP turbine was spinning at 6,000 rpm and had a calculated isentropic efficiency of 90.2%, while the IP turbine and LP turbine were spinning at 3,000 rpm and had the calculated isentropic efficiencies of 88.9% and 86.0%, respectively.

The 6,000 rpm HP shaft was connected through a gearbox to the 3,000 rpm IP- and LP shaft, which drive a 3,000 rpm generator. The design point efficiencies for the gearbox and the generator were 98.69% and 98.27% respectively. The pumps, such as, for example, the feedwater pumps, in the steam cycle were modelled with an isentropic efficiency of 75%.

The energy utilization in the HRSG is discussed more in section 2.3.3, in which Figure 2.15 shows the T-Q chart (temperature vs. energy chart) for the HRSG design.

### 2.1.6 Flue gas condenser

The working medium leaving the economizer in the HRSG has a temperature of 70 °C at the design point. For an alternative OCC configuration might the temperature vary within the range of, at least, 70 to 130 °C depending on the steam cycle design, e.g. the number of steam pressure levels and the pinch-point in the LP economizer have a clear influence on the temperature level. The majority of this mass flow (about 90 -wt.%) is recirculated back toward the gas turbine compressor inlet, but before it can be re-injected into the compressor inlet it has to be cooled, cleaned and slightly reheated. By adding a flue gas condenser in the form of a wet cooling tower at the cold end of the HRSG, both the cooling and cleaning can be achieved in one single unit (Figure 2.2). The basic working principle of the cooling tower is to spray in recirculated water at the top of the tower. The water then drains down through surface-enhancing plates, where the water interacts with the (counter-current) upwards-flowing working medium, which gets cooled. The velocity of the working medium rising up through the tower has to be kept sufficiently low to avoid water carryover. The velocity limit depends on the size of the water droplets and the design of the tower, but a velocity in the order of 2 m/s can be used as an indicative figure, which corresponds to an estimated cross-section radius of about 5.0 m [65]. As the working medium is cooled below its dew point, some of the steam condenses and falls down to the bottom of the tower, where it is collected to be reused as a cooling medium. In addition to cooling the working medium the water spray also acts as a scrubber, which purifies the working medium from determinable substances, such as acids, potential soot particles and deposits, which might be chemically aggressive to the material and also risk plugging cooling holes in the turbine airfoils. The cooling water that is collected at the bottom of the condenser tower is itself cooled through an external heat drain, presumably a seawater cooler or external cooling tower depending on the available cooling medium at the site. A part of the cooling water stream is also passed through a water treatment plant to ensure high quality before it is reinjected into the top of the cooling tower. The cooling tower is not associated with any water consumption, as there will be a surplus of water available from the condensing of steam formed in the gas turbine combustion, and neither is it any major energy consumer either, as its consumption is mainly associated with pumping water and a facility for the water clean-up. The pressure drop of the flue gas across the flue gas condenser was assumed to be 20 mbar.

### 2.1.7 Recirculation, pre-heating and $CO_2$ separation

The working medium that has been passed through the cooling tower is split into two streams, one major stream that is recirculated back towards the gas turbine unit's compressor inlet and

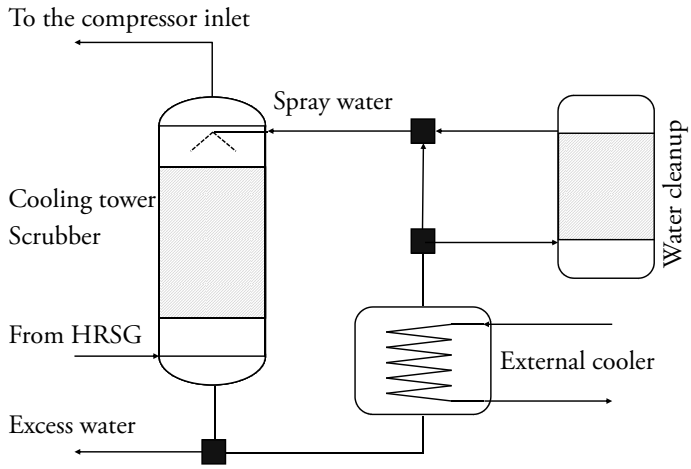


Figure 2.2: Layout of the combined wet cooling tower and scrubber, for cooling and cleaning the working medium prior to the recirculation and the $CO_2$ bleed

one minor $CO_2$ stream that is bleed off to be sequestrated. The mass of the minor $CO_2$ bleed stream keeps the mass balance stable by balancing the fuel flow and the oxygen supply injected into the cycle in the gas turbine combustion and potential minor leakages out of the cycle. The total mass of the bleed stream is about 26 kg/s or 10 -wt.% of the total recirculated mass flow, including the condensed excess water in the cooling tower, which is drained off separately in the condenser.

The composition in the $CO_2$ bleed stream is about 85 -wt.% $CO_2$, 10 -wt.% $H_2O$ and a few percentage points of mainly the enriched non-condensable gases argon and nitrogen (Table 2.1). The composition of the bleed stream depends mainly on the temperature in the cooling tower, and hence the amount of $H_2O$ that is condensed and separated prior to the bleed, and to a minor extent on the composition of the fuel and oxidizer streams. The ratio between the $CO_2$ and $H_2O$ will therefore vary slightly if the condenser temperature, the fuel composition and the composition of the oxygen stream are changed. The $CO_2$ bleed stream is passed through a compressor- and pump train with intermediate cooling, to separate the $H_2O$ from the $CO_2$ and compress the $CO_2$ to a state applicable for transportation and sequestration. By using intermediate cooling the water is condensed and separated from the stream. This reduces the mass flow of the bleed stream and lowers its temperature, both of which reduce the work for the $CO_2$ compression. The required state of the delivered $CO_2$ stream from the compressor train depends on the utilization area, but it is likely to be delivered as a virtually pure $CO_2$ stream in a supercritical state.

$CO_2$ compression represents the second largest efficiency penalty in the total OOC efficiency, after the oxygen production in the ASU. The energy consumption depends on the configuration of the compressor train and the number of inter-coolers. The full compressor train was not modelled thermodynamically in the process simulation. The approach was instead to penalize the cycle with a specific energy consumption for the compression of the $CO_2$ bleed stream to its final delivery state of 140 bar, used in this investigation. A common

approach is to apply a fixed specific energy consumption in kW/kg wet $CO_2$. This method is not preferable when the flue gas condenser temperature affects the water content directly and, thereby, also the energy consumption despite a constant dry $CO_2$ mass flow. The method used to avoid this undesirable influence was to include the compression of the bleed stream to 3.5 bar and the subsequent cooling to 40 °C in the thermodynamic cycle simulation. From this specific state of 3.5 bar and 40 °C, where the water content is independent of the condenser temperature, a specific energy cost of 315 kW/kg wet $CO_2$ was then used to represent the energy cost for the compression to 140 bar. The total energy consumption was 6.5 MW, which reduces the total power plant efficiency by 2.6 percentage points.

The $CO_2$ stream might need to be further treated by removing traces of impurities depending on the storage site or its utilization. The acceptable level of impurities depends on the applications of the $CO_2$ stream even for similar application and it is therefore difficult to specify it accurately on a general basis [35]. The energy consumption for any after treatment was not considered in the $CO_2$ compression cost and, if required, this cost has to be accounted for separately.

The working medium is saturated with steam in the flue gas condenser as it is cooled down to, and below, its dew point. A high moisture content is a problem as there is an obvious risk of formation of water droplets through condensation in the compressor bellmouth and in its front stages, where the static temperature is reduced as the fluid is accelerated to a high absolute Mach number. The absolute Mach number reaches for example about 0.6 at the inlet to rotor 1 and about 0.9 at the inlet to stator 1. Water droplets in the compressor inlet risk to causing erosion and corrosion to the compressor airfoils and the droplets can themselves also act as a scrubber and, by precipitation, enrich aggressive impurities on the compressor airfoils. The working medium is therefore passed through a preheater to protect the first compressor stages. The preheater increases the temperature by a few degrees (about 3-5 °C), which reduces the relative humidity down to approximately 80%, or less. As the preheating itself both require an additional heat energy supply and increases the compressor work it penalizes the cycle performance (from a thermodynamic perspective) and the amount of preheating should therefore be kept at a fairly low (but still sufficiently high) level.

The working medium is passed through an inlet filter before it is recirculated back to the compressor inlet, to capture any debris that might slip through the clean-up plant and potential deposits from the recirculation pipes. A conventional gas turbine air filter design is likely to be appropriate to use as the working medium is preheated down to a relative humidity of approximately 80% or less, which reduces the risk of water carryover. The energy consumption for the preheating is 4.5 kJ/kg recirculated working medium, or about 1.0 MW in total for the OCC design. This energy supply was modelled by using a heat exchanger that utilizes low-pressure feedwater as the heat source, but for a simpler and less integrated cycle design an electric heater is an alternative.

## 2.2 Working medium

*This section describe the properties of the $CO_2$-rich working medium and compare it against either air or the flue gas in a typical conventional natural gas-fired combined cycle power plant at typical compressor and turbine gas states.*

In the OOC's topping cycle the composition of the working medium is different from that in a conventional natural gas-fired CCPP, where the working medium consists of either air (in the compressor) or a flue gas (in the turbine). Therefore, the gas properties of the working medium are also significantly different in the two power plants. The composition of the working medium at the oxy-fuel gas turbine's compressor inlet has a composition of 84.6 -wt.% $CO_2$, 8.8 -wt.% $H_2O$, 3.9 -wt.% Ar, 2.6 -wt.% $N_2$ and 0.1 -wt.% $O_2$ at a gas state of 64.7 °C and 1.015 bar (Table 2.1). The higher mass fraction of argon (3.9 -wt.% Ar) in the working medium compared to air (1.27 -wt.% Ar) is due to the fact that argon does not get efficiently separated in a cryogenic ASU and, thereby, gets enriched in the recirculated cycle, as discussed in section 2.1.3. The gas properties with respect to the specific heat at constant pressure ($c_p$), the isentropic exponent ($\gamma$), the speed of sound ($a$), the dynamic viscosity ($\mu$) and the compressibility factor ($Z$) are clearly different for the $CO_2$-rich working medium compared to air at similar states (Table 2.2 and 2.3).

Table 2.2: The composition and gas properties of the working medium in an oxy-fuel gas turbine, compared to the gas properties of air or flue gas, at the same gas state

| | | Compressor | | | | Turbine | | | |
|---|---|---|---|---|---|---|---|---|---|
| | | Inlet | | Outlet | | Inlet (CT) | | Outlet (PT) | |
| | | OCC | CCPP | OCC | CCPP | OCC | CCPP | OCC | CCPP |
| $CO_2$ | [-wt.%] | 84.6 | 0.1 | 84.6 | 0.1 | 80.3 | 7.6 | 81.2 | 6.0 |
| $H_2O$ | [-wt.%] | 8.9 | 0.6 | 8.9 | 0.6 | 13.4 | 6.8 | 12.5 | 5.5 |
| Ar | [-wt.%] | 3.9 | 1.3 | 3.9 | 1.3 | 3.7 | 1.2 | 3.7 | 1.2 |
| $N_2$ | [-wt.%] | 2.6 | 75.1 | 2.6 | 75.1 | 2.5 | 73.0 | 2.5 | 73.5 |
| $O_2$ | [-wt.%] | 0.1 | 23.0 | 0.1 | 23.0 | 0.1 | 11.3 | 0.1 | 13.9 |
| Temperature ($T$) | [°C] | 64.7 | 64.7 | 438.6 | 438.6 | 1340.0 | 1340.0 | 612.0 | 612.0 |
| Pressure ($p$) | [bar] | 1.015 | 1.015 | 31.2 | 31.2 | 30.31 | 30.31 | 1.080 | 1.080 |
| Molar mass ($M$) | [g/mol] | 38.38 | 28.85 | 38.38 | 28.85 | 36.32 | 28.23 | 36.73 | 28.36 |
| Gas constant ($R$) | [kJ/(kg K)] | 216.7 | 288.2 | 216.7 | 288.2 | 228.9 | 294.5 | 226.3 | 293.1 |
| Specific heat ($c_p$) | [kJ/kg] | 0.961 | 1.012 | 1.192 | 1.084 | 1.484 | 1.336 | 1.298 | 1.33 |
| Isentropic exp. ($\gamma$) | [–] | 1.29 | 1.40 | 1.22 | 1.36 | 1.18 | 1.28 | 1.21 | 1.33 |
| Speed of sound ($a$) | [m/s] | 307 | 369 | 434 | 529 | 661 | 781 | 493 | 587 |

These differences give rise to several design-related questions, such as what is the preferred overall OCC layout and gas turbine unit's PR, and its influence on the cooling medium consumption and the effect on the Mach number in the turbomachinery design. There was also uncertainty over whether the traditional correlation-based 1D and 2D design tools and design methods could still be used or not. These questions are addressed in the subsequent section 2.3 and in Chapter 3, 4 and 5.

The gas properties at the inlet and outlet of the compressor and turbines are given in Table 2.2, where they are compared against the properties for either air or a flue gas at the same state. The gas states are not the same in the OCC and in a conventional natural gas-fired CCPP, and therefore for completeness the gas properties for the states in a typical natural gas-

Table 2.3: The composition and gas properties in the gas turbine for a typical natural gas-fired combined cycle power plant

| | | Compressor | | Turbine | |
|---|---|---|---|---|---|
| | | Inlet | Outlet | Inlet | Outlet |
| $CO_2$ | [-wt.%] | 0.1 | 0.1 | 7.2 | 5.6 |
| $H_2O$ | [-wt.%] | 0.6 | 0.6 | 6.4 | 5.2 |
| Ar | [-wt.%] | 1.3 | 1.3 | 1.2 | 1.2 |
| $N_2$ | [-wt.%] | 75.1 | 75.1 | 73.1 | 73.6 |
| $O_2$ | [-wt.%] | 23.0 | 23.0 | 12.0 | 14.5 |
| Temperature ($T$) | [°C] | 15.0 | 451.0 | 1445 | 565 |
| Pressure ($p$) | [bar] | 1.013 | 21.4 | 20.4 | 1.04 |
| Specific heat ($c_p$) | [kJ/kg] | 1.010 | 1.087 | 1.342 | 1.170 |
| Isentropic exp. ($\gamma$) | [−] | 1.40 | 1.36 | 1.28 | 1.33 |
| Speed of sound ($a$) | [m/s] | 340.9 | 532.9 | 804.4 | 572.1 |

fired CCPP are also shown in Table 2.3. These tables are based on the actual gas composition present in the OCC and a typical composition in a conventional CCPP, which is also given in the Tables. That is not the case for the illustrated variation in the specific heat ($c_p$), isentropic exponent ($\gamma$) and dynamic viscosity ($\mu$), all with respect to the temperature in Figure 2.3 and 2.4 and 2.5, where 100% $CO_2$ is compared against air for pressures between 1 and 40 bar. The reason for comparing pure $CO_2$, instead of a gas mixture as in Table 2.2 and 2.3, is because of the complexity with a changing composition of the working medium throughout the cycle, regarding both pressure and temperature. Therefore, there is some deviation between the numbers shown in the graphs and those given in the tables. The difference is mainly because the water content of about 10 -wt.% is not taken into account in the graphs.

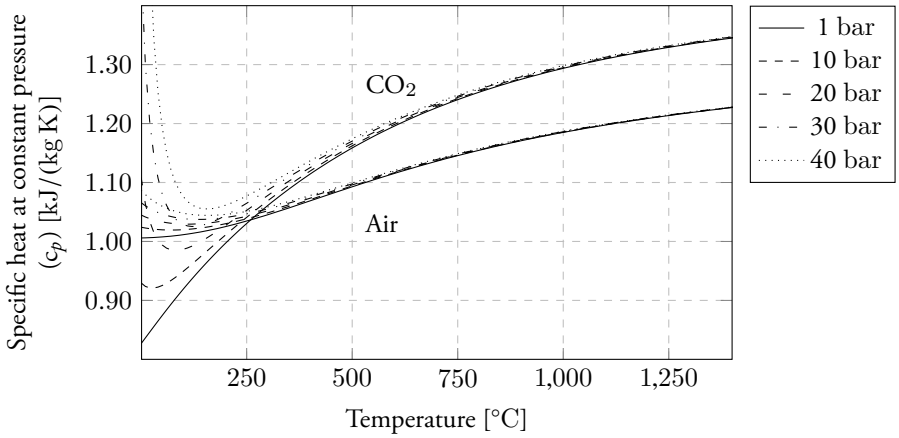


Figure 2.3: Specific heat at constant pressure vs. temperature, for air and $CO_2$.

The $CO_2$-rich working medium deviates significantly from an ideal gas, unlike air, which has a fairly ideal behaviour at the gas states concerned. This can be seen from the fact that the compressibility factor ($Z$) given by Equation 2.2 deviates greatly from 1.0 for $CO_2$ in Figure 2.6. Air, on the other hand, has a much more ideal behaviour and its compressibility factor ($Z_{Air}$) is close to 1.0 for the gas states concerned as seen in Figure 2.7 (note the different

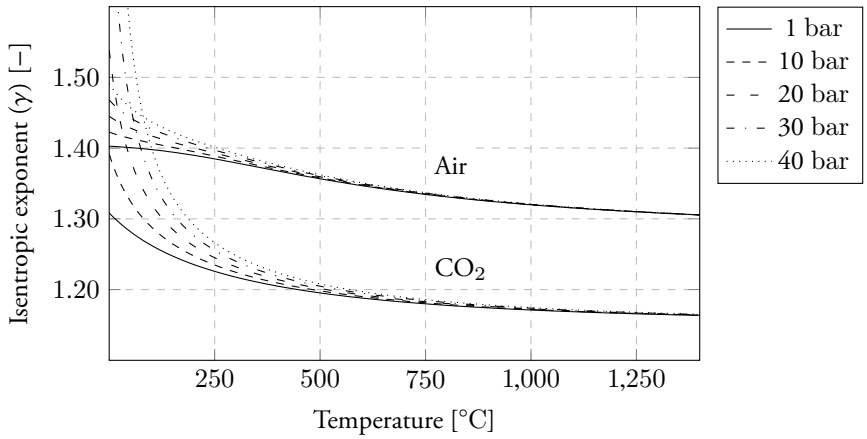


Figure 2.4: Isentropic exponent vs. temperature, for air and $CO_2$.

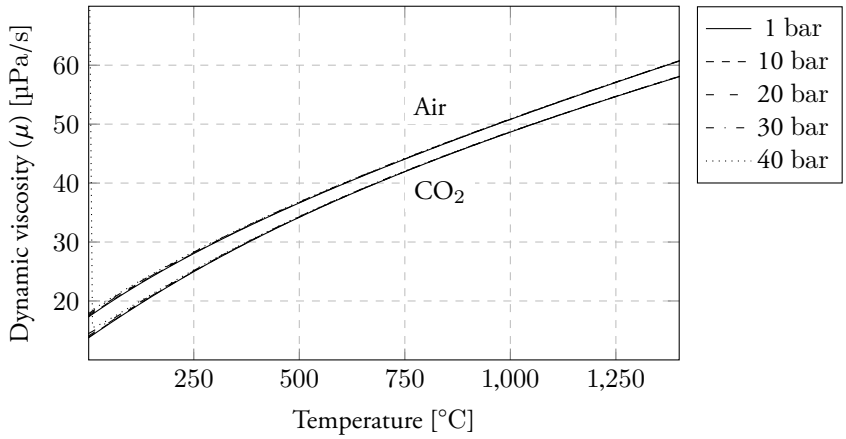


Figure 2.5: Dynamic viscosity vs. temperature, for air and $CO_2$.

scale on the y-axis in the two figures). This deviation from the ideal gas law for the $CO_2$-rich working medium implies that it is essential to use real gas data in the calculations.

$$Z = \frac{pv}{RT} \tag{2.2}$$

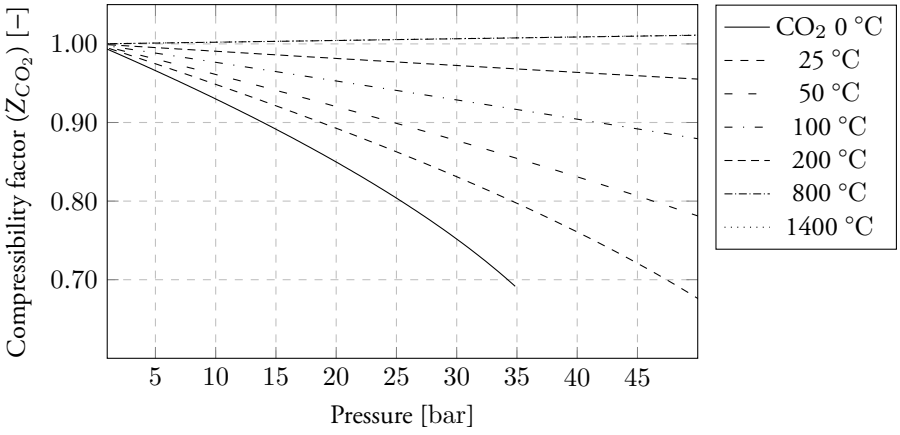


Figure 2.6: Compressibility factor, for $CO_2$ ($Z_{CO_2}$).

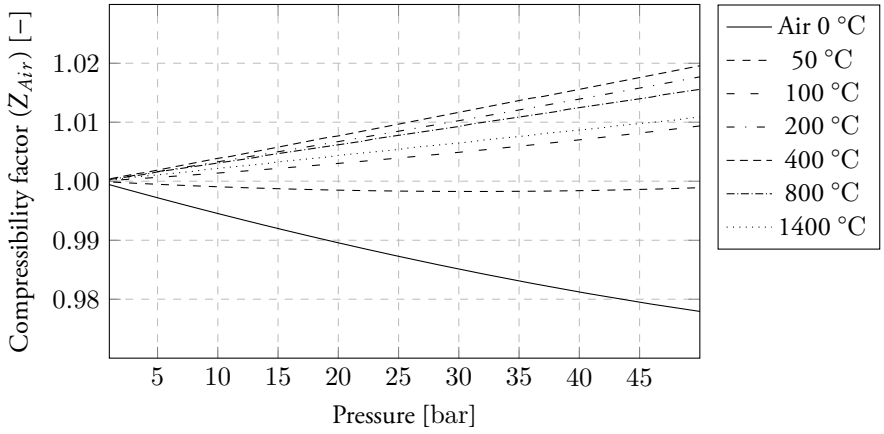


Figure 2.7: Compressibility factor, for air ($Z_{Air}$).

## 2.3 Cycle optimization

*This section describes the approach used to determine the preferred cycle design and discusses the different design parameters that were investigated, namely the gas turbine pressure ratio (PR), the exhaust gas temperature (EGT) from the gas turbine unit's, the cooling medium consumption ($m_{cool}$), the turbine disc sealing consumption ($m_{seal}$) and the preferred amount of cooling of the recirculated working medium. The effect on the HRSG and steam cycle design of the $CO_2$-rich working medium is also discussed in this section.*

### 2.3.1 Gas turbine pressure ratio and exhaust gas temperature

Designing a CCPP and optimizing the design of the embedded components, e.g. the gas turbine unit, from scratch is an art in itself, regardless of whether it is a conventional CCPP or an OCC. The design optimization is, in its simpler form, associated with major uncertainties, while when increasing the model complexity the optimization in many aspects quickly risks becoming neither foreseeable nor manageable. What makes the design optimization especially problematic is the question of how different parameters, assumptions and design choices affect each other. The optimization process is therefore a multidimensional problem where the key to enabling an efficient design process is to achieve a sound balance between the complexity of the initial modelling, its turnaround time and its accuracy. The multidimensional nature can be exemplified by the many design choices that have to be addressed almost immediately for the gas turbine design. Questions that arise include the shaft configuration, the gas turbine unit's pressure ratio, the number of compressor stages and turbine stages, the number of cooled stages, the exhaust gas temperature from the gas turbine unit, assumable component efficiencies, assumable cooling medium consumption and, on top of this, predicting the trends of how these parameters influence each other.

To avoid the initial oxy-fuel combined cycle design being optimized against improper design parameters it was a priority to achieve a cycle model that predicted the trends correctly. That is because, in the initial design phase, it is more important to predict the trends correctly than that the absolute levels for the final design are absolutely correct. That is because there is a major risk that the overall design turns out to be a sub-optimal design if the trends are not captured correctly in the initial design. A suboptimal design results in lost performance for the entire power plant that cannot be fully compensated for, even by optimal designs of the individual subcomponents. Certain design decisions tend, however, to be based on the absolute performance levels and therefore the prediction of the absolute levels is still important.

Analysing the cycle design was basically about considering and relating the different design choices to the available technologies that are either governing, guiding or limiting it and to ensuring that the design fulfilled the specification. The main technologies that generally need to be considered are the combustion, the turbine cooling, the HRSG and the steam cycle technologies. These technology levels must also reflect the size of the power plant, as the available technologies are size dependent. The design specifications for the OCC included, amount others, a power plant in the range of 115-125 MW. The OCC design should also, to the greatest extent possible, be based on current state-of-the-art technology to avoid having to develop any new technologies or components that were not required for obvious reasons. That is because all components or technologies that are not already mature risk challenging the feasibility of bringing the OCC concept to the market within the foreseeable future.

It was decided early that the combustor outlet temperature (COT) would be 1,340 °C,

which is in the range from 1,319 °C to 1,425 °C commonly used for oxy-fuel combined cycles [62, 15, 81, 49, 75, 70], although COT of 1,232 °C [59] and 1,600 °C [81] have been used too.

A COT of 1,340 °C is a relatively conservative temperature compared to today's modern gas turbine technology standard. Mitsubishi Heavy Industries have, for example, a turbine inlet temperature of 1,600 °C in their J-series gas turbines [39, 82]. The decision to use a COT of 1,340 °C was justified with regard to the relatively high gas turbine PR required for a certain temperature ratio (TR) across the turbines because of the different gas properties, as discussed in the following section. It was not desirable either to further complicate the design of the combustion system with a too high COT, as a completely new design of the combustion system is already required for the oxy-fuel combustion. The reason for not reducing the COT further was that it would reduce the specific power and the total efficiency of the OCC and with that also the OCC's competitiveness.

It was decided to limiting the admission data for the steam cycle to 565 °C and 100 bar, which can also seem slightly conservative, as there are steam cycles with higher admission data. These high admission steam cycles (i.e. 585-600 °C [64, 38]) are, however, mainly for the larger power cycle segment, and with higher admission data for the OCC in a 1-1 gas- and steam turbine configuration the volume flow into the HP steam turbine is getting too low for a good HP turbine design (i.e. blade height). The volume flow into the HP turbine was 1.50 $m^3/s$, at 565 °C and 100 bar. To increase the performance of the OCC either the steam temperature could have been increased towards 580-585 °C, or a reheat cycle been used or a combination of both an increased temperature and a reheat could have been used. These options were not investigated further for the design case of the OCC; instead higher steam data was considered as an upgrade opportunity for larger OCC power plants with either multiple gas turbine unit configurations such as 2-1 or 3-1, or larger OCC gas turbine units, or when high admission steam turbines for lower volume flows become more commercially available. For a conventional CCPP of similar power size the design procedure would (most likely) be to based on the highest manageable COT, without an all too high cooling medium consumption[i], chose a gas turbine PR that results in an EGT that is about 20-25°C higher (or slightly more) than the HP steam temperature. For example, designing for an EGT of 585-600 °C for a HP steam temperature of 565 °C. Depending on the COT, this would correspond to a gas turbine PR of about 18-22, which is in line with the efficiency optimum for a CCPP as shown by Horlock [45] and the commercially available CCPP [2, 4]. There are, however, conventional CCPPs with both higher and lower PRs and EGTs available in the market [2, 4]. Designing these CCPPs with an, for the CCPP efficiency, optimal gas turbine PR is not an issue as the optimal PR is modest even for a state-of-the-art COT (i.e. a J-series of 1,600°C).

The design of the OCC was more complicated than it would have been for a CCPP, because the OCC design also needs to consider some additional aspects related to the gas properties, which affect and complicate the design further. These effects on the design are mainly related to the lower isentropic exponent ($\gamma$), compared to a conventional flue gas. The design is also affected by the different variations in specific heat ($c_p$) and the lower speed of sound ($a$) for the $CO_2$-rich working medium. The lower isentropic exponent of the working medium in the OCC calls for a higher gas turbine PR to achieve the same gas temperature ratio (TR) in the turbine(s), as in a conventional CCPP for the same COT. To illustrate the increased need

[i] I.e. the highest manageable temperature if one imagines mixing the working medium at the turbine inlet with the turbine cooling medium, all prior to the turbine inlet.

for a higher PR in the oxy-fuel gas turbine unit, compared to a conventional gas turbine, the relation between the TR $(T_1/T_2)$[ii] and the PR $(p_1/p_2)$ is shown for air and $CO_2$ in Figure 2.8. As mentioned in section 2.2, the $CO_2$-rich working medium does not behave fully as an ideal gas, but to give an idea of how the pressure and temperature relate to each other the isentropic relation between the temperature and pressure for an ideal gas can be used (Equation 2.3). From this graph (Figure 2.8) it can be seen that for a TR of 1.75 the required PR for air is about 10, while a PR of about 44 is required for the same TR for $CO_2$. It also appears that the derivative declines with an increasing PR, hence the benefits of further increasing the PR decline.

$$\frac{T_1}{T_2} = \left(\frac{p_1}{p_2}\right)^{\left(\frac{\gamma-1}{\gamma}\right)} \tag{2.3}$$

The calculations were made in the process simulation tool Krawal Modular for an inlet temperature $(T_1)$ of 1340 °C (1613 K) and an outlet pressure $(p_2)$ of 1.0 bar, without any cooling medium and with an isentropic efficiency of 100%, and reflect therefore not entirely a real engine behaviour. Included in the figure is also the average isentropic exponent $(\gamma_{avg.})$ calculated as a straight average between the inlet and outlet $(\gamma_{avg.} = 0.5\,(\gamma_1 + \gamma_2))$ to show its variation.

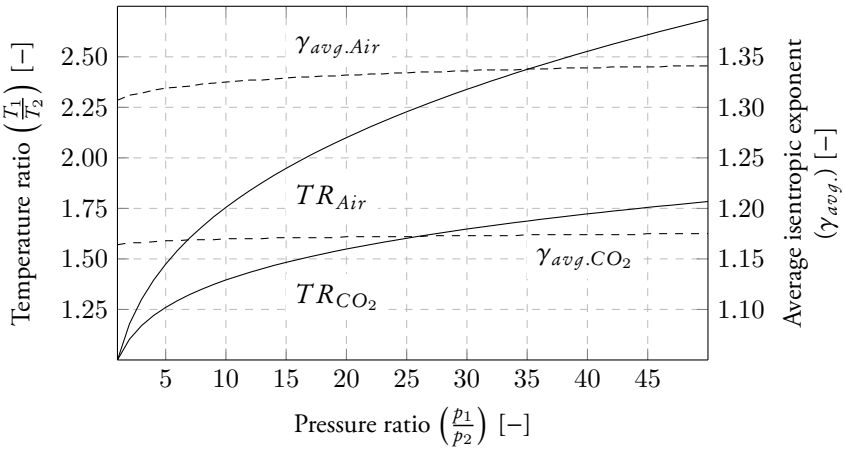


Figure 2.8: The isentropic relation between the temperature ratio (in Kelvin) and the pressure ratio, for $CO_2$ and air. The average isentropic exponent $\gamma_{avg.}$ is also seen. Derived with a $T_1$ of 1613 K (1340 °C) and a $p_2$ of 1.0 bar.

The influence that the gas turbine unit's PR has on the OCC's efficiency, the EGT, the SAS consumption and the temperature into the power turbine, for a constant COT, was important to consider during the cycle design. These relations were, therefore, investigated through a parameter study in the process simulation tool, in publication II [25]. The investigation was made through including a gas turbine model in the process simulation, in which every turbine stage was modelled individually to enable the prediction of the turbine cooling and disc sealing

[ii] in Kelvin (K)

medium consumption for each stage. It should be noted that a twin-spool gas turbine unit was used for the investigation in publication II [25] and not a single-shaft GG with a free PT, which was the final design chosen for the gas turbine's shaft configuration. Therefore, the numbers in Figure 2.9, 2.10, 2.11 and 2.12 do not fully agree with the final design figures for the gas turbine unit. The overall trends and conclusions from this study are nevertheless still considered valid and are as follows.

Firstly, increasing the PR reduces the EGT from the gas turbine unit, and as long as the EGT is above 590 °C this has a positive effect on the cycle performance. That is because the super-heater pinch-point can then be decreased down towards its lower limit, which for the OCC design was set to 25 °C. The reason for the increased performance is that the exhaust heat energy can then be better utilized in the steam cycle (i.e. less exergy losses).

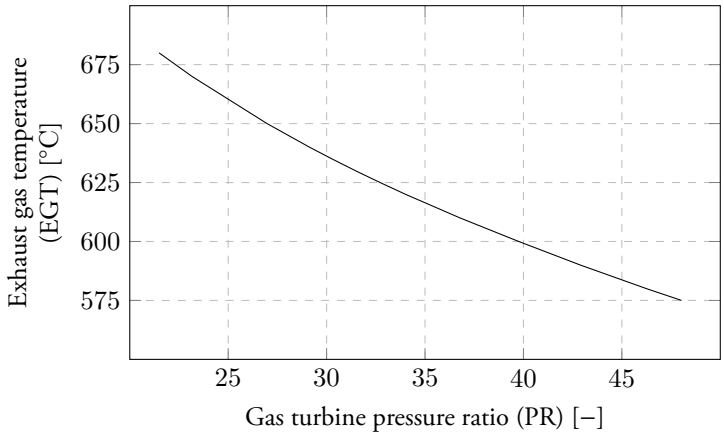


Figure 2.9: The effects on the exhaust gas temperature of the gas turbine's pressure ratio.

An increased PR is, however, likely to result in a need for additional compressor stages and possibly additional turbine stage(s), too. The efficiency of both a compressor and a turbine is reduced with an increasing PR and especially if the increased PR is to be handled by an increased stage load ($\psi$), instead of adding additional compressor stages and/or turbine stages.

The working medium consumption for the secondary-air-system (SAS) that provides the working medium for the turbine cooling and disc sealing also increases with a rising gas turbine PR, as seen in Figure 2.10. The increase is mainly the result of an increasing temperature of the cooling medium ($T_c$) and a higher density ($\rho$) of the disc sealing medium, both caused by the higher PR. Thereby, the SAS flow to the HP turbine increases with a rising PR. The increased compressor work results also in a longer expansion in the compressor turbine(s), which also reduces the temperature of the working medium ($T_g$) in the power turbine. If the temperature in the power turbine is reduced below the acceptable metal temperature of the airfoils can the PT be uncooled. The effect from the increasing compressor work on the temperature into the PT is seen in Figure 2.11, and the influence is further discussed in section 5.2. This reduced temperature of the working medium ($T_g$) in the power turbine results in the SAS consumption in the power turbine being reduced with an increasing PR. Therefore, there are two counteracting effects on the total SAS consumption, i.e. the increasing SAS consumption in the HP turbine because of an increasing temperature of the cooling medium and the declining cooling need in the power turbine as the temperature of the working

medium ($T_g$) is reduced in the PT. At a PR above 40, the gas temperature into the power turbine is below 900 °C which was the assumed maximum metal temperature in the stage cooling model for the gas turbine unit's PT in the process simulation tool. The effect of this is that the counter acting effect from a decreasing PT cooling ceases at a PR of 40, which is seen as an increased derivative for the total SAS consumption at about 40 bar in Figure 2.10. (This maximum metal temperature is however, dependent on the blade material of choice.)

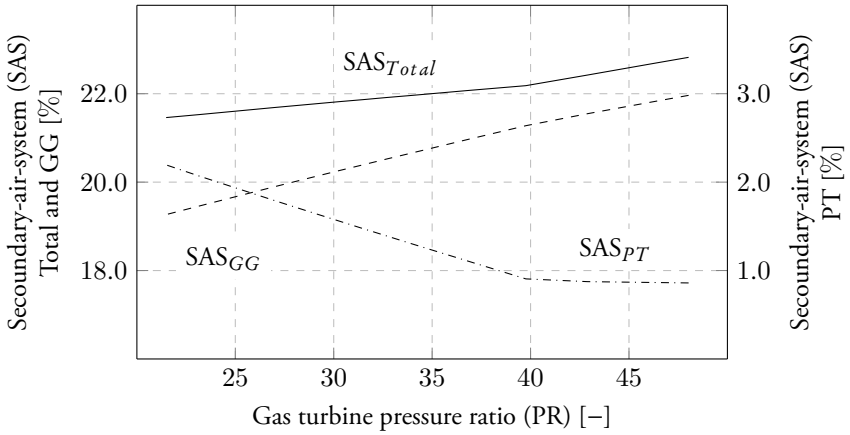


Figure 2.10: The effects on the SAS consumption of the gas turbine's pressure ratio for the GG, PT and the total, as a percentage of compressor inlet mass flow. The SAS consumption for the GG is the sum of the HP- and LP turbines.

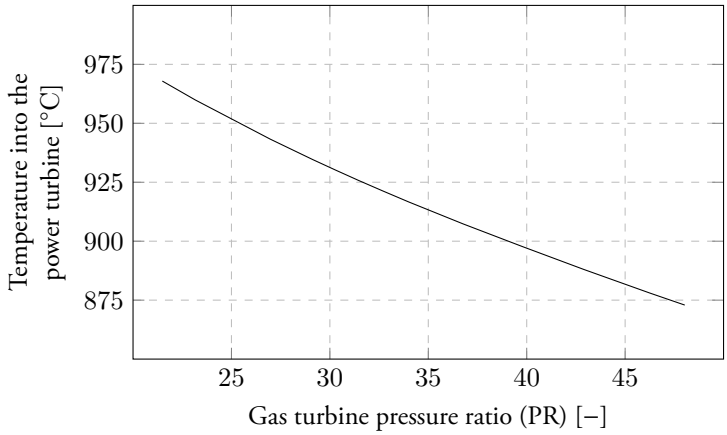


Figure 2.11: The effects on the temperature into the power turbine of the gas turbine's pressure ratio.

The compressor outlet temperature is also increased by a higher pressure ratio (i.e. compressor work), which for a specific COT reduces the temperature rise in the combustor and, thereby, the specific work of the OCC. The influence of the gas turbine unit's PR on the EGT

and the total OCC efficiency are seen in Figure 2.9 and 2.12 [25]. The trend is that the gain in total cycle efficiency declines and eventually flattens out towards the higher PRs. The efficiency optimum was found to be at a PR of about 45 and increasing the PR further reduces the total plant efficiency. That is as expected and is consistent with a conventional CCPP, apart from the fact that CCPPs have their efficiency optimum at a lower PR of about 18-22 [4]. Increasing the PR penalizes the cycle efficiency of the OCC slightly more than an increasing PR does to a CCPP. That is because the compression of the externally provided oxygen stream is less efficient than if being compressed in the gas turbine unit's compressor together with the main working medium, as in a conventional gas turbine.

A design trade-off for the OCC was between aiming for the peak cycle efficiency through choosing a PR in the range of 40-45 with the increased design complexity it brings, and a slight reduction of a few tenths of percentage point in total cycle efficiency to gain from the reduced design complexity that reducing the PR down towards the range of 30 entails. The conclusion was that the last tenths of percentage point were not worth the extra design complexity of the gas turbine unit and, therefore, was the OCC finally designed with a PR of 31.0.

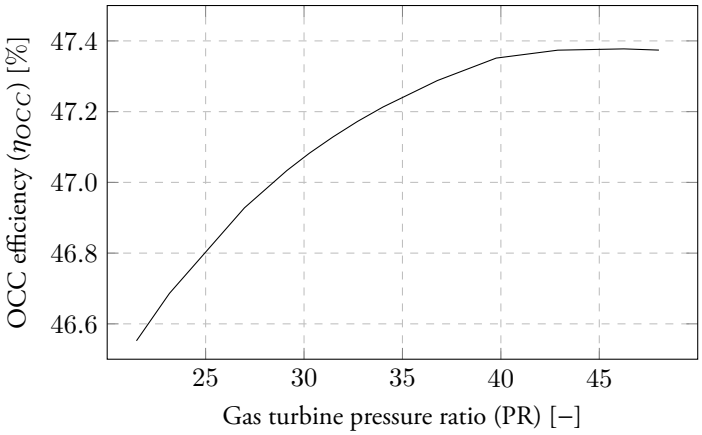


Figure 2.12: The effects on the total cycle efficiency of the gas turbine's pressure ratio.

### 2.3.2 Turbine cooling and disc sealing flow

For the quality of the conceptual design, it is important to predict the consumption of the turbine cooling medium and the disc sealing flows (disc purge flows). These two flow types are both summarized in the collective name "secondary-air-system" (SAS), which reflects that it is a secondary fluid stream that is bleed off from the compressor, mainly for protection of the turbines. A first assessment of the SAS consumption was required in the initial cycle study before any qualitative aerodynamic calculations, such as a 1D mid-span or 2D through-flow design, had been performed. This means that there was no actual turbine geometry to base the SAS estimation on and, therefore, some simple and general models were required for the first predictions. The turbine cooling and the disc sealing flow consumption are governed by two separate requirements and by different flow physics and these were, thus, predicted by two separate models.

The disc's sealing flows ($m_{seal}$) are fed up between the turbine discs and into the main gas

path. The purpose of these flows are to control the temperature of the discs and by pressurize the disc cavity and seal of the disc gap, prevent the hot working medium in the gas path from being ingested down between the discs. Avoiding hot gas ingestion is crucial, as the discs' material cannot withstand either the high temperature of the working medium in the gas path or the thermal stresses that high temperature gradients might cause. The disc sealing flows were predicted as the minimum flow that is required to avoid hot gas ingestions between the discs. The predictions were made according to the well-established method of Bayley and Owen (Equation 2.4) [11]. In this equation, $k$ represents the disc gap opening, $s$ the effectiveness of the sealing and $\rho$ the fluid density, $\omega$ the angular rotation of the disc and $r$ the disc rim radius.

$$m_{seal} = k \cdot s \cdot \rho \cdot \omega \cdot r^2 \tag{2.4}$$

The turbine cooling medium consumption ($m_c$) is primarily influenced by the suitable metal temperature ($T_m$) of the airfoils for a given load and lifetime, the cooled surface area ($A$), the gas temperatures ($T_g$) of the working medium, the temperatures of the cooling medium ($T_c$), the specific heat of the working medium ($c_{p,g}$) and the specific heat of the cooling medium ($c_{p,c}$). From these parameters three dimensionless groups can be derived that represent the heat-load ($m^*$), cooling effectiveness ($\varepsilon_c$) and cooling efficiency ($\eta_c$) (Equations 2.5, 2.6 and 2.7).

**Heat-load** ($m^*$)

$$m^* = \frac{m_c \cdot c_{p,c}}{HTC \cdot A} \tag{2.5}$$

**Cooling effectiveness** ($\varepsilon_c$)

$$\varepsilon_c = \frac{T_g - T_m}{T_g - T_c} \tag{2.6}$$

**Cooling efficiency** ($\eta_c$)

$$\eta_c = \frac{T_{c,out} - T_{c,in}}{T_m - T_{c,in}} \tag{2.7}$$

Rearranging Equations 2.5, 2.6 and 2.7 gives a relation between the three dimensionless parameters.

$$m^* = \frac{\eta_c}{\varepsilon\,(1-\varepsilon)} \tag{2.8}$$

This is an established set of equations, commonly referred to as the "m-STAR model", which enables calculations of the cooling medium consumption based on the cooling efficiency and effectiveness [10, 40, 44]. These equations are based on physical relations and were derived for conventional air-breathing gas turbines. To make this set of equations appropriate for predicting the turbine cooling medium consumption for different gas properties and gas state, as in the oxy-fuel gas turbine, some modifications were made. It was required, however, that

the prediction model still had to remain simple and robust to be applicable as early as in the preliminary design of the OCC in the process simulations tool and that its computing time was not allowed to limit studies of a range of different cases. A weakness with this set of equations that leads to a considerable uncertainty in the predicted results is that it is difficult to come up with representative values of the considered parameters, when applied early on in the design. There is, therefore, a risk of obtaining a significant error in the estimation of the total turbine cooling medium consumption through estimating some of the parameters slightly inaccurately. To reduce the uncertainty the method used was to instead predict relative changes from a reference design that utilized a similar cooling technology and as similar operation condition as possible, instead of predicting absolute values. As only relative variations have an impact on the result, this approach made the analysis less sensitive.

Two parameters that both have a large influence on the cooling medium consumption and are difficult to estimate from scratch for a new turbine are the cooled turbine area ($A$) and a representative average heat transfer coefficient ($HTC$). The cooled turbine area ($A$) is related to the volume flow ($V$) and therefore was the change in cooled turbine area correlated against the change in the volume flow ($dA/dV$). The relation between the cooled surface area and the volume flow was determined by redesigning a turbine with different volume flows, while keeping typical stage parameters constant. The designs were made in a 1D mid-span design tool and by analysing these results the derivative was found to be in the range from 0.5 to 0.75. The cooled surface area ($A$) comprises both the airfoils and the hub- and tip platform and the range depends on the assumptions made, such as how the aspect ratio and solidity were assumed to vary. The heat transfer coefficient ($HTC$) is influenced by a large variety of parameters, where the different gas composition in the OCC is the most significant contributor relative to the HTC in a conventional gas turbine. The change in the flow field that results from the different turbine geometry and the fact that the gas state is different also has an effect on the HTC. The HTC was correlated through the dimensionless quantities of the Nusselt number ($Nu$), the Prandtl number ($Pr$) and the Reynolds number ($Re$). Rearranging these dimensionless groups showed that the HTC is a function of the specific heat ($c_p$), thermal conductivity ($\lambda$), velocity ($C$), pressure ($p$), dynamic viscosity ($\mu$), density ($\rho$) and a characteristic length ($L$). Before being used, this fairly complicated relationship was simplified to a more applicable form by using the ideal gas law and a few assumptions [25].

The prediction models for the disc sealing flow and the turbine cooling medium consumption required some additional parameters that are not provided by a traditional process simulation. The additional parameters required were some basic turbine geometry parameters, such as for example the number of turbine stages, the radii of the gas path and the shaft speed. To attain these parameters a broad design of the gas path of the gas turbine unit was carried out in parallel with the process simulation. This broad design of the gas turbine also provided the necessary inputs (e.g. gas path geometry and gas state) for the SAS calculations as well as a first assessment of what the preferred gas turbine unit's design ought to be like.

### 2.3.3 Influences on the steam cycle

The HRSG and steam cycle has the same purpose in the OCC as in a conventional CCPP in that it recovers heat from the gas turbine unit's exhaust flow and utilizes it for driving the steam cycle. As discussed in section 2.3.1, the lower isentropic exponent calls for a higher PR in the gas turbine unit for the same TR across the turbines. A trade-off was, therefore, to allow a slightly higher EGT into the HRSG than necessary for a typical super-heater pinch-

point of about 25 °C. The final oxy-fuel combined cycle design has an EGT of about 613 °C and a high-pressure steam temperature of 565 °C, i.e. a pinch-point of 48 °C. That is an unnecessarily high super-heater pinch-point and a steam temperature of about 585 °C would suit this high EGT well.The high super-heater pinch-point in the HRSG reduces, however, the need for multiple pressure levels in the steam cycle. That is consistent with a supplementary fired CCPP, which generally only has one pressure level [18]. The reason that fewer steam pressure levels are required is because of the higher steam mass flow that is generated in the high pressure evaporated, when more exhaust heat is available above the evaporators pinch-point (for a certain steam pressure). This results in a higher water flow through the economizer(s), which entails a better matching between the available exhaust heat below the pinch-point and the economizer's water flow. However, the HRSG inlet temperature in the OCC does not get near to the temperatures in a supplementary fired HRSG and a two-pressure level steam cycle design was preferred over a one-pressure level design.

The effect mentioned above is primarily a result of the lower isentropic exponent of the working medium. Another difference in the gas properties, which results in an interesting design aspect of the HRSG design, is the variation in specific heat with respect to the temperature. The relation was shown in Figure 2.3, but is reproduced for the temperature range of interest for the HRSG in Figure 2.13. For air, the variation of the specific heat in the temperature range from 0 to 700 °C has an almost linear but weak concave variation and decreases from about 1.15 kJ/(kg K) at 700 °C down to about 1.0 kJ/(kg K) at 0 °C. In the same temperature range the specific heat for $CO_2$ has a convex shape with a more rapidly decreasing trend from about 1.22 kJ/(kg K) at 700 °C down to 0.83 kJ/(kg K) at 0 °C. The two graphs cross each other at about 260 °C, which means that $CO_2$ has a higher specific heat above this temperature and a lower specific heat below it. This large variation in specific heat for $CO_2$ results in more specific heat energy being available at temperatures above this crossover (at 260 °C) than in a conventional CCPP's flue gas, while the available specific heat energy is less in the lower temperature range. The available heat energy in the HRSG for the OCC and a conventional CCPP is illustrated in Figure 2.14, which shows the heat energy for the two power cycles compared between the same temperature interval (610- 70 °C), which are typical temperature levels for an OCC. To attain the same total heat energy in both cycles the $CO_2$ mass flow was reduced to 91.5% of the flue gas mass flow in the CCPPs.

It can be seen that for an EGT of 610 °C, an evaporation pressure of 106 bar and a pinch-point of 10 °C (corresponding to a gas temperature of 325 °C) there is about 10 kJ/s or 2.5% more heat energy available in the gas for evaporating and super-heating the steam in the OCC, than in a conventional CCPP. The heat energy available in the gas below this temperature of 325 °C down to 70 °C is at the same time about 3.1% less in the OCC (Figure 2.14). This might seem insignificant, but it should be considered against the fact that the exhaust mass flow is 245 kg/s and that this behaviour also results in an improved energy match between the flue gas and steam cycle in the OCC. This is in turn likely to result in a lower gas temperature out of the HRSG, i.e. the OCC has a gas temperature of 70 °C leaving the HRSG which is below the typical temperature in a two-pressures CCPP. Therefore, by attaining a lower stack temperature in the OCC the total energy utilization is increased further, which is not captured in Figure 2.14, where both the OCC and the CCPP are compared between the same temperature levels. The favourable variation of the specific heat results in there being more energy available at the high temperatures and less energy at the low temperatures in the HRSG, which enhances a steam cycle design with fewer steam pressure levels. This strengthens the effect that a higher EGT (i.e. high super-heater pinch-point) has on the need for fewer steam

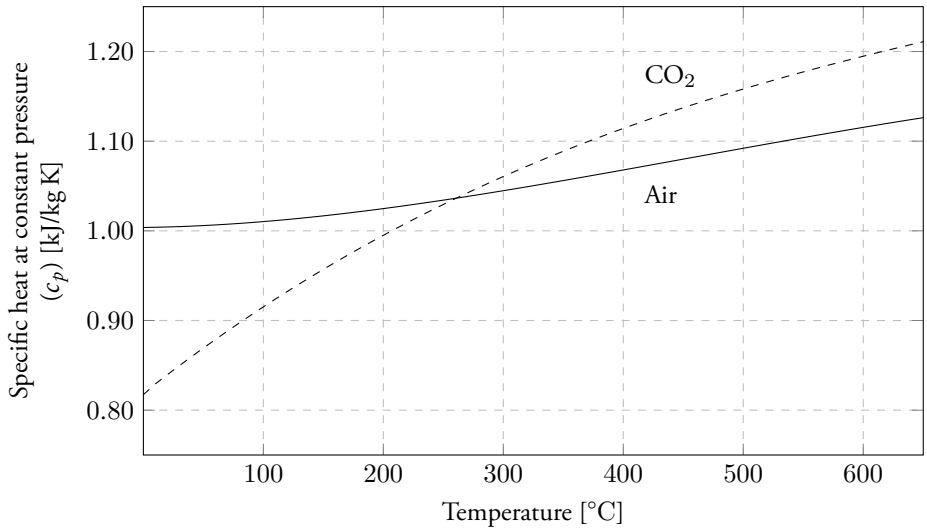


Figure 2.13: Specific heat at constant pressure ($c_p$) for $CO_2$ and the flue gas in a conventional CCPP.

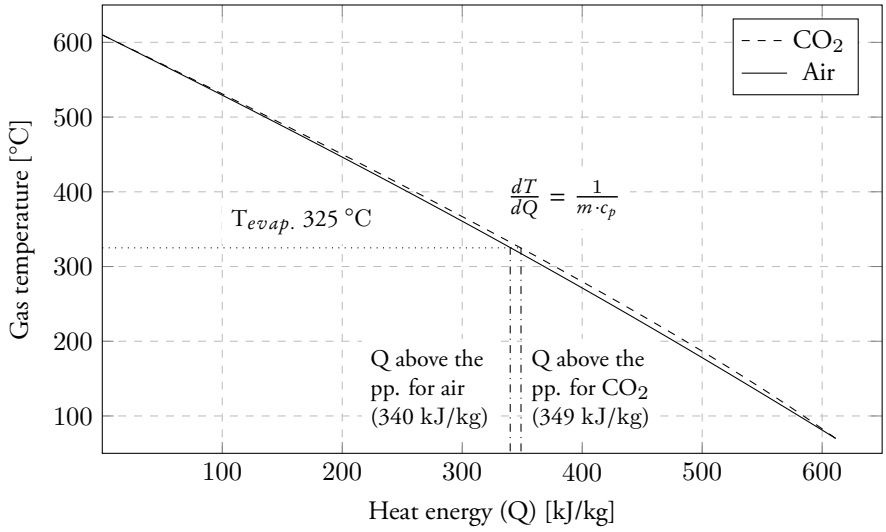


Figure 2.14: T-Q chart showing the variation in gas temperature (T) vs. extracted heat energy (Q), for $CO_2$ and air.

pressure levels.

The energy utilization in the HRSG for the OCC design is shown in the T-Q chart (temperature vs. heat energy) in Figure 2.15. The higher HRSG inlet temperature related to the COT and the lower outlet temperature from the HRSG means that the steam cycle represents a slightly larger portion of the total plant power. In a traditional CCPP the steam cycle represent about a third of the total plant power, while the steam cycle in an OCC tends to be a few percentage points higher. For this OCC design the gross power ratio between the gas turbine unit and steam turbine is 63.0%/37.0%. This does not include the energy cost of the oxygen production for the gas turbine combustion, which if accounted for would shift the ratio more towards the steam cycle (i.e. 55.0%/45.0%).

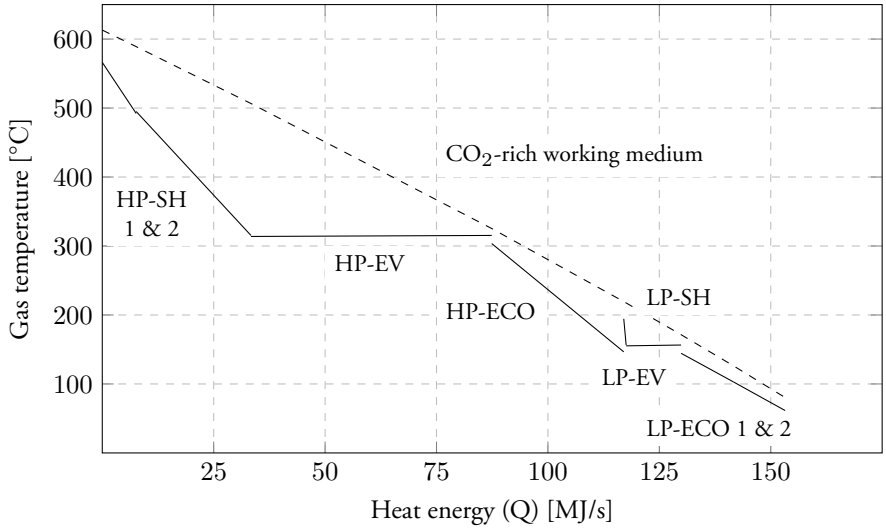


Figure 2.15: Energy utilization in the HRSG for the oxy-fuel combined cycle design.

### 2.3.4 Cooling and pre-heating of the recirculated working medium

As the compressor inlet temperature is controlled in the OCC the effects on the cycle design of varying the flue gas condenser temperature were investigated in publication II [25]. It was found that cooling the working medium has a variety of effects on the cycle, of which some counteract and others reinforce each other. The different effects are summarized below and discussed in more detail in publication II. Increasing the cooling (i.e. a lower temperature of the working medium at the compressor inlet) results in a reduced steam content in the working medium. A lower steam content reduces, in turn, the specific compressor work and, through a reduced heat transfer coefficient, the heat load on the turbines' hot section. The isentropic coefficient also gets reduced, which leads to the need for a slightly higher PR for the same TR in the turbines. The effect of the working medium being colder is also a reduced specific compressor work, a reduced temperature of the cooling medium and correspondingly a reduced turbine cooling medium consumption. The reduced compressor outlet temperature increases the firing window in the combustor and, hence, the specific gas turbine power. If, on the other hand, the cooling gets reduced (i.e. a higher temperature of the working medium

at the compressor inlet), less heat is rejected from the cycle and, thereby, the size of the flue gas condenser and the required temperature of the cooling medium for the flue gas condenser are reduced too.

The OCC efficiency optimum was found to be in the range of 40 °C to 65 °C with no further efficiency gain from cooling further below 60 °C. In several publications has a condenser temperature of 19-25 °C been used [59, 15, 70]. A design temperature of 60 °C was considered preferable after considering the optimum range and design aspects, such as the condenser size and the requirement for the available cooling medium temperature for the flue gas condenser.

### 2.3.5 Preferred cycle design

*This section summarizes the proposed design of the oxy-fuel combined cycle that was used for the proceeding design of the gas turbine unit.*

The proposed oxy-fuel combined cycle design consists of a twin-pressure steam cycle, with admission data of 100 bar and 565 °C at the HP steam turbine inlet and of 4.5 bar and 195 °C in the LP steam cycle (according to section 2.1.5). The topping cycle comprises a gas turbine unit with a COT of 1,340 °C and a PR of 31.0 at the design point. The compressor inlet mass flow is 220 kg/s, the compressor inlet temperature is 64.7 °C with a relative humidity of 80% and the EGT into the HRSG is 613 °C. The gross cycle power is 153.7 $MW_{el}$ and the net power 119.9 $MW_{el}$. The oxy-fuel combined cycle was calculated to have a gross power of 153.7 $MW_{el}$, a net power of 119.9 $MW_{el}$ and a net efficiency of 48.2%, which includes the energy cost for the $CO_2$ compression and the external $O_2$ production.

In the collaborative project OxyGT [65] was it concluded that the expected cost for a mature OCC power plant would be about 15-20% higher than for a conventional CCPP, which should be considered as relatively affordable. That is if excluding cost for the ASU and the $CO_2$ compression train, if including the costs of the ASU and the $CO_2$ compressor train will the cost of the entire power plant, obviously be higher.

# 3 The impact on the gas turbine design

*In this chapter the overall design requirements for the gas turbine unit, which were set by the broad conceptual cycle design, are described. The specific influences on the gas turbine unit arising because of its operation in an oxy-fuel combined cycle are also discussed in this chapter.*

*The subject was investigated in the following publications:*
**Publication I:** *Conceptual Design of a Mid-sized Semi-closed Oxy-fuel Combustion Combined Cycle, GT2011-46299 [60]*
**Publication II:** *Optimization of an Oxy-fuel Combined Cycle Regarding Performance and Complexity Level, GT2013-94755 [25]*
**Publication V:** *Aerodynamic Gas Turbine Compressor Design for an Oxy-fuel Combined Cycle, GT2015-42028 [23]*
**Publication VI:** *Aerodynamic Turbine Design for an Oxy-fuel Combined Cycle, GT2016-56439 [24]*

The overall performance requirements for the gas turbine unit were specified by the broad conceptual design of the oxy-fuel combined cycle, described in Chapter 2. The design then proceeded by designing the gas turbine unit to meet these overall performance requirements. The broad design criteria and boundary conditions for the gas turbine unit's design were that it should have a compressor inlet mass flow of 220 kg/s at a temperature of 64 °C, a pressure ratio (PR) of 31.0 and a combustion outlet temperature (COT) of 1340 °C. The shaft power from the gas turbine should be 100 MW, corresponding to an exhaust gas temperature (EGT) of about 610 °C. The total medium consumption for the secondary-air-system (SAS) was also estimated to be 22.8% of the compressor inlet mass flow (Chapter 2). The aim with the conceptual design of the gas turbine unit was to find a preferred design compromise that meets these requirements and restrictions. That involved, for example, deciding on a preferred shaft configuration, the flow matching between the compressor and turbines, the number of turbine stages, the shaft speed and a first estimation of the gas path's geometrical shape. Although the concept phase is approximate, it is important as it sets the basis for avoiding sub-optimization and, thereby, to achieving a competitive overall gas turbine unit design. The different design criteria for the OCC gas turbine unit, because of the gas properties of the $CO_2$-rich working medium, resulted in an unexplored design space where especially the higher pressure ratio resulted in a need to explore different shaft configurations for the gas turbine unit. There were several different gas turbine shaft configurations that could have meet these design requirements. For a gas turbine designed mainly for operation in a conventional CCPP, i.e. without the intention of being used for mechanical drive, the choice of shaft configuration would be more apparent. That is, a gas turbine design for a conventional CCPP would (most likely) be a single-shaft gas turbine design, as is evident if one examines the shaft

configuration of gas turbines designed mainly for a CCPP [4]. That is because a single-shaft gas turbine unit has the advantage of being a simpler design with the potential for an enhanced diffuser design, a cold-end driven generator, with no need for a power turbine overhang, fewer bearings and potentially fewer turbine stages too. A single-shaft gas turbine design also has the advantage of an improved part-load performance, through the ability to reduce the mass flow (by variable guide vanes) and thereby maintain a high COT over a wider part-load range. However, remember that the pressure ratio for a newly designed gas turbine unit for a conventional CCPP would probably be about 18-22, which should be compared with the pressure ratio of 31.0 in the OCC gas turbine unit. The different shaft configurations mainly considered for the oxy-fuel gas turbine unit were: a single-shaft, a single-shaft gas generator with free power turbine, a twin-spool gas generator with the low-pressure turbine also acting as the power turbine and a twin-spool gas generator with a free power turbine. Some other more novel designs with a geared twin-speed compressor driven by a single compressor turbine were also investigated [65], but these concepts were considered too complex to proceed with. The different shaft configurations were explored by conducting broad concept studies of them. These concept studies provide preliminary information about typical parameters, such as the gas path geometry, shaft-speed(s), turbines' stage count and the gas states at the interfaces to the gas turbine unit's compressor and turbines.

The two parameters that influenced the selection of the gas turbine unit's shaft configuration most were the shaft power of the power turbine and the total gas turbine unit's PR.

Firstly, because the shaft power was about 100 MW it was decided that the generator should be direct-driven by the power turbine (i.e. no gearbox). A direct driven configuration is common for large gas turbine and, despite the available gearboxes [58] this approach seemed appropriate for the 100 MW oxy-fuel gas turbine unit. The motive was to save the cost of a gearbox and to avoid the gearbox loss. For a direct-driven generator the speed of the power turbine is fixed to 3000- or 3600 rpm for 50- and 60 Hz respectively.

Secondly, the relatively high pressure ratio of 31.0 combined with the low temperature rise of 375 °C in the compressor results in a large variation in the volume flow between the compressor inlet and outlet. A single-shaft compressor design becomes, therefore, more difficult as a large variation in the volume flow hampers the matching between the front- and rear compressor stages, while maintaining a sufficiently high blade speed in the rear stages.

Commercial compressor designs with pressure ratios of 30 or above are only common in aero-derivatives, where this is achieved by twin-spool compressor configurations [4]. An exception to this is the gas turbine models GT24 and GT26, which achieve a PR of 35.4/35.0 in their 22-stage compressor [4]. For a twin-spool compressor configuration there is no need for this trade-off between high blade speed and the blade height in the rear compressor stages. That is because both can be achieved by positioning the high-pressure spool at a lower diameter to increase the blade height, and then compensate for the reduced blade speed with a higher shaft speed of the high-pressure spool. A twin-spool configuration would, therefore, facilitate the aerodynamic design, but it would also increase the complexity and cost of the machine. For an industrial gas turbine unit, such as the oxy-fuel gas turbine, it is preferred to have a single-shaft compressor design.

A single-shaft configuration with a shaft speed of 3000 rpm, which would be the obvious choose for a conventional CCPP with a gas turbine shaft power of about 100 MW or above [4], was also considered. (For a smaller conventional CCPP the preferred shaft configuration would still be a single-shaft gas turbine, but with a gearbox to allow for a higher shaft speed [4].) This shaft configuration was rejected because of the large change in the volume flow

throughout the compressor, which would result in too low blade velocities in the rear compressor stages if the blade height was to be maintained at an adequate level (the compressor design is discussed in more detail in Chapter 4). A single-shaft gas generator with a free power turbine was, therefore, chosen as the preferred shaft configuration for the gas turbine unit.

# 4 Compressor design

*This chapter describes the design process for the compressor, discusses some general design parameters and presents the final compressor design.*

*The subject was discussed in the following publications:*
**Publication IV:** *The Influence from the Working Medium on the Profile Loss in Compressor and Turbine Airfoils, GT2014-25069 [26]*
**Publication V:** *Aerodynamic Gas Turbine Design for an Oxy-fuel Combined Cycle, GT2015-42028* [23]

## 4.1 Scope of the compressor design

Designing conventional axial compressors is a well-explored and -documented engineering art, but when it comes to designing compressors for application in an oxy-fuel gas turbine the amount of information in the public domain is sparse, although some preliminary mid-span designs have been published [60, 37, 62]. A subset of this thesis was, therefore, to investigate and carry out a conceptual aerodynamic design of an axial compressor suitable for an oxy-fuel gas turbine application. This compressor design task was, through the conceptual design of the gas turbine unit (described in Chapter 3), narrowed down to focus on demonstrating the feasibility of achieving the compression with a single-shaft compressor design at a satisfyingly high efficiency. That was instead of the initially intended twin-spool compressor configuration as used in publication III [25]. In the following sections the aerodynamic design process for the single-shaft compressor is described and certain design parameters are addressed both generally and specifically exemplified with design figures from the final compressor design.

## 4.2 Compressor design process

The aerodynamic compressor design follows as a natural sequence after the conceptual design of the gas turbine units has determined the boundaries and specified the performance requirements for the compressor. The boundaries and performance requirements at the design point are summarized in Table 4.1.

The same fundamental physical laws govern the aerodynamic compressor design whether it is a conventional air-breathing compressor or a compressor design for an oxy-fuel application. The approach was, therefore, to treat the design in a similar manner as the design of a conventional compressor. Nevertheless, the different gas properties of the working medium and specific design requirements for the OCC influenced the design trade-off and determined what was achievable or not. Aerodynamically the conceptual compressor design can be divided into three steps: the 1D mid-span design, the 2D through-flow and the 3D steady-state analysis. The 1D mid-span and 2D through-flow calculations rely mainly on correlations for predicting

Table 4.1: Design boundaries and performance requirements for the compressor design

| Parameter | Unit | Value | | |
|---|---|---|---|---|
| Temperature in/out | [°C] | 63.5 | 438.5 | |
| Pressure in/out | [bar] | 1.013 | 31.42 | |
| Mass flow in/out | [kg/s] | 219.8 | 197.7/168.4 | |
| Bleed mass flows | [kg/s] | 8.35 | 13.85 | 29.3 |
| Bleed flow pressure | [bar] | 8.5 | 16.9 | 31.4 |

the losses and flow deviations. These correlations are based on dimensionless numbers and are kept simple to make them universal and with a short execution time. They have historically been derived for conventional engines and are, thus, based upon experimental cascade tests, test compressors and numerical analyses. For the compressor design for an oxy-fuel combined cycle, this entailed a risk of errors when extrapolating these correlations into the $CO_2$-rich working medium. Therefore, the utility of these correlations was tested by numerically investigating the difference in the profile loss and the flow deviation between air and the $CO_2$-rich working medium for a compressor cascade. The profile loss and flow deviation were compared with each other and with loss model correlations. The conclusions from this investigation was that the correlations are considered reliable for using for design calculations with a $CO_2$-rich working medium (see publication IV [26]).

Now back to the aerodynamic compressor design process, which started with a 1D mid-span calculation. The mid-span calculation set several typical compressor design parameters, such as for example the stage count, stage loading ($\psi$), stage flow coefficient ($\phi$), stage pressure ratio ($PR_{st.}$) and the shape of the gas path.

When the 1D mid-span design results had been determined, the next design step was to create a 2D model for the through-flow program. The through-flow program used was HT0300, which originates from Hearsey [43]. This program has been further developed at Siemens to include models for the losses and flow deviation that match the behaviour of our house-style compressor blade geometries and a model for span-wise mixing of the entropy generated along the endwalls. The 2D design was tuned until a flow field was attained throughout the compressor that fulfilled the requirements established by the 1D design and that had an appropriate radial distribution of the flow field and the stage parameters.

A strength with the 1D mid-span and 2D through-flow design- and analysis tools is the simplicity of controlling them and their short execution time. This enables a wide range of different designs to be investigated in a time-efficient manner. These two initial 1D and 2D design phases were given a considerable emphasis to ensure that correct design choices were made, so that the design satisfied both the intended compressor performance and the overall design requirements of the gas turbine unit. That is because it becomes much harder and far more time-consuming to change the design to any appreciable extent when the design has continued into the 3D design phase, without first going back to the 1D and/or 2D design tools again. The 1D and 2D design sets, beside for the design parameters stated above, also the wall hade angles, radial distribution etc., and roughly some 80% of the final design is set by the first 20% of the time that is spent in the 1D and 2D design phase.

The third design step was to generate the 3D blading, adapted for the 3D flow solver Multip, to fine-tune the design and validate the results. Multip is a steady-state 3D flow solver that was

originally developed by Denton at Cambridge University [30]. The program has been further developed at Siemens to, for example, be able to utilize a variable specific heat at constant pressure ($c_p$), which is of great importance for an oxy-fuel compressor design.

## 4.3 Design parameters

The main purpose of the axial compressor is to compress the working medium in an efficient and stable manner. The specific design to achieve this can differ quite significantly between different compressor designs, depending on the application and design philosophy. However, considering the broad overall picture, all compressor designs follow and fall within the same fairly tight design space. This section describes the working principle of a compressor through several design parameters, gives some guidance and presents the corresponding design parameters that were chosen for the oxy-fuel compressor. The fundamental flow physics and design methods are only covered broadly, as this section is not intended to be comprehensive on the design method. For further descriptions of the basic compressor design, the reader is referred to public literature of educational textbooks dealing with this subject, for example Cumpsty [21] and Wennerstrom [78]. Some basic understanding and guidelines concerning the aerodynamic compressor design that can be complementary were also given in the present author's licentiate thesis [22].

Before proceeding with describing some basic compressor design parameters it is appropriate to describe the nomenclature of a compressor cascade. A typical blade-to-blade cross section of a row is shown in Figure 4.1.

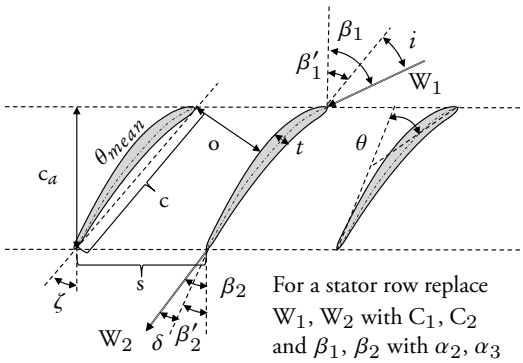


Figure 4.1: A blade-to-blade cross section of a compressor row.

| | Unit | Description |
|---|---|---|
| c | [m] | Chord |
| $C_2$, $W_1$ | [m/s] | Inlet flow |
| $C_3$, $W_2$ | [m/s] | Outlet flow |
| $c_a$ | [m] | Axial chord |
| o | [m] | Throat |
| s | [m] | Pitch |
| t | [m] | Maximum blade thickness |
| $\alpha_2$, $\beta_1$ | [°C] | Inlet flow angle |
| $\alpha_3$, $\beta_2$ | [°C] | Outlet flow angle |
| $\alpha'_2$, $\beta'_1$ | [°C] | Inlet metal angle |
| $\alpha'_3$, $\beta'_2$ | [°C] | Outlet metal angle |
| $\delta$ | [°C] | Deviation angle |
| $i$ | [°C] | Incidence angle |
| $\theta$ | [°C] | Camber angle |
| $\zeta$ | [°C] | Stagger angle |

Table 4.2: Compressor cascade nomenclature

A compressor stage consists of two rows of airfoils, first a rotating rotor row followed by a stationary stator row. The total stage work ($\Delta h_0$) is added in the rotor row, while the static pressure rise occurs in both the rotor and stator row. The static pressure rise is achieved by repeatedly in each row diffusing a part of the fluid's velocity component ($W_1$ or $C_2$) (dynamic pressure) into a static pressure rise. That is achieved by increasing the flow area, by turning the flow axial. Turning the flow axial in one coordinate system (e.g. the relative coordinate system for a rotor row) gets the fluid accelerated relative to the other coordinate system (e.g. the

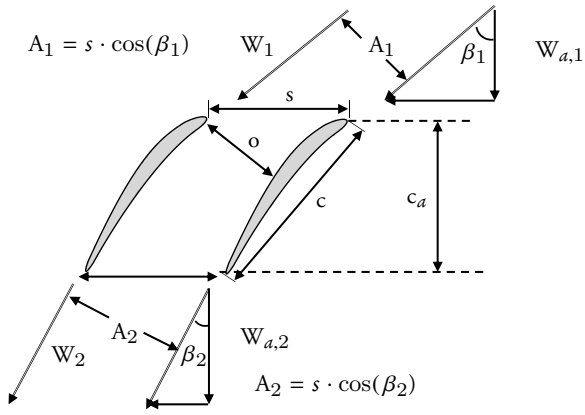


Figure 4.2: Diffusion of a part of the dynamic pressure into a static pressure rise, by turning the relative velocity ($W_1$) towards the axial direction and increase the flow area.

stationary coordinate system for a stator row) which enables the diffusion process to proceed continually in the subsequent row and stages. The flow turning from $\beta_1$ to $\beta_2$ is illustrated in Figure 4.2 for a rotor row in the relative coordinate system.

### 4.3.1 Dimensionless stage parameters and stage characteristic

It is common practice to establish some dimensionless stage parameters to describe the process, repeated in each row, in which a part of the dynamic pressure is diffused into a static pressure. These parameters describe the velocity triangles in each stage as dimensionless and enable the stage performance to be calculated. The main parameters are the stage load ($\psi$), flow coefficient ($\phi$) and stage reaction ($\Lambda$).

The degree of reaction in a stage is the ratio between the static enthalpy- or pressure increase in the rotor row and the total increase across the stage (Equation 4.1 and 4.2), hence it expresses the ratio of the flow diffusion between the rotor and stator. A low reaction means that the majority of the static pressure rise occurs in the stator row and the reverse for a high stage reaction. The stage load and flow coefficient are the most common design parameters, and these two parameters were mainly used to control the design. The degree of reaction was more the result of the design with respect to other design parameters, hence it was not used to control the design to any significant extent. The reaction was indeed supervised to ensure a positive static pressure rise over the entire span of the airfoil in each row.

**Enthalpy-based stage reaction ($\Lambda_h$)**

$$\Lambda_h = \left( \frac{h_{2,s} - h_{1,s}}{h_{3,s} - h_{1,s}} \right) \tag{4.1}$$

**Pressure-based stage reaction** $\left(\Lambda_p\right)$

$$\Lambda_p = \left(\frac{p_{2,s} - p_{1,s}}{p_{3,s} - p_{1,s}}\right) \tag{4.2}$$

The specific work input in a stage is the blade velocity ($U$) times the change in the tangential swirl component ($\Delta C_\theta$) according to Euler's equation (Equation 4.3) [78].

$$\Delta h_0 = \int c_p(T) \cdot dT = U_2 \cdot W_{\theta 2} - U_1 \cdot W_{\theta 1} \tag{4.3}$$

The stage load expresses the dimensionless work input normalized with the blade velocity square and can be expressed by Equation 4.4 if the blade speed $U_1$ and $U_2$ is constant, i.e. neglecting the radial change of the flow stream across the blade. The total stage pressure ratio is then given by Equation 4.5, where $\eta_s$ is the isentropic efficiency.

**Stage load** ($\psi$)

$$\psi = \frac{\Delta h_0}{U^2} = \frac{W_{\theta 2} - W_{\theta 1}}{U} \tag{4.4}$$

**Stage pressure ratio** ($PR_{st.}$)

$$PR = \frac{p_{03}}{p_{01}} = \left[1 + \eta_s \cdot \frac{\Delta T_{0\,st.}}{T_{01}}\right]^{\left(\frac{\gamma}{\gamma - 1}\right)} \tag{4.5}$$

The ratio between the axial velocity ($C_a$) and the blade speed ($U$) is frequently used and defined as the dimensionless flow coefficient ($\phi$) (Equation 4.6).

**Flow coefficient** ($\phi$)

$$\phi = \frac{C_a}{U} \tag{4.6}$$

It is justifiable to assume that the outlet flow angles ($\beta_2$, $\alpha_1$) from each row are virtually stable for a compressor stage that operates in its stable operation range, where the stage pressure ratio is well below its surge margin (SM). That is because the boundary layers are attached to the airfoil within this operation range and therefore the flow deviation ($\delta$) on the outlet flow angles ($\beta_2, \alpha_1$) is in principle constant. The stage load can then be expressed by Equation 4.7, which describes the relation between the stage load ($\psi$) and flow coefficient ($\phi$) for different flow angles ($\beta_2$, $\alpha_1$) [21]. Equation 4.7 is a linear equation where $[\tan(\alpha_1) - \tan(\beta_2)]$ determines the slope of the relations between the stage load and the flow coefficient.

$$\psi = 1 - \phi\,[\tan(\alpha_1) - \tan(\beta_2)] \tag{4.7}$$

An open stage design with a relatively high axial flow, hence low blade stagger and small flow angles ($\alpha_1$, $|\beta_2|$), is herein referred to as a "high-flow stage" (Figure 4.3b).

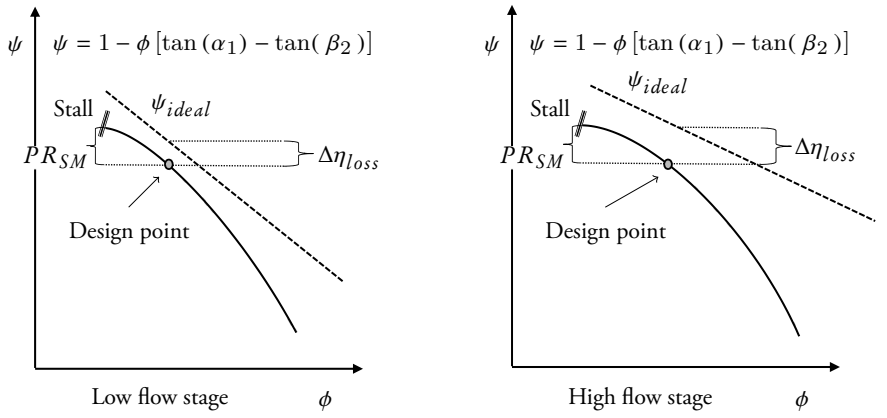


(a) A closed, low-flow stage, has a steeper stage characteristic.

(b) An open, high-flow stage, has a flatter stage characteristic.

Figure 4.3: Theoretical stage characteristics for a low- and a high-flow stage.

The reverse is true for a closed stage design with larger flow angles ($\alpha_1$, $|\beta_2|$) and higher blade stagger, which is herein refereed to as a "low-flow stage" (Figure 4.3a). A low-flow stage design has a steeper stage characteristic with a stronger stage load response to fluctuations in the flow coefficient. This more rapid stage load response has a stabilizing effect on the compressor stage matching.

A high-flow stage can (theoretically) produce a higher stage work than a low-flow stage, which is an advantage as it reduces the stage count and is thereby a drive towards high-flow stage designs. A (theoretical) drawback with high-flow stage designs is that they tend to have somewhat lower efficiency at the design point. The reason for this is that all stages must be designed with a certain pressure ratio stall margin ($PR_{SM}$) at the design point. If the stall margin is to be constant in both a high- and low-flow stage design, then the flow coefficient at the design point has to be increased more in a high-flow stage design than in a low-flow stage design, relative to the respective stage's stall limit. That is because of the flatter stage characteristic in a high-flow stage than in a low-flow stage design. This means that the difference between the ideal stage load ($\psi_{ideal}$) and the real stage load ($\psi$) is larger in a high-flow stage, which increases the efficiency loss ($\Delta\eta_{loss}$), as illustrated in Figure 4.3.

The reasoning above is around one specific radial span height (e.g. mid-span). When considering the full blade span, it turns out that the design space for the flow coefficient at the mid-span is quite limited. That is because of the three-dimensional nature of the flow and the large variation in blade speed ($U$) across the blade span. Satisfying the radial equilibrium, with an uniform work input across the span height, implies that the rotor hub section will have a high flow turning while the rotor tip section will have an almost flat blade profile. The large variation of the flow field (i.e. blade profile) over the span height is illustrated by the difference in the 2D blade-to-blade blade profiles for Rotor 1 at the hub-, mid-, and tip section in Figure 4.4a. It can be seen that the hub section has a low stagger and a quite large camber with an almost axial outlet angle, while the tip section has a higher stagger with a low camber. It can also be seen that the front of the tip section has a very flat profile initially, with its small

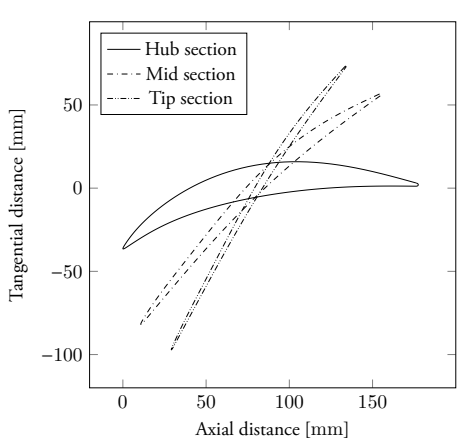


(a) The 2D cross sections for the hub-, mid-, and tip section.

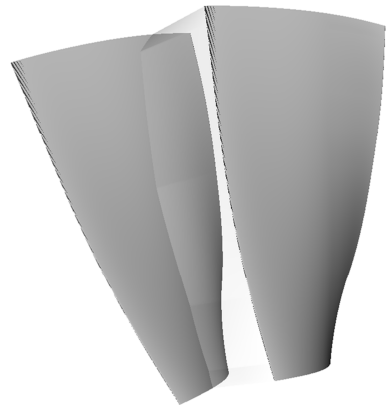

(b) 3D compressor rotor.

Figure 4.4: Compressor rotor 1.

camber towards the back. The reason for the straight profile at the front and the late camber is because of the shock wave that is situated in the front. The blade profile at the mid section is somewhere between the two.

The design space for the flow coefficient at the mid-section is therefore generally limited to about 0.45-0.70. Some recommended ranges for the flow coefficient given in literature are 0.50-0.70 [31], 0.3-0.9 [36], 0.5-0.75 [77] and around 0.5 [21] and for the mid-span stage load ($\psi$) to be 0.2-0.5 (typically 0.35) [36], 0.25-0.5 [77] and 0.3-0.5 [31].

The mid-span flow coefficients and the stage load for the OCC's compressor design are seen in Figure 4.5.

## 4.4 Design philosophy

*The key to all successful compressor design is achieving a sound balance between the many design parameters. That is no less true for the oxy-fuel compressor design, with its relatively high pressure ratio, large volume flow ratio and low speed of sound. The following section discusses and explain the motives for some of the design choices that were made for the oxy-fuel compressor.*

The shaft speed of the entire gas generator is to a large extent determined by the velocity triangles in the compressor's front stage. The interaction between the geometrical hub-to-tip ratio, axial Mach number, relative tip Mach number, shaft speed and stage work had, therefore, to be considered together. For the certain compressor inlet mass flow, set by the cycle design, the compressor design was striving toward a high shaft speed, while still avoiding a too high relative rotor tip Mach number ($Ma_{w,tip}$) or a too high axial Mach number ($Ma_a$). These design parameters are all interlinked with each other and a change in one influence in general the choice of several other parameters through either forcing or enabling the other to be

changed too. No complete conclusions can therefore be derived by considering the parameters separately, but let's nevertheless investigate the trend of how a variation of one parameter affects the design. That aim to attain a fundamental understanding of who each individual design parameter affect the overall compressor design, if the other design parameters are kept constant, as far as possible.

The hub-to-tip ratio ($r_{hub}/r_{tip}$) describes the radius ratio between the blade hub and blade tip. For a constant shaft speed, mass flow and axial Mach number, hence constant inlet area, the following occurs. Increasing the hub-to-tip ratio correspond to shifting the gas path towards a larger mean diameter and a reduced effective gas path height, i.e. shorter blades situated at a larger compressor diameter. For a constant shaft speed, this increases the average blade speed ($U$) and for a constant IGV swirl it also increases the relative tip Mach number. For the reverse the opposite is true, videlicet that a reduced radius ratio ($r_{hub}/r_{tip}$) results in a smaller overall compressor diameter with longer blades and lower blade velocities. For a certain stage load ($\psi$), this results in a reduced stage pressure ratio.

The axial inlet Mach number ($Ma_a$) affect the axial inlet flow path area and by increasing the axial Mach number is the axial gas path area and the compressor's mean diameter reduced. Increasing the axial Mach number also increases the stage work potential (i.e. high-flow stage) and, therefore, a fairly high axial Mach number is preferable. Increasing the axial Mach number too much risk, however, to choke the compressor at off-design operation. Too high axial Mach number also limits the potential for future upgrading of the compressor mass flow. It is recommended to keep the axial inlet Mach number $Ma_a$ below 0.65-0.70 in the front stage, at the design point. In literature, some recommended ranges for the axial Mach number throughout the compressor are 0.3-0.6 (typical 0.5) [36] and 0.4-0.6 [77]. These figures relate more to the stages in the compressor, and axial Mach number can be both higher in the front stage(s) and lower in the rear stage(s).

In reality, all modern axial compressors are designed to have the first stages transonic to increase the stage pressure ratio and enable a higher shaft speed. The relative tip Mach number ($Ma_{w,tip}$) can, to some extent, be, and is generally too, controlled by applying a current rotating swirl at the tip by an inlet guide vane (IGV) in front of rotor 1 and by variable guide vanes (VGV) in the following front stages.

The OCC compressor inlet was designed with a hub-to-tip ratio of 0.54, an axial inlet Mach number of 0.63 and a relative inlet tip Mach number of 1.29 and 1.11 for the first two rotor rows, while the third rotor was just below 1.00. In literature it is commonly recommended to keep the hub-to-tip ratio above 0.65 [77] and the relative tip Mach number below 1.3-1.4 [77, 36]. The total inlet flow area to rotor 1 is 1.07 $\mathrm{m}^2$ with an r.m.s. blade speed of 325 $\mathrm{m/s}$.

Considering the same design parameters at the compressor outlet resulted in a trade-off between keeping up the blade speed by increasing the mean radius and avoiding too short blade heights (i.e. avoiding too high hub-to-tip ratios). The axial Mach number was reduced in the rear stages to increase the axial flow area and, thereby, enable longer blades and a reduced hub-to-tip ratio. Reducing the axial Mach number also has a positive effect on the pressure loss in the compressor diffuser, but it should not be reduced too far as it also reduces the stage work capacity and the surge margin of the stage. For the OCC compressor design an axial outlet Mach number of 0.27 was used, despite this the hub-to-tip ratio was as high as 0.91, which corresponds to a stator height of 36 $\mathrm{mm}$. In literature it is commonly recommended to keep the hub-to-tip ratio below 0.92 at the outlet [77], and the exit Mach number below 0.35 (ideally <0.25) [77]. Concerning the mechanical stresses in the discs, also the blade rim and tip speed were recommended to be kept below 500 $\mathrm{m/s}$ at the blade tip and 350-

380 m/s at the blade hub (i.e disc rim) for titan discs. For nickel alloy discs, with titan blades it were recommended to stay below 400 m/s and 350-380 m/s at the blade tip, respective blade hub [77, 36, 21]. The compressor design and the chosen design parameters were verified through comparing the flow field at the compressor inlet by dimensionless parameters. By comparing these dimensionless parameters an improved understanding of the complexity and design challenges was obtained. The method was to compare the mass flow that a scaled compressor design would get if scaled to 3000 rpm ($m_{3000rpm}$) while keeping the inlet velocity triangle constant to the design. A parameters for the 3000 rpm mass flow can be derived, as in Equation 4.8, by combining the dimensionless speed with the dimensionless mass flow [23]. The corresponding 3000 rpm mass flow for the OCC compressor, corrected to standard air and ISO conditions, is 951 kg/s. This high figure reflects a high but feasible technical challenge with today's state-of-the-art technology. As a comparison such high 3000 rpm mass flows are commonly only seen for large conventional gas turbines (i.e. SGT6-8000H with 921 kg/s, Fr 7HA-02 with 995 kg/s) while medium-sized gas turbines with a power of less then 150 MW generally have a 3000 rpm mass flow below 700 kg/s, derived from data from Gas Turbine World [2].

$$m_{3000} = m_{Des} \cdot \left(\frac{N_{Des}}{N_{Ref}}\right)^2 \cdot \frac{p_{Ref}}{p_{Des}} \cdot \left(\frac{\gamma_{Ref}}{\gamma_{Des}}\right)^{\frac{3}{2}} \cdot \sqrt{\frac{T_{Ref} \cdot R_{Ref}}{T_{Des} \cdot R_{Des}}} \tag{4.8}$$

The stage load ($\psi$) and flow coefficient ($\phi$) were determined in the 1D mid-span design and the common design range are 0.3-0.45 for the stage load and 0.45-0.70 for the flow coefficient. The oxy-fuel compressor was designed within these ranges, as shown in Figure 4.5. The first two stages are transonic and were designed with higher stage loads (0.386/0.354) than the subsequent stages to allow for a reduced stage load in the subsequent stages. The design philosophy was to have the intermediate stages modestly loaded with a small and smooth decline trend of the stage load (from 0.349 to 0.335) and then unload the last three stages more steeply. The idea behind this is that the intermediate stages, which are less affected by off-design operation, can be designed for a higher stage load and/or more efficiently, as their required operation envelope is smaller. The last rear stages are those that are most affected by a rising total compressor pressure ratio and therefore tend to stall first and needs, thus, to have a wider operating range. Remember also that the axial Mach number in the last stage was reduced down to 0.27, in favour of an increased blade height, which has a negative effect on the surge margin. The stage loads of the last three stages were therefore reduced (0.328-0.308) to compensate for this through improving their surge margin and the operation envelope of the entire compressor.

The flow coefficient decreases from the inlet value of 0.61 in stage two down to the exit value of about 0.53. The first stage has a slightly lower flow coefficient (0.58) and two temporary reductions are also seen after stages 7 and 11 because of the compressor bleeds.

There is a strong incentive to increase the stage work to reduce the stage count, cost and weight of the compressor. Fundamentally the main physical limit for increasing the stage work is that the flow brakes down when the stage load increases too far and the diffusion gets too severe, which results in boundary layer separation. The stability of the boundary layer is affected by several parameters, which to a certain extent can be influenced by the design choices.

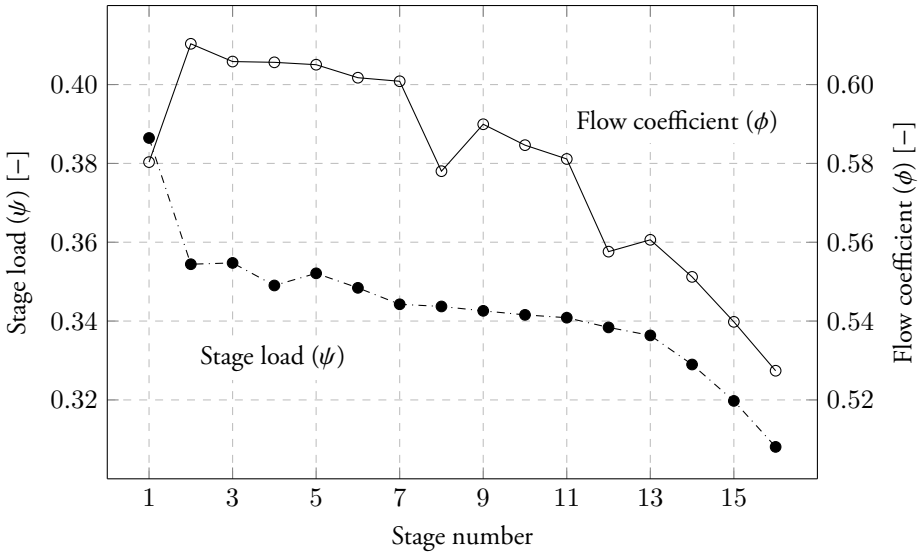


Figure 4.5: Stage parameters: the stage load ($\psi$) and the flow coefficient ($\phi$), at the mid-span section.

A key ability in the 1D and 2D design is predicting the diffusion limit to avoid separation. The deHaller coefficient [28], the Diffusion factor (DF) [51] and the Equivalent diffusion factor [51] are all example of traditional parameter for correlating the diffusion limit. They tend to be of different detail levels and correlate against somewhat different flow physics, but basically they are all approximate correlations. These parameters were more profound discussed in the present author's licentiate thesis [22].

The total stage work can be expressed by Equation 4.11 through combining Euler's equation (Equation 4.3) with the diffusion factor (Equation 4.10). This equation shows that the the work capacity is direct proportional to the solidity ($\sigma$), the blade speed, the relative inlet velocity, the diffusion factor and the deHaller coefficient.

**deHaller coefficient**

$$\text{deHaller coefficient} = \frac{W_2}{W_1} \text{ or } \frac{C_2}{C_3} \tag{4.9}$$

**Diffusion Factor**

$$DF = 1 - \frac{W_2}{W_1} + \frac{\Delta W_\theta}{2 \cdot \sigma \cdot W_1} \tag{4.10}$$

**Stage work**

$$\Delta h_0 = 2 \cdot \sigma \cdot U \cdot W_1 \cdot \left( DF - 1 + \frac{W_2}{W_1} \right) \tag{4.11}$$

The deHaller coefficient relates the velocity ratio between the inlet and the outlet of a row, without considering any geometrical parameters, such as blade curvature or solidity. That makes the correlation insensitive to variations in the airfoil design, but the deHaller coefficient is simple and, therefore, appropriate for the initial design. The deHaller coefficients for the OCC's compressor can be seen in Figure 4.6 for the mid-span of the rotor and stator rows, respectively. The traditional recommendation is to keep the velocity ratio above 0.70-0.72[i], which corresponds to diffusing about 0.51-0.44% of the dynamic pressure (incoming velocity) into a static pressure.

Figure 4.6 shows that the velocity ratio in the first rotor was 0.68, which is slightly outside the recommended range and might appear inappropriate, but it is not considered an issue. Firstly, a large amount of the pressure rise in the first rotor is achieved by a shock wave. The deHaller coefficient was derived for subsonic airfoils, and not transonic designs, and therefore the pressure rise from the shock wave is not accounted for. Secondly, the deHaller coefficient was derived assuming well-designed blade profiles, but still of a somewhat dated blade style. For a modern controlled diffusion airfoil the limit of 0.70 can certainly be slightly undercut.

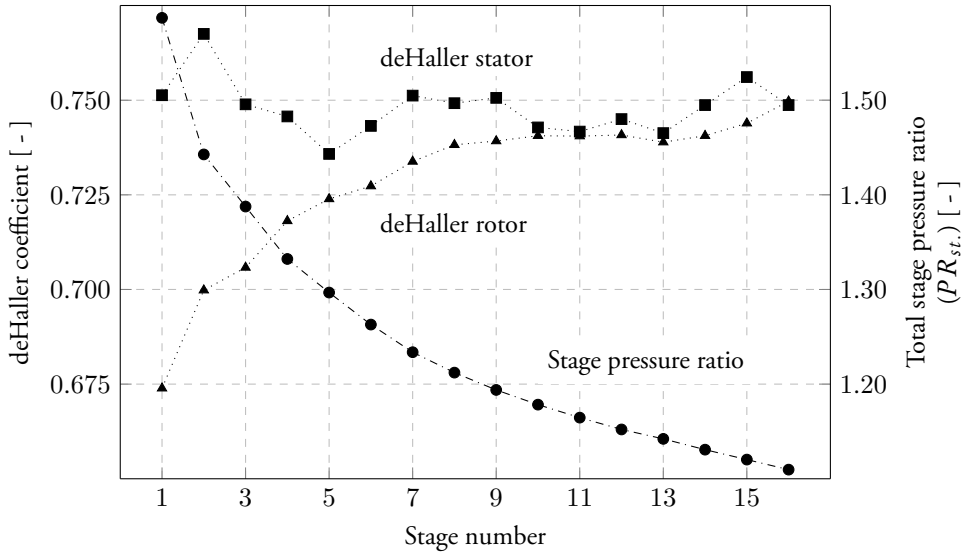


Figure 4.6: Total stage pressure ratio ($PR_{st.}$) and the deHaller coefficient for the rotors and stators, at the mid-span section.

The hub section is the part of the airfoil span that is most prone to stalling because of the lower blade velocity, relative to the rest of the span. The design philosophy used to improve the flow field at the hub sections, hence surge margin, was to increase the axial flow velocity ($C_a$) towards the hub section by opening up the stator hub section axial ($\alpha_3$). This was mainly applied to the front stages, which, because of their length, have a larger span vice variation in the blade velocity. By increasing the axial velocity in the highly cambered hub section the flow turning angles can be somewhat reduced for a certain stage work (a constant swirl), as discussed in section 4.4. The span vice variation in the axial velocity field ($C_a\,(r)$) can be seen in Figures 4.7 and 4.8.

[i] deHaller's original recommendation was $\geq 0.75$.

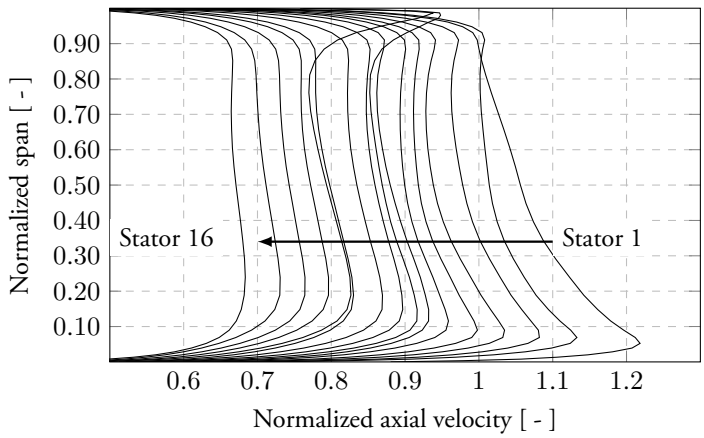


Figure 4.7: Normalized axial velocity component out of the stator rows over the normalized span height.

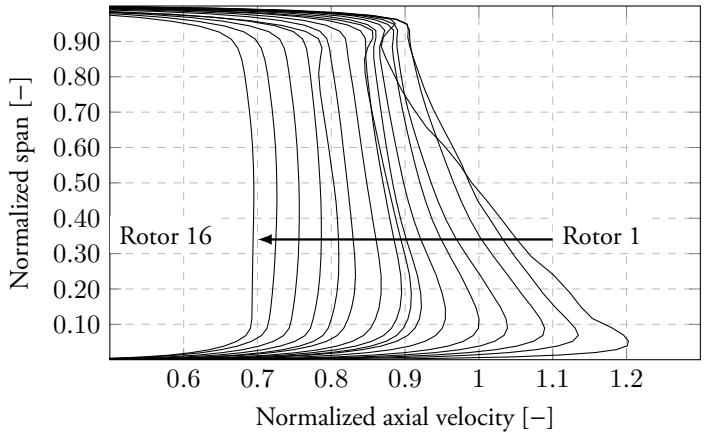


Figure 4.8: Normalized axial velocity component out of the rotor rows over the normalized span height.

Table 4.3: Design parameters for the compressor

| Parameter | Unit | Value | |
|---|---|---|---|
| Shaft speed | [rpm] | 5,700 | |
| Hub-to-tip ratio in/out | [–] | 0.54 | 0.91 |
| Hub- and tip radius R1 in/EGV out | [m] | 0.355/0.661 | 0.380/0.416 |
| Axial Mach number in/out | [–] | 0.63 | 0.27 |

The compressor design was evaluated by plotting the stage load ($\psi$), the flow coefficient ($\phi$), the deHaller coefficient and the throttle number ($\tau$) ($\frac{\psi}{\phi^2}$) as seen in Figure 4.9. The throttle number is the ratio between the stage load and the square of the flow coefficient (Equation 4.12), defined as the inverse of Traupel's "Drosselzahl" ($\frac{\phi^2}{\psi}$) [74]. The throttle number can be interpreted as the slope of the stage characteristic (stage work relative to the flow coefficient) for the compressor stage and is a complement to the discussion about the stage characteristic in section 4.3.1 and Equation 4.7. A high throttle number means that the stage load ($\psi$) is high relative to the flow coefficient ($\phi$). That implies a low-flow stage with a steeper derivative of the work characteristic, compared to a stage with a lower throttle number (a high-flow stage). Most conventional compressor stages tend to fall within a quite limited design space regarding stage load, flow coefficient and with a throttle number of around unity, as indicated by the shaded box in Figure 4.9. It turned out that the compressor stages for the oxy-fuel compressor also falls within this design space, as indicated by the crosses that represents the oxy-fuel compressor stage in Figure 4.9.

The lines of constant deHaller coefficients in Figure 4.9 are derived assuming a repeated stage design with constant axial velocity and a degree of reaction of 0.60 according to Equation 4.13, as proposed by Aungier [9]. This assumption is obviously not fully met by the actual OCC's compressor design, which for example, has a varying axial velocity, flow angles and degree of reaction throughout the stages. The degree of reaction for the stages at the hub-, mid, and tip section is shown in Figure 4.10. Accordingly the design do not coincides fully with the indicated lines of constant deHaller coefficients, but these are not that far off and give a good indication of the design.

$$\text{Throttle number} = \frac{\psi}{\phi^2} \tag{4.12}$$

$$\frac{W_2}{W_1} = \sqrt{\frac{\phi^2 + (\psi/2 - \Lambda_h)^2}{\phi^2 + (\psi/2 + \Lambda_h)^2}} \tag{4.13}$$

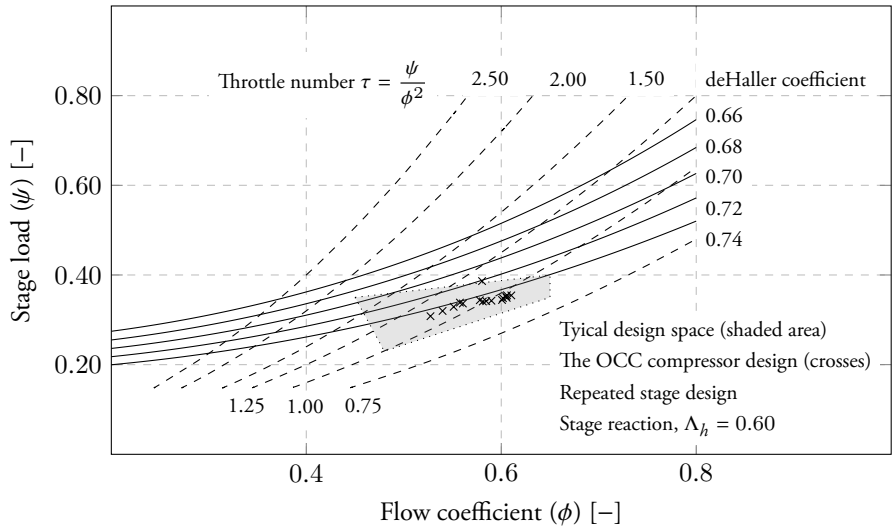


Figure 4.9: Rotor loading for the compressor at the mid-span. *(The indicated lines of constant deHaller coefficients assumes a repeated stage design with constant axial velocity and a stage reaction of 0.60.)*

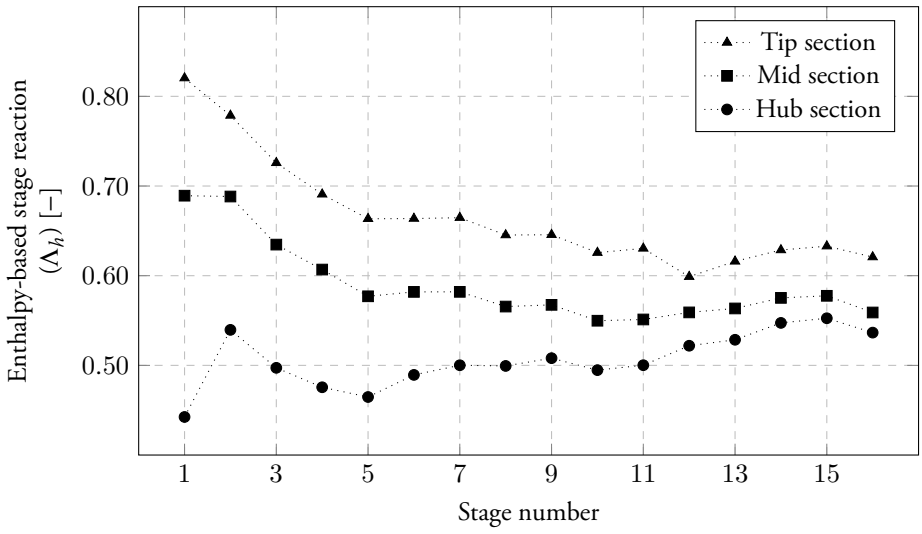


Figure 4.10: Enthalpy-based stage reaction for the compressor, at the hub-, mid-, and tip section.

# 5 Turbine design

*This chapter describes the design process for the turbines, discusses some general design parameters and presents the final turbine design.*

*The subject was discussed in the following publications:*
**Publication IV:** *The Influence from the Working Medium on the Profile Loss in Compressor and Turbine Airfoils, GT2014-25069 [26]*
**Pupblication VI:** *Aerodynamic Turbine Design for an Oxy-fuel Combined Cycle, GT2016-56439 [24]*

## 5.1 Scope of the turbine design

Designing conventional turbines is a well-established engineering art, but just as for the compressor design, the information on how to conduct a turbine design for application in an oxy-fuel gas turbine unit is sparse in the public domain. Therefore, a subset of this thesis aimed at investigating and carry out an aerodynamic design of the turbines for the oxy-fuel gas turbine unit. The intention was to investigate whether the turbine design for an oxy-fuel gas turbine unit, operating with a $CO_2$-rich working medium, is feasible with today's state-of-the-art technology and through using conventional design methods. The conceptual aerodynamic design was carried out through a typical conceptual design loop, which included the 1D mid-span, 2D through-flow and 3D steady-state design and analysis calculations. The design covered both the compressor turbine and the power turbine. Analogously to the compressor, the 1D mid-span and 2D through-flow tools rely on correlations for predicting the aerodynamic losses and the flow deviation. These correlations were derived for conventional turbines, as pointed out in the previous Chapter 4, section 4.2. The utilization of these conventional air-based correlation models for the oxy-fuel turbine design raised, therefore, the question of whether they could still be used or not. Their applicability for turbines, operating with the $CO_2$-rich working medium present in an oxy-fuel turbine, was investigated in publication IV [26], where it was concluded that they could be used for the design of (at least) lightly- to modestly loaded airfoils. The reason for the caution for more heavily loaded airfoils is uncertainty over the limit of the boundary layer separation, a limit that was not specifically investigated in publication IV [26].

The previous design work performed through the cycle simulation, the broad overall gas turbine unit design and the compressor design formed the basis of specifying the boundary conditions and the design criteria to be met by the compressor turbine and power turbine. The main design criteria are summarized in Table 5.1 and 5.2. The gas state between the two turbines was determined through an iterative process and is, strictly speaking, neither boundary conditions nor a design criteria.

Table 5.1: Boundary condition and design criteria for the compressor turbine

| Parameter | Unit | Value | |
|---|---|---|---|
| Shaft power | [MW] | 86.5 | |
| Temperature in/out | [°C] | 1,340 | 930 |
| Pressure in/out | [bar] | 31.1 | 7.2 |
| Mass flow in/out | [kg/s] | 193.1 | 236.1 |
| Cooling flow | [kg/s] | 43.0 | |
| Shaft speed | [rpm] | 5,700 | |

Table 5.2: Boundary condition and design criteria for the power turbine

| Parameter | Unit | Value | |
|---|---|---|---|
| Temperature in/out | [°C] | 930 | 612 |
| Pressure in/out | [bar] | 7.2 | 1.11 |
| Mass flow in/out | [kg/s] | 236.2 | 244.4 |
| Cooling flow | [kg/s] | 8.2 | |
| Shaft speed | [rpm] | 3,000 | |

## 5.2 Turbine design process

The conceptual aerodynamic turbine design phase, following after the broad overall gas turbine unit's design parameters were specified, can virtually be divided into a number of sub-steps. The main steps are the 1D mid-span design, the 2D through-flow design, the 2D blade-to-blade profiling, the stacking of the airfoils and the 3D steady-state analysis. The mechanical integrity of the turbines' discs', blade's foot attachment and the blades was also considered briefly through 1D steady-state calculations. This was to reduce the risk that the conceptual aerodynamic design had an unrealistic mechanical design, which could not be fulfilled without redesigning the aerodynamics.

The 1D mid-span design was the first step in the turbines design process. This design determined essentially all the typical broad design parameters, such as, for example, the stage count, the blade solidity, the stage loading, the flow coefficient, the stage reaction, the stage pressure ratio, the total turbine pressure ratio and the basic geometrical shape of the turbines' gas path. The 1D design is essential for the achievable performance of the final turbine design, hence its success. The 1D design was, therefore, given a considerable emphasis to ensure that the design satisfied the requirements. For the mid-span design of the turbines Siemens in-house programs Mac II was used for the design and Mac I for the analysis, which are both included in the turbine design's shell program T-Design.

The 1D design also provided additional data regarding the turbine geometry and the gas state throughout the turbines. This enabled the turbine cooling prediction from the process simulation, described in section 2.3.2, to be revised more accurately.

The proceeding design step was to carry out the 2D through-flow design to obtain a radial span-wise variation of the flow field that met the intended 1D design. Special attention was given to the flow field near the end-walls to ensure positive hub reactions (i.e. an accelerating

flow) and to avoid too high exit Mach numbers at any span height of the airfoils. Blade stacking design features, such as, twisting, leaning, sweeping and end-wall profiling can be used too to improve the reaction, the losses and the exit Mach number, particularly in the hub- and tip sections. The blade stacking and end-wall profiling generate these beneficial effects through altering the radial pressure gradient by creating a favourable radial flow-field curvature. Stacking strategies can also be used to unload the end-walls and, thereby, reduce the end-wall losses. The fundamental effects from various stacking strategies were discussed by Havakechian and Denton [41, 42].

Inverse twisting was applied to the stator vanes, through opening up the stator outlet flow angle ($\alpha_2$) more axially towards the tip section. The benefit of opening up the stator tip is that it creates a more uniform radial variation of the relative inlet flow angle ($\beta_2(r)$) to the succeeding rotor. This results in the rotor blade getting less twisted over its span height. Inverse twisting also allows for a higher flow acceleration in the rotor tip section, which has the positive effect of increasing the blade turning at the rotor tip section. Avoiding highly twisted blades is especially important for cooled blades, as it enhances the casting of the blade's cooling system. For the 2D through-flow design the in-house program Beta2d was used for the design and for the 2D analysis Beta2a was used. These two through-flow programs are also included in the turbine design's shell program T-Design. The stacking strategy was applied in the 2D design, but because of its largely 3D nature, its effect was captured first in the 3D analysis.

The 3D flow solver Multall was used to fine-tune the design and validate the results. Multall is a steady-state 3D flow solver that was originally developed by Denton at Whittle Lab in Cambridge [29]. The program version used for this study has been further developed at Siemens and particularly important for this study of an OCC was the adaptation to enable utilization of a variable specific heat ($c_p$).

The 3D airfoils (stator and rotor) were generated by stacking several 2D blade profile cross-sections above each other. Three to five 2D blade-to-blade cross-sections were used to form each airfoil, by interpolating the blade profile geometry in between these sections (Figure 5.1, 5.4). That is, for most cases, a sufficient number of cross-sections for the conceptual design. The final design of the airfoils will, however, benefit from a denser radial cross-section profiling to enable a more precise shape, not least for more novel 3D-shaped blades. The profiling of these 2D cross-sections was done with the 2D profiling and 3D stacking tool Cato, which is a Siemens in-house program too. The 2D blade profiles were designed with Bézier curves to allow for a smooth curvature and analysed two-dimensionally with a MISES flow solver [33]. The boundary conditions for the MISES analysis of each cross-section were obtained from the 2D through-flow analysis. The airfoils were designed to have a light- to modest blade loading with a Mach number distribution (e.g. front-, mid-, aft-loaded) that is consistent with traditional turbine designs. A significant emphasis was devoted to obtaining a smooth, positive and continuous blade curvature on the suction side. The mid-span cross-section and the blade curvature of rotor 2 in the compressor turbine and rotor 3 in the power turbines can be seen in Figure 5.2 and 5.5. In Figure 5.3 and 5.6 the mid-span cross-sections and the aft-loaded velocity profiles for the same two blades can be seen.

In general, the 3D design do not improve the turbine design substantially (especially not during the concept phase), but it risks to degrading the performance if not carried out carefully. The 3D calculations are instead mainly used to analyse the flow field to verify the design against the predictions from the correlation-based 1D and 2D tools. Minor design improvements can nevertheless be achieved by fine-tuning the blade design in the 3D design. Performance improvements from the 3D effects that airfoil stacking features such as twisting,

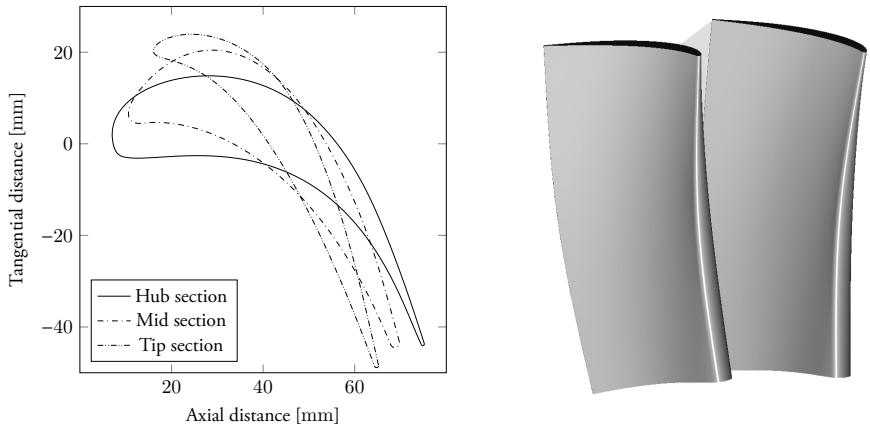


(a) The 2D cross-sections for the hub-, mid- and tip section.

(b) The 3D blade profile generated by stacking the 2D cross-sections.

Figure 5.1: Rotor 2 in the compressor turbine.

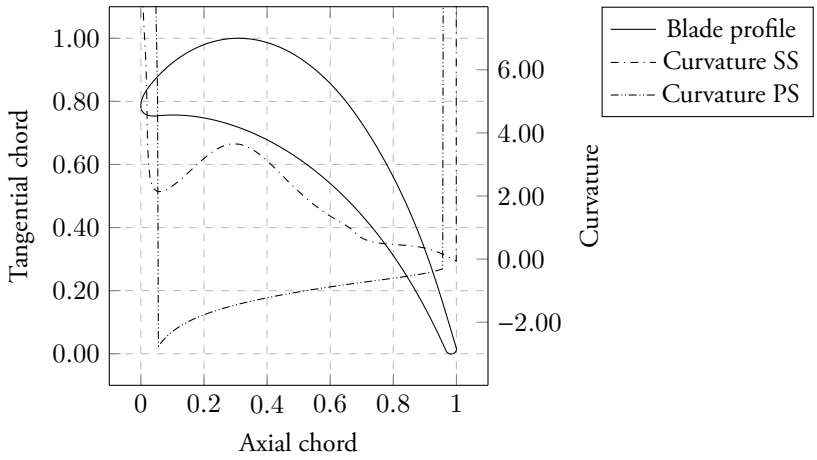


Figure 5.2: Mid-span cross-section and blade curvature for rotor 2, in the compressor turbine.

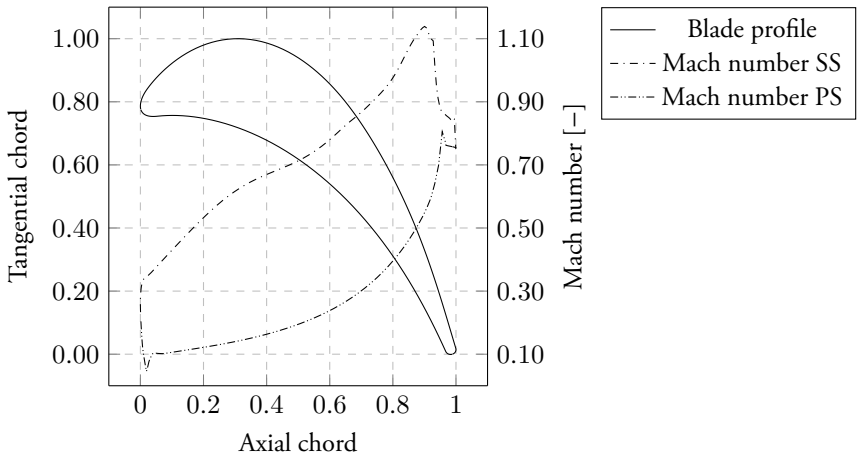


Figure 5.3: Mid-span cross-section and Mach number for rotor 2, in the compressor turbine.

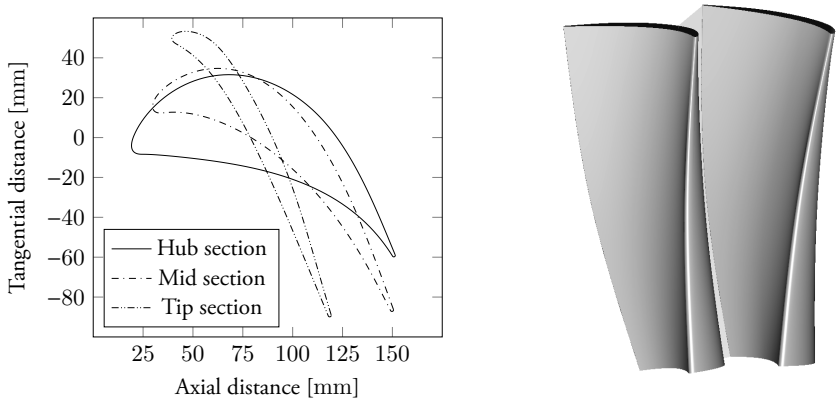


(a) The 2D cross-sections for the hub-, mid- and tip section.

(b) The 3D blade profile generated by stacking the 2D cross-sections.

Figure 5.4: Rotor 3 in the power turbine.

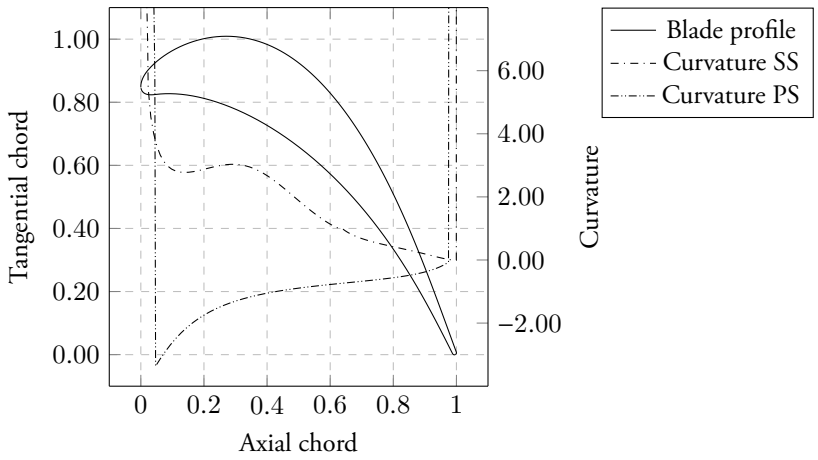


Figure 5.5: Mid-span cross-section and blade curvature.

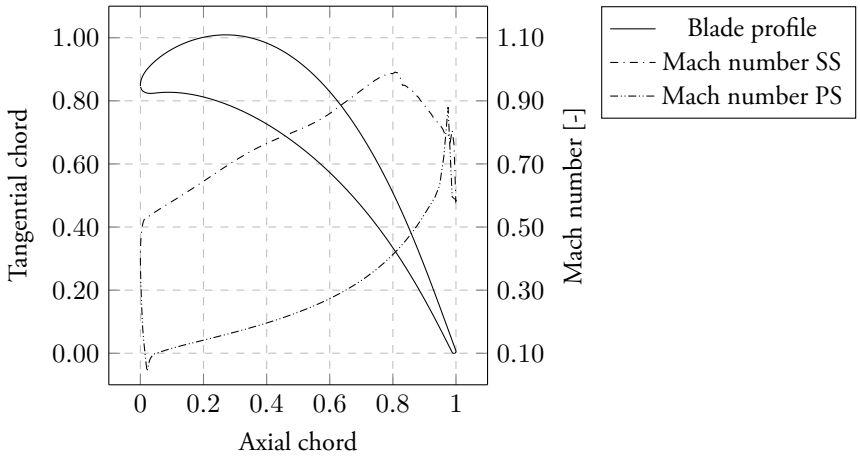


Figure 5.6: Mid-span cross-section and Mach number.

leaning, sweeping and end-wall profiling have on the flow field are also more accurately captured in the 3D analysis, than in the 1D and 2D design and analysis tool previously used.

**Turbine intermediate duct:**

*This section discusses the matching between the consumed compressor work and the provided compressor turbine work, and the effects it has on the temperature between the compressor turbine and power turbine. This temperature is important as it influences the design decision of whether to design with or without any considerable turbine intermediate duct.*

When designing a twin-shaft gas turbine unit, the temperature of the working medium out of the compressor turbine (CT) and into the power turbine (PT) is a crucial parameter that needs to be considered carefully. The reason for this is that the temperature of the working medium tends to exceed the temperature limit for conventional uncooled PT material (for an acceptable lifetime). The tendency to exceed the temperature limit is indeed present with today's drive towards both increasingly higher combustion outlet temperatures (COT) and higher exhaust gas temperature (EGT) into the HRSG. Exceeding this temperature limit results in some stage(s) in the PT needing to be cooled. This complicates the design of the PT and the design of the secondary-air-system (SAS), which then needs to feed a second turbine with a cooling medium. For a certain COT and cooling technology this is, however, inevitably something that the turbine design has to cope with.

Another consequence that an elevated temperature after the CT has, is that any turbine intermediate duct (TID) between the CT and PT would also need to be cooled. This increases the cooling medium consumption and decreases the total gas turbine efficiency. Future engine upgrades through increasing the COT will also be aggravated by a cooled TID. A TID is, however, a design choice and not an inevitable must. The need for a TID can be avoided by designing the CT and PT with similar diameter, hence allowing them to fit each other geometrically and, thereby, keeping the TID small or preferably completely avoided. The problem with an elevated gas temperature after the CT stated above is an issue for both conventional twin-shaft gas turbine units and the oxy-fuel gas turbine design, but the tendency with an elevated temperature is more severe for the oxy-fuel gas turbine design. The reason for this is mainly the considerably larger variation in specific heat with respect to temperature ($c_p(T)$) for the $CO_2$-rich working medium than for the flue gas in a conventional gas turbine unit. The variation in specific heat is shown in Figure 2.3 in section 2.2 for air and $CO_2$. In that figure it can be seen that in the temperature range from 600 °C to 1,400 °C, where the turbines operate, the specific heat for $CO_2$ is about 7-10% higher than for air. This results, for a certain specific turbine work, in the temperature reduction being less in the CT in an oxy-fuel gas turbine then in a conventional gas turbine unit. In the lower temperature range from about 0 °C to 500 °C where the compressor operates the ratio between the specific heat of the two gases is different to that in the high-temperature region. At this temperature range the difference in specific heat between the two gases is less, and in the lowest temperature span from 0 °C to about 260 °C (depending on the pressure) the specific heat for $CO_2$ is less than for air. Above this temperature of about 260 °C the specific heat for $CO_2$ is higher than that for air, and the two curves diverge from each other.

It has previously been shown that the temperature rise in the oxy-fuel compressor is about 375 °C (from 63 °C to 438 °C) for a pressure ratio of 31.0. The temperature rise in a conventional gas turbine compressor, designed for a combined cycle, is typically about 420-430 °C

(e.g. from 15 °C to 435-445 °C) for a typical pressure ratio of 20-21. The temperature rise in the oxy-fuel compressor is, hence, less than in a conventional gas turbine compressor. The combined effect of both the temperature rise being less and the working medium having a lower average specific heat results in the specific compressor work being less in the oxy-fuel compressor than in a conventional gas turbine compressor. The lower compressor work and the higher specific turbine work, for a certain temperature reduction in the oxy-fuel gas turbine, results in turn in the temperature after the CT being higher in the oxy-fuel gas turbine, than the temperature in a conventional gas turbine unit, for the same COT and EGT. This effect is enhanced slightly further by the external feed stream of oxygen that is compressed externally and does not increase the gas turbine unit's compressor work, but contributes to the work output in the CT.

The total effect from these contributions is that the temperature after the CT in an oxy-fuel gas turbine is elevated by about 25-55 °C compared to a conventional gas turbine unit for the same COT and EGT. The magnitude of the temperature difference depends on several design parameters, such as the COT, gas turbine unit's PR, component efficiencies, SAS consumption and the steam content in the OCC's working medium. The trend is that the temperature difference between an oxy-fuel gas turbine and a conventional gas turbine unit declines with rising COT (1,000-1,500 °C). That is because, if the COT is increased, it also calls for a higher PR to keep the EGT into the HRSG constant at a temperature suitable for the steam cycle. Increasing the PR means that the difference in the specific compressor work between the oxy-fuel and a conventional gas turbine unit decreases, as the specific heat for $CO_2$ is higher than that for air above 260 °C. The temperature level after the CT is, therefore, important to consider for the oxy-fuel gas turbine design as it tends to be higher than in a comparable conventional gas turbine unit.

The process simulations of the overall oxy-fuel combined cycle showed that the gas temperature after the CT was about 930 °C at the design point. This temperature is above the acceptable metal temperature of traditional PT blade material and implied that the first PT stage needs to be cooled. It also implies that any TID would need to be cooled, which, as stated above, results in a performance penalty and impedes further engine upgrades by increasing the COT. A turbine design aimed at minimizing, or completely avoiding the TID was therefore investigated.

Designing the turbines (i.e CT and PT) to fit each other geometrically to avoid a TID was a trade-off between suitable blade speeds in both turbines, a proper exhaust flow area from the PT and avoiding severe hade angles along the end-walls. The shaft speed of the CT was set by the compressor design, as it is the first stage in the compressor that is most sensitive to the matching of the flow field and compressor geometry. This design trade-off between the compressor geometry and shaft speed was discussed in section 4.4 and publication V [23]. The final design choice was a gas generator shaft speed of 5,700 rpm at the design point. The maximum acceptable blade speed sets virtually an upper limit to the mean blade diameter of the CT. The CT inlet can neither be allocated at too large a diameter as the blade height then tend to be too short for an adequate aerodynamic design (i.e. low hub-to-tip ratio).

The PT generator was determined to be direct driven, which for a two-pole 50 Hz generator determines that the shaft speed is 3,000 rpm and the corresponding figure for a two-pole 60 Hz generator is 3,600 rpm. The aerodynamic design focused on the 3,000 rpm case, since it is most challenging from an aerodynamic point of view. That is because if the aerodynamic design is satisfied at 3,000 rpm then the aerodynamic design for 3,600 rpm is most likely to be achieved by redesigning the airfoils.

Positioning the turbines (CT and PT) at similar diameters, to keep the TID short, implied a compromise for the PT design, as the blade speed in the PT inevitably becomes lower than the aerodynamic optimum. This results in additional stages in the PT, if the stage load is to be kept at the same level. This design trade-off was not obvious and an alternative design was to increase the blade speed by positioning the PT at a larger diameter and, thereby, reduce the required stage count down to three, from the present four-stages. A three-stage design would result in a large cooled TID to accommodate the radial shift of the gas path and therefore the three-stage PT design was rejected. Adding an extra PT stage, instead of a TID, is justified by the fact that the duct would have to be cooled, whilst an additional PT stage (to a first order) does not increases the total turbine cooling consumption. A possible approach might, however, be to examine the possibility of using other more temperature resistant materials. Another aspect is that a four-stage PT will have yet another disc gap to seal, but a second order effect is that the disc rim for all stages will be situated at a smaller mean diameter, which reduces the sealing medium consumption in each. A schematic view of the turbines and the turbine intermediate duct can seen in Figure 5.7.

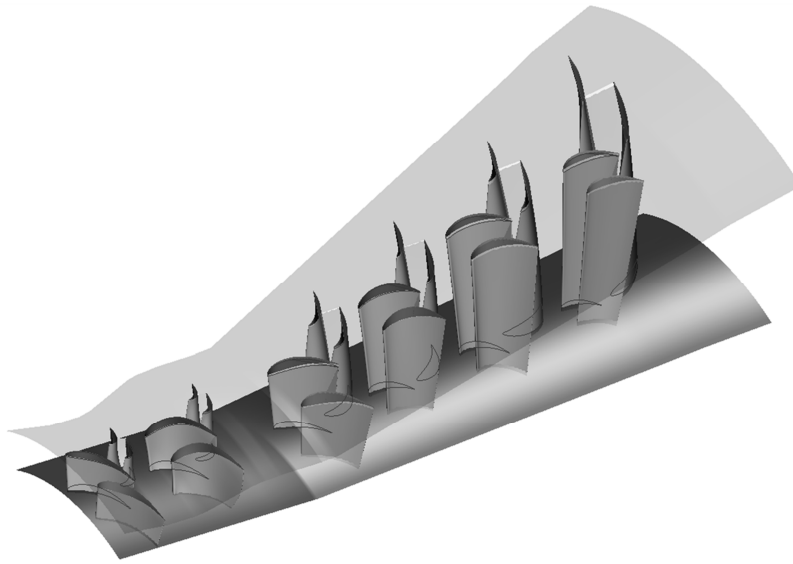

Figure 5.7: Schematic view of the turbines and the turbine intermediate duct.

Because more energy is available for the PT in the oxy-fuel gas turbine, as a result of the lower specific compressor work, another outcome is that the OCC gas turbine has a higher specific power, than a conventional gas turbine. The increase in specific power is dependent on the same design parameters as discussed above, but as indicative figures the specific power is increased by about 40% for a combustor outlet temperature of 1,000 °C and by about 20% for a combustor outlet temperature of 1,500 °C. The specific power for the OCC's gas turbine is 410 kW/kg.

In the initial concept phase of the OCC, performed in the process simulation tool, the turbine cooling was predicted through a modified version of the common m-STAR model (Equations 2.5, 2.6, 2.7 and 2.8) and the disc sealing consumption by a traditional correlation (Equation 2.4), both described in section 2.3.2. These predictions were revised to better reflect the design through still using the same equations, but based on the geometry and gas temperatures from the turbines' 1D mid-span design. When proceeding with the design from the concept phase into the final turbine design this method has to be further refined through more detailed heat transfer analyses and cooling schemes of the individual rows for a more precise prediction. But for the concept phase, this method is considered to be a balanced trade-off between accuracy and time consumption.

## 5.3 Design parameters

*In the present author's licentiate thesis the fundamental working principle of a turbine was discussed, several basic turbine stage parameters described and some general recommendations given. This is not repeated in this doctoral thesis, instead the reader is referred to the author's licentiate thesis [22] or other textbooks such as "Axial and Radial Turbines" by H Moustapha et.al. [54], for a more fundamental and general understanding. This section is intended to merely repeat the parameter definitions, provide the corresponding design values used for the OCC's turbine design and when appropriate comment on these too.*

Before proceeding with the design parameters it is appropriate to repeat the geometrical parameters of a turbine airfoil as shown in Figure 5.8 and Table 5.3 [22]. This figure illustrates a rotor row, but it is analogous with a stator row with the exception that the indices 1 and 2 are used for the in- and outlet instead of 2 and 3. A typical flow field through a turbine stage and its corresponding velocity triangles can be seen in Figure 5.9a and 5.9b [22].

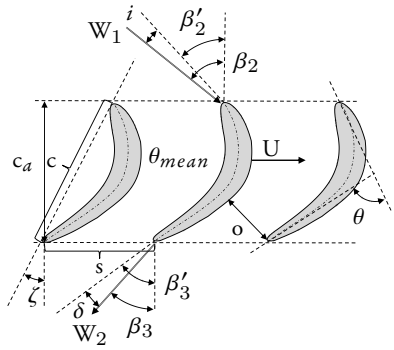


Figure 5.8: Flow- and geometrical parameters in a turbine cascade.

| | Unit | Parameter |
|---|---|---|
| c | [m] | Chord |
| $c_a$ | [m] | Axial chord |
| $W_1$ | [m/s] | Inlet flow |
| $W_2$ | [m/s] | Outlet flow |
| $\beta$ | [°C] | Flow angle |
| $\beta'$ | [°C] | Blade metal angle |
| $\zeta$ | [°C] | Blade stagger |
| $\theta$ | [°C] | Blade camber |
| $\theta_{mean}$ | [°C] | Mean blade camber line |
| s | [mm] | Pitch |
| $i$ | [°C] | Incidence angle |
| $\delta$ | [°C] | Deviation |
| o | [mm] | Throat |

Table 5.3: Turbine nomenclature

It is common to express the axial velocity ($C_a$) as dimensionless by the flow coefficient ($\phi$) by dividing ($C_a$) by the blade velocity ($U$) (Equation 5.1). In the same manner the stage work

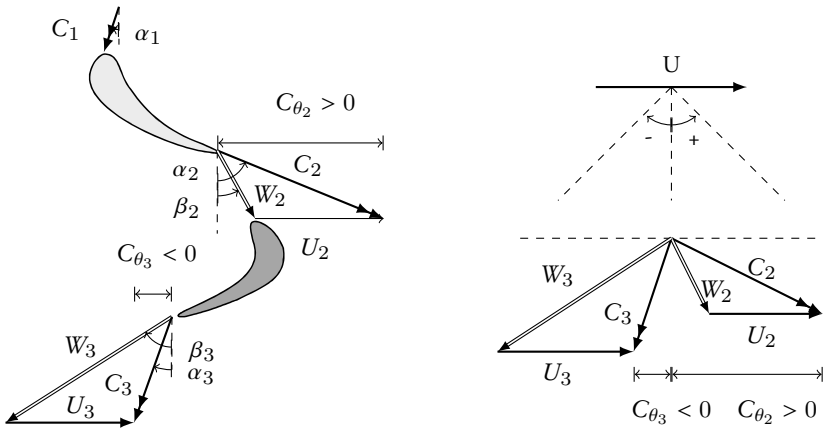


(a) Flow field. (b) Velocity triangles.

Figure 5.9: Flow field and velocity triangles in a turbine row (reaction stage).

can be expressed as dimensionless by the stage load ($\psi$), by dividing the total enthalpy drop ($\Delta h_0$) by the blade velocity square ($U^2$) (Equation 5.2). If the axial velocity ($C_a$) is constant throughout the row and there is no radial shift of the streamline, the stage load can also be expressed by the flow coefficient ($\phi$) and the blade angles ($\beta_2, \beta_3$) (Equation 5.3), the same way as in a compressor stage (Equation 4.7).

Some recommended figures for the stage load and flow coefficient in the literature is to keep the flow coefficient within the range of 0.20-0.50 and the stage load within the range of 1.0-2.50 [31].

**Flow coefficient ($\phi$)**

$$\phi = \frac{C_a}{U} \tag{5.1}$$

**Stage load ($\psi$)**

$$\psi = \frac{\Delta h_0}{U^2} = \frac{U\,(C_{\theta 2} - C_{\theta 3})}{U^2} \tag{5.2}$$

$$\psi = \frac{\Delta h_0}{U^2} = \frac{C_a\,[\tan(\beta_2) - \tan(\beta_3)]}{U} = \phi\,[\tan(\beta_2) - \tan(\beta_3)] \tag{5.3}$$

When examining the turbine designs for the OCC it can be seen that the CT was designed with the relatively conservative stage loads of 1.32 for stage 1 and 1.21 for stages 2 (Table 5.4). One reason for this low stage work was the variation in specific heat of the working fluid and the external feed stream of oxygen, which both result in a slightly lower compressor work than for a conventional gas turbine, as discussed previously in section 5.2. An alternative design

with a single-stage CT was also considered, but a single-stage design would require significant compromises as both the stage load and blade velocity would have to be increased too far, which would result in both too skewed velocity triangles and high blade- and disc stresses [24]. A single-stage CT design was, therefore, not considered preferable over the chosen two-stage design.

The stage loads for the four-staged PT were 1.52, 1.57, 1.44 and 1.08 for the respective stages. The corresponding exit Mach number from the stator and rotor in the respective stages were 0.59/0.65, 0.66/0.73, 0.73/0.80 and 0.75/0.76 as shown in Table 5.5. Both the stage loads and exit Mach numbers are quite low and, if necessary, they could have been higher without causing any problems. A stage load of about 1.7-1.9 and an exit Mach number of around 0.90-0.95 are not expected to cause severe problems. A three-stage PT was therefore also investigated, but there were some issues with a three-stage turbine design that made this option unfavourable. Firstly, the stage load for the last stage in the PT cannot deviate significantly from 1.0-1.1 if the flow field is to remain uniform and axial into the diffuser, which is crucial for a high diffuser recovery and, thereby, total performance. Hence, if the blade velocity remains constant for the last stage (i.e. constant mean diameter), the stage work ($\Delta h_0$) in the last stage is also virtually constant. That implies that to enable a three-stage PT design the stage work currently done in the first three-stages must be extracted in just two-stages. The stage loads for these two stages were then too high for a satisfying performance level. A second alternative was to also increase the blade speed, by increasing the mean blade diameter for all stages in the PT. This would require a large TID which, as discussed previously in section 5.2, was not desirable. Under these conditions a three-stage PT design was therefore not considered preferable over the chosen four-stage PT design [24].

**Enthalpy-based stage reaction ($\Lambda_h$)**

$$\Lambda_h = \frac{h_{2,s} - h_{3,s}}{h_{1,s} - h_{3,s}} \tag{5.4}$$

The degree of reaction of a turbine stage represents the ratio between the static enthalpy- or static pressure drop in the rotor and the total drop across the entire stage and the enthalpy-based reaction is defined by Equation 5.4. The mid-span reaction is normally around 0.5 [77], as that gives an uniform distribution of the work between the stator and rotor in a stage. For cooled stages, it can be beneficial to reduce the reaction slightly towards 0.4-0.45 to reduce the relative gas temperature in the rotor, and values as low as 0.3 have been suggested [77]. It is more important, however, to ensure that the reaction at the hub section remains positive all the time because a negative hub reaction means a diffusive flow with a risk of flow separation. It is recommended to keep the hub reaction above 0.2 [77]. The enthalpy-based reactions at the hub- and tip section for the CT and PT are given in Table 5.4 and 5.5. It can be seen that the hub reactions are well above 0.2 for all stages and that the lowest reaction is in the last long PT stage, which has a hub reaction of 0.34 at the design. The r.m.s. blade speed (U) is also seen in Table 5.4 and 5.5, typical recommended values are to keep the discs' rim speed below 400 m/s in the CT and 350 m/s in the PT [77].

The aerodynamic blade load for the airfoils (stator and rotor) can be assessed by the Zweifel coefficient ($Zw$) [83] (Equation 5.5). The aerodynamic load depends on the stage load and the axial solidity ($\sigma_a$), which expresses the ratio between the axial blade chord ($c_a$) and its pitch ($s$). The Zweifel coefficient is typically in the range of 0.8-1.1 [31], but it can be beneficial to increase it slightly above unity to reduce the cooled airfoil area through a lower solidity.

Table 5.4: Stage parameters for the compressor turbine

| Parameter | Unit | Stage 1 | Stage 2 |
|---|---|---|---|
| Blade velocity | [m/s] | 394 | 411 |
| Pressure ratio s-s/ t-t | [–] | 2.06/1.98 | 2.25/2.13 |
| Stage loading ($\psi$) | [–] | 1.32 | 1.21 |
| Flow coefficient ($\phi$) | [–] | 0.38 | 0.41 |
| Reaction hub/ tip ($\Lambda_h$) | [–] | 0.53/0.57 | 0.44/0.52 |
| Absolute exit flow angle | [°] | - | 11.2 |
| Isentropic exit Mach number Stator/ Rotor | [–] | 0.74/0.87 | 0.85/0.87 |
| Zweifel coefficient (Zw) Stator/ Rotor | [–] | 0.52/0.65 | 0.67/0.61 |

Table 5.5: Stage parameters for the power turbine

| Parameter | Unit | Stage 1 | Stage 2 | Stage 3 | Stage 4 |
|---|---|---|---|---|---|
| Blade velocity | [m/s] | 234 | 256 | 286 | 307 |
| Pressure ratio s-s/t-t | [–] | 1.48/1.41 | 1.65/1.57 | 1.86/1.74 | 1.82/1.70 |
| Stage loading ($\psi$) | [–] | 1.52 | 1.57 | 1.44 | 1.08 |
| Flow coefficient ($\phi$) | [–] | 0.59 | 0.52 | 0.53 | 0.56 |
| Reaction hub/tip ($\Lambda_h$) | [–] | 0.45/0.54 | 0.47/0.55 | 0.45/0.56 | 0.34/0.54 |
| Absolute exit flow angle | [°C] | - | - | - | 4.9 |
| Isentropic exit Mach number Stator/Rotor | [–] | 0.59/0.65 | 0.66/0.73 | 0.73/0.80 | 0.75/0.76 |
| Zweifel coefficient (Zw) Stator/Rotor | [–] | 1.19/0.93 | 0.92/0.90 | 0.87/0.85 | 0.89/0.91 |

As can be seen in Table 5.4, the Zweifel coefficient for the compressor turbine is less than what is traditionally recommended, which corresponds to a larger wet turbine area to cool. The reason for this is the quite low stage work in combination with the fact that the solidity cannot be reduced too low while maintaining a suitable number of airfoils and aspect ratio (AR). The blade counts in the CT were 31, 61, 37 and 72, and the aspect ratio and solidity can be seen in Figure 5.10. The Zweifel coefficients for the turbines are given in Table 5.4 and 5.5.

**Zweifel coefficient** ($Zw$)

$$Zw = \frac{2 \cdot s \cdot \rho_{out} \cdot V_{a,out} \cdot (V_{\theta,in} - V_{\theta,out})}{c_a \cdot [1 + (H_{in}/H_{out})] \cdot (p_{0,out} - p_{out})} \text{, Note [i]} \tag{5.5}$$

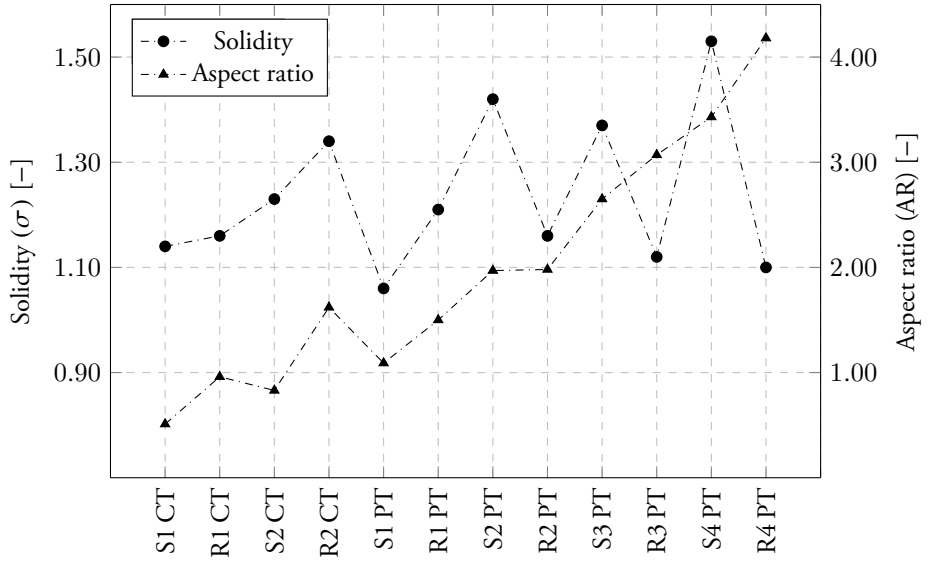


Figure 5.10: The solidity and the aspect ratio for the turbines.

The "true" solidity ($\sigma = c/s$) and the aspect ratio ($AR = h/s$) are plotted in Figure 5.10 for each row in the CT and PT, respectively. The solidity is within a range from 1.0 to 1.55 for both turbines, which is within the range of conventional turbine designs. The aspect ratio starts at about 0.8 in the first stator in the CT and increases up to about 4.2 for the last rotor in the PT. That is also within the range to expect for a conventional turbine design.

[i] $H_{in}/H_{out}$ is the ratio between the stream tube height at the inlet and outlet.

# 6 Concluding remarks

*The doctoral thesis and the six publications are summarized in this chapter along with the key conclusions, which answer the objective questions.*

The main objective of this doctoral thesis was to bring the oxy-fuel combined cycle to the next technical readiness level by investigate and extend the research of its thermodynamic cycle design and the conceptual aerodynamic design of the gas turbine unit's turbomachinery. The work has identified, analysed and proposed a thermodynamic cycle design of an OCC, through carry out a process simulation. Based on the design requirements set by the cycle design, was a suitable shaft configuration for the gas turbine unit proposed. The proposed gas turbine unit was a single-shaft gas generator, with a free power turbine.

For this gas turbine unit, conceptual aerodynamic designs were carried out for the compressor, the compressor turbine and the power turbine. The design loop covered the 1D mid-span, the 2D through-flow design and the 3D steady-state analysis of both the compressor and the two turbines. It was concluded that the conceptual aerodynamic design loop for both compressors and turbines can be performed with conventional design tools, if these are adapted to the gas properties for the $CO_2$-rich working medium. No major issues were identified in either the process simulation of the OCC, or in any of the more detailed aerodynamic compressor and turbine designs for the gas turbine unit.

## 6.1 The oxy-fuel combined cycle

A major difference in the cycle design of the OCC and its embedded gas turbine unit is the call for a higher PR to achieve, for a certain COT, a suitable EGT into the HRSG. That is a result of the different gas properties for the $CO_2$-rich working medium in the OCC. Another difference is that the design and performance of the steam cycle is improved by the different variation in the specific heat of the $CO_2$-rich working medium, than for a conventional flue gas. That is because, compared to a conventional CCPP, there is more energy available at the high temperatures in the HRSG and less at the low temperatures in the OCC, which enhances the energy utilization and thereby reduces the need for additional steam pressure levels.

## 6.2 Compressor design for the gas turbine

The high pressure ratio required in the oxy-fuel combined cycle and the modest temperature rise in the compressor is a challenge for the compressor design, as it results in a large variation in the volume flow throughout the compressor. This large change in volume flow between the compressor inlet and its outlet makes it more difficult to achieve a high pressure ratio in a single-shaft compressor design. That is because the rear stages get a low blade speed as a result of the need to maintain the blade height at a reasonable level for efficiency reasons, which

forces the design of the rear stages towards a lower mean diameter than at the compressor inlet. It was concluded that reducing the overall gas turbine unit's pressure ratio below the OCC's efficiency optimum, to facilitate a single-shaft compressor design instead of a twin-spool compressor design, was a sensible trade-off. After this reduction of the pressure ratio, down to 31.0, it was shown that the aerodynamic compressor design was feasible to carry out as a single-shaft compressor, and by using today's state-of-the-art technology. The final compressor design was a single-shaft 16-stage compressor, with a design mass flow of 219.8 kg/s, a shaft speed of 5,700 rpm and a pressure ratio of 31.0. The calculated performance figures achieved a satisfying isentropic efficiency ($\eta_s$) of 90.1%, a polytropic efficiency ($\eta_p$) of 92.8% and a surge margin of 25.5%.

## 6.3 Turbine design for the gas turbine

The aerodynamic turbine design and analyses made through the 1D mid-span, 2D through-flow, and steady-state 3D analysis showed that the turbines design are feasible with today's state-of-the-art technology, by using conventional design methods while remaining within our design expertise. Because of the different variation in the specific heat, with respect to temperature for the $CO_2$-rich working medium, the gas temperature after the CT is higher in the oxy-fuel gas turbine unit, than in a conventional gas turbine unit with similar COT and EGT. Because of this elevated gas temperature it is not desirable to have a TID, as the duct would need to be cooled. The CT and PT were, therefore, designed to match each other geometrically without any TID. The final design was a two-stage CT and a four-stage PT, with a calculated isentropic total-to-total efficiency of 86.7% for the CT and 92.6% for the PT.

## 6.4 Overall

The oxy-fuel combined cycle was calculated to have a overall net efficiency of 48.2%, which includes the energy cost for the $CO_2$ compression and the external $O_2$ production. The expected net efficiency for a commercial OCC is in the range of 47- 50%, which is some 7- 12% points less than for a conventional CCPP of similar size. The main additional efficiency penalty, compared to a conventional CCPP, originates from the $O_2$ production in the ASU. Therefore, this efficiency gap of 7- 12% can be reduced further if any of the more novel and less energy-demanding ASU technologies make it to the market in the near future.

# 7 Summary of papers

## 7.1 Conceptual Design of a Mid-sized Semi-closed Oxy-fuel Combustion Combined Cycle

This paper presents a study of a semi-closed oxy-fuel combustion combined cycle (SCOC-CC) with a net power output with a size of 100 MW. The heat and mass balance calculations were conducted in the commercial program IPSEpro, which was linked with NIST-REFPROP to enable the use of real gas data necessary at the high pressures present in the SCOC-CC.

The gas turbine's turbomachinery equipment was modelled with in-house mean-line programs from Lund University and Chalmers University. The mean-line programs for the turbine design (LUAX-T) and compressor design incorporate features as stage loading, loss modelling, cooling and some geometric features to generate more accurate results. A total gas turbine pressure ratio of 39 was chosen to match the combustion outlet temperature (COT) of 1,400 °C.

A single-shaft gas turbine configuration was the chosen shaft configuration for the design. One of the main issues identified was the gas turbine exit Mach number, which should preferably be kept below 0.60 and axial for the diffuser design, thereby requiring a lightly loaded last turbine stage.

The required cooling medium flow was calculated to be 26.2%, which is comparable to a conventional gas turbine. The compression was carried out in a 18-stage compressor and the expansion in a four-stage turbine.

The conceptual design of the SCOC-CC process has a net efficiency of 47%. One conclusion was that a twin-shaft gas turbine design would be beneficial from an aerodynamic perspective, however the advantages of a twin-shaft design must be weighed against retaining the inherent simplicity and low cost of a single-shaft design.

The present author's contribution to this paper was of a consultative nature through contributing expertise regarding the design of conventional gas turbines and combined cycle power plants. The knowledge of how to carry out the design of conventional gas turbines and power plants is key to enabling the design of more novel designs as required for the SCOC-CC. E. Thorbergsson and T. Gronstedt carried out the compressor design and wrote this section of the paper, M. Sammak and M. Genrup carried out the turbine design and simulation, K. Jonshagen developed advanced components for the cycle design in Ipse-Pro and M. Thern assisted in developing the method for calculating with real gas data properties.

## 7.2 Optimization of an Oxyfuel Combined Cycle Regarding Performance and Complexity Level

As there is no oxy-fuel combined cycle in commercial operation yet, it is of major importance to establish and motivate a design of a competitive OCC that does not include any unconventional features, beyond what is state-of-the-art in gas turbine technology today, as any unconventional features could challenge the feasibility of bringing the OCC concept to the market in a reasonable time. To find and propose a preferred cycle design that would be competitive, was the effect on the OCC from a few different cycle parameters investigated in the publication.

The investigated design parameters were, the temperature of the recirculated working medium, the gas turbine pressure ratio, the compressor outlet temperature (COT) and, hence, the temperature into the HRSG and its effect on the thermodynamic design of the HRSG and steam cycle. The OCC was modelled in an advanced heat and mass balance program, with stage-level capabilities. For the gas turbine unit a cooling model was used, which kept the metal temperature of all cooled turbine stages constant, while seeking the optimum pressure ratio.

The working medium in an OCC, which consist of mainly $CO_2$ and some $H_2O$, has a significantly lower isentropic coefficient than the flue gas in a conventional gas turbine, hence the OCC requires a higher pressure ratio. However, a high gas turbine pressure ratio increases the complexity of the machine, which must be weighed against the gain in efficiency.

This trade-off was considered and an OCC design was proposed, with a combustor outlet temperature of 1,340 °C and a pressure ratio of 34. This pressure ratio is somewhat lower than the optimum, from an cycle efficiency point of view. However, the reduced pressure ratio significantly eases the complexity of the compressor design. This somewhat lower gas turbine pressure ratio also makes more energy available for the bottoming cycle. For the proposed cycle, 38% of the power output is produced in the steam cycle, which is higher than for the conventional combined cycle where typically a third of the power is produced in the bottoming cycle.

The recirculated flue gas was cooled to 60 °C. Further cooling would remove more moisture which is positive, but it also rejects more heat from the cycle, which has a negative impact on the cycle efficiency.

As the specific heat for the flue gas in the OCC behaves differently compared to a conventional combined cycle, is there more energy available at the high temperatures while there is less energy at low temperatures in the HRSG. This results in that an OCC achieves an enhanced heat recovery, compared to the conventional combined cycle.

The present author's contribution to this publication was through setting up the investigation and designing the oxy-fuel combined cycle in the process simulation tool, Krawal Modular. The external gas turbine model, which enabled the influence from the different design parameters on the cycle design to be take into account, e.g. the turbine cooling medium consumption, was also built by the present author. The same applies to the execution of the parameter study on the oxy-fuel combined cycle's topping cycle, which formed the basis for determining the final cycle design. K. Jonshagen investigated the influences on the HRSG and steam cycle design further. The present author and K. Jonshagen analysed the results together and wrote the paper under supervision from M. Sjoedin and M. Genrup.

## 7.3 Concept for a Combustion System in Oxyfuel Gas Turbine Combined Cycles

Two alternative SCOC-CCs with different $H_2O$ content, due to different conditions for condensation of water, in the recirculated working medium ($CO_2/H_2O$) have been investigated and benchmarked against each other. The SCOC-CC alternative with the lower moisture content showed the highest thermodynamic potential and was selected for further study. The cycle was optimized in an advanced in-house heat- and mass balance program (Krawal Modular) and this optimized cycle formed the basis for a design study of the combustion process.

A conceptual combustion system was developed, where three different combustor feed streams were to be controlled independently: the natural gas fuel, the oxidizer consisting mainly of oxygen plus some impurities, and the recirculated $CO_2$-rich working medium. A key issue was how to maintain high combustion efficiency over the entire load range while using as little oxidizer as possible, and with emissions (NOx, CO, UHC) within given constraints. Other important challenges were related to combustion stability, heat transfer and cooling, and material integrity, all of which are indeed affected when changing the working medium. The combustor concept was evaluated both through a simplified approach using laminar flame speed and flame temperature of an air case as a basis and by a more refined reactor network analysis using the Chemkin software package. The results indicate that the working medium share going to the burner should be in the range 0.5– 0.6, with the rest being used for dilution downstream of the primary flame zone. A schematic design of the OCC combustor with swirl stabilizers and a cylindrical combustion chamber was provided.

The present author and M. Sjoedein performed the process simulations of the oxy-fuel combined cycle. The present author also investigated several different shaft configurations for the gas turbine unit, through performing preliminary designs of gas turbine units suitable for an oxy-fuel combined cycle. M. Siljan performed the HMOC (High Moisture Oxyfuel Cycle) simulations and M. Siljan, M. Sjoedein and the present author together wrote the section in the paper describing the design and analysis of the cycles. J. Janczewski, Ø. Langørgen, M. Seljeskog and M. Ditaranto carried out the combustion analysis and design and wrote this section of the paper. S G. Sundkvist and M. Bysveen were project managers of OXYGT, and coordinated and supervised the writing of the paper.

## 7.4 The Influence from the Working Medium on the Profile Loss in Compressor and Turbine Airfoils

This paper focused on numerically investigating how the $CO_2$-rich working medium in an oxy-fuel combined cycle affects the aerodynamic loss in the turbomachinery design. This is important to investigate as it is current practice today to design turbomachinery using 1-D and 2-D flow tools, which primarily rely on loss models derived for air engines through tests, experiments and numerical calculations. Another aspect that was considered was how to assess the influence on the total profile loss in a turbomachine conducting the same total work ($m \cdot \Delta h_0$), with either air or $CO_2$ as the working medium.

The study was conducted on typical compressor and turbine airfoils using a steady-state Navier-Stokes 3D flow solver. This type of solver can resolve the boundary layer (y+ of about unity) instead off relying upon a boundary layer equation, thereby eliminating the latter as a source of error. The results were compared with the predicted profile loss from loss correlations derived for conventional gas turbine applications, aimed at investigating their applicability for $CO_2$.

The hypothesis was that the profile loss (for a fixed cascade geometry) depended on the viscosity, and that changes in the viscosity would affect the profile loss. This trend was observed, for example, when changing the working medium from air to $CO_2$, as the profile loss coefficient (Yp) for the compressor was reduced by about 25% and for the turbine by 6%. The finding regarding the wet area was that it would increase by about 20% for $CO_2$, compared to air.

The observed difference in profile loss (Yp) was relatively small at the design point and, thus, it is the author's opinion that loss correlations derived for air are also considered safe to use for the design point calculations when the working medium is $CO_2$. However, there is a certain risk involved that air-based loss models are not capable of predicting the behaviour over the full operating range, as the boundary layers risk behaving in a different manner. The finding that the profile loss for $CO_2$ was somewhat less than for air, must be put in relation to the increase in total wet area of some 20% for the whole compressor/turbine, which counteracts the gain.

The present author designed the 3D airfoils used for the investigation for both the compressor and the turbine. The 3D airfoils were formed by stacking several carefully designed 2D blade profile cross-sections. The present author also meshed, pre-processed, performed and post-processed the 3D calculation in CFX and its associated programs. The same applies to the design of the methodology for the investigation, the analysis of the results and the writing of the paper. M. Genrup and M. Thern supervised the present author during the investigation and the writing of the paper.

## 7.5 Aerodynamic Gas Turbine Compressor Design for an Oxy-fuel Combined Cycle

This publication investigated the aerodynamic compressor design for a gas turbine unit operating in an oxy-fuel combined cycle. The key difference in this cycle is the working medium, which mainly consists of $CO_2$ (80-95 -wt.%), $H_2O$ (5-15 -wt.%) and a few percentage points of enriched $N_2$ and Ar. This $CO_2$-rich working medium has significantly different gas properties compared to air, which is the working medium in a conventional gas turbine unit. The difference affects the design requirements on the compressor and the gas state throughout the compressor. For example, a pressure ratio of 31.0 was required, while the speed of sound at the compressor inlet was 10-17% less than for air.

The design loop for the conceptual aerodynamic compressor design covered the 1D mid-span, 2D through-flow and steady-state 3D calculations. The work demonstrated the feasibility of achieving the compression in a single-spool compressor design with today's state-of-the-art technology.

The final design was a single-shaft 16-stage compressor, with a design mass flow of 219.8 kg/s, a shaft speed of 5,700 rpm and a pressure ratio of 31.0. The calculated performance figures achieved a satisfactory efficiency level of 90.1% isentropic ($\eta_s$) and 92.8% polytropic ($\eta_p$), while maintaining a surge margin of 25.5%.

The present author designed the methodology for the investigation. The entire conceptual design loop for the compressor, covering the 1D mid-span, the 2D through-flow design and the steady-state 3D analysis, was carried out by the present author, who also analysed the results and drew conclusions through the writing of the paper. M. Genrup supervised the present author during the investigation and the writing of the paper.

## 7.6 Aerodynamic Turbine Design for an Oxy-fuel Combined Cycle

This publication investigated the conceptual aerodynamic design of the turbines for a gas turbine units operating in an oxy-fuel combined cycle. The key difference in this cycle is the $CO_2$-rich working medium, which mainly consists of $CO_2$ (80-95 -wt.%) and $H_2O$ (5-15 -wt.%) with a few percentage points of enriched $N_2$ and Ar. The difference in the gas properties for this $CO_2$-rich working medium compared to conventional flue gases affects, among other things, both the operation and design of the gas turbine unit's turbines. The conceptual aerodynamic turbine design for operation with this $CO_2$-rich working fluid was investigated through a typical turbine aero-design loop, which covered the 1D mid-span, 2D through-flow and 3D blade profiling designs and the steady-state 3D validation. The design was carried out through the use of conventional design methods and design criteria, in order to investigate whether any significant departures from conventional turbine design methods were required.

The survey revealed some minor deviations in design considerations, yet it showed that the turbine design is feasible with today's state-of-the-art technology, using conventional design practices and methods.

The turbine design was a two-stage compressor turbine and a four-stage power turbine, without any substantial turbine intermediate duct. That was because of the elevated gas temperature after the compressor turbine. The isentropic total-to-total efficiency ($\eta_{s_{t-t}}$) for the compressor turbine and the power turbine was calculated to 86.7% and 92.6%, respectively.

The present author designed the set-up of the study. The entire design of both the compressor turbine and the power turbine was carried out by the present author. The conceptual turbine design loop covered the 1D mid-span, the 2D through-flow and the steady-state 3D analysis of both turbines. The same applies to the analysis of the results, drawing of conclusions and to the writing of the paper. M. Genrup supervised the present author during the investigation and the writing of the paper.

# Bibliography


[1] Surface temperature analysis. `http://data.giss.nasa.gov/gistemp/abstemp.html`. "Last accessed March 2016".

[2] *Gas Turbine World 2014 performance specs 30th Edition*, vol. 44. General Electric Company, 2014.

[3] Adoption of the Paris Agreement, Durban Platform for Enhanced Action (decision 1/cp.17) adoption of a protocol, another legal instrument, or an agreed outcome with legal force under the Convention applicable to all parties. Tech. rep., 2015.

[4] *Gas Turbine World 2015 performance specs 31st Edition*, vol. 45. General Electric Company, 2015.

[5] Key world energy statistics 2015. Tech. rep., International Energy Agency (IEA), 2015.

[6] Global CCS Institute. `http://www.globalccsinstitute.com/projects/large-scale-ccs-projects`, 2016. "Last accessed January 2016".

[7] Allis, R., Chidsey, T., Gwynn, W., Morgan, C., White, S., Adams, M., and Moore, J. Natural $CO_2$ reservoirs on the Colorado Plateau and southern Rocky Mountains: Candidates for $CO_2$ sequestration. In *Proceedings of the First National Conference on Carbon Sequestration*, pp. 14--17.

[8] Amann, J.-M., Kanniche, M., and Bouallou, C. Natural gas combined cycle power plant modified into an $O_2/CO_2$ cycle for $CO_2$ capture. *Energy Conversion and Management 50*, 3 (2009), 510--521.

[9] Aungier, R. H. *Axial-flow compressors: a strategy for aerodynamic design and analysis 2003*. New York ASME Press, 2003.

[10] Barry, B. The aerodynamic penalties associated with turbine blade cooling. *Von Karman Inst. for Fluid Dyn. Turbine Blade Cooling 36 p(SEE N 79-18979 10-07)* (1976).

[11] Bayley, F. J., and Owen, J. The fluid dynamics of a shrouded disk system with a radial outflow of coolant. *Journal of Engineering for Gas Turbines and Power 92*, 3 (1970), 335--341.

[12] Birol, F. World energy outlook 2013. Tech. rep., International Energy Agency (IEA), 2013.

[13] Birol, F. Energy and climate change world energy outlook special report. Tech. rep., 2015.

[14] Boden, T., and Marland, G. Global $CO_2$ emissions from fossil-fuel burning, cement manufacture, and gas flaring: 1751-2007. *Carbon Dioxide Information Analysis Center, Oak Ridge National Laboratory, Oak Ridge, TN, USA* (2010).

[15] Bolland, O., and Mathieu, P. Comparison of two co 2 removal options in combined cycle power plants. *Energy Conversion and Management 39*, 16 (1998), 1653--1663.

[16] Bolland, O., and Saether, S. New concepts for natural gas fired power plants which simplify the recovery of carbon dioxide. *Energy Conversion and Management 33*, 5 (1992), 467--475.

[17] Bolland, O., and Undrum, H. A novel methodology for comparing $CO_2$ capture options for natural gas-fired combined cycle plants. *Advances in Environmental Research 7*, 4 (2003), 901--911.

[18] Chattopadhyay, P. *Boiler operation engineering: Questions and answers*. McGraw-Hill Education, 2013.

[19] Christensen, T., Barseth, K., Hainriii, S., and De Mayer, H. Jet engine with carbon capture, 2011. US Patent App. 13/811,753 US20130119667A1.

[20] Crastan, V. *Global energy economics and climate protection report 2009*. Springer Science & Business Media, 2010.

[21] Cumpsty, N. A. *Compressor aerodynamics*. Longman Scientific & Technical, 1989.

[22] Dahlquist, A. Initial aerothermal design considerations for an oxyfuel combined cycle. *Licentiate Thesis Lund University* (2014).

[23] Dahlquist, A., and Genrup, M. Aerodynamic gas turbine compressor design for an oxy-fuel combined cycle. In *ASME Turbo Expo 2015: Turbine Technical Conference and Exposition* (2015), American Society of Mechanical Engineers, pp. V003T06A001--V003T06A001.

[24] Dahlquist, A., and Genrup, M. Aerodynamic turbine design for an oxy-fuel combined cycle. In *ASME Turbo Expo 2016: Turbine Technical Conference and Exposition* (2016), American Society of Mechanical Engineers.

[25] Dahlquist, A., Genrup, M., Sjoedin, M., and Jonshagen, K. Optimization of an oxyfuel combined cycle regarding performance and complexity level. In *ASME Turbo Expo 2013: Turbine Technical Conference and Exposition* (2013), American Society of Mechanical Engineers, pp. V002T07A011--V002T07A011.

[26] Dahlquist, A., Thern, M., and Genrup, M. The influence from the working medium on the profile loss in compressor and turbine airfoils. In *ASME Turbo Expo 2014: Turbine Technical Conference and Exposition* (2014), American Society of Mechanical Engineers, pp. V02CT38A003--V02CT38A003.

[27] Darde, A., Prabhakar, R., Tranier, J.-P., and Perrin, N. Air separation and flue gas compression and purification units for oxy-coal combustion systems. *Energy Procedia 1*, 1 (2009), 527--534.

[28] De Haller, P. Das verhalten von tragflügelgittern in axialverdichtern und im windkanal. *Brennstoff-Wärme-Kraft (BWK) 5*, 10 (1953), 333--37.

[29] Denton, J. Multistage turbomachinery flow calculation program MULTALL. *Whittle Laboratory, University of Cambridge, UK*.

[30] Denton, J. Multistage turbomachinery flow calculation program-MULTIP. *Whittle Laboratory, University of Cambridge, UK* (1999).

[31] Denton, J. Introductory review of basic principles. *Cambridge Turbomachinery Course 1* (2012), 1--31.

[32] Dlugokencky, E., and Tans, P. National Oceanic and Atmospheric Administration Earth System Research Laboratory. www.esrl.noaa.gov/gmd/ccgg/trends/, 2016. "Last accessed February 2016".

[33] Drela, M., and Youngren, H. A user's guide to MISES 2.63.

[34] ElKady, A. M., Evulet, A., Brand, A., Ursin, T. P., and Lynghjem, A. Application of exhaust gas recirculation in a DLN F-class combustion system for postcombustion carbon capture. *Journal of Engineering for Gas Turbines and Power 131*, 3 (2009), 034505.

[35] ENCAP - WP 1.1. Reference cases and guidelines for technology concepts No 55431.

[36] Farokhi, S. *Aircraft propulsion*. John Wiley & Sons, 2014.

[37] Franco, F., Mina, T., Woolatt, G., Rost, M., and Bolland, O. Characteristics of cycle components for $CO_2$ capture. In *Proceedings of 8th International Conference on Greenhouse Gas Control Technologies, Trondheim, Norway* (2006).

[38] GE Power. Combined cycle steam turbines power and performance. `gepower.com` GEA32228. "Last accessed March 2016".

[39] Hada, S., Tsukagoshi, K., Masada, J., and Ito, E. Test results of the world's first 1,600 °C J-series gas turbine. *Mitsubishi Heavy Industries Technical Review 49*, 1 (2012), 18.

[40] Halls, G. Air cooling of turbine blades and vanes: An account of the history and development of gas turbine cooling. *Aircraft Engineering and Aerospace Technology 39*, 8 (1967), 4--14.

[41] Havakechian, S. Denton, J. 3D blade stacking strategies and understanding of flow physics in low pressure steam turbines part I 3D Stacking mechanisms. In *ASME Turbo Expo 2015: Turbine Technical Conference and Exposition*.

[42] Havakechian, S. Denton, J. 3D blade stacking strategies and understanding of flow physics in low pressure steam turbines part II Stacking equivalence and differentiators. In *ASME Turbo Expo 2015: Turbine Technical Conference and Exposition*.

[43] Hearsey, R. Program HT0300 NASA 1994 version. *Doc. No. D6-81569TN, Volumes 1* (1994).

[44] Holland, M., and Thake, T. Rotor blade cooling in high pressure turbines. *Journal of aircraft 17*, 6 (1980), 412--418.

[45] Horlock, J. *Advanced gas turbine cycles*. Elsevier Science Ltd, 2013.

[46] ICO2N. Integrated $CO_2$ Network. `http://www.ico2n.com/`, 2013. "Last accessed February 2016".

[47] IEA. $CO_2$ emissions from fuel combustion highlights 2013. Tech. rep., International Energy Agency (IEA), 2014.

[48] Kehlhofer, R., Hannemann, F., Rukes, B., and Stirnimann, F. *Combined-cycle gas & steam turbine power plants*. Pennwell Books, 2009.

[49] Kvamsdal, H. M., Jordal, K., and Bolland, O. A quantitative comparison of gas turbine cycles with $CO_2$ capture. *Energy 32*, 1 (2007), 10--24.

[50] Lemmon, E., Huber, M., and McLinden, M. NIST standard reference database 23 ver 8.0. *National Institute of Standards and Technology, Gaithersburg, MD* (2007).

[51] Lieblein, S., Schwenk, F. C., and Broderick, R. L. Diffusion factor for estimating losses and limiting blade loadings in axial-flow-compressor blade elements. Tech. rep., DTIC Document, 1953.

[52] Massachusetts Institute of Technology (MIT). The carbon capture and sequestration technologies program. `http://sequestration.mit.edu/index.html`. "Last accessed February 2016".

[53] Metz, Bert, Davidson, Ogunlade, de Coninck, Heleen, Loos, Manuela, Meyer, and Leo. IPCC special report on carbon dioxide capture and storage. Tech. rep., IPCC, Geneva (Switzerland). Working Group III, 2005.

[54] Moustapha, H., Zelesky, M. F., Baines, N. C., and Japikse, D. *Axial and radial turbines*, vol. 2. Concepts NREC Wilder, VT, 2003.

[55] NRG. Petra Nova. `http://www.nrg.com/sustainability/strategy/enhance-generation/carbon-capture/wa-parish-ccs-project/`, 2016. "Last accessed January 2016".

[56] Pfaff, I., and Kather, A. Comparative thermodynamic analysis and integration issues of CCS steam power plants based on oxy-combustion with cryogenic or membrane based air separation. *Energy Procedia 1*, 1 (2009), 495--502.

[57] Pupo, R. Adiabatic flame temperature for combustion of methane. *Undergraduate Journal of Mathematical Modeling: One+ Two 3*, 2 (2011), 6.

[58] RENK. High Speed Power Gears. `www.renk.eu`.

[59] Riethmann, T., Sander, F., and Span, R. Modelling of a supercharged semi-closed oxyfuel combined cycle with $CO_2$ capture and analysis of the part-load behavior. *Energy Procedia 1*, 1 (2009), 415--422.

[60] Sammak, M., Genrup, M., Thorbergsson, E., and Grönstedt, T. Conceptual mean-line design of single and twin-shaft oxy-fuel gas turbine in a semi-closed oxy-fuel combustion combined cycle. In *Proceedings of ASME Turbo Expo 2012: Power for Land, Sea and Air. June 11-15, 2012, Copenhagen, Denmark*, vol. Volume 3, pp. 289--297.

[61] Sammak, M., Jonshagen, K., Thern, M., Genrup, M., Thorbergsson, E., Gronstedt, T., and Dahlquist, A. Conceptual design of a mid-sized semi-closed oxy-fuel combustion combined cycle. In *ASME 2011 Turbo Expo: Turbine Technical Conference and Exposition* (2011), American Society of Mechanical Engineers, pp. 253--261.

[62] Sanz, W., Jericha, H., Bauer, B., and Gottlich, E. Qualitative and quantitative comparison of two promising oxy-fuel power cycles for $CO_2$ capture. *Journal of Engineering for Gas Turbines and Power 130*, 3 (2008), 031702.

[63] SaskPower. Boundary dam saskpower, 2016. `http://saskpowerccs.com/ccs-projects/boundary-dam-carbon-capture-project/`.

[64] Siemens AG. Industrial steam turbines, the comprehensive product range from 2 to 250 megawatts. `siemens.com/energy/steamturbines` E50001-G410-A101-V4-4A00. "Last accessed March 2016".

[65] SINTEF Energi AS, Siemens AS Norway, Siemens Industrial Turbomachinery AB, Nebb Engineering AS, Lund University. OxyGT final technical report. Tech. rep., CLIMIT, 2014.

[66] Statoil. Sleipner West. `http://www.statoil.com/en/TechnologyInnovation/NewEnergy/Co2CaptureStorage/Pages/SleipnerVest.aspx`, 2014. "Last accessed January 2016".

[67] Statoil. Snohvit. `http://www.statoil.com/en/TechnologyInnovation/NewEnergy/Co2CaptureStorage/Pages/Snohvit.aspx`, 2014. "Last accessed January 2016".

[68] Stéphenne, K. Start-up of world's first commercial post-combustion coal fired CCS project: Contribution of Shell Cansolv to SaskPower Boundary Dam ICCS project. *Energy Procedia 63* (2014), 6106--6110.

[69] Sundkvist, S., Dahlquist, A., Janczewski, J., Sjödin, M., Bysveen, M., Ditaranto, M., Langørgen, ., Seljeskog, M., and Siljan, M. Concept for a combustion system in oxyfuel gas turbine combined cycles. In *ASME Turbo Expo 2013: Turbine Technical Conference and Exposition* (2013), American Society of Mechanical Engineers, pp. V002T07A005--V002T07A005.

[70] Tak, S. H., Park, S. K., Kim, T. S., Sohn, J. L., and Lee, Y. D. Performance analyses of oxy-fuel power generation systems including $CO_2$ capture: comparison of two cycles using different recirculation fluids. *Journal of mechanical science and technology 24*, 9 (2010), 1947--1954.

[71] The Energy Department's Fossil Energy. Pre-combustion carbon capture research. `http://energy.gov/fe/science-innovation/carbon-capture-and-storage-research/carbon-capture-rd/pre-combustion-carbon`, 2013. "Last accessed January 2016".

[72] Torp, T., and Gale, J. Demonstrating storage of $CO_2$ in geological reservoirs: The Sleipner and SACS projects. *Energy 29*, 9 (2004), 1361--1369.

[73] Tranier, J., Perrin, N., and Darde, A. Update on advanced developments for ASU and $CO_2$ purification units for oxy-combustion (Air Liquide, France). In *3rd Meeting of the Oxy-Fuel Combustion Network (IEAGHG International Oxy-Combustion Network)* (2008), Yokohama Japan.

[74] Traupel, W. *Thermische Turbomaschinen: Erster Band Thermodynamisch-strömungstechnische Berechnung*. Springer-Verlag, 2013.

[75] Ulizar, I., and Pilidis, P. Handling of a semiclosed cycle gas turbine with a carbon dioxide-argon working fluid. In *ASME 1999 International Gas Turbine and Aeroengine Congress and Exhibition* (1999), American Society of Mechanical Engineers, pp. V002T04A015--V002T04A015.

[76] Van der Merwe, J. Environmental and material influences on the stress-corrosion cracking of steel in $H_2O$-CO-$CO_2$ solutions. *International Journal of Corrosion 2012* (2012).

[77] Walsh, P. P., and Fletcher, P. *Gas turbine performance*. John Wiley & Sons, 2004.

[78] Wennerstrom, A. J. *Design of highly loaded axial-flow fans and compressors*. 2000.

[79] White, and Don. Monitoring $CO_2$ storage during EOR at the Weyburn-Midale Field. *The Leading Edge 28*, 7 (2009), 838--842.

[80] White Rose CCS. `http://www.whiteroseccs.co.uk/`, 2016. "Last accessed January 2016".

[81] Yang, H., Kang, D., Ahn, J., and Kim, T. Evaluation of design performance of the semi-closed oxy-fuel combustion combined cycle. *Journal of Engineering for Gas Turbines and Power 134*, 11 (2012), 111702.

[82] Yuri, M., Masada, J., Tsukagoshi, K., Ito, E., and Hada, S. Development of 1600 c-class high-efficiency gas turbine for power generation applying j-type technology. *Mitsubishi Heavy Industries Technical Review 50*, 3 (2013), 1--10.

[83] Zweifel, O. The spacing of turbo-machine blading, especially with large angular deflection. *Brown Boveri Rev. 32*, 12 (1945), 436--444.

Publication I

# Conceptual Design of a Mid-sized Semi-closed Oxy-fuel Combustion Combined Cycle

Sammak, M., Jonshagen, K., Thern, M., Genrup, M.,

Thornbergsson, E., Gronstedt, T., **Dahlquist, A.,**

ASME Turbo Expo 2011, GT2011-46299

**Proceedings of ASME Turbo Expo 2011**
**GT2011**
**June 6-10, 2011, Vancouver, British Columbia, Canada**

# GT2011-46299

# CONCEPTUAL DESIGN OF A MID-SIZED SEMI-CLOSED OXY-FUEL COMBUSTION COMBINED CYCLE

*** Majed Sammak, Klas Jonshagen, Marcus Thern, Magnus Genrup**
Lund University
SE-221 00 Lund, Sweden
**Corresponding author. Tel: +46 76 236 3637*
*E-mail address: majed.sammak@energy.lth.se*

**Egill Thorbergsson, Tomas Grönstedt**
Chalmers University of Technology
SE-412 96 Gothenburg, Sweden

**Adrian Dahlquist**
Siemens Industrial Turbomachinery AB
SE-612 83 Finspong, Sweden

## ABSTRACT

This paper presents the study of a mid-sized semi-closed oxy-fuel combustion combined cycle (SCOC-CC) with net power output around 108 MW. The paper describes not only the power balance and the performance of the SCOC-CC, but also the conceptual design of the SCOC turbine and compressor. A model has been built in the commercial heat and mass balance code IPSEpro to estimate the efficiency of semi-closed dual-pressure oxy-fuel combustion combined cycle using natural gas as a fuel. In order to obtain the real physical properties of the working fluids in IPSEpro, the code was linked to the NIST Reference Fluid Thermodynamic and Transport Properties Database (REFPROP).

The oxy-fuel turbine was modeled with the in-house Lund University package LUAX-T. Important features such as stage loading, loss modeling, cooling and geometric features were included to generate more accurate results. The oxy-fuel compressor has been modeled using a Chalmers university in-house tool for conceptual design of axial compressors. The conceptual design of the SCOC-CC process has a net efficiency of 47 %. The air separation unit and $CO_2$ compression reduce the cycle efficiency by 10 and 2 percentage points, respectively.

A single-shaft configuration was selected for the gas turbine simplicity. The rotational speed chosen was 5200 rpm and the turbine was designed with four stages. All stage preliminary design parameters are within ranges of established industrial axial turbine design limits. The main issue is the turbine exit Mach number; the stage must be lightly loaded in terms of pressure ratio to maintain the exit Mach number below 0.6. The compressor is designed with 18 stages. The current value of the product of the annulus area and the blade rotational speed squared ($AN^2$) was calculated and found to be $40 \cdot 10^6$.

Keywords: SCOC-CC, Oxy fuel, gas turbine, mid-sized dual pressure combined cycle, $CO_2$.

## NOMENCLATURE

| | |
|---|---|
| A | Area [$m^2$] |
| C | Blade chord [m] |
| $C_m$ | Meridional velocity [m/s] |
| CCS | Carbon capture and storage |
| cp | Specific heat capacity [kJ/kg.K] |
| Cp | Pressure recovery coefficient [-] |
| HP | High pressure |
| HRSG | Heat recovery steam generator |
| HTC | Heat transfer coefficient [$W/m^2.K$] |
| LP | Low pressure |
| $\dot{m}$ | Mass flow [kg/s] |
| $m^*$ | Dimensionless mass flow [-] |
| M | Molecular mass [kg/kmol] |
| *M* | Mach number [-] |
| N | Rotational speed [rpm] |
| P | pressure [bar] |

| | |
|---|---|
| PR | Pressure ratio [-] |
| r | Radius [m] |
| R | Gas constant [kJ/kg °C] |
| SCOC-CC | Semi-closed oxy-fuel combustion combined cycle |
| T | Temperature [°C or K] |
| U | Blade speed [m/s] |

**Greek symbols**

| | |
|---|---|
| $\gamma$ | Gamma [-] |
| $\Delta$ho | Stage work |
| $\varepsilon$ | Cooling effectiveness [-] |
| $\eta$ | Efficiency [%] |
| $\eta_p$ | Polytropic efficiency [-] |
| $\Lambda_p$ | Reaction degree based on pressure |
| $\rho$ | Density [kg/m$^3$] |
| $\varphi$ | Flow coefficient [-] |
| $\psi$ | Blade loading coefficient [-] |

**Subscripts**

| | |
|---|---|
| ax | Axial |
| d | Discharge |
| h | hub |
| i | Inlet |
| m | Meridional |
| rel | Relative |
| rtr | Rotor |
| str | Stator |
| ti | Total inlet |
| td | Total discharge |
| t | Tip |

## INTRODUCTION

Secure, reliable and affordable energy supply is needed for economic growth. However, the increase in the carbon dioxide ($CO_2$) emissions associated with oil, coal and natural gas is a cause of major concern. Over the past decade, reducing carbon emissions and their impact on climate change has become the major focus of researchers and scientists. One option that has broad potential is $CO_2$ capture and storage; however, considerable development is needed to enable scale-up for industrial applications, and to make it more economical.

A number of power plant concepts for $CO_2$-neutral power production have been developed. All have advantages and disadvantages, and no single technique has shown to be superior in terms of performance and cost. The choice of capture technology is determined largely by the process conditions under which it the process must operate. Current carbon dioxide capture systems for power plants have the potential to capture some about 85-95 % of the $CO_2$ produced [1]. However, carbon capture and compression come at a price, namely a decrease in performance of the plant.

One promising candidate for the separation of carbon dioxide emitted by power plants is the semi-closed oxy-fuel combustion combined cycle (SCOC-CC). SCOC-CC concept is based on replacing air with oxygen in the combustion of the fuel so that the main products of combustion will be carbon dioxide and water. The steam is condensed in the flue gas condenser, while the $CO_2$ rich flue gas is separated into two streams. The main stream is re-circulated to the gas turbine, while the much smaller bleed stream is compressed for transport and storage [1].

Previous published work on SCOC-CC has been focused on large single-shaft gas turbines. There are several publications from ENCAP, Bolland and Sanz [2-9], among others. This paper differs from the previous work in that the studied SCOC-CC cycle is a mid-sized cycle with net power output around 108 MW and a gas turbine rotational speed of 5200 rpm leading to fewer stages in the compressor. The issues of air separation and CO2 transport and storage are not discussed although their impact is taken into consideration in the cycle assessments.

The change in the compressor working fluid, from air to $CO_2$, requires a number of important changes in the properties for the design of the gas turbine compressor, combustion chamber, and turbine.

Table 1 presents the main thermodynamic properties of air and carbon dioxide at 15 °C and 1 bar.

**Table 1: Thermodynamic properties of air and carbon dioxide at 15 °C and 1 bar [10].**

| *Thermodynamic properties* | *Units* | *Air* | *Carbon dioxide* |
|---|---|---|---|
| $C_p$ | kJ/kg °C | 1.005 | 0.846 |
| $C_v$ | kJ/kg °C | 0.718 | 0.657 |
| R | kJ/kg °C | 0.287 | 0.189 |
| $\gamma$ | - | 1.4 | 1.289 |
| $\rho$ | kg/m$^3$ | 1.2 | 1.84 |
| M | kg/kmol | 28.9 | 44.01 |

From Table 1 it can be seen that the carbon dioxide has a lower value of gamma $\gamma$ and a higher density than air. The speed of sound in the denser gas will be slower, and this will have a great impact on the design of the gas turbine. Issues such as Mach numbers in the turbomachinery components and maintaining a high performance in the bottoming cycle will have to be addressed.

Land based gas turbines can be categorized as single-, twin- or three-shaft units. The single-shaft configuration is less complex, but has poor torque characteristics for mechanical drive. The gas turbine mass flow can be controlled using a fixed-speed, single-shaft turbine by means of the variable guide vanes. This means that part-load operation can be achieved with a, more-or-less, nominal firing level, maintaining a high exhausts temperature over a wide load range. This feature

results in high combined-cycle performance. A multi-shaft unit typically has about twice the full-load torque at starting speed, and is capable of satisfying both electric power and mechanical drive applications. Thus, a SCOC-CC plant based on a single-shaft turbine offers several advantages.

## THE SEMI-CLOSED OXY-FUEL COMBUSTION COMBINED CYCLE PROCESS

Figure 1 show a schematic of the SCOC-CC cycle. The SCOC-CC consists of five main parts: the topping cycle, the bottoming cycle, the air separation unit, the $CO_2$ compression and the flue gas condenser. A brief description of the proposed SCOC-CC is given below.

The topping cycle consists of a compressor, a combustion chamber and a turbine.
*Compressor:* The compressor working fluid consists mainly of $CO_2$ re-circulated from the flue gas condenser. (The flue gas is divided into two streams; about 93 % being returned to the compressor). As a direct consequence of the high $CO_2$ content, the pressure ratio in the SCOC-CC is calculated to 39, which is higher than the operating pressure ratio for a conventional industrial gas turbine.
*Combustion Chamber:* In the SCOC-CC, combustion of hydrocarbons is performed in oxygen with a purity of 95 % at close to the stoichiometric conditions. The oxygen is obtained from the air separation unit. The SCOC-CC combustion chamber products are thus quite different from conventional combustion chamber products. The outlet temperature from the combustion chamber is set to 1400 °C. This gives a good turbine effect taking into consideration material limitation in the turbine as well as cooling effectiveness that is a function of degree of technology. The theoretical flame temperature in the combustion chamber may reach 3500 °C [1] while the actual flame temperature is lower. This is considerably higher than any state-of-the-art gas turbine can handle, and must be addressed in subsequent design phases.
*Turbine:* Due to the high temperature at the turbine inlet the turbine is cooled with $CO_2$ from the compressor. The mass flow of the cooling $CO_2$ is about 30 % of the turbine inlet mass flow. The flue gas is expanded in the turbine to a pressure of 1.06 bar (including the diffuser loss), resulting in a temperature of 620 °C.

The bottoming cycle main components are the heat recovery steam generator (HRSG) and steam turbine and condenser. The heat recovery system employs two pressure levels. A third level would probably give better performance, but is not considered here due to the cost. The heat recovery steam generator has a standard configuration including a low-pressure (LP) economizer, a low-pressure evaporator, a low-pressure superheater, a high-pressure (HP) economizer, a high-pressure evaporator and finally a high-pressure superheater. The HP inlet steam temperature is set at 565 °C and a pressure of 127 bar at steam quality around 85 %. The static pressure of the condenser is set to 0.034 bar, assuming a cooling water temperature of 15 °C. The performance of the steam turbine has been assessed in detail with the Siemens in-house design code for steam turbines, however, due to the proprietary nature of this information; no details can be given here. The deaerator is operating at 105 °C and the energy is taken from the LP-economizer. The deaerator outgoing water is cooled by the incoming condensate, to approximately 50 °C. This is limited by the requirement of a temperature difference of 13 °C for efficient deaeration. This configuration increases the temperature of the inlet water in the economizer which prevents flue-gas condensation. The flue-gas exit temperature from the HRSG is of 64 °C is lower than for a regular dual-pressure combined cycle and this is due to the fact that the specific heat of the flue gas is lower than in a conventional cycle.

The flue gas condenser is assumed to be a packed column. The purpose of this is to condense water from the exhaust gases and remove pollutants and non-condensed gases from the flue gas. The flue gas leaving the flue gas condenser consists mainly of $CO_2$ with a temperature around 20 °C. Most of the $CO_2$, around 93 %, is recycled to the compressor, while the remainder is bled off and compressed for storage.

$CO_2$ is compressed and liquefied at a pressure of 200 bar to enable transport and storage in the dense phase.

There are three commercially available methods of separating air, namely; cryogenic separation, pressure swing absorption, and membranes. The very large quantities of oxygen required in oxy-fuel combustion can only be produced economically using cryogenic separation [9,11].

## MODELING AND PROCESS SIMULATION

All thermodynamic and process simulations were performed using the commercial software IPSEpro, developed by SimTech Simulation Technology [12]. This software allows the implementation of user-defined fluid properties to simulate the real gas properties of the working fluids. The physical properties of water and steam were calculated using the standard IAPWS-IF97 formulations in IPSEpro [12]. IPSEpro was linked to the NIST Reference Fluid Thermodynamic and Transport Properties Database (REFPROP) to obtain more realistic results [13].

Modeling of e.g. turbomachinery components becomes more intricate with rigorous-state models. The assumption of the reversible polytropic path for the compression works should not be used, since they are typically derived from semi-perfect gas models. Instead, one should use the basic state equations for such process.
The Mallen-Saville model [14, 15] was implemented in this study.

$$T\ \mathrm{ds/dT} = constant \quad (1)$$

$$\Delta H_p = \Delta H - (S_d - S_i)(T_{td} - T_{ti})/\ln(T_{td} - T_{ti}) \quad (2)$$

$$\eta_p = \Delta H_p / \Delta H \quad (3)$$

The polytropic efficiency calculated by the model was 92 %.

The SCOC-CC was designed as a mid-sized plant. Such a plant would typically have two pressure levels in the bottoming cycle, in contrast to larger plants with three pressure levels and reheat. Choosing a smaller plant offers the possibility of using geared gas- and steam turbines, hence allowing compact parts to be used. Bolland and Mathieu found that the difference between dual- and triple-pressure steam cycles was very small [9].

The work necessary to obtain oxygen with 95% purity from air has been estimated to approximately 900 kJ/kg $O_2$ and 325 kJ/kg $O_2$ for compression [2]. The energy required for $CO_2$ compression from 1 to 200 bar for transport and storage has been estimated to be 350 kJ/kg $CO_2$ [2].

The thermodynamic states and compositions of the streams are given in Tables 2 and 3 respectively. Table 4 lists the main cycle parameters.

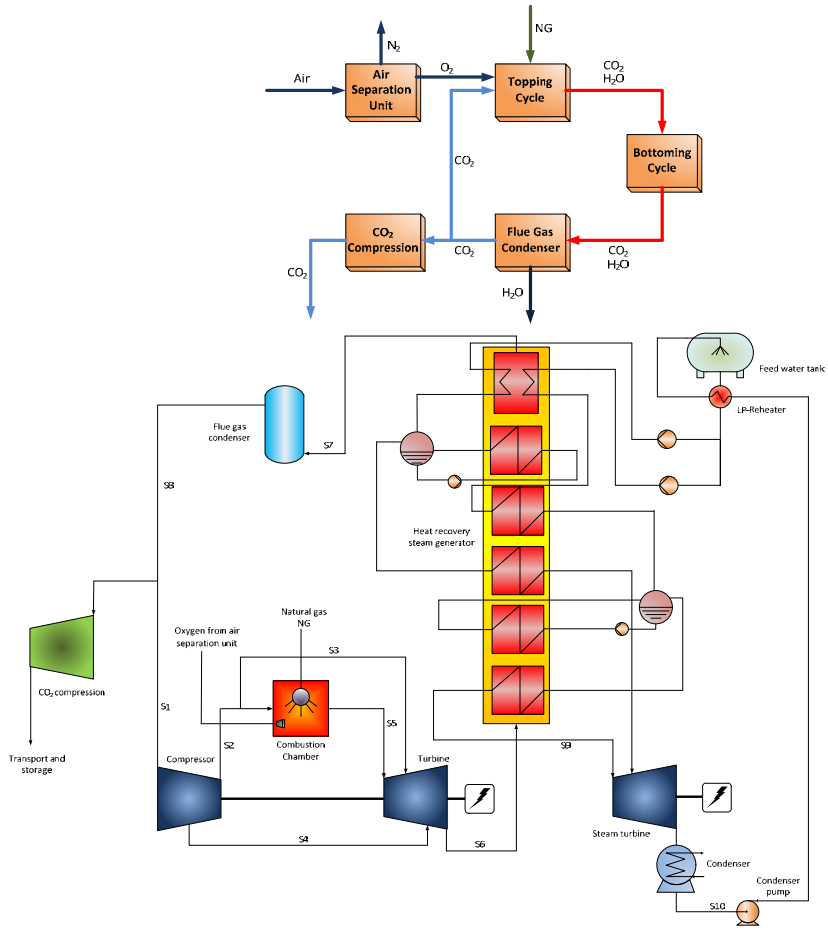


**Figure 1: Principle flow scheme for SCOC-CC.**

**Table 2: Composition of streams S1-S5.**

| *Stream* | *Unit* | *S1* | *S2* | *S3* | *S4* | *S5* |
|---|---|---|---|---|---|---|
| T | °C | 20 | 394 | 394 | 265 | 1400 |
| P | bar | 1.013 | 39 | 39 | 14 | 39 |
| m | kg/s | 190 | 171 | 31 | 19 | 164 |
| $CO_2$ | %wt | 92 | 92 | 92 | 92 | 86.5 |
| $N_2$ | %wt | 2.85 | 2.85 | 2.85 | 2.85 | 2.7 |
| Ar | %wt | 4.06 | 4.06 | 4.06 | 4.06 | 3.8 |
| $H_2O$ | %wt | 0.97 | 0.97 | 0.97 | 0.97 | 6.8 |
| $O_2$ | %wt | 0.11 | 0.11 | 0.11 | 0.11 | 0.11 |

**Table 3: Composition of streams S6-S10.**

| *Stream* | *Unit* | *S6* | *S7* | *S8* | *S9* | *S10* |
|---|---|---|---|---|---|---|
| T | °C | 620 | 64 | 20 | 565 | 26 |
| P | bar | 1.013 | 1.013 | 1.013 | 127 | 0.034 |
| m | kg/s | 214 | 214 | 204 | 35.6 | 39.5 |
| $CO_2$ | %wt | 87.7 | 87.7 | 92 | 0 | 0 |
| $N_2$ | %wt | 2.7 | 2.7 | 2.85 | 0 | 0 |
| Ar | %wt | 3.9 | 3.9 | 4.06 | 0 | 0 |
| $H_2O$ | %wt | 5.5 | 5.5 | 0.97 | 100 | 100 |
| $O_2$ | %wt | 0.11 | 0.11 | 0.11 | 0 | 0 |

**Table 4: SCOC-CC cycle power balance.**

| | *Unit* | |
|---|---|---|
| Compressor mass flow | kg/s | 190 |
| Compressor pressure ratio | - | 39 |
| Combustor outlet temp. | °C | 1400 |
| Gas turbine power, Turbine | MW | 156 |
| Gas turbine power, Compressor | MW | 67 |
| Gas turbine power | MW | 87 |
| Total heat input | MW | 230 |
| Steam turbine power | MW | 49 |
| Gross power output | MW | 136 |
| Gross efficiency | % | 59 |
| $O_2$ generation+compression | MW | 23 |
| $CO_2$ compression to 200 bar | MW | 5 |
| Net power output | MW | 108 |
| Net efficiency | % | 47 |

The designed process has a net effect of 108 MW and a net efficiency of 47 %. The penalties for air separation and compression are 10 % while $CO_2$ compression is 2 %.

## CONCEPTUAL DESIGN OF THE SCOC-CC GAS TURBINE

As with the compressor, the working fluid in the turbine is mainly $CO_2$, with a purity of almost 92 %. Changing the fundamental physical properties of the working fluid will have a significant impact on the design of the turbine. The standard set of design rules for a normal gas turbine can therefore not be directly applied to the design of a SCOC cycle. The SCOC-CC turbine has been modeled with the Lund University in-house turbine design tool [1]LUAX-T. The code is a reduced-order throughflow tool which is capable of designing highly cooled turbines. The code uses the [2]AMDC-KO-MK loss model and fundamental equations for momentum, energy and continuity for assessing losses due to cooling, purging and packing flows.

The chosen layout is a straight forward $CO_2$-cooled single-shaft unit. As mentioned the principal reasons for a single-shaft are the simplicity and related low cost. Furthermore, a single-shaft unit offers significantly less complexity in terms of shaft and bearing systems. Since there is no need for a collector with cold-end drive a more efficient exhaust system could be designed [16]. A conical diffuser can reach a recovery level of 0.8 in comparison to 0.6-0.7 for a system with a 90° bend. Figure 2 presents turbine exhaust diffuser performance which presents the relation between the pressure recovery coefficient and the static/total outlet pressure. A single-shaft unit has typically a beam type rotor whereas the twin-shaft needs bearings within the high pressure section of the gas turbine. Before describing the features of a SCOC turbine, it is instructive to discuss the design of a conventional (air and flue gas) single-shaft unit. One of the most critical design choices is the speed level since it has a profound impact on the stage count and cost.

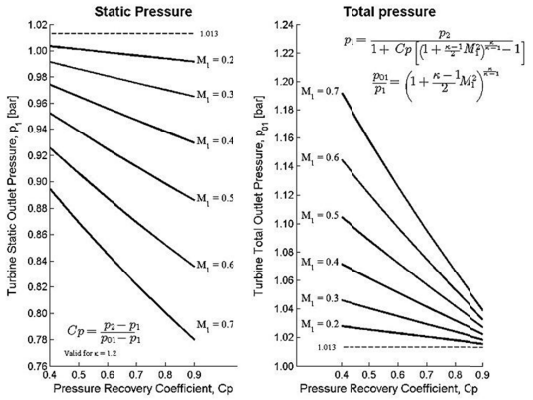


**Figure 2: Turbine exhaust diffuser performance.**

[1] LUAX-T is freely available for academic work outside Lund University.

[2] AMDC-KO-MK: Ainley+Mathieson+Dunham+Came-Kacker+Okapuu- Moustapha+Kacker [17]

### *The SCOC-CC Turbine design*

The rotational speed is typically set by either the turbine exhaust Mach number at a maximum available $AN^2$ (~root stress level) or the relative tip Mach number at the first compressor rotor. The importance of the $AN^2$ parameter cannot be overemphasized since a reduction from e.g. $50{\cdot}10^6$ to $40{\cdot}10^6$ may translate into two additional compressor stages. The exit Mach number is preferable within the range of 0.5-0.6 while the maximum tip Mach number is in the order of 1.3 [16]. The meridional Mach number should be less than 0.7 at the compressor inlet.
The heavy gas introduces issues with the last stage loading due to the low speed of sound. For reasonable exit losses, the last turbine stage should be designed with an exit Mach number below 0.6 (see figure 2).

The pressure ratio of the last stage needs to be low, but still give sufficient rotor turning to keep blade frequency high enough in order to avoid rotor dynamic difficulties. One can argue whether a twin-shaft unit should provide a better platform. The additional freedom of having another speed level would be advantageous in terms of optimizing the loading distribution. The speed level was calculated to 5200 rpm and the first turbine stage rim speed to 380 m/s. The calculated rotation speed takes into account the aerodynamics requirements that are leveling between exit Mach number and the last stage loading coefficient. The relative tip Mach number of the first compressor stage does not pose any limitations at the chosen speed level. Efficient gears are available exceeding 100 MW. The associated losses are approximately 1.2 % and 0.6 % for normal and vacuum respectively.

The first stage has almost no inner wall hade, while the later next one has about eight degrees. The first two rotors are cylindrical to satisfy minimum running clearance requirements. The outer wall hade was set to a maximum of 25° to maintain a maximum opening of approximately 35°. These values are somewhat arbitrary, but well within current practice. The actual limitations must be assessed in a later, more detailed design phase. With these design constraints, the exit Mach number is 0.60 and the value of $AN^2$ is close to $40{\cdot}10^6$. The last rotor has a mid-span turning exceeding 65°. A three-stage design would not be realistic, even at higher speed, due to the inherent limitation on the exit Mach number. Figure 3 presents the annulus of a four stages SCOC designed turbine.

The designed four stages SCOC turbine flow coefficients, stage loading coefficients and reactions degree of the four-stage are presented in Table 5.

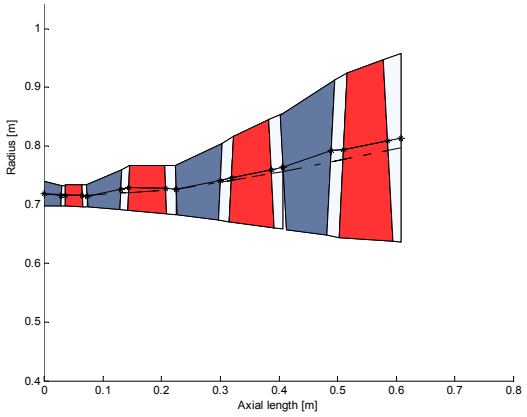


**Figure 3: Annulus of the conceptual design of the SCOC turbine.**

**Table 5: Turbine design data.**

| | *Stage 1* | *Stage 2* | *Stage 3* | *Stage 4* |
|---|---|---|---|---|
| $\Delta h_0/U^2$ | 1.7 | 1.3 | 1.1 | 1.0 |
| $\bar{\psi}$ | | 1.30 | | |
| $C_m/U$ | 0.39 | 0.39 | 0.42 | 0.44 |
| PR | 2.57 | 2.32 | 2.34 | 2.74 |
| $\Lambda_p$ | 0.30 | 0.38 | 0.38 | 0.40 |
| $\varepsilon_{str}/\varepsilon_{rtr}$ | 0.47/0.4 | 0.28/0.16 | 0.05/0 | - |

The combustor outlet temperature was set to 1400 °C to obtain high power density and good cycle performance. This level of firing requires an efficient cooling system. The firing level alone is not sufficient to describe the required cooling, and the cooling effectiveness must be used to describe the cooling duty (ε). At first glance, the values of the cooling effectiveness are low – and well within common practice. The cooling flows can be assessed with the standard m-star model [17].

$$\varepsilon = \frac{T_{gas.rel} - T_{metal}}{T_{gas.rel} - T_{cool.rel}} \quad \varepsilon = \frac{m^* \eta_{cool}}{1 + m^* \eta_{cool}} \quad m^* = \frac{\dot{m}_{cool} \cdot c_{p.cool}}{HTC \cdot 2.2 \cdot C \cdot h} \qquad (4)$$

Equations (4) provide a link between the thermodynamic properties of the cycle, the maximum metal temperature, the level of technology and the velocity triangles. All temperatures should be relative, since both the inlet temperature and coolant temperature are dependent on the velocity triangles. The relative inlet temperature can be controlled effectively by lowering the reaction level. Another possibility is to reduce the relative inlet velocity by using a lower value of $C_m/U$, resulting in lower local heat transfer at the first part of the blade. However, it is not possible to assess this heat transfer with a mid-span code. The present version of LUAX-T has three different ways of mixing coolant into the main stream, namely: (i) film, (ii) trailing-edge ejection, and (iii) packing and cavity purge flows. Losses due to coolant- and packing flows are assessed by conservation of momentum and energy. The

mixing routines result in a non-linear system that must be solved iteratively for conservation of mass. Film losses are assessed through a generic free stream velocity distribution and the Hartsel mixing method [18]. The generic velocity distribution assumes a certain loading distribution and suction-side diffusion level. Injection positions, angles and momentum ratios are typical in terms of normal showerhead and profile configurations. Common practice is not to have injection cooling after the throat point – driven by that the loss scales with Mach number squared.

The total cooling flow, including 1.5 % per disc cooling and packing, is 49.8 kg/s or 26.2 % of the compressor inlet flow. This figure is rather high, and must be further investigated. The specific heat ratio between air and carbon dioxide is about 1.2, and a corresponding influence on cooling consumption is to be expected by virtue of the medium alone. It should be borne in mind that the m-star model typically underestimates the total cooling flow for highly fired engines. It is common to introduce an adjustment factor which is dependent on the firing level. Early profiling and a heat transfer code should be able to verify the coolant consumption in a later design stage. The drop in combustion pressure is a limiting factor in terms of the pressure difference for film cooling of the first vane. For a normal gas turbine, the pressure drop should not fall below 3 % to ensure sufficient film pressure drop. The entire cooling and secondary air system must be analyzed before any firm conclusions can be drawn.

### *The SCOC-CC compressor design*

As mentioned previously the design of the SCOC-CC compressor is constrained by the relative tip Mach number of the first rotor. To allow a high blade speed and keep first stage transonic losses down an inlet guide vane is employed. Here, a 15° swirl was selected. This was a sufficient level for the relatively moderate Mach number that resulted from the design process described below.

Reducing the flow coefficient at the first stage will help to keep the first stage specific work up. For a given hub tip ratio reducing flow speed will increase speed at the blade mid allowing a higher first stage temperature rise to be achieved for a given stage loading parameter $\psi$. However, it is usually desirable to reduce axial flow speed and the flow coefficient through the compressor to allow a relatively low flow coefficient at the compressor exit. This makes the process of establishing a desirable surge margin easier. In fact, it is possible to select a somewhat higher first stage flow factor and simultaneously obtain an operation point close to the minimum tip Mach number, i.e. close to the minima of the family of curves presented in Figure 4. This will reduce the transonic losses incurred in the first stage rotor. Here, a first stage hub tip ratio of 0.483 is selected together with a flow factor of 0.65.

To keep blade lengths at a reasonable level and thereby limit tip leakage losses in the last stages of the compressor the hub-tip ratio must be kept at a reasonable number. Here a constraint of 0.92 in exit hub tip ratio has been imposed together with an axial exit Mach number of 0.25. Together with the mass flow, the compressor efficiency and the pressure ratio the hub tip ratio limit will define the compressor exit tip and hub radius; here these numbers turn out to be 0.374 and 0.345 meters respectively.

To ensure that accurate thermodynamic gas properties are obtained the Chalmers university in-house tool for conceptual compressor design couples the REFPROP tool to the compressor design process.

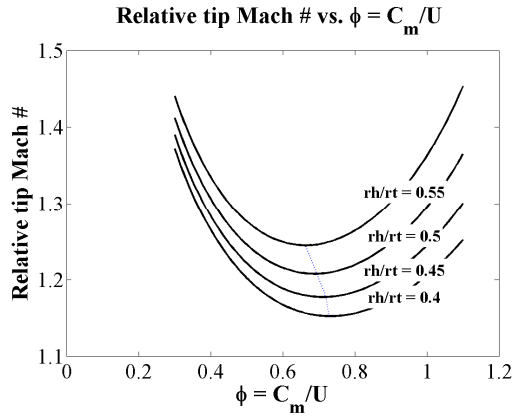


**Figure 4: First stage rotor relative tip Mach number as a function of flow coefficient for a range of hub-tip-ratios (0.4, 0.45, 0.50, 0.55).**

The resulting compressor is an 18-stage design. It should be noted that the initial assumption of a first stage rotor hub-tip ratio of 0.50 and the limiting hub tip ratio of 0.92 at the compressor exit produced an annulus very close to a constant hub design after the first stage. Data on axial flow velocities, blade speeds at blade mid, flow coefficients, stage loading coefficients, stage hub tip ratio, relative tip Mach numbers and stage pressure ratios have been collected in Table 6. A cross sectional drawing of the compressor annulus is reproduced in Figure 5.

The design studies carried out strongly suggest that the number of stages and the feasibility of a single-shaft compressor are quite sensitive to the exit hub tip ratio. Reducing the allowable exit hub tip ratio to 0.90 typically adds 2-4 stages on the compressor due to the reduced blade speed. This gives some insight into how the selection of single-shaft compressor architecture imposes restrictions on the pressure ratio of the cycle. Increasing the pressure ratio further will necessitate that the annulus is allowed to move to lower radii, a decreasing hub radius design, to allow the shorter blades arising from the

increased pressure and density to stay within the hub tip ratio bound. This will add stages rapidly making the single-shaft design less attractive for very high cycle pressure ratios.

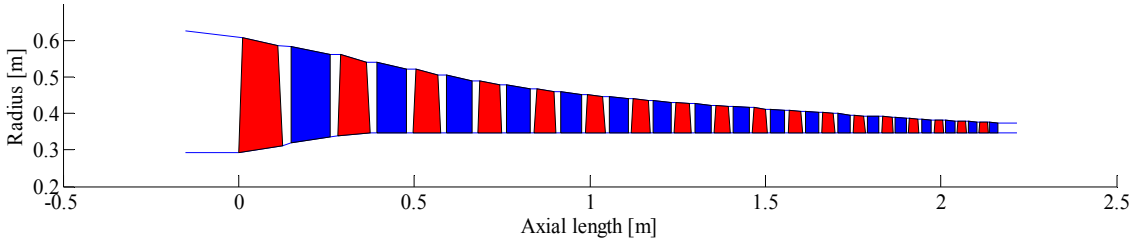


**Figure 5: Annulus of the conceptual design of the SCOC compressor.**

**Table 6: SCOC-CC compressor data.**

| *Stage* | | *1* | *3* | *5* | *7* | *9* | *11* | *13* | *15* | *17* | *18* |
|---|---|---|---|---|---|---|---|---|---|---|---|
| $C_{ax}$ | [m/s] | 155 | 138 | 127 | 117 | 106 | 100 | 100 | 100 | 100 | 100 |
| $U_m$ | [m/s] | 246 | 232 | 219 | 212 | 208 | 204 | 201 | 199 | 197 | 196 |
| $\varphi_m$ | - | 0.63 | 0.60 | 0.58 | 0.55 | 0.51 | 0.49 | 0.50 | 0.50 | 0.51 | 0.51 |
| $\psi_m$ | - | 0.45 | 0.45 | 0.45 | 0.45 | 0.45 | 0.45 | 0.45 | 0.45 | 0.45 | 0.45 |
| rh/rt | - | 0.55 | 0.68 | 0.75 | 0.79 | 0.83 | 0.85 | 0.88 | 0.90 | 0.91 | 0.92 |
| $M_{reltip}$ | - | 1.12 | 0.85 | 0.73 | 0.65 | 0.60 | 0.56 | 0.53 | 0.50 | 0.48 | 0.47 |
| PR | - | 1.52 | 1.37 | 1.28 | 1.23 | 1.19 | 1.17 | 1.15 | 1.14 | 1.13 | 1.12 |

## CONCLUSION

This paper presents the conceptual design of a mid-sized, semi-closed dual-pressure oxy-fuel combustion combined cycle and the conceptual design of a SCOC turbine and compressor. The SCOC-CC model was based on the heat and mass balance code IPSEpro. The physical properties of the gases were calculated using values determined by NIST software REFPROP.

The designed SCOC-CC process has a net power output of 108 MW and 47 % efficiency. Note that all values exclude parasitic losses and step-up transformer losses. The air separation unit reduces the net efficiency by 10 percentage points while the $CO_2$ compression reduces it by another 2 percentage points.

The overall compressor pressure ratio is 39 which is higher than the operating pressure ratio for a conventional industrial gas turbine. The combustion outlet temperature is set to 1400 °C. The turbine requires an efficient cooling system to maintain blade metal temperature within the limits. The total calculated cooling flow is 49.8 kg/s or 26.2 % of the compressor inlet flow.

A four-stage, single-shaft gas turbine configuration was chosen for simplicity. The rotational speed selected was 5200 rpm. The turbine exit Mach number was maintained below 0.60. The compressor was designed with 18 stages. The current value of $AN^2$ was found to be $40 \cdot 10^6$.

The last stage loading issue together with the relative low compressor rotor inlet Mach number suggests that a twin-shaft unit is a better candidate for optimal turbomachinery operation. Furthermore a twin-shaft design would allow the gas generator to operate at a higher speed level making the compressing system more compact as well as providing an optimized power turbine at a lower speed level. However, the advantages of a twin-shaft design must always be weighed against retaining the inherent simplicity and low cost of the simple cycle single-shaft design.

## ACNOWLEDGEMENTS

This research has been funded by the Swedish Energy Agency, Siemens Industrial Turbomachinery AB, Volvo Aero Corporation and the Royal Institute of Technology through the Swedish research code TURBO POWER, the support of which is gratefully acknowledged. The authors would also like to acknowledge David Olsson and Jonas Svensson for developing the LUAX-T turbine design tool. The detailed steam turbine calculations would not have been possible without the assistance from Specialist Åke Göransson (Siemens).

## REFERENCES


[1] Metz, B., Davidson, O., Coninck, H., Loos, M., Meyer, L., 2005, "IPCC Special Report on Carbon Dioxide Capture and Storage", Cambridge University, ISBN-13 978-0-521-86643-9.

[2] Sanz, W., Jericha, H., Bauer, B., Göttlich, E., 2005, "Qualitative and Quantitative Comparison of Two Promising Oxy-Fuel Power Cycles for CO2 Capture", Journal of Engineering for Gas Turbines and Power, **130**.

[3] Bolland, O., Saether, S., 1992, "New concepts for natural gas fired power plants which simplify the recovery of carbon dioxide", Energy Convers.Mgmt, **33**, (5-8), pp. 467-475.

[4] Woollatt,G., Franco, F., 2009, "Natural gas oxy-fuel cycles-Part 1: Conceptual aerodynamic design of turbo-machinery components", Energy Procedia, **1**, pp. 573-580.

[5] Rezvani, S., Bolland, O., Franco, F., Huang, Y., Span, R., Keyser, J., Sander, F., Mcllveen-Wright, D., Hewitt, N., 2009, "Natural gas oxy-fuel cycles-Part 3: Economic Evaluation", Energy Procedia, **1**, pp.565-572.

[6] Bolland, O., Kvamsdal, H.M, Boden, J. C., 2005, " A compison of the efficiencies of the oxy-fuel power cycles water cycle, Graz cycle and Matiant cycle", Carbon dioxide capture for storage in deep geologic formations, **1**.

[7] Bolland, O., Undrum, H., 2003, "A novel methodology for comparing CO2 capture options for natural gas-fired combined cycle plants", Advanced in Environmental Research, **7,** pp. 901-911.

[8] Hammer, Th., Keyser, J., Bolland, O., 2009, "Natural gas oxy-fuel cycles-Part 2: Heat transfer analysis of a gas turbine" Physics Procedia, **1,** pp. 557-564.

[9] Bolland, O., Mathieu, P., 1998, "Comparison of two $CO_2$ removal options in combined cycle power plants", Energy Convers. Mgmt, **39**, (16-18), pp. 1653-1663.

[10] Cengel, Y., Boles, M., 2002, "Thermodynamics an engineering approach", 4th ed, ISBN 0-07-112177-3.

[11] Allam, R., White, V., 2005, "The oxyfuel baseline: revamping heaters and boilers to oxyfiring by cryogenic air separation and fuel gas recycle", Carbon dioxide capture for storage in deep geologic formations, **1**.

[12] IPSEpro, 2003, SimTech Simulation Technology (SimTech), Graz, Austria.

[13] REFPROP, Version 8, Standard Reference Data Code, National Institute of Standard and Technology.

[14] Aungier, R., 2003, "Axial-Flow Compressor", ISBN 0-7918-0192-6.

[15] Mallen, M., Saville, G., 1977, "Polytropic processes in the performance prediction of centrifigual compressors", Institution of mechanical engineers, London, United Kingdom, pp. 89-96.

[16] Walsh, P.P., Fletcher, P., 1998, "Gas Turbine Performanc" ISBN 0-632-04874-3.

[17] Moustapha, H., Zelesky, M F., Baines, N., Japikse, D., 2003, "Axial and Radial Turbine", Concepts ETI, ISBN 0-933283-12-0.

[18] Hartsel, E., "Prediction of effects of mass transfer cooling on the blade row efficiency of turbine airfoils", General Electric Company, Evendale, ohio.

Publication II

# Optimization of an Oxy-fuel Combined Cycle Regarding Performance and Complexity Level

**Dahlquist, A.,** Genrup, M., Sjoedin, M., Jonshagen, K.,

ASME Turbo Expo 2013, GT2013-94755

**Proceedings of the ASME Turbo Expo 2013: Power for Land, Sea and Air**
**GT2013**
**June 3-7, 2013, San Antonio, Texas, USA**

# GT2013-94755

## Optimization of an Oxyfuel Combined Cycle Regarding Performance and Complexity Level

**[*] Adrian Dahlquist[1], Magnus Genrup[2], Mats Sjoedin[1], Klas Jonshagen[1]**

[1]Siemens Industrial Turbomachinery AB
SE-612 83 Finspong, Sweden
**Corresponding author. Tel: +46 70-967 06 88*
*E-mail address: Adrian.Dahlquist@siemens.com*

[2]Lund University
SE-221 00 Lund, Sweden

### ABSTRACT

The aim of this paper is to establish and motivate the design parameters of a 125 MW Oxyfuel Combined Cycle (OCC) also referred to as the Semi-Closed Oxyfuel-Combusted Combined Cycle (SCOC-CC). This paper proposes a compatible OCC that does not include any unconventional features, beyond what is state-of-the-art in gas turbine technology today. Such features could challenge the feasibility to bring the concept to the market in a reasonable time.

The OCC requires a higher pressure ratio compared to a conventional combined cycle in order to achieve exhaust conditions that fit the design of the bottoming cycle. However, a high gas turbine pressure ratio increases the complexity of the machine and must be weighted against the gain in efficiency. The OCC gas turbine is modeled using a cooling model which keeps the metal temperature of all cooled turbine stages constant while seeking the optimum pressure ratio.

As the cycle is semi-closed the compressor inlet temperature is a design parameter: it is shown that there is an efficiency optimum clearly in the range of what is normally achievable. As the gas properties of the OCC flue gas differ from the conventional plant, the effects of this on the HRSG design are explored.

**Keywords:** SCOC-CC, Oxyfuel, mid-sized dual pressure combined cycle, $CO_2$, CCS.

### NOMENCLATURE

| | |
|---|---|
| A | Area [$m^2$] |
| CCS | Carbon Capture and Storage |
| COT | Combustor Outlet Temperature |
| $c_p$ | Specific heat [kJ/kg K] |
| dA/dV | Change in cooled turbine area with gas volume flow [$m^{-1}$] |
| EGT | Exhaust Gas Temperature [°C] |
| GT | Gas Turbine |
| $h_{HTC}$ | Heat transfer coefficient [W/$m^2$ K] |
| HP-ST | High Pressure Steam Turbine |
| HRSG | Heat Recovery Steam Generator |
| k | Conductivity [W/m K] |
| NGCC | Natural Gas fired Combined Cycle |
| OCC | Oxyfuel Combined Cycle |
| p | Pressure [bar] |
| PR | Pressure ratio [-] |
| Pr | Prandtl [-] |
| R | Gas constant [kJ/kg K] |
| SAS | Secondary-Air-System |
| SCOC-CC | Semi-Closed Oxyfuel Combustion Combined Cycle |
| ST | Steam Turbine |
| T | Temperature [°C] |
| V | Volume flow [$m^3$/s] |

### SUBSCRIPT

| | |
|---|---|
| 1 | Inlet |
| 2 | Outlet |
| ap | Approach point [°C] |
| CC | Combined-Cycle |
| evap | Evaporation (temperature) [°C] |
| exit | HRSG exit |
| fw | Feedwater |
| GT | Gas Turbine |
| new | New |
| net | Netto |
| $noCO_2tre$ | without the cost for $CO_2$ treatment and compression of the bleed stream |
| pp | Pinch-point |
| ref | Reference condition |

| | |
|---|---|
| s | Isentropic |
| ST | Steam Turbine |

## GREEK SYMBOLS

| | |
|---|---|
| $\varepsilon$ | Effectiveness [-] |
| $\Phi$ | Heat load [-] |
| $\eta$ | Efficiency [-] |
| $\mu$ | Kinematic viscosity [$m^2/s$] |
| $\gamma$ | Isentropic exponent [-] |
| $\rho$ | Density [$kg/m^3$] |

## INTRODUCTION

Oxyfuel combustion refers to combustion of fuel using pure oxygen rather than normal air. In this way, very high temperatures can be achieved but when applied to carbon capture in power plants this is not the aim. Here the idea is to avoid having non-condensable gases such as nitrogen in the flue gas. After the steam generator the $CO_2$ can be separated by simply condensing the steam formed in the combustion process. The concept is well developed for coal-fired power plants and pilot plants are in operation both in Germany and Australia[1],[2].

The OCC is a power cycle designed for $CO_2$ capture with similarities to the conventional combined cycle power plant. The top cycle is a semi-closed gas turbine cycle with a working fluid mainly consisting of carbon dioxide, a small amount of steam (5-30 wt-%) and enriched noble gases. Fuel and oxygen are injected into the combustion chamber, operating in close to stoichiometric conditions. After expansion in the turbine and cooling in the HRSG the gas stream formed in the combustion is cooled, the steam part is partially condensed in a flue gas condenser and the surplus water is drained out of the cycle. Some of the gaseous part of the stream mainly containing carbon dioxide is bled off and prepared for either utilization in the industry, e.g. for Enhanced Oil Recovery, or the $CO_2$ is transported for final storage.

The aim of this paper is to establish an OCC cycle that is feasible in a near future. The cycle should suit both the power industry and the Enhanced Oil Recovery market and therefore a unit size of approximately 125 $MW_{el}$ is chosen.

One of the key parameters in an OCC design is the gas turbine pressure ratio. In ref [2], Yang et al. suggests a pressure ratio of 60, which is higher than previous investigations. Sammak et al. [4] have 37, Franco et al. [5], Sanz et al. [6] have 40 and Bolland and Mathieu [7] found an efficiency optimum at a pressure ratio of 30. The pressure ratio also affects the cooling flow which in turn has a significant influence on the efficiency. In order to create an accurate pressure ratio to efficiency optimization this work implements a Secondary-Air-System model. The approach here differs from what Yang et al. [2] did in the sense that the blade metal temperature is kept constant not only in the first stage but in all cooled turbine stages. By doing so the variation of heat drop per stage is accounted for while varying the pressure ratio.

Another design parameter that has been neglected in the published work is the compressor inlet temperature. For a closed / semi-closed cycle this is a design parameter which has an impact on the specific work and efficiency. Reference [3]-[7] uses temperatures reaching from 18 °C to 25 °C which is more or less the minimum value achievable at their plant conditions. The influence from increasing the compressor inlet temperature is investigated in the present work; the preferred temperature was, however, found to be at a higher level than the mentioned values.

The paper also addresses the influence on the bottoming cycle design from the fact that the gas properties of the OCC flue gas differs from the conventional NGCC plant. The behavior of specific heat vs. temperature influences the choice of pressure levels in the HRSG design.

## CYCLE SETUP

The OCC consists of a topping cycle, gas turbine with recirculated working fluid, and a bottoming cycle that consists of a conventional two-pressure steam cycle. The topping cycle consists of a power generating gas turbine with a combustion system operating on mainly recirculated working fluid, a pure $O_2$ stream and a fuel stream. The layout of the OCC plant and its components is seen in Appendix 1 and the numbers in brackets correspond to its sections. From the GT exhaust {7} the flue gas passes through the HRSG transferring heat to the bottoming cycle. From the HRSG outlet {13} the flue gas is recirculated via a flue gas cooler/condenser where the working fluid is cooled and some of the steam is condensed before the partial bleed of the gaseous remains of the fluid. From the working fluid, consisting mainly of $CO_2$, steam and enriched Argon, Nitrogen, and Oxygen, a stream is bled off for Carbon Capture and Storage (CCS) {44}. Before entering the compressor the working fluid is preheated, to reduce RH to 80 %, in a heat exchanger {14} utilizing feed water before it enters the compressor inlet {1}.

The bottoming cycle consists of a conventional two-pressure HRSG as the preferred concept for efficiency, cost and complexity for an OCC at this size. The simulations are based on a seawater-cooled condenser operating at 0.045 bar and above 15 % moisture content (15 °C inlet, 25 °C outlet and 6 °C terminal temperature difference).

## METHOD

The OCC cycle was simulated in the Siemens standard process simulation tool Krawal-modular. The Krawal tool is an advanced heat and mass balance program with stage level capabilities. It is based on real gas properties and has a matrix type solver. The optimized cycle configuration setup is shown in Appendix 1. The influence of varying a number of different parameters was evaluated to come up with the best compromise between efficiency, design challenge, complexity and cost to ensure an attractive product with high availability. The calculation approach is to use variable geometries of all

components and keep the net power output constant. Doing so makes the mass flow vary through each case and each case can be considered as a new design.

The investigated principal parameters are:

- Pressure ratio for the gas turbine compressor and the corresponding flue gas temperature into the HRSG
- Temperature of the recirculated working fluid into the gas turbine compressor
- HRSG and bottoming cycle design

**Table 1: Component performance and boundary conditions**

| Aggregates | Parameter | Unit | Value |
|---|---|---|---|
| ***GT Compressor*** | | | |
| LPC/HPC | $\eta_s$ | % | 90.5/90.0 |
| ***Combustor*** | | | |
| Air to Fuel ratio | $\lambda$ | - | 1.01 |
| ***GT Turbine*** | | | |
| HPT/LPT/PT | $\eta_s$ | % | 87.0/87.0/91.5 |
| HPT | COT | °C | 1340 |
| ***Steam Turbine*** | | | |
| HP1/HP2/LP | $\eta_s$ | % | 90.2/88.9/86.0 |
| HPST | p | bar | 100 |
| HPST | T | °C | 565 |
| LPST | p | bar | 5.00 |
| Condenser | p | bar | 0.045 |
| ***HRSG*** | | | |
| dP gas | dp | bar | 0.038 |
| pp evap | $T_{pp}$ | °C | 8.00 |
| ap evap | $T_{ap}$ | °C | 5.00 |
| ***Auxiliary*** | | | |
| Fuel compressor | $\eta_s$ | % | 80.0 |
| $O_2$ compressor | $\eta_s$ | % | 80.0 |
| Pump | $\eta_s$ | % | 75.0 |
| Gear box | $\eta$ | % | 98.0 |
| Generator | $\eta$ | % | 98.4 |

N.B. The presented efficiencies are isentropic.

The gas turbine and steam turbine are modeled in sections containing one or more stages. Each compressor and turbine section was simulated with a constant, but individual isentropic efficiency (Table 1). The stage count for the gas turbine HPT/LPT/PT was 1, 2 and 3, respectively.

The Secondary-Air-System (cooling and sealing flow) was divided into two parts, turbine cooling and turbine disk sealing. The turbine cooling system design is based on an assumption of 850 °C metal temperature. The turbine disk cooling and sealing flow (to prevent hot gas ingestion) were predicted according to Balay & Owen [14].

The turbine cooling was predicted with an extended version of the common m*-method that utilize effectiveness ($\varepsilon$), efficiency ($\eta$) and heat load ($\Phi$) [13].

**Cooled turbine area:**

$$A_{new} = \underbrace{dA/dV}_{\substack{\text{constant} \\ 0.5\text{-}0.75}} \cdot \underbrace{(V_{new} - V_{ref})/V_{ref}}_{\frac{1}{V}dV} + A_{ref} \quad (1)$$

**Heat transfer correlation:**

$$h_{HTC,new} = h_{HTC,ref} \cdot \left( \frac{k_{new}}{k_{ref}} \cdot \left( \frac{\mu_{ref}}{\mu_{new}} \right)^{4/5} \right) \cdot \frac{1}{\left( \frac{p_{ref} \cdot R_{new} \cdot T_{new}}{p_{new} \cdot R_{ref} \cdot T_{ref}} \right)^{4/5} \cdot \left( \frac{V_{new}}{V_{ref}} \right)^{1/10}} \cdot \left( \frac{Pr_{new}}{Pr_{ref}} \right)^{1/3} \quad (2)$$

The reason for the enhanced cooling calculation is to capture the effect on the heat transfer from the gas properties of the new working medium. The additional parameters, incorporated to handle these effects, are variation in cooled turbine area with gas volume flow (dA/dV, Eq 1) and change in heat transfer coefficient (HTC, Eq 2) due to the gas composition and flow conditions. The ratio between the cooled area and volume flow was calculated to be in the range of 0.5-0.75. A conservative approach using 0.75 was applied. The variation in heat transfer coefficient is evaluated with Eq.2. Equation 2 is based on a flat plate turbulent flow assumption. The benefit of this approach is to predict the relative change from a known reference case utilizing similar cooling technology. This approach makes the analysis less sensitive to the absolute values as only relative variations influence the result.

Natural gas was used in the calculations and was delivered to the plant at a pressure of 30.0 bar and a temperature of 15.0 °C. For further compression to suit the combustor a compressor with an isentropic efficiency of 80.0 % was used and the fuel composition is shown in Table 2.

The oxygen used for the combustion is supplied by an air separation unit (ASU) at 1.20 bar and 30.0 °C at a cost of 735 kW/kg and further compression was made with a isentropic efficiency of 80.0 %. The purity of the delivered stream was 95.0 wt % $O_2$ with additional 3.0 wt- % Ar and 2.0 wt- % $N_2$ (Table 2).

**Table 2: Fuel and ASU composition**

| | | |
|---|---|---|
| ***Fuel Composition*** | | |
| $CH_4$ | wt-% | 89.0 |
| $C_2H_6$ | wt-% | 7.00 |
| $C_2H_8$ | wt-% | 1.00 |
| $nC_4H_{10}$ | wt-% | 0.0500 |
| $iC_4H_{10}$ | wt-% | 0.0500 |
| $C_5H_{12}$ | wt-% | 0.0100 |
| $N_2$ | wt-% | 0.980 |
| $CO_2$ | wt-% | 2.00 |
| LHV | kJ/kg | 46 502 |
| ***ASU Composition*** | | |
| $O_2$ | wt-% | 95.0 |
| Ar | wt-% | 3.00 |
| $N_2$ | wt-% | 2.00 |

## GAS TURBINE PRESSURE RATIO

The linchpin of the OCC is the gas turbine pressure ratio. In order to achieve an exhaust gas temperature suitable for the bottoming steam cycle a significantly higher pressure ratio is required, compared to a conventional air-based cycle. The underlying reason for this is that the working fluid consists mostly of $CO_2$ which has a low isentropic exponent ($\gamma$) compared to air, e.g. at 1000 °C and 30 bar $\gamma_{CO2} = 1.174$ while $\gamma_{Air} = 1.321$. If the GT should operate at a combustor outlet temperature (COT) comparable to a conventional GT while utilizing the same temperature drop in the GT the overall pressure ratio has to be raised considerably, [2], [4], [8]. The alternative of reducing the COT is devastating for the efficiency of the cycle.

For a combined-cycle gas turbine the required exhaust gas temperature (EGT) depends on the ability of the steam cycle to utilize reheat. This work treats a 125 $MW_{net}$ power plant which typically comprises a single or dual-pressure steam cycle without reheat with an admission temperature of 565 °C. For this an EGT of 590 °C – 600 °C would be suitable; however this will require a GT pressure ratio above 40. The pressure ratio vs. net cycle efficiency (including $O_2$ compression) diagram in Figure 1 is calculated using a COT of 1340 °C, a dual-pressure steam cycle with fixed steam data and a total net power output of 125 $MW_{net}$ i.e. the GT mass flow varies.

The minimum realistic EGT required for a steam admission temperature of 565 °C is set to 590 °C, but to investigate a wider span of GT pressure ratios and to show a more complete picture of the behavior, EGTs down to 575 °C are included in Figure 1. The efficiency vs. pressure ratio diagram flattens out at a pressure ratio of about 40 which corresponds to the pressure ratio used by Franco et al. [5] and Sammak et al. [4]. A high EGT reduces the enthalpy drop per stage in the turbine (for a fixed number of stages) which will result in higher gas temperatures on the later stages and increased cooling demands. This can be handled either by increased cooling flow, which is the approach here, or increased cooling technology level. In the worst case more components have to be cooled. In the last two stages creep is also an important issue to be considered for high EGT and the realistic limit is probably around 640 °C – 650 °C but for completeness EGT's up to 680 °C has been investigated.

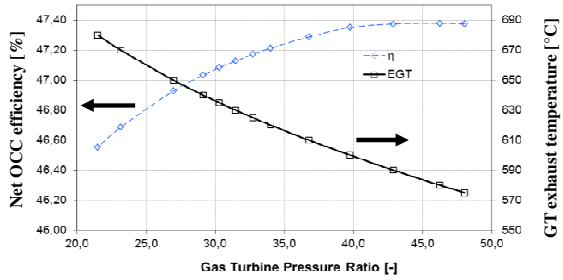


**Figure 1: OCC efficiency and EGT vs. GT pressure ratio**

Figure 1 shows that, when increasing the pressure ratio from 29.1 (corresponding to an EGT of 640 °C) to 42.9 (and an EGT of 590 °C) the efficiency increases by 0.34 %-points (from 47.03 % to 47.37 %). This increase in efficiency is not negligible, but the leap in pressure ratio from 29.1 to 42.9 is considered too large and therefore hard to motivate from a gas turbine design point of view. It could also be seen that the efficiency curve flattens out for pressure ratios above 40. That is due to the increasing SAS flows followed by rising temperatures through the rear part of the GT. Increasing PR would also require additional stages in both the compressor and turbine. Designing a GT for pressure ratios above 40 is challenging even for a conventional machine and normally requires a two-spool compressor configuration. Conventional GTs with high PR are e.g. RR Trent 60 (34), GE LMS100PB (44), LM 6000PG (35), Alstom GT26 (34) [10]. For an OCC that has a working fluid with much lower speed of sound, e.g. at 50 °C and 30bar, it is only 78 % of that for air (279 m/s compared to 360 m/s), a high-pressure ratio design would be an even tougher task for the compressor.

To facilitate the technical challenge for the compressor design a pressure ratio of 34 corresponding to an EGT of 620 °C is chosen. This generates temperature margins to include reheat in the steam cycle or possibility to increase steam admission temperature towards 600 °C. A lower pressure ratio in the top cycle releases potentially more enthalpy drop to be utilized in the steam cycle; a pressure ratio of 34 leaves 38 % of the power to be produced in the steam cycle. This figure is typically 33 % for conventional NGCC and hence the steam cycle efficiency will have a somewhat higher impact on the total efficiency. A lower pressure ratio also reduces the power needed for $O_2$ compression.

To summarize; the design choice regarding the temperature into the HRSG is based on total plant efficiency, GT pressure ratio and the temperature level through the GT stages, where additional cooling requirements are considered. Summarizing these aspects, the preferred choice is the case with a HRSG temperature of 620 °C, Figure 2. The temperature out of the flue gas condenser was considered in this investigation and will be further described in the following section.

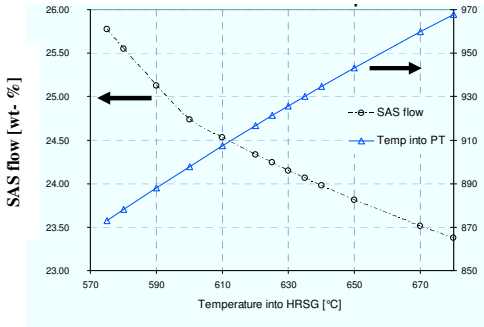


**Figure 2: Influence of different HRSG temperatures on the OCC for a constant HP steam temperature of 565 °C**

## TEMPERATURE OF THE RECIRCULATED FLUID

It is common fact that the output from a GT (and NGCC) decreases as the ambient temperature increases. The inlet temperature is a design parameter for an OCC since there is a dedicated cooling plant (more correctly, a flue gas condenser). This means that the inlet temperature to the GT can be controlled.

After the condenser only a small part corresponding to the $CO_2$ and steam formed in the combustion is bled off for further treatment prior to final $CO_2$ storage. The remaining part is cooled and dried before being recirculated back to the compressor inlet. Depending on the steam cycle configuration, number of pressure levels, reheat etc. the flue gas temperature after the HRSG varies from approximately 130 °C to 65 °C which is higher than what is preferable for the compressor inlet and therefore cooling is required. Recirculation of flue gases also introduces purification requirement and removal of impurities and moisture. The principle risk is concentration of detrimental substances that may be aggressive to the material as well as to prevent particles (e.g. soot) from clustering and plugging cooling holes.

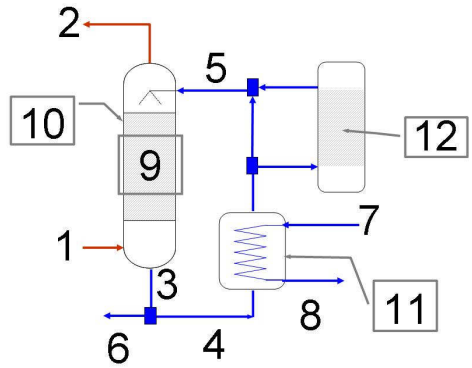


**Figure 3: Flue gas condenser**

**Table 3: Flue gas condenser**

| Nr | Description | Note |
|---|---|---|
| | ***Streams*** | |
| 1 | Flue gas inlet | From HRSG |
| 2 | Flue gas outlet | To pre-heater & GT inlet |
| 3 | Water outlet | Condensed water |
| 4 | Recirculated water | |
| 5 | Condenser spray | |
| 6 | Surplus water | Bleed off surplus water |
| 7 | External cooling inlet | |
| 8 | External cooling outlet | |
| | ***Aggregates*** | |
| 9 | Surface enhancing plates | Increase the area for cooling and condensing |
| 10 | Flue gas condenser | Acts as a scrubber as well |
| 11 | External cooler | |
| 12 | Water cleaner | Cleaning a part stream of the water |

The cooling and cleaning of the flue gas prior to recirculation can be treated relatively simply with a flue gas condenser that also acts as a scrubber, (the number in brackets corresponds to Figure 3). The proposed design of this flue gas condenser is to have a wet cooling tower {10} where recirculated water is sprayed in at the top {5}, where it interacts with the counter-current upward-flowing flue gas that is cooled down and condensed. The flue gas is fed into the bottom of the tower {1}, flowing up through surface-enhancing plates {9} where it condenses and is cooled below its water dew point. At the bottom of the tower both the cooling water and the flue gas condensate are collected {3}, cooled in an external seawater condenser {11} and the main stream is recirculated back to the

spray nozzles {5}. The condensing of the flue gas also acts as a scrubber and the recirculated water needs to be passed through a water treatment plant {12} before being recirculated to the spray nozzles to ensure high water quality. Only a part stream should be fed through the water treatment for size reasons. The flue gas condensate is drained from the cycle in the flue gas condenser {6}. A schematic sketch of a flue gas condenser which has to be designed to prevent from water carry-over is shown in Figure 3 and Table 3.

At the top of the flue gas condenser tower the flue gas is collected, {2}, led to a splitter where a part stream is bled off for CCS. The $CO_2$ compression train consists of a series of compressors and water-cooled intercoolers. The remaining flue gas is then recirculated back to the compressor inlet via a heat exchanger that heats the flue gas, to reduce RH down to 80 %. The reason for this preheating, although it adds compressor work and costs heat, is to prevent water droplets and corresponding corrosion and erosion of the first stages of the low pressure compressor. Another reason for preventing compressor inlet condensation is that the condensed water droplets turn the compressor itself into an effective scrubber. This means that minute levels of impurities can be enriched on the blading, causing severe corrosion attacks.

To evaluate the preferred temperature of the recirculated fluid, simulations covering the temperature range from 25 °C to 80 °C were performed. To ensure that the correct GT pressure ratio was selected the condenser temperature span (25 °C to 80 °C) was also included when exhaust gas temperatures from 590 °C to 640 °C were investigated. In all the simulations the total OCC net power was kept at 125.0 $MW_{net}$ by letting the GT's exhaust mass flow vary (approximately between 245 to 275 kg/s at GT outlet), see Figure 4 (d). The GT combustion outlet temperature (COT) was set to 1340 °C whilst the pressure ratio (and SAS flow) was allowed to vary. The results from this investigation are presented in Table 4 and Figure 4. HRSG temperatures (between 590 °C to 640 °C) other than 620 °C were regarded as undesirable since there was no efficiency gain and other aspects such as cooling, cost etc. favored neither high nor lower temperatures. The total cycle efficiency varies from 47.04 at 25 °C to 47.21 at 60 °C and then drops to 46.90 at 80 °C.

The preferred temperature of the recirculated flue gas from the condenser is dependent on a number of counteractive effects, the most important ones are:

***Increased Cooling***

**1.** *Reduced steam content*

1.1. Reduced specific compressor work

1.2. Reduces the heat load on the turbine hot section as the conductivity to viscosity ratio increases with water content.

1.3. Reduces turbine heat drop that increases the required GT pressure ratio as $H_2O$ has a higher isentropic exponent than $CO_2$.

**2.** *Colder GT inlet*

2.1. Reduced specific compressor work

2.2. Reduction in cooling fluid temperature and corresponding required cooling mass flow to the turbine as compressor discharge temperature is reduced.

2.3. Extended firing window (reduced compressor discharge temperature) and hence increased specific GT power (for constant gas composition).

***Reduced Cooling***

**3.** Less heat rejected from the cycle

**4.** Reduced size of the flue gas condenser.

All these points influence the cycle in one way or the other. Some of them reinforce each other while some counteract each other.

**Table 4: Effect on the OCC of condenser temperatures from 25°C to 80°C**

| Section | Unit | | | | | | | |
|---|---|---|---|---|---|---|---|---|
| Flue Gas Condenser Temp | [°C] | 25 | 30 | 40 | 50 | 60 | 70 | 80 |
| Net efficiency | [%] | 47.04 | 47.08 | 47.15 | 47.20 | 47.21 | 47.15 | 46.90 |
| Efficiency | [%] | 49.68 | 49.74 | 49.85 | 49.96 | 50.07 | 50.17 | 50.25 |
| No $CO_2$ treatment | | | | | | | | |
| Compressor (outlet) | | | | | | | | |
| P | [MW] | 82.8 | 85.2 | 90.3 | 95.6 | 101.4 | 107.7 | 114.8 |
| PR | [-] | 34.1 | 34.4 | 34.7 | 34.6 | 34.0 | 32.6 | 30.3 |
| m | [kg/s] | 236.5 | 237.5 | 238.6 | 238.2 | 235.3 | 228.5 | 215.9 |
| T | [°C] | 386.5 | 396.8 | 417.6 | 438.5 | 459.5 | 480.9 | 502.5 |
| High pressure turbine (inlet) | | | | | | | | |
| p | [bar] | 32.1 | 32.3 | 32.6 | 32.5 | 32.0 | 30.7 | 28.5 |
| m | [kg/s] | 212.8 | 213.6 | 214.8 | 214.6 | 212.4 | 207.0 | 196.7 |
| T | [°C] | 1340 | 1340 | 1340 | 1340 | 1340 | 1340 | 1340 |
| V | [m3/s] | 22.8 | 22.8 | 23.0 | 23.6 | 24.7 | 26.6 | 30.1 |
| Power turbine (inlet) temp | [°C] | 944 | 940 | 933 | 925 | 917 | 908 | 898 |
| Power turbine (outlet) | | | | | | | | |
| P | [MW] | 106.5 | 106.2 | 105.5 | 104.7 | 103.8 | 102.8 | 101.9 |
| p | [bar] | 1.08 | 1.08 | 1.08 | 1.08 | 1.08 | 1.08 | 1.08 |
| m | [kg/s] | 265 | 266 | 267 | 267 | 264 | 257 | 245 |
| T | [°C] | 620 | 620 | 620 | 620 | 620 | 620 | 620 |
| SAS* | [wt-%] | 24.76 | 24.67 | 24.52 | 24.40 | 24.33 | 24.34 | 24.48 |
| m fuel | [kg/s] | 5.714 | 5.709 | 5.701 | 5.695 | 5.693 | 5.701 | 5.731 |
| $O_2$** | [MW] | 29.47 | 29.49 | 29.50 | 29.46 | 29.35 | 29.16 | 28.91 |
| Bottoming cycle | | | | | | | | |
| P | [MW] | 59.9 | 60.3 | 61.2 | 62.1 | 63.2 | 64.3 | 65.8 |
| Q transferred in HRSG | [MW] | 163600 | 164700 | 167100 | 169700 | 172600 | 176100 | 180400 |
| $CO_2$ compression | [MW] | 7.01 | 7.05 | 7.15 | 7.31 | 7.56 | 8.00 | 8.93 |
| $H_2O$ content*** | [wt-%] | 6.87 | 7.24 | 8.36 | 10.29 | 13.53 | 18.95 | 28.29 |

* percent of HPT inlet mass flow
**ASU production cost [kW/kg $O_2$] +
compression from ASU delivery pressure to combustor pressure
*** water content at Low Pressure Compressor inlet

When increasing the cooling of the recirculated flue gas the gas properties change both regarding temperature and composition due to increased steam condensation. These effects reduce the specific compressor work i.e. more heat drop is available for the power turbine. With a colder compressor

working temperature, the temperature raise over the combustor is increased (given that COT is kept constant). However, less vapor content equals lower specific heat of the working fluid and hence less fuel is required to raise the temperature in the combustor per unit mass flow. A lower specific heat of the working medium also mean that more total mass flow is required for a given total plant power output, see Figure 4 (d).

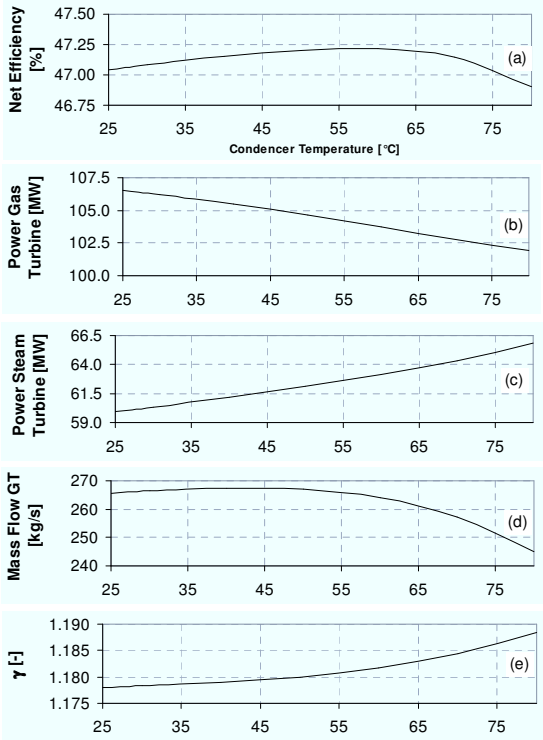


**Figure 4: Effect on the OCC of condenser temperatures from 25°C to 80°C**

The Secondary-Air-System (SAS) is affected by the condenser temperature due to the altering of the gas composition of the cooling flows, see Eq. (2). The fact that the SAS mass flow changes with changing working fluid also has a small impact on the pressure ratio. This is also due to the change in cooled turbine area generated by the differences in total volume flow between the cases with high and low moist content in the re-circulated gas.

Another remark is that there is a minor variation in the GT pressure ratio in the simulations in order to maintain the flue gas temperature to the HRSG inlet. The reason for this is that as the condenser temperature varies, so does the working fluid composition (primary the $H_2O$ content) and thereby the isentropic exponent ($\gamma$), see Figure 4 (e).

Seen from the perspective of net efficiency there is no clear performance optimum, but the preferred range is between 40 °C and 70 °C, see Figure 4 (a). This is not the only important parameter in an OCC design and considering performance, manufacturability, availability and working fluid composition the preferred choice of the recirculated working fluid is 60 °C. This temperature does not stretch the flue gas condenser or the compressor design too much and still the water content is maintained relatively low at compressor inlet (13.5 wt-%) which is preferred from both a GT cooling and a general mechanical strength perspective. The lowest temperature levels introduce an unfortunate cooling demand for the PT blading. The reason for this is the reduced specific compressor turbine work. This is not desirable from a design and robustness view since the PT should normally be designed for a longer life than the gas generator.

The overall effect is that more cooling shifts the power production towards the gas turbine, see Figure 4 (b), (c).

## COMPRESSION OF $CO_2$

Simulation of the $CO_2$ compression train is not within the scope of this work, however previous experience shows that several intercooling stages is to be preferred and the rejected heat is assumed not to be useful in the cycle, e.g. ENCAP and DECARBit suggested 3 stages with intercooling to 18 °C [11], [12]. A common approach is to specify the power consumption via a fixed cost in kW/kg wet $CO_2$ e.g. the ENCAP project [11], suggested a cost of 340 kW/kJ wet $CO_2$ for a delivery pressure of 110 bar. This method is not preferable in a study where the flue gas condenser temperature is investigated. This temperature has a direct influence on the wet $CO_2$ stream's mass flow and thus the assumed power consumptions even when the dry $CO_2$ mass flow is constant. Instead, the first compressor stage and intercooling with $H_2O$ separation was included in the calculations, to 3.5 bar, 40 °C and 3.06 wt-% $H_2O$ and from this condition, which is identical for all cases, to a final delivery state of 140 bar a fixed power consumption of 315 kW/kg wet $CO_2$ was used. The figure is not arbitrarily set and reflects current technologies. This cost excludes any treatment of impurities such as deoxidization that is necessary for Enhanced Oil Recovery (probably not required for other CCS technologies such as e.g. aquifer). Therefore, depending on the field of application for the $CO_2$ stream, there is room for improvements and/or variations in plant performance. To demonstrate the performance cost for the $CO_2$ treatment and enhance comparison of the cycle results, data for net cycle efficiency without $CO_2$ treatment/compression are presented as well ($\eta_{noCO2tre}$), Table 4.

## HRSG AND BOTTOMNING CYCLE DESIGN

As for the common natural gas fired combined cycle (NGCC) the OCC utilizes a heat recovery steam generator (HRSG) to recover energy from the GT exhaust. The concept is virtually the same as for a conventional NGCC, but as the cycle is semi-closed it would be possible to utilize a pressurized HRSG as suggested by Riethmann et al. [9] However, this will significantly add complexity and cost to the plant.

As was stated earlier in accordance with Bolland and Mathieu [7] and Yang et al. [3] the OCC has a rather flat efficiency optimum toward GT pressure ratio, see Figure 1. Therefore the pressure ratio was set to a lower value than would be optimum in an efficiency perspective. This reduced expansion in the GT, rendering a higher GT exhaust temperature for a fixed GT COT, and that relatively more power is produced in the bottoming cycle. With a higher exhaust temperature the need for multiple pressure levels is reduced. This is in accordance with the externally fired combined cycle which typically only utilizes one pressure level. The basic explanation for this is that when more energy is available above the evaporator pinch-point more steam is produced and hence the water flow through the economizer is higher. With a larger economizer flow more energy can be extracted below the pinch-point which is fixed for all design cases using the same evaporator pressure.

The major difference in the bottoming cycle from the conventional combined cycle is the flue gas properties of the OCC. First of all the density is higher, which will have a slight positive effect on the heat transfer compared to a convectional HRSG. Secondly, instead of nitrogen the OCC flue gas contains a large amount of $CO_2$ which is a more aggressive substance;, however it is not likely that under the prevailing circumstances this will require more expensive materials in the HRSG. More important for the layout and design of the bottoming cycle is that the specific heat ($c_p$) of the flue gas differs non-linearly compared to the conventional combined cycle.

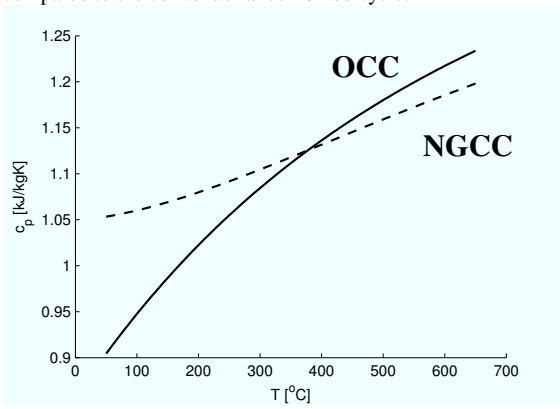


**Figure 5: Specific heat ($c_p$) vs. temperature for the OCC flue gas (solid line) and the conventional combined cycle (dashed line)**

Figure 5 shows that in the high temperature part of the HRSG the specific heat of the flue gas for the OCC is higher and hence more energy is available here. However, at lower temperatures the specific heat of the OCC drops and becomes significantly lower compared to the conventional combined cycle. This behavior will actually make it easier to achieve a high HRSG efficiency as the major limiting factor for good heat recovery is the economizer i.e. the low temperature part of the HRSG. The mass flow in the steam cycle is set by the amount of energy available in the evaporator and this mass flow is the only available heat sink in the economizer. If the specific heat is lower here the exit temperature of the flue gas will be lower according to Eq.3, 4.

$$\left( \dot{m} \cdot \int_{T_2}^{T_1} c_p \cdot dT \right)_{water} = \left( \dot{m} \cdot \int_{T_2}^{T_1} c_p \cdot dT \right)_{flue\ gas} \quad (3)$$

or

$$\left( \dot{m} \cdot \int_{T_{fw}}^{T_{evap}} c_p \cdot dT \right)_{water} = \left( \dot{m} \cdot \int_{T_{exit}}^{T_{evap}+T_{pp}} c_p \cdot dTc_p \right)_{flue\ gas} \quad (4)$$

For a single-pressure HRSG working below the gas turbine with 620 °C exhaust gas temperature (EGT), the HRSG exit temperature will be approximately 10 °C lower compared to flue gas produced by a typical air-breathing GT with the same EGT (132 °C vs. 141.5 °C). The corresponding figure for a dual-pressure HRSG is 6.5 °C (73.5 °C vs. 80 °C). For this particular case the power output is 7 % higher for the OCC steam cycle in the dual-pressure case and 8 % for the single-pressure case. The reason for the higher output is that more steam is produced in the high-pressure evaporator. The advantage is slightly less in the dual-pressure case since the conventional combined cycle produces more steam in the low-pressure part. This corresponds to what was expected from figure 3.

## SUMMARY OF PREFERRED CYCLE LAYOUT

The suggested 125 $MW_{net}$ OCC is shown in Appendix 1. It comprises a gas turbine using a combustor outlet temperature of 1340 °C and a pressure ratio of 34. This pressure ratio is somewhat lower than the optimum from an efficiency point of view; however the reduced pressure ratio significantly eases the compressor complexity. A lower pressure ratio makes more energy available for the bottoming cycle. For the proposed cycle 38 % of the power output is produced in the steam cycle which is higher than for the conventional combined cycle where typically 1/3 of the power is produced in the bottoming cycle.

The recirculated flue gas is cooled to 60 °C; further cooling will remove more moisture which is positive but it also rejects more heat from the cycle. The cooling is performed in a water scrubber which also will clean the gas stream.

The OCC flue gas behaves differently compared to the conventional combined cycle. In the HRSG the specific heat is higher at high temperatures while it is less at low temperatures. The result is that an OCC will achieve a better heat recovery compared to the conventional combined cycle. The advantage is smaller for multi-pressure steam cycles.

## DISCUSSION & CONCLUSION

The Semi-Closed Oxyfuel Combustion Combined Cycle is a competitive concept towards a $CO_2$ free and environmentally friendly power production. In order to gain market acceptance, the design has to provide competitive performance, robustness and simplicity – for maximum costumer value. It is also important to understand the market demand in terms of operability as this will have a major impact on the GT configuration concept and combustor design.

The optimum pressure ratio for the current cycle is found at about 45; however, the optimum is rather flat and choosing a pressure ratio of 34 only penalizes the cycle by 0.16 efficiency points. The lower pressure ratio renders a high exhaust gas temperature at 620 °C. This level is high but still within current last-stage design practice. It also provides a good opportunity for easy upgrades in the future by raising the HP-ST live steam temperature towards 590-600 °C, or by steam reheat.

It has been shown that in an efficiency perspective it is not preferable to cool the recirculated exhaust gases as far as possible (dictated by the heat sink). For this particular cycle the efficiency optimum is found at 60 °C. It is advantageous to design the scrubber/exhaust gas condenser with an overcapacity that will allow further cooling to handle peak loads.

Another finding is that the gas properties of OCC are well suited for the bottoming cycle. Compared to the conventional combined cycle more energy is available in the high-temperature region while the opposite is true in the low-temperature parts. The consequence is that a single-pressure bottoming cycle will achieve better HRSG efficiency than the standard combined cycle but the benefit is less for multiple pressure plants.

## ACKNOWLEDGMENTS

The authors would like to acknowledge Siemens Industrial Turbomachinery AB, Finspong, Sweden for the permission to publish this paper. Additionally the authors acknowledge all Siemens employees involved in the project.

## REFERENCES

[1] L. Strömberg, Lindgren G., Jacoby J., Giering R., Anheden M., Burchhardt U., Altmann H., Kluger F., Stamatelopoulos G.N., Update on Vattenfall's 30 MWth oxyfuel pilot plant in Schwarze Pumpe, Energy Procedia, Volume 1, Issue 1, February 2009, Pages 581-589, ISSN 1876-6102, 10.1016/j.egypro.2009.01.077.

[2] P. J. Cook, Demonstration and Deployment of Carbon Dioxide Capture and Storage in Australia, Energy Procedia, Volume 1, Issue 1, February 2009, Pages 3859-3866, ISSN 1876-6102, 10.1016/j.egypro.2009.02.188.

[3] H. J. Yang, D. W. Kang, J. H. Ahn, T. S. Kim "Evaluation of Design Performance of the Semi-Closed Oxy-Fuel Combustion Combined Cycle" ASME Turbo Expo GT2012-69141

[4] M. Sammak, Thorbergsson E., Gronstedt T., Genrup M. "Conceptual Mean-Line Design of Single and Twin-Shaft Oxy-Fuel Gas Turbine in a Semi-Closed Oxy-Fuel Combustion Combined Cycle" ASME Turbo Expo GT2012-69470

[5] Franco, F., Mina, T., Woolatt, G., Rost, M., Bolland, O., 2006, "Characteristics of Cycle Components for $CO_2$ Capture", Proceedings of 8th International Conference on Greenhouse Gas Control Technologies, Trondheim, Norway

[6] W. Sanz, Jericha H., Bauer B., Göttlich E., "Qualitative and Quantitative Comparison of Two Promising Oxy-Fuel Power Cycles for $CO_2$ Capture" ASME Turbo Expo GT2007-27375

[7] O. Bolland and Mathieu, P., Comparison of two $CO_2$ removal options in combined cycle power plants, Energy Conversion and Management, Volume 39, Issues 16–18, November–December 1998, Pages 1653-1663, ISSN 0196-8904, 10.1016/S0196-8904(98)00078-8.

[8] E. Thorbergsson, Gronstedt T., Sammak M., Genrup M. "A Comparative Analysis of Two Competing Mid-Size Oxy-Fuel Combustion Cycles" ASME Turbo Expo GT2012-69676

[9] T. Riethmann, Sander F., Span R, Modelling of a supercharged semi-closed oxyfuel combined cycle with $CO_2$ capture and analysis of the part-load behavior, Energy Procedia, Volume 1, Issue 1, February 2009, Pages 415-422, ISSN 1876-6102, 10.1016/j.egypro.2009.01.056.

[10] Gas Turbine World 2010 GTW Handbook, Volume 28

[11] N. A. Røkke, Langørgen Ø., Enabling pre-combustion plants—the DECARBit project, Energy Procedia, Volume 1, Issue 1, February 2009, Pages 1435-1442, ISSN 1876-6102, 10.1016/j.egypro.2009.01.188

[12] ENCAP - WP 1.1 Deliverable D1.1.1 & D1.1.2 Reference cases and guidelines for technology concepts Vattenfall A/S Report No.: 55431 Issue No. 4 pg.28 February 2008 Vattenfall A/S Report No. 55431, issue no. 4

[13] Grieb, H. "Projektierung von Turboflugtriebwerken" 2004, ISBN 978-3-7643-6023-8 F.J Bayley and J.M. Owen, "The Fluid Dynamics of a Shrouded Disk System With a Radial Outflow of Coolant", Journal of Engineering for Power Transactions of the ASME, July 1970 pp 335-340

[14] U. P. Phadke and J. M.Owen, "Aerodynamic aspects of the sealing of gasturbine rotor-stator Part 1: The behavior of simple shrouded rotating-disk systems in a quiescent environment" 1988, Int. J. Heat and Fluid Flow, Vol. 9 No.2, June 1988

**APPENDIX 1**

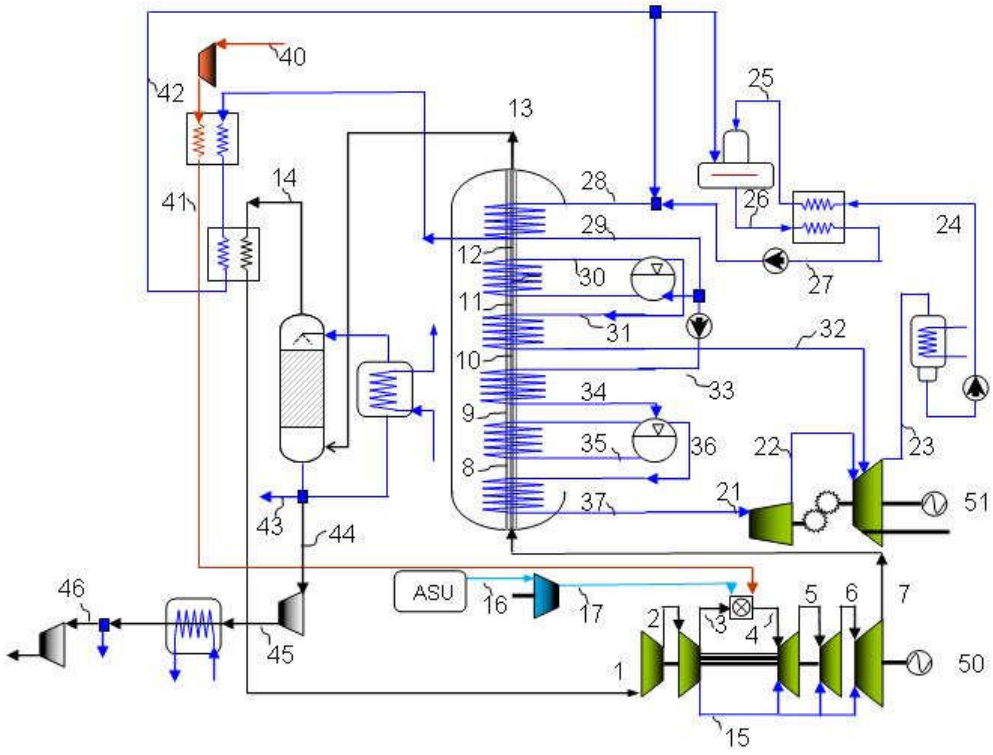


**Figure 6: OCC plant layout**

**Table 5: Summary of main parameters for the OCC concept**

**Temperature, pressure and mass flow**

| Nr | T [°C] | p [bar] | m [kg/s] |
|---|---|---|---|
| 1 | 63.76 | 0.991 | 235.1 |
| 2 | 246.0 | 6.50 | 235.1 |
| 3 | 460.2 | 33.9 | 183.7 |
| 4 | 1340 | 32.1 | 212.5 |
| 5 | 1074 | 13.8 | 243.9 |
| 6 | 917.1 | 6.89 | 260.9 |
| 7 | 620.0 | 1.08 | 263.9 |
| 8 | 507.7 | --- | --- |
| 9 | 322.7 | --- | --- |
| 10 | 206.7 | --- | --- |
| 11 | 205.2 | --- | --- |
| 12 | 159.8 | --- | --- |
| 13 | 66.20 | 1.04 | 263.9 |
| 14 | 60.00 | 1.04 | 235.1 |
| 15 | 460.2 | 33.9 | 51.40 |
| 16 | 30.00 | 1.20 | 23.10 |
| 17 | 576.2 | 33.4 | 23.10 |
| 21 | 565.0 | 100 | 45.41 |
| 22 | 288.1 | 13.7 | 45.41 |
| 23 | 31.00 | 0.0450 | 51.51 |
| 24 | 31.00 | 0.0450 | 51.51 |
| 25 | 31.00 | 4.00 | 51.51 |
| 26 | 105.0 | 1.21 | 67.22 |
| 27 | 58.40 | 1.21 | 67.22 |
| 28 | 61.30 | 13.5 | 74.95 |
| 29 | 146.9 | 5.00 | 74.95 |
| 30 | 151.8 | 5.00 | 30.52 |
| 31 | 151.9 | 5.00 | 6.104 |
| 32 | 180.7 | 4.33 | 6.104 |
| 33 | 149.0 | 108 | 45.41 |
| 34 | 309.8 | 105 | 45.41 |
| 35 | 314.0 | 105 | 315.6 |
| 36 | 314.8 | 105 | 45.41 |
| 37 | 566.2 | 103 | 45.41 |
| 40 | 15.00 | 30.0 | 5.694 |
| 41 | 120.0 | 37.1 | 5.694 |
| 42 | 85.00 | 5.00 | 7.736 |
| 43 | 60.00 | 1.01 | 10.56 |
| 44 | 60.00 | 1.04 | 18.24 |
| 45 | 184.4 | 3.50 | 18.24 |
| 46 | 40.00 | 3.50 | 16.75 |

**Power [$MW_{el}$]**

| Nr | Power [$MW_{el}$] |
|---|---|
| 50 | 103.8 |
| 51 | 63.16 |

**Composition [wt- %]**

| Nr | $CO_2$ | $H_2O$ | $N_2$ | Ar | $O_2$ |
|---|---|---|---|---|---|
| 1 | 84.28 | 9.004 | 2.811 | 3.800 | 0.1086 |
| 4 | 80.09 | 12.94 | 2.690 | 3.636 | 0.1039 |
| 7 | 80.91 | 12.64 | 2.700 | 3.648 | 0.1042 |
| 44 | 84.28 | 9.004 | 2.811 | 3.800 | 0.1086 |
| 46 | 91.79 | 0.8939 | 3.062 | 4.139 | 0.1182 |

Publication III

# Concept for a Combustion System in Oxy-fuel Gas Turbine Combined Cycles

Sundkvist, S.G., **Dahlquist, A.**, Janczewski, J., Sjoedin, M., Bysveen, M., Ditaranto, M., Langørgen, Ø., Seljeskog, M., Siljan, M.,

ASME Turbo Expo 2013, GT2013-94180

**Sven Gunnar Sundkvist**
Siemens Industrial Turbomachinery AB,
Finspong SE-612 83, Sweden
e-mail: sven-gunnar.sundkvist@siemens.com

**Adrian Dahlquist**
Siemens Industrial Turbomachinery AB,
Finspong SE-612 83, Sweden
e-mail: adrian.dahlquist@siemens.com

**Jacek Janczewski**
Siemens Industrial Turbomachinery AB,
Finspong SE-612 83, Sweden
e-mail: jacek.janczewski@siemens.com

**Mats Sjödin**[1]
Siemens Industrial Turbomachinery AB,
Finspong SE-612 83, Sweden
e-mail: mats.sjodin@siemens.com

**Marie Bysveen**
SINTEF Energi AS,
Trondheim NO-7465, Norway
e-mail: marie.bysveen@sintef.no

**Mario Ditaranto**
SINTEF Energi AS,
Trondheim NO-7465, Norway
e-mail: mario.ditaranto@sintef.no

**Øyvind Langørgen**
SINTEF Energi AS,
Trondheim NO-7465, Norway
e-mail: oyvind.langorgen@sintef.no

**Morten Seljeskog**
SINTEF Energi AS,
Trondheim NO-7465, Norway
e-mail: morten.seljeskog@sintef.no

**Martin Siljan**
Nebb Engineering AS,
Asker NO-1383, Norway
e-mail: martin.siljan@nebb.com

# Concept for a Combustion System in Oxyfuel Gas Turbine Combined Cycles

*A promising candidate for $CO_2$ neutral power production is semiclosed oxyfuel combustion combined cycles (SCOC-CC). Two alternative SCOC-CCs have been investigated both with recirculation of the working fluid (WF) ($CO_2$ and $H_2O$) but with different $H_2O$ content due to different conditions for condensation of water from the working fluid. The alternative with low moisture content in the recirculated working fluid has shown the highest thermodynamic potential and has been selected for further study. The necessity to use recirculated exhaust gas as the working fluid will make the design of the gas turbine quite different from a conventional gas turbine. For a combined cycle using a steam Rankine cycle as a bottoming cycle, it is vital that the temperature of the exhaust gas from the Brayton cycle is well-suited for steam generation that fits steam turbine live steam conditions. For oxyfuel gas turbines with a combustor outlet temperature of the same magnitude as conventional gas turbines, a much higher pressure ratio is required (close to twice the ratio as for a conventional gas turbine) in order to achieve a turbine outlet temperature suitable for combined cycle. Based on input from the optimized cycle calculations, a conceptual combustion system has been developed, where three different combustor feed streams can be controlled independently: the natural gas fuel, the oxidizer consisting mainly of oxygen plus some impurities, and the recirculated working fluid. This gives more flexibility compared to air-based gas turbines, but also introduces some design challenges. A key issue is how to maintain high combustion efficiency over the entire load range using as little oxidizer as possible and with emissions ($NO_x$, CO, unburnt hydrocarbons (UHC)) within given constraints. Other important challenges are related to combustion stability, heat transfer and cooling, and material integrity, all of which are much affected when going from air-based to oxygen-based gas turbine combustion. Matching with existing air-based burner and combustor designs has been done in order to use as much as possible of what is proven technology today. The selected stabilization concept, heat transfer evaluation, burner, and combustion chamber layout will be described. As a next step, the pilot burner will be tested both at atmospheric and high pressure conditions.* [DOI: 10.1115/1.4027296]

## Introduction

It is envisaged in the EU 2050 energy roadmap (published by the European Commission in Dec. 2011) that energy supply from electricity is assumed to grow significantly until 2050. It is also stated that 97–99% of electric power production from fossil fuels must be equipped with $CO_2$ capture by 2050.

The opportunities for near-term implementation of low and zero-emission fossil fuel power generation using carbon capture and storage (CCS) is emerging in niche markets. This is primarily motivated by regulations following a growing awareness regarding the potential impact of climate-change and partly the opportunities for use of carbon dioxide ($CO_2$) with enhanced oil recovery (EOR). However, there remain significant technology, engineering, investment, and political barriers that need to be overcome before CCS can be accepted as commercially mature for the power generation industry and the finance community.

One of the three main routes for CCS is the oxyfuel route. The literature regarding gas fired oxyfuel power plants is mainly referring to semiclosed oxyfuel combustion cycles and a modified Graz cycle variant [1]. SCOC-CC are promising candidates for CCS power plants due to their relative simplicity compared to other carbon capture cycles and their independence of chemicals.

These cycles are well suited for all types of pure hydrocarbon fuels such as natural gas and for gasified biomass or coal (syngas). The concept mainly includes turbomachinery equipment well known to utility companies and excludes chemical industry equipment.

A drawback of the oxyfuel concept is the need for an air separation unit (ASU) for the generation of oxygen. The ASU generates both high investment cost and a large foot print, and it also contributes significantly to a reduction in plant net efficiency due to its high energy consumption. However similar types of drawbacks appear in close to all other $CO_2$ capture concepts, e.g., post combustion capture concepts with monoethanolamine (MEA) scrubbing.

[1]Corresponding author.
Contributed by the Combustion and Fuels Committee of ASME for publication in the Journal of Engineering for Gas Turbines and Power. Manuscript received February 25, 2014; final manuscript received March 10, 2014; published online May 2, 2014. Assoc. Editor: David Wisler.

This paper presents results from a feasibility project called OXYGT (oxyfuel gas turbine combined cycle), the objective of which is to investigate the performance of a proposed commercial SCOC-CC in the 125 MW range. The objectives for the OXYGT phase 1 are (1) to assess the market potential for the oxyfuel technology including the produced $CO_2$, (2) to assess the technical and economic performance of the oxyfuel engine, and (3) to prepare for a demonstration of a natural gas fired oxyfueled gas turbine in a pilot plant. The overall objective for the whole oxyfuel project (phase 1–3) is to develop a natural gas fired oxyfuel combined cycle power plant concept (CCPP) for demonstration in a commercial scale power plant.

The development work in the project phase 1 is based on optimization of two slightly different oxyfuel power plant concepts with the aim to select one of them as a starting point for developing a concept for a combustion system in the selected SCOC-CC. The project is carried through in a partnership between a turbine manufacturer (Siemens), an engineering company (Nebb Engineering), two partners representing research institutes and academia (SINTEF, Lund University), and the funding organization Gassnova.

## Oxyfuel Plant Concept

The main idea behind oxyfuel cycles is to avoid mixing carbon dioxide with nitrogen ($N_2$), which complicates the carbon capture process. By using pure oxygen ($O_2$) instead of air in the combustion process, the combustion products can be reduced to mainly steam ($H_2O$) and $CO_2$. $CO_2$ can then be separated by simply condensing the steam downstream of the heat recovering unit.

The oxygen is generated in an air separation unit. There are three main techniques used in air separation units: cryogenic, membrane, or adsorption. For large scale $O_2$ generation, a cryogenic process is presently the only feasible choice, even if ionic transport membrane (ITM) based pilot plants are in operation today. It should be noted that with a cryogenic process, argon cannot be separated. A cryogenic process means that the gas components are separated by condensation at low temperatures obtained in a refrigeration process. In a cycle perspective, there might be possibilities to integrate the ASU process with the compression of $CO_2$ after the power plant. To reach the high pressures of the $CO_2$ (100–200 bar depending on storage conditions) and low temperatures that are required for final storage, the $CO_2$ will first be compressed to condensation pressure and then pumped to the final pressure.

It should be emphasized that oxyfuel power cycles are only suitable for carbon capture power plants and will never be able to compete with conventional power plant cycles in terms of efficiency and cost of electricity if $CO_2$ is not taxed or utilized as a commodity.

The SCOC-CC consists of a topping Brayton cycle and a bottoming Rankine cycle and has, therefore, obviously many similarities with a regular combined cycle power plant. This makes the SCOC-CC a promising candidate for carbon capture and storage due to its relative simplicity compared to other CCS concepts. It is mainly the topping gas turbine and the working fluid that differ from a conventional CCPP plant. First of all, the WF in the cycle is mainly $CO_2$ and $H_2O$ (diluted with small amounts of $O_2$, Ar, and $N_2$). Secondly, the combustion chamber is operated close to stoichiometric conditions with pure oxygen as the oxidizer. The combustion product that consists of $CO_2$ and $H_2O$ expands through the turbine. The turbine cooling is provided with a $CO_2$/$H_2O$ mixture as coolant extracted from the compressor.

The pressure ratio of the oxyfuel gas turbine is much higher (about 40) compared to a conventional combined cycle gas turbine (about 18) due to the relatively low specific heat ratio for $CO_2$. The heat recovery steam generator (HRSG) does not differ from the one in a regular CCPP in other ways than that the WF is $CO_2$/$H_2O$ instead of flue gas, nor does the steam cycle.

## The Oxyfuel Combustion Combined Cycle

The first of the two investigated and optimized semiclosed oxyfuel combustion combined cycles is very similar to a recirculated conventional combined cycle. It is named the oxyfuel combined cycle and has got the acronym OCC (see Fig. 1). The main difference, except from the working medium, is that the compression is mechanically divided into two compressors with different rotational speeds to manage to keep up efficiency for all compressor stages and to prove good working condition for the driving turbines. This solution is triggered by the high pressure ratios needed and the low speed of sound in the working medium.

After the HRSG, the exhaust gas is cooled below the dew point of $H_2O$ generating a liquid stream of water. The main part of the exhaust gas is recirculated to the compressor inlet, and the rest is bled off for treatment to export conditions. The bleed stream is compressed, intercooled, and separated into $CO_2$ and water, and the $CO_2$ is pumped to final storage pressure. Since the working medium is cooled down below the dew point of $H_2O$ before the recirculation, the compressor has to be protected from erosion of the inlet stages by reduction of the relative humidity in the stream.

The recycled gas will have a moisture content of about 15 vol. % before the condensation, and 7 vol. % after the condensation. This cycle has been simulated for two turbine inlet temperature (TIT) levels, 1340 °C and 1420 °C, but the following is mainly describing the 1340 °C version.

## The High Moisture Oxyfuel Combustion Cycle

The second investigated and optimized semiclosed oxyfuel combustion cycle is named the high moisture oxyfuel cycle and has got the acronym HMOC (see Fig. 2). This is a slightly more advanced cycle compared to the OCC but still similar to a recirculated conventional combined cycle plant. There are two main differences compared to the OCC:

(1) There is no cooling/condensation after the HRSG, but instead an intercooler is placed between the two compressors. This has three effects: first it will keep a high efficiency for all compressor stages, and second it will reduce the compressor work. Further, water is condensed out in the intercooler at elevated pressure, which enables utilization of the condensation energy in the bottoming Brayton cycle.
(2) The bleed is located between the compressors, generating a higher inlet pressure for the $CO_2$ compressor train. This saves at least one stage in the $CO_2$-compressor train.

The recycled gas will have a moisture content of about 40 vol. % before the condensation and 36 vol. % after the condensation.

## Method

The method used for the investigation and comparison of the two SCOC-CC cycles was to simulate them at a detailed level using process simulation tools (Siemens in-house tool KRAWAL that is used for tender calculations of combined cycle power plants, and the commercial tool HYSYS). First the plant boundary conditions and the performance characteristics of the individual components were specified for a fair comparison. Then the two cycles were simulated and optimized individually for maximum efficiency and manufacturability and compared to decide which concept would be the preferred choice for design regarding turbomachinery and combustor.

## Results

**Compressor Data.** Compressor data are shown in Table 1. For the OCC cycle, results from two slightly different design concepts are provided to show the tradeoffs in performance for an enhanced turbomachinery design of the gas turbine. The difference between these cycles is the gas turbine exhaust temperature, which is either 590 °C or 630 °C, referred to as OCC 590 and OCC 630.

It is seen that the HMOC compressor power requirement for generating an outlet pressure around 40 bar is higher than in the OCC 590 case, despite the latter having a higher outlet pressure

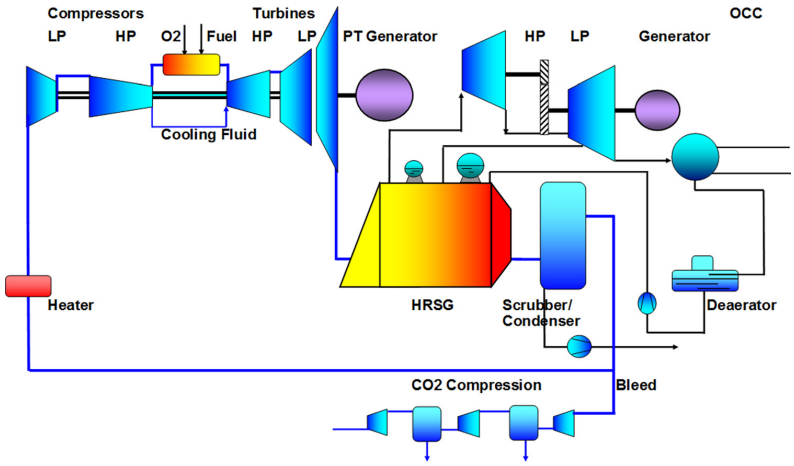


Fig. 1 Layout of the OCC

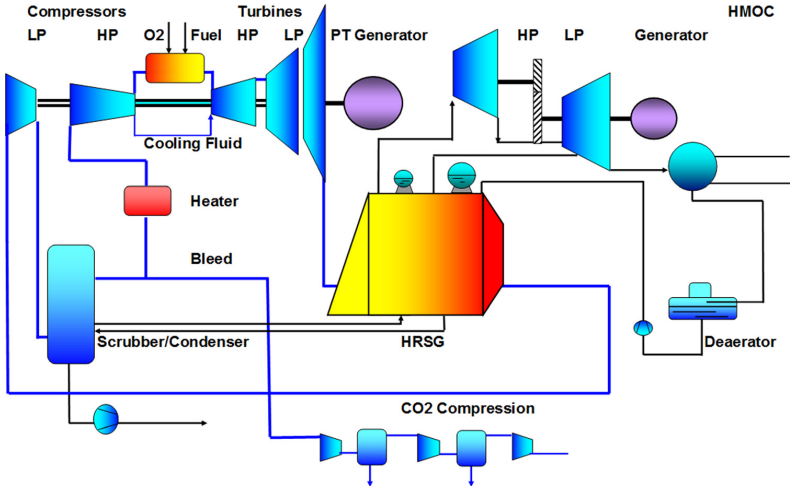


Fig. 2 Layout of the HMOC

Table 1 Compressor data

| | HMOC | OCC 590 | OCC 630 |
|---|---|---|---|
| GT compressor power (MW) | 108.45 | 104.18 | 87.73 |
| Compressor outlet pressure (bar) | 10 (after compr 1)<br>40 (after compr 2) | 46.99 | 34.69 |
| Compressor outlet temperature (°C) | 358 (after compr 1)<br>311 (after compr 2) | 460.5 | 418.8 |
| Compressor inlet temperature (°C) | 98 (compr 1)<br>136 (compr 2) | 43–44 | 43–44 |
| Mass flow rate (kg/s) | 230.1 (compr 1)<br>198.8 (compr 2) | 242.0 | 228.5 |

and that the HMOC compressor is intercooled. The main reasons for this high power consumption are probably that the compressor inlet temperature in the HMOC cycle is much higher, since no external cooling has been applied to the gas stream prior to the low pressure (LP) compressor inlet, and that the moisture content is relatively high due to the high media pressure and temperature in the cooling/extraction part of the cycle. Since the HMOC compressor is intercooled, one would expect that the required compressor power would be lower than for the OCC compressor. However, this could perhaps be partly offset by the fact that the

HMOC compressor also performs part of the $CO_2$ compression work that in the OCC is performed by the $CO_2$ compression train.

In the HMOC cycle, the bleed stream is extracted after the intercooler between the compressors, where the moisture content in the working fluid also is controlled. The water mole fraction in the LP compressor is 0.403 whereas in the high pressure (HP) compressor it is reduced to 0.359. The mass flow difference in the simulated case is 31.3 kg/s, which means that 31.3 kg/s excess water in the gaseous phase are compressed from atmospheric pressure to 10 bar in the LP compressor. This generates additional compressor work to be compensated for by the utilization of the heat of vaporization in the Rankine cycle.

The temperature in the cooling/extraction part of the OCC cycle should be >40 °C. The heater in front of the LP compressor raises the temperature to 43–44 °C, i.e., significantly lower than for the HMOC cycle. The slight preheating of 3–4 °C is included in order to reduce the relative humidity of the inlet stream down to 80% to avoid condensation in the compressor inlet.

**Power Generation Data.** Power generation data are shown in Table 2. As seen, the steam turbine power is more than 10 MW higher in the HMOC cycle than in any of the two OCC cycles due to utilization of the heat of vaporization in the Brayton cycle. Another effect of this is that the LP steam mass flow becomes very high in the HMOC cycle generating problems to use a one casing steam turbine train.

**Oxygen Production Data.** The ASU power is slightly higher and the $O_2$ compression power is slightly lower for the HMOC than for the OCCs, but there is no significant difference in the auxiliary power consumption for the different cycles (cf. Table 3).

## Oxyfuel Plant Concepts: Discussion and Conclusions

The preferred design of the SCOC-CC is the OCC cycle working with a flue gas temperature entering the HRSG of 630 °C. The OCC has clearly higher efficiency than the HMOC without any clear disadvantages in either design complexity or cost. The reduction in efficiency by changing the HRSG entry temperature from 590 °C to 630 °C is more than well-compensated by the enhancement in the turbomachinery design. The main reason for the lower efficiency of the HMOC ought to be found in how the cycle concept affects the gas turbine compressor work in addition to the lower temperature of the WF entering the combustion chamber. The choice of the design parameters for these cycles is triggered mainly by the following reasons:

- High pressure ratios are needed for this type of cycle but the experience of high pressure ratios is limited.

**Table 2 Power generation**

| | HMOC | OCC 590 | OCC 630 |
|---|---|---|---|
| Power turbine power (MW) | 98.54 | 106.6 | 101.0 |
| Power turbine inlet temperature (°C) | 879 | 912.3 | 948.8 |
| Steam turbine power (MW) | 70.46 | 55.28 | 58.57 |
| HP steam pressure (bar) | 66 | 95.0 | 92.0 |
| HP steam mass flow (kg/s) | 26.8 | 39.8 | 43.8 |
| LP steam pressure (bar) | 2.7 | 4.59 | 8.0 |
| LP steam mass flow (kg/s) | 74.0 | 7.23 | 4.42 |
| Plant Net efficiency (%) | 41.9 | 48.1 | 47.9 |

**Table 3 Oxygen production data**

| POWER (MW) | HMOC | OCC 590 | OCC 630 |
|---|---|---|---|
| ASU power | 17.57 | 16.65 | 16.72 |
| $O_2$ compression power | 11.82 | 14.05 | 12.34 |
| Sum | 29.39 | 30.70 | 29.06 |

- The efficiency versus pressure ratio gradient in the OCC cycle is not that steep, and a high oxyfuel turbine exhaust gas temperature can in the future be, to some extent, compensated for by high steam turbine inlet temperatures, around 600 °C. In this study, the live steam temperature was restricted to 565 °C due to present limitations of live steam temperature for this size of steam turbines.
- High pressure ratio also generates higher working media mass flow, which indicates that the specific work output is going down as pressure is increased.

A pressure ratio of about 35 is chosen as the most favorable for the future development of this concept. This generates a plant efficiency slightly below 48%. This is, according to the reasoning above, a suitable design point for the cycle, which limits the leaps in technology for an implementation of these ideas into hardware.

The increase in TIT from 1340 °C to 1420 °C emphasizes the need for really high pressure ratios, and still the Brayton cycle exhaust temperature tends to become too high to be efficiently utilized in the bottoming cycle. The increase in efficiency is very limited compared to the increased cost of the equipment and the increased maintenance of the Brayton cycle gas path parts. Designing the cycle for very high pressure ratios (about 50) for TIT 1420 °C is not justified by the gain in efficiency. Higher Brayton cycle TIT must include more innovative cycle solutions to be justified.

Some of the arguments from the OCC results are also valid for the HMOC. A pressure ratio of about 40 is chosen as the most favorable for the future development of the HMOC concept. This generates a plant efficiency slightly below 42%.

The opening statement that oxyfuel power cycles are only suitable for carbon capture plants and will never be able to compete with conventional power plant cycles in terms of efficiency is still valid. The calculated efficiency for the OCC close to 48% still keeps the question open if there is a market for this type of plant if $CO_2$ is a commodity. To generate such relatively high plant efficiencies from an oxyfuel power plant, the Brayton cycle equipment ought to be designed for a pressure ratio in the range of 35–40 combined with a TIT of 1340 °C. Design parameters in that range generate favorable plant performance if future developments of power plant equipment for this type of concepts are pursued. This statement is of course linked to the validity of the prerequisites. If breakthroughs in technology affecting the prerequisites are performed, these assumptions may change. To generate a better established view on the possibilities regarding this type of plant, the next step ought to be a more thorough investigation of the conditions in the rotating equipment regarding gas path design.

## Combustion Concept

The aim of the present work on the OXYGT combustion concept is to develop a design basis on how to arrange the different streams into the combustor matching both the requirements of flame stability, temperature level, and heat transfer, as well as complying with the relevant emission requirements. This is done using thermodynamic and chemical kinetic analysis both on a global basis and by reactor network representation of the combustor.

The combustor of the OXYGT gas turbine will have three inlet streams; the fuel which in the present work is natural gas, the working fluid from the compressor consisting mainly of $CO_2$ and $H_2O$ recycled from the exhaust, and the separate oxidizer stream from the ASU consisting mainly of oxygen. This means that a new burner and combustor concept have to be developed. The three-stream configuration seems to be more complicated than in the air-case. On the other hand, it also provides more freedom with respect to injection, mixing, and combustor operation over the gas turbine load range.

Combustion behavior studies relevant to the OXYGT gas turbine have been done theoretically using thermodynamic and chemical kinetic numerical tools (e.g., Refs. [2,3]), as well as experimentally at small scale (e.g., Refs. [4,5]). From these studies, some main challenges can be highlighted.

First, the combustor should preferably operate close to stoichiometric conditions in order to save costly oxygen. This may result in improper fuel burn-out and excessive CO emissions. This near stoichiometric combustion requirement is a large difference compared to traditional air-based gas turbines, which operate at large $O_2$ excess.

Next, the reactivity and flame stability in the primary zone are affected and will be highly dependent on the local ratio of oxygen to $CO_2$. The reactivity of a combustible mixture can be evaluated by the laminar flame speed $S_L$. As shown in Ref. [4], the laminar flame speed for stoichiometric combustion of methane in an $O_2$/$CO_2$ mixture is just around 10 cm/s when the volumetric $O_2$ concentration is as for air. This is only one-fourth compared to methane-air and implies higher possibility of poor flame stability. In order to achieve the same flame speed as for the air-case, the oxygen concentration in the $O_2$/$CO_2$ mixture has to be raised to about 38 vol. %. However, this also increases the adiabatic flame temperature to about 2110 K, being 160 K above the methane-air value. The challenge appears to be the trade-off between excessive local temperature and flame stabilization. Optimal design will need different oxygen/working fluid ratios in the different combustor zones in order to match the different temperature and stabilization requirements.

Further, in order to save energy in the ASU, the oxidizer stream will contain small amounts of impurities ($N_2$ and Ar). Nitrogen, combined with the possibility of local high temperatures in the flame zone, may generate thermal $NO_x$.

Finally, the heat transfer will be altered. The emissive power of the combustion products in oxyfuel combustion will be about five times higher compared to the air case. Heat transfer analysis of the gas turbine hot gas path [6] shows that for a SCOC-CC case at pressure ratio 40 and with recirculation after condensation, thermal radiation increases with 30% compared to a natural gas fired CCPP case at pressure ratio 17. The convective heat transfer may also be affected, depending on the final combustor design with respect to flow conditions, velocities, and cooling schemes.

## Combustor Representation and Simulation Tools

A schematic diagram of the model combustor is shown in Fig. 3. In the present combustion analysis model, the WF from the compressor can be split in three streams. One stream $a_1$ is going through the burner together with fuel and oxidizer. The stream $a_2$ is also fed to the primary zone while stream $a_3$ is the main dilution stream fed downstream the primary zone. One main target of the analysis is to evaluate the ratio between these WF streams.

The arrows $a_1$, $a_2$, and $a_3$ show the positions of the WF streams into the combustor. In addition, they are distributed evenly around the combustor circumferentially. The composition of the WF streams used in the combustion calculations is as given in Table 4. It contains mostly $CO_2$ plus some small amount of water vapor, argon, nitrogen, and a minor amount of oxygen. The arrow into the center of the burner shows the inlet position of the fuel stream. Its composition, as used in the combustion calculations, is given in Table 4. The fuel stream contains mainly methane with smaller amounts of ethane, propane, and nitrogen. The oxidizer stream inlet is indicated with an arrow, and its composition is given in Table 4 as well. In addition to oxygen, it contains some smaller amounts of nitrogen and argon.

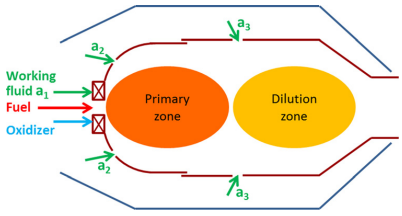


**Fig. 3 Schematic model of the combustor**

**Table 4 Inlet streams to the combustor section**

| Item | Unit | OCC | Base cases |
|---|---|---|---|
| *Fuel stream* | | | |
| $CH_4$ | vol. % | 92.6 | 92.6 |
| $C_2H_6$ | vol. % | 4.5 | 4.5 |
| $C_3H_8$ | vol. % | 2.2 | 2.2 |
| $N_2$ | vol. % | 0.7 | 0.7 |
| Temperature | °C | 10 | 10 |
| *Oxidizer stream* | | | |
| $O_2$ | vol. % | 95.0 | 95.0 |
| $N_2$ | vol. % | 2.0 | 2.0 |
| Ar | vol. % | 3.0 | 3.0 |
| Temperature | °C | 333 | 40 |
| *WF stream* | | | |
| $CO_2$ | vol. % | 90.3 | 100 |
| $H_2O$ | vol. % | 1.8 | 0 |
| Ar | vol. % | 5.1 | 0 |
| $N_2$ | vol. % | 2.7 | 0 |
| $O_2$ | vol. % | 0.06 | 0 |
| Temperature | °C | 422 | 25/400 |
| *Combustion chamber* | | | |
| Pressure | bar(a) | 37 (34[a]) | 1/5/2010/30/40 |
| TIT | °C | 1400 (1340[a]) | — |
| Equivalence ratio | – | 0.995 | 1.0 |
| $O_2$ excess | vol. % | 0.5 | 0 |

[a]Optimized cycle value.

The oxyfuel combined cycle was the preferred alternative from the cycle analysis, and data only for this cycle will be presented. In addition a base case has been analyzed to check the influence of the WF temperature and the effect of combustor pressure. For simplicity, this base case is run with pure $CO_2$ as WF as shown in Table 4.

The pressure and TIT deviate somewhat from the final optimized values in the cycle analysis. The combustion study has used preliminary data from the thermodynamic cycle analysis (37 bar/1400 °C) instead of the data from the optimized cycle analysis (34 bar/1340 °C) as the optimized cycle data were not available when the combustion calculations were started. It has been shown by a parametric variation on pressure and WF dilution that these deviations have no significant influence on the conclusions of the combustion analysis.

In the present report, the CHEMKIN-PRO combustion calculation package [7] has been used to calculate combustion properties. The software uses idealized homogeneous reactors as the basis. Inhomogeneity, flow effects, and incomplete mixing will not be reflected in the results. However, the results will give a good representation of the chemical kinetics and flame temperatures. By arranging several reactors in a reactor network, it is possible to mimic the combustor in a better way.

As a chemical kinetic reaction mechanism, the GRI-Mech 3.0 [8] has been used. It consists of 325 reactions and 53 species and is one of the most widely used mechanisms for gas combustion.

## Basic Combustion Properties

The adiabatic flame temperature $T_{ad}$ and the laminar flame speed $S_L$ are seen as the two most important combustion parameters with respect to evaluating the trade-off between flame temperature and flame stability. In the air-case, these parameters are commonly presented as a function of the mass of air to the mass of fuel ratio (AFR), which is a measure of the flame dilution.

In the present work, an equivalent term for oxyfuel combustion has been defined as the mass of the WF plus oxidant to the mass of fuel $(m_{WF} + m_{OX}) / m_F$. This term is named WOF ratio (WF plus oxidant to fuel) and analogous to the AFR. As long as the oxygen is supplied at least in stoichiometric proportion, the additional oxygen and WF act as a diluent to the flame in terms of

thermodynamics, whether it is $CO_2$ and $H_2O$ in the oxyfuel case or $N_2$ in the air case. The stoichiometric amount of oxygen for the fuel in Table 4 is 3.90 $kg_{O2}/kg_{fuel}$. The difference between the AFR and WOF ratio in order to achieve equal value of some combustion property is just a consequence of the different properties of the diluting components, e.g., such as $CO_2$ having higher heat capacity than $N_2$.

The laminar flame speed $S_L$ and adiabatic flame temperature $T_{ad}$ for the base case are shown in Figs. 4 and 5 as function of combustor pressure and WF inlet temperature versus dilution represented by the WOF ratio on the abscissa axis. In these calculations, the combustor is treated as a perfectly stirred reactor (PSR) without any flow splits.

For equal dilution and WF temperature, the laminar flame speed decreases with increasing pressure. Therefore, the oxyfuel case follows the general trend known from air-based systems. The difference in flame speed between the high and low pressure decreases when the WOF is increased. The flame speed difference between the 30 bar and the 40 bar cases is generally very small and in principle negligible at the higher WOF ratios.

The adiabatic flame temperature shows an increase with pressure for equal dilution and WF temperature. Also, here the difference between the 30 bar and 40 bar cases is very small and vanishes more or less completely at the higher WOF ratios.

## Combustor Flow Estimates From the Basic Properties

The laminar flame speed and the adiabatic flame temperature of the OCC case are shown in Fig. 6 as a function of dilution (WOF ratio). In this case, the pressure is 37 bar and both the WF and the oxidizer streams are at elevated temperatures as given in Table 4. The equivalence ratio is kept constant at 0.995 so the variation in WOF ratio is only caused by variation in the amount of WF.

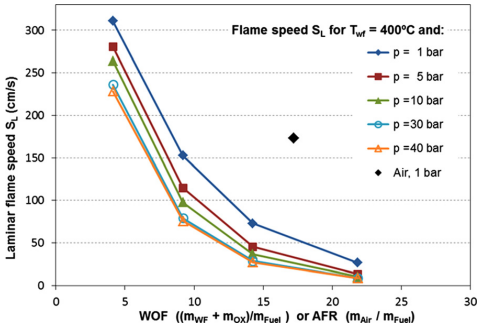


**Fig. 4 Laminar flame speed for the base case as a function of dilution with working fluid**

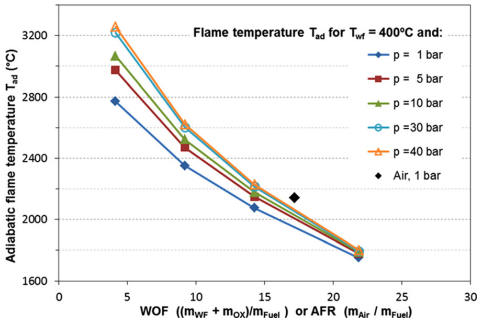


**Fig. 5 Adiabatic flame temperature for the base case as a function of dilution with working fluid**

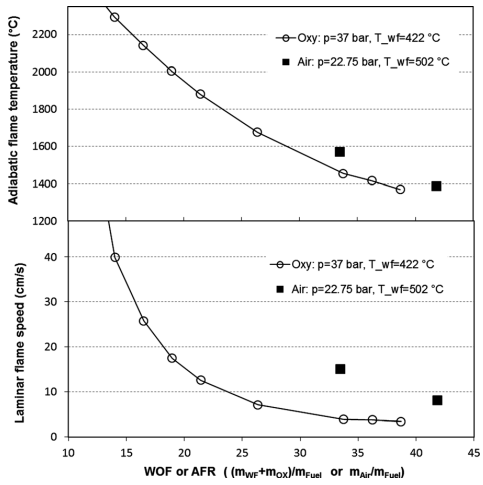


**Fig. 6 Adiabatic flame temperature (above) and laminar flame speed (below) for the OCC case as a function of dilution with working fluid and comparison with relevant data from an air case**

A representative gas turbine air case is also shown in the same figure as a function of AFR. The lower AFR point of 33.5 represents a lean primary flame zone, and the high AFR point of 41.8 represents the combustor outlet conditions. The fuel composition is the same as for the OCC case.

A first estimate on the WF flow split for the OCC combustor has been made based on a comparison between the adiabatic flame temperatures and the laminar flame speeds of the OCC case and the air case. First, the amount of dilution to the OCC combustor primary zone ($a_1 + a_2$ in Fig. 3) is found from the requirement of having the same laminar flame speed as the primary zone of the air case as indicated by the arrows in the lower part of Fig. 6. This will, however, create a much higher temperature compared to the air case but is nevertheless chosen as a starting point. The additional WF to be fed to the dilution zone ($a_3$ in Fig. 3) is decided from the requirement of having the same outlet temperature as the air case as indicated with arrows in the upper part of Fig. 6.

The results of this estimation are summarized in Table 5. Some important design issues can be highlighted: First, the WF split to the dilution zone ($a_3$ in Fig. 3) should be about half (0.52) of the total WF to the combustor.

**Table 5 Combustor flow estimates**

| | | Air case | Oxy case |
|---|---|---|---|
| Power input (fired heat) | MW | 260 | 260 |
| Fuel heat content (LHV) | MJ/kg | 48.3 | 48.3 |
| Fuel mass flow | kg/s | 5.4 | 5.4 |
| Combustor pressure | bar a | 22.75 | 37.0 |
| Air mass flow to PZ | kg/s | 179.9 | — |
| Working fluid mass flow to PZ | kg/s | — | 86.4 |
| Oxidizer mass flow to PZ | kg/s | — | 22.3 |
| Burnt mixture leaving PZ | kg/s | 185.2 | 114.1 |
| Burnt mixture leaving PZ | $m^3/s$ | 43.9 | 15.3 |
| Dilution stream (a3, air or WF) | kg/s | 45.0 | 94.8 |
| Air for dilution/air total | — | 0.20 | — |
| WF for dilution/WF total | — | — | 0.52 |
| Burnt mixture leaving combustor | kg/s | 230.2 | 208.8 |
| Burnt mixture leaving combustor | $m^3/s$ | 48.9 | 19.3 |
| Burnt mixture density | $kg/m^3$ | 4.7 | 10.8 |
| Burnt mixture sound speed | m/s | 789 | 633 |
| Burnt mixture Prandtl number | — | 0.81 | 0.86 |

The volumetric flow into the primary zone is much smaller for the OCC case than the air case. This may affect aerodynamics such as sizing of swirl and recirculation. The volumetric flow of burnt mixture out of the primary zone is just above one-third of the air case. The total volumetric flow out of the combustor is less than half of the air case.

It should be noted that the results from these estimates are highly dependent on the prerequisites made, the most important one being the laminar flame velocity in the primary zone (PZ). However, this calculation gives several insights into the complexity of converting a gas turbine from air to oxyfuel mode as exemplified below.

Even though the volumetric flow for the OCC case is much smaller than the air case, it does not necessarily imply a considerable reduction in size. One interesting exercise is to look at the Reynolds number at the combustor outlet for the air and OCC case in Table 5. The dynamic viscosity is nearly the same; about $5.9 \times 10^{-5}$ for both streams. If, as an example, the Reynolds number were to be kept constant for the two cases it would imply that $(V * D)_{OCC} = 0.43 * (V * D)_{air}$, where V is the flow velocity and D is the related flow diameter. The constraint giving equal Reynolds number for these two cases will then be $D_{OCC} = (D_{air}/0.43) * (VF_{OCC}/VF_{air})$, where $VF_{OCC}$ and $VF_{air}$ are the volumetric flows in the oxyfuel combined cycle case and the air case, respectively. For the volumetric flows given at the combustor outlet (i.e., "burnt mixture leaving combustor" in Table 5) this means that $D_{OCC} = 0.92 * D_{air}$. Therefore, the flow diameter for the OCC case should be only marginally smaller than for the air case if the Reynolds numbers were to be equal. In this case, the velocity of the OCC case must be about half of the air case meaning that the residence time will increase, something which may be beneficial for fuel and CO burn-out.

Under the constraint of equal Reynolds number, the Mach number for the OCC case would be just 58% of the air case at the combustor outlet. In order for the Mach numbers to be equal, the OCC diameter should be 0.7 times the air value. Because of the lower sound speed in the OCC case, the velocity will of course still be lower than the air case, but the Reynolds number will be about 31% higher.

The convective heat transfer coefficient increases with both the Reynolds and Prandtl number. An increase in Reynolds number would, thus, mean that the convective heat transfer would increase since the Prandtl numbers are fairly equal. This increase will add to the possible increase in thermal radiation.

## Reactor Network Calculations

A reactor network setup of the model combustor configuration in Fig. 3 was made in the CHEMKIN-PRO package. This gives a better representation of the combustor than one single PSR since the flow and chemistry interaction will be more realistic. The reactor network representation is shown in Fig. 7. The fuel, a share $a_1$ of the WF and most of the oxidizer stream (75%) are fed to a near burner mixing zone with short residence time. This zone is modeled as a PSR. A small portion (30%) of recirculated hot gas from the flame zone is also fed back to the mixing zone. Next follows the main flame zone, which is also modeled as a PSR. Here, the rest of the oxidizer is fed together with the share $a_2$ of the WF and 70% of the recirculated hot gas. 20% of the gas leaving the flame zone reactor is sent back as hot gas recirculation. Thereafter the dilution zone follows where the share $a_3$ of the WF is injected. No streams enter after the dilution zone. The next zone is a post dilution zone modeled as a plug flow reactor (PFR). Finally, the flow in the turbine stages is included in the model in order to take into account any slow chemistry. Since CO burn out is expected to be challenging in oxyfuel combustion due to the high concentrations of $CO_2$, the additional residence time in the turbine can affect the final composition at the gas turbine outlet. The turbine PFR has a gradual pressure and temperature decrease down to the turbine outlet conditions of about 630 °C and nearly atmospheric pressure.

The network calculations were done for a large range of WF splits with the purpose to find optimum values from an emission point of view and to verify whether these values match the estimated value of the $a_3$ share of about 0.5 found in the Combustor Flow Estimates From the Basic Properties section. The different values of $a_3$ calculated are 0.15, 0.25, 0.40, 0.60, and 0.80. For each of these $a_3$ values, the share between $a_1$ and $a_2$ were varied so that $a_1/(a_1 + a_2)$ went from 0.05 to 0.95.

For some cases, with low $a_1$ there is a very rapid ignition already in the mixing zone and the temperature immediately becomes very high. Except from this the results clearly indicate that the share between $a_1$ and $a_2$ is of minor importance compared to the variation in $a_3$. The rest of the results are, therefore, only for the cases where $a_1$ and $a_2$ are equal so that $a_1/(a_1 + a_2)$ is 0.5. For the species concentrations only the results downstream the dilution zone are shown. Then all the feed streams have entered the combustor and the concentrations are directly comparable. Concentrations are given as ppmv (parts per millions volumetric) without standard corrections as is normally done for air-based cases.

Figures 8 and 9 show the temperatures and CO concentrations. A high amount of WF in the primary zone (low $a_3$) gives low temperatures in the mixing and flame zone. On the contrary, a low amount of WF to the primary zone (high $a_3$) causes excessively high temperature in the flame zone. The CO in the dilution zone becomes high and so does the $O_2$ concentration (not shown here). As discussed in Ref. [1] this is probably due to the increased importance of the dissociation reactions of $H_2O$ and $CO_2$ at high temperatures, which results in higher emissions of CO and $O_2$. In addition this high flame zone temperature generates a considerable amount of $NO_x$, the level being around 800 ppm at the outlet.

The case that seems to give the best results is the one with $a_3$ equal to 0.4. It shows the lowest CO values, the temperature in the mixing zone indicates more rapid ignition than the other cases, and the flame zone temperature is below 1800 °C. The $NO_x$ concentration at the outlet (not shown here) is only about 2 ppm. Even though this case provides the lowest CO emission among

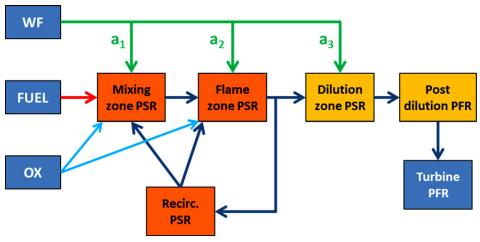


**Fig. 7 Reactor network representation of the model combustor**

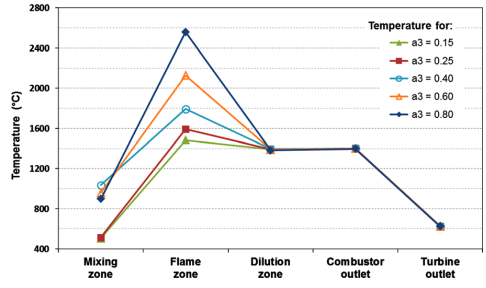


**Fig. 8 Temperature through combustor and turbine as a function of the working fluid share $a_3$ to the dilution**

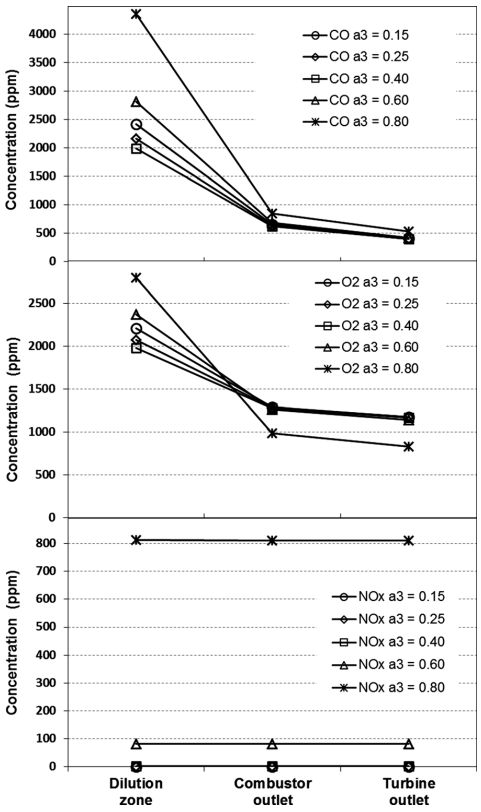


**Fig. 9 CO, $O_2$, and $NO_x$ concentration as a function of the working fluid share $a_3$ to the dilution zone**

the cases calculated here, the actual value of about 500 ppm is still rather high. In addition, the CO value is not at a stationary level at the outlet of the combustor and some CO oxidation continues through the turbine. This is not desirable.

Better CO burn-out can be achieved with higher $O_2$ excess. The case of $a_3 = 0.4$ has been run again but now with different oxygen excess, ranging from 0.5 vol. % to 5.2 vol. % (equivalence ratio from 0.995 to 0.95). In addition, the total amount of WF has been slightly increased in order to reduce the TIT from about 1400 °C as in the former case down to about 1340 °C, which is the value from the more optimized cycle.

The results are shown in Fig. 10. First, the increase in total WF contributes to a slight decrease in both temperature and CO as seen from the curves that are comparable with the results of Fig. 8 and Fig. 9 (excess $O_2$ equal to 0.5 vol. %). Next, the increase in $O_2$ excess reduces the CO significantly and less CO burn-out is happening in the turbine. However, the reduced CO comes at the cost of increased $O_2$ production in the ASU and $O_2$ emissions.

It should be noted again that the present calculations use idealized homogeneous reactors and the effects of inhomogeneity and incomplete mixing will not be captured. In the real case, it is likely that such effects will be present to some degree and most probably contribute to increased CO emissions. The combustion calculation package used in the present work (CHEMKIN-PRO) does have the possibility to use nonhomogeneous reactors where incomplete mixing can be taken into account through mixing models and choice of mixing parameters. This is a sensitivity study on its own and has not been included in the present paper but is relevant for further work.

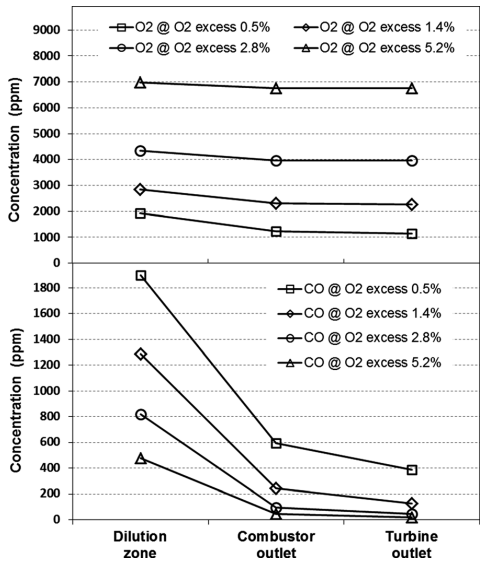


**Fig. 10 CO and $O_2$ concentration as a function of oxygen excess for the case with $a_3$ equal to 0.4**

## Overall Combustor Geometry

The concept of the test combustor incorporates features that have been gained from rules used in Siemens for design of gas turbine combustors. Similar design principles will be applied for both testing in the HP test rig at SINTEF and in an anticipated continuation in a project Phase 2 in a small scale gas turbine pilot plant at Lund University. Overall, the design scheme of the test combustor is shown in Fig. 11, which also shows the flow path of the working fluid.

The basic features of the OXYGT combustor are as follows:

- burner with radial swirler: swirl number close to the critical, i.e., the flame will be stabilized by the central recirculation zone
- fuel is injected through fuel pegs in the inlet to the radial swirl generator
- secondary fuel is injected axially in the center of the burner
- oxidizer ($O_2$) is mixed with the WF in a dome upstream the swirl generator with the help of a flow conditioner for a homogeneous mixture
- cylindrical combustion chamber (can or silo) with a smooth expansion (quarl) between the burner outlet and the flame tube
- combustor liner is cooled with the dilution portion of WF ($a_3$) by convection
- the dilution WF enters the hot gas duct in the transition part, which is also a mechanical connection to the outlet duct in the test rig and to the turbine nozzle guide vane in the pilot turbine

## Combustion Concept: Discussion and Conclusions

The OXYGT combustion concept has first been evaluated by a simplified approach matching the laminar flame speed and the adiabatic flame temperature of the oxyfuel case with a relevant reference air case. The results show that the WF split should be 0.48/0.52 through the burner and for dilution, respectively. In this case, the volumetric flow of burnt mixture out of the primary zone is just above one-third of the air case whereas the total volumetric flow out of the combustor is less than half of the air case.

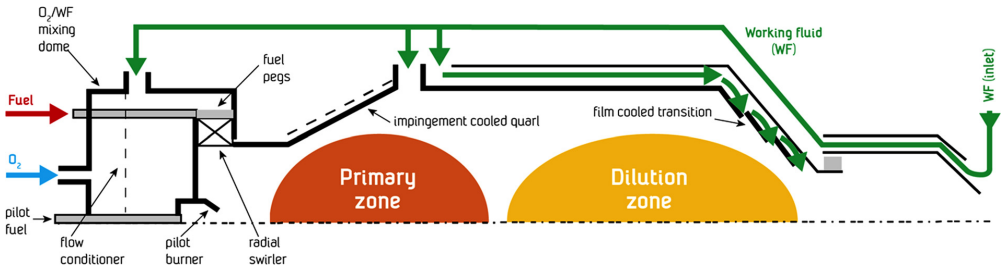


**Fig. 11 Overall design features of the OXYGT test combustor**

Reactor network calculations have been done to evaluate temperatures and emissions. In this analysis, it is found that the WF split should be around 0.6 through the burner and 0.4 for dilution. The flame zone temperature is below 1800 °C, and the $NO_x$ concentration at the combustor outlet is only about 2 ppm. A higher WF share through the burner would reduce the flame zone temperature further, but the laminar flame speed will then be low and flame stability will be affected.

CO burn-out is very dependent on the $O_2$ excess. At an $O_2$ excess of 0.5% compared to stoichiometric value, CO is 600 ppmv at the combustor outlet and 400 ppmv at the turbine outlet. At an $O_2$ excess of 5.2% the CO values are 43 and 20 ppmv at combustor and turbine outlet, respectively. In this case, a lot of extra $O_2$ has to be produced in the ASU, being costly in terms of efficiency loss.

It should be noted that in the oxyfuel case, the exhaust is not liberated to air but will go to storage or be used for EOR. There will be other requirements on the composition and values have been provided both from the Dynamis project [9] and from NETL [10]. The values from the reactor network analysis fall generally well within the given limits except for the CO limit given by NETL and for the $O_2$ concentration if the stream is to be used for EOR. The CO limit given by NETL is 35 ppmv and is just the time weighted average concentration. This seems to be a very stringent limit for the concentration within a pipeline since any leakage will be diluted, which is used as methodology by Dynamis. The Dynamis requirement of 2000 ppmv CO will be of no problem according to the reactor network analysis.

A schematic design of the OXYGT combustor has been provided. The burner will be swirl stabilized by radial swirlers, and there will be a cylindrical combustion chamber (can or silo) with a smooth expansion between burner outlet and the flame tube. The combustor liner is to be cooled with the dilution portion of the WF by convection. The next step will be to manufacture a burner–combustor arrangement that will be tested both at atmospheric and pressurized conditions in a dedicated oxyfuel test facility [11].

## Summary and Conclusions

The results from the cycle comparison show that the more straight forward OCC cycle with low steam content has a clearly higher efficiency (~48%) without any clear disadvantages in either design complexity or cost than the more advanced HMOC cycle with high steam content in the WF that generates a lower efficiency (~42%). The preferred design for the SCOC-CC is the OCC cycle working with a flue gas temperature entering the HRSG of 630 °C. There is a slight reduction in efficiency (0.2%) in the OCC by changing the HRSG entry temperature from 590 °C to 630 °C, but this is more than well compensated for by the enhancement in the turbomachinery design.

The main reason for the lower efficiency of the HMOC ought to be found in how the cycle concept affects the gas turbine compressor work, in addition to the lower temperature of the WF entering the combustion chamber. The LP compressor work is increased due to the higher temperature level at the compressor inlet and the ballast steam that is condensed and extracted after the LP compressor.

These drawbacks are not fully compensated by the reduced power consumption in the $CO_2$ compression train, the HP compressor, and the power generated from the heat of condensation in the LP steam cycle.

The general conclusion from this oxyfuel cycle comparison is that the OCC seems more promising from a number of reasons and that the future combustion development will be concentrated on this cycle.

The OXYGT combustor concept has been evaluated both by a simplified approach using laminar flame speed and flame temperature of an air case as basis and by more refined reactor network analysis using the CHEMKIN software package. The results indicate that the WF share going to the burner should be in the range 0.5–0.6, while the rest is used for dilution downstream of the primary flame zone. This WF fluid split gives the best compromise between flame zone temperature, flame zone laminar flame speed, and flame stability as well as emission levels. $NO_x$ emissions are low, about 2 ppm, while the CO emissions are very much dependent on the $O_2$ excess. An $O_2$ excess of 0.5% compared to stoichiometric value gives CO emissions of 400 ppm while an excess of 5.2% gives 20 ppm. This additional $O_2$ will imply higher duty on the ASU, which is costly in terms of efficiency.

The exhaust will be subject to storage or EOR. Compared to requirements and guidelines given by the EU project Dynamis and NETL of the US, the present numerical reactor network analysis falls generally well within the given limits except for the CO limit given by NETL and for the $O_2$ concentration if the stream is to be used for EOR.

A schematic design of the OXYGT combustor has been provided. The burner will be swirl stabilized and there will be a cylindrical combustion chamber. The combustor liner cooling will be provided by the dilution portion of the WF by convection. The next step will be to manufacture a burner and combustor arrangement that will be tested both at atmospheric and pressurized conditions in a dedicated oxyfuel test facility.

## Acknowledgment

The research leading to these results has received funding from the CLIMIT program in Norway through Project No. 212784 OXYGT, in addition to contribution from the partners. The authors acknowledge the partners SINTEF Energi AS, Siemens Industrial Turbomachinery AB, Siemens AS, Nebb Engineering AS, and Lund University.

## Nomenclature

AFR = air/fuel ratio
ASU = air separation unit

$a_1$, $a_2$, $a_3$ = stream split of WF
CCPP = combined cycle power plant
CCS = carbon capture and storage
D = diameter (m)
EOR = enhanced oil recovery
GT = gas turbine
HMOC = high moisture oxyfuel cycle
HP = high pressure
HRSG = heat recovery steam generator
ITM = ionic transport membrane
LHV = lower heating value (kJ/kg)
LP = low pressure
m = mass (kg)
MEA = monoethanolamine
$NO_x$ = nitrogen oxide
OCC = oxyfuel combined cycle
OX = oxidant
OXYGT = oxyfuel gas turbine cycle feasibility project
PFR = plug flow reactor
ppmv = parts per millions volumetric
PSR = perfectly stirred reactor
PZ = primary zone
Q = specific heat flow (kW/kg)
$S_L$ = laminar flame speed
SCOC-CC = semiclosed oxyfuel combustion combined cycle
T = temperature (°C)
TIT = turbine inlet temperature (°C)
UHC = unburnt hydrocarbons
V = velocity (m/s)
VF = volumetric flow ($m^3$/s)
WF = working fluid
WOF = ratio working fluid plus oxidant to fuel ratio

## Subscripts

ad = adiabatic
air = air stream
L = laminar
OCC = oxyfuel combined cycle
OX = oxidant

## References


[1] Jericha, H., Sanz, W., and Göttlich, E., 2006, "Design Concept for Large Output Graz Cycle Gas Turbines," ASME Paper No. GT2006–90032.
[2] Liu, C. Y., Chen, G., Sipöcz, N., Assadi, M., and Bai, X. S., 2012, "Characteristics of Oxy-Fuel Combustion in Gas Turbines," Appl. Energy, **89**(1), pp. 387–394.
[3] Hasegawa, T., 2012, "Combustion Performance in a Semiclosed Cycle Gas Turbine for IGCC Fired With CO-Rich Syngas and Oxy-Recirculated Exhaust Streams," ASME J. Eng. Gas Turbines Power, **134**(9), p. 091401.
[4] Ditaranto, M., and Hals, J., 2006, "Combustion Instabilities in Sudden Expansion Oxy-Fuel Flames," Combust. Flame, **146**(3), pp. 493–512.
[5] Kutne, P., Kapadia, B. K., Meier, W., and Aigner, M., 2011, "Experimental Analysis of the Combustion Behavior of Oxyfuel Flames in a Gas Turbine Model Combustor," Proc. Combust. Inst., **33**(2), pp. 3383–3390.
[6] Hammer, Th., Keyser, J., and Bolland, O., 2009, "Natural Gas Oxy-Fuel Cycles—Part 2: Heat Transfer Analysis of a Gas Turbine," Energy Procedia, **1**(1), pp. 557–564.
[7] Reaction Design, 2011, "CHEMKIN-Pro Release 15112 2011," http://www.reactiondesign.com/lobby/open/index.html
[8] GRI-Mech, 1999, "GRI-Mech Version 3.0 7/30/99 CHEMKIN Format," http://www.me.berkeley.edu/gri_mech/
[9] EU FP6 Project Dynamis, 2007, "Dynamis CO2 Quality Recommendations," Public Report No. 019672/D3.1.3.
[10] NETL, 2012, "CO2 Impurity Design Parameters," National Energy Technology Laboratory, Public Report No. DOE/NETL-341/011212.
[11] Ditaranto, M., 2011, "Description of a High Pressure Oxy-Fuel Combustion Facility HIPROX," 2nd Oxyfuel Combustion Conference, Yeepoon, Australia, September 12–16.

Publication IV

# The Influence from the Working Medium on the Profile Loss in Compressor and Turbine Airfoils

**Dahlquist, A.,** Thern, M., Genrup, M.,

ASME Turbo Expo 2014, GT2014-25069

**Proceedings of the ASME Turbo Expo 2014: Power for Land, Sea and Air**
**June 16-20, 2014, Düsseldorf, Germany**

**GT2014-25069**

# The influence from the working medium on the profile loss in compressor and turbine airfoils

**Adrian Dahlquist**

Siemens Industrial
Turbomachinery AB
SE-612 83 Finspong, Sweden
*Corresponding author.*
E-mail address:
Adrian.Dahlquist@siemens.com

**Marcus Thern**

Lund University
SE-221 00 Lund, Sweden

**Magnus Genrup**

Lund University
SE-221 00 Lund, Sweden

## ABSTRACT

A number of CCS-technologies are currently being developed for the reduction of $CO_2$ emissions from thermal power stations. One such technology is the oxyfuel process, in which a mixture of $CO_2$ and steam is used as the working medium. The semi-closed oxyfuel combustion combined cycle (SCOC-CC) is an oxyfuel cycle where the working medium mainly consists of $CO_2$ (85-95%).

Current practice is to design turbomachinery using 1D and 2D flow tools, which primarily rely on loss models derived from experiments with air. For the oxyfuel case, the losses are hence extrapolated from air to a $CO_2$/ steam mixture, which can have adverse effects on the accuracy of the loss model.

Therefore, the applicability and accuracy in using profile loss correlations derived with air when changing the working medium to the oxyfuel like environment of pure $CO_2$ was investigated. The reason that 100% $CO_2$ was chosen as the working medium and not a $CO_2$/ $H_2O$ mixture is that the water content present is relatively low and varies from case-to-case. Hence, a general water content could not be specified that was relevant for all cases. The study was done with typical compressor and turbine airfoils using a steady-state Navier-Stokes' 3D flow solver. This solver type can resolve the boundary layer ($y^+$ of about unity) rather than relying upon a boundary layer equation, - hence eliminating the latter as a source of error.

The hypothesis was that the profile loss depended on the viscosity, and that amendments to the viscosity would affect the profile loss. This trend was observed, e.g. when changing the working medium from air to $CO_2$, the profile loss coefficient ($Y_p$) for the compressor was reduced with 25% and for the turbine with 6%, respectively.

A slight difference in profile loss for an individual cascade was found when changing the working medium from air to $CO_2$. Theoretically, this difference leads to an increased mismatch of the stages downstream even at design point, and thus increases the losses and reduces the stability. However, the difference in profile loss is relatively small at the design point, and thus it is the authors' opinion that the practical effect will be quite small. Therefore, it is considered safe to use loss correlations derived from air for design point calculations even when the working medium is $CO_2$. However, there is a certain risk involved that air- based loss models are not capable of predicting the behavior over the full operating range, as the boundary layers risk to behave in a different manner.

Another aspect that was considered is how the wet surface area (physical size) of a turbomachine performing the same work ($m \cdot \Delta h_0$) will change between the two gases. This is important as the total profile loss in a whole compressor or turbine is directly proportional to this change. The conclusion was that the total wet area would increase by some 20% for $CO_2$ compared to air.

**Keywords:** $CO_2$, profile loss, oxyfuel, SCOC-CC, CCS

## NOMENCLATURE

| | |
|---|---|
| A | Speed of sound [m/s] |
| BL | Boundary layer |
| CCS | Carbon capture and sequestration |
| $C_d$ | Dimensionless boundary layer dissipation coefficient [-] |
| $c_p$ | Specific heat at constant pressure [kJ/kg·K] |
| EGR | Exhaust gas recirculation |
| h | Specific enthalpy [kJ/kg] |
| M | Molecular mass [g/mol] |
| m | Mass flow [kg/s] |
| Ma | Mach number [-] |
| P | Pressure [bar] |
| PR | Pressure ratio [-] |
| S | Entropy generation [kJ/K] |

| | |
|---|---|
| s | Specific entropy generation [kJ/kg·K] |
| SCOC-CC | Semi-closed oxyfuel combustion combined cycle |
| T | Temperature [K] |
| TR | Temperature ratio [-] |
| $u^*$ | Friction velocity [m/s] |
| V | Volume [$m^3$] |
| $w_{s,Area}$ | Specific work capacity per unit area [$kJ/m^2 \cdot s$] |
| x, y, z | Cartesian coordinates |
| Y | Distance from wall [m] |
| $y^+$ | Non-dimensional wall distance [-] |
| $Y_p$ | Pressure based profile loss coefficient [-] |

### SUBSCRIPT

| | |
|---|---|
| 0 | Total |
| in | Inlet/ upstream in the relative frame to the blade. E.g. stationary for a stator and relative to a blade. |
| out | Outlet/ downstream in the relative frame to the blade. E.g. stationary for a stator and relative to a blade. |
| Irrev | Irreversible |
| Chord | Blade chorda |

### GREEK SYMBOLS

| | |
|---|---|
| Γ | Isentropic exponent [-] |
| P | Density [$kg/m^3$] |
| ν | Kinematic viscosity [$m^2/s$] |
| μ | Dynamic viscosity [Pa·s] |
| $\tau_{wall}$ | Wall shear stress [Pa] |
| ∞ | Free stream |
| $\delta^*$ | Mass flow displacement thickness [-] |
| θ | Momentum flow displacement thickness [-] |
| λ | Thermal conductivity [W/m·K] |

## INTRODUCTION

The world is now entering an era where there is a large focus on managing global warming. To accomplish this, a key aspect is to reduce the man-made carbon dioxide emissions by using CCS technologies. Therefore several organizations around the world are developing oxyfuel technology to demonstrate its suitability and gain market acceptance [1], [2].

One such promising technology is the oxyfuel combustion process, wherein the fuel is combusted with pure oxygen to produce mainly carbon dioxide and water. This technology is commonly referred to as oxyfuel, or more specifically as e.g. a SCOC-CC [3] or a Graz cycle [4] when the technology is used in the context of a gas turbine. The process is "semi-closed" since the surplus carbon dioxide is, after condensation, extracted for after-treatment and final compression.

The SCOC-CC process is similar to an ordinary combined cycle process since it is using a conventional steam bottoming cycle. In the toping cycle, on the other hand, the working medium consists of mainly $CO_2$, some steam, and minor traces of other no condensable gasses. The $CO_2/H_2O$ ratio varies slightly depending on the setup of the power plant, i.e. the condensing temperature of the recirculated medium.

This working medium mixture is indeed very different from the medium in a conventional gas turbine. Therefore the applicability and accuracy in using profile-loss correlations derived with air when changing the working medium to the oxyfuel like environment of pure $CO_2$ was investigated. The reason that 100% $CO_2$ was chosen as the working medium and not a $CO_2/H_2O$ mixture is that the water content present is relatively low and varies from case-to-case. Hence, a general water content could not be specified that was relevant for all cases. Regarding the profile losses in turbomachinery design, with steam as the working medium, there is also a substantial amount of knowledge to acquire from design of steam turbines.

Previous studies have shown that, even when proper dimensionless numbers are being used in the characteristics, there is a certain difference in the behavior for different medium and its associated isentropic coefficients [5], [6]. R. Canepa and A. Satta [7] conducted numerical studies on the influence from exhaust gas recirculation (EGR). In their study, they found that the current turbomachinery components would still function well with 40% EGR. However the change in working medium composition with 40% EGR is far less then what present in an SCOC-CC, and the exact influence on the efficiency could not be drawn from this as the non-dimensional parameters of the stages were allowed to change with gas composition. In other studies, it has been concluded that there is for certain a need to conduct new designs of the turbomachinery when changing working medium as severely as from air to $CO_2$ [8].

All new designs of a turbomachinery equipment start with a process simulation to establish the overall design parameters for each gas turbine component. After this, the next step is to commence with a 1D and 2D aerodynamic design before being carried into the subsequent blade-to-blade environment, quasi 3D and finally, full 3D Navier-Stokes' solvers. Today it is still safe to state that most flow path features like stage loadings, flow coefficients, reaction, number of blades, wall hade angles, etc., are set very early in the design phase. Once the initial design phase has been completed, it is indeed costly to introduce any major changes to the design. The reason for this is that the detailed design, stress analysis and cooling design have commenced. It is therefore important that the initial 1D and 2D calculations are of a sufficiently high quality to ensure the right decisions are made at the start. Again, it is safe to claim that some 80 percent of the design is carried out in the first 20 percent of the time – hence a need for accurate loss models.

The 1D mid-span and the 2D through-flow solvers rely on correlations for predicting the losses and flow deviation. These correlations have historically been derived primarily from experimental tests (cascade tests) and secondarily from numerical calculations and test compressors/ turbines. These experiments have been carried out by utilizing air, and in some cases even steam or flue gas, as the working medium.

Some of the more prominent correlations are e.g. Dunham & Came [9], Kacker & Okapuu [10], Craig & Cox [11], Denton [12], Mamaev [13] and Wright and Miller [14]. This implies that there is a need to validate if these 1D/ 2D correlations are applicable to other gases as well, (e.g. $CO_2$), to ensure that the design can be optimized in 1D and 2D.

These correlations are, to a large extent, based on dimensionless numbers with the intention to make them universal. They are also derived using simplifications and assumptions that may render in problems when extrapolating into another working medium. Their validity has been investigated by examining the profile loss for different gas compositions. The invested gases were air, $CO_2$ and two fictive gasses modeled with either a high- or low dynamic viscosity, whilst keeping all other properties as for regular $CO_2$. The main gas properties for these gases are seen in Table 1-2.

Table 1: Summary of the main gas properties in the compressor

| Compressor at 70°C, 1 bar | | *Air* | *$CO_2$* | *High Viscosity* | *Low Viscosity* |
|---|---|---|---|---|---|
| Molar mass (M) | (g/mol) | 28.96 | 44.01 | 44.01 | 44.01 |
| Specific gas constant (R) | (J/kg·K) | 287.11 | 188.92 | 188.92 | 188.92 |
| Density ($\rho$) | (kg/m$^3$) | 1.02 | 1.55 | 1.55 | 1.55 |
| Speed of sound (a) | (m/s) | 371 | 286 | 286 | 286 |
| Specific Heat ($c_p$) | (kJ/kg·K) | 1.009 | 0.893 | 0.893 | 0.893 |
| Isentropic coefficient ($\gamma$) | (-) | 1.400 | 1.274 | 1.274 | 1.274 |
| Dynamic viscosity ($\mu$) | ($\mu$Pa·s) | 20.60 | 17.08 | 100.0 | 0.10 |

Table 2: Summary of the main gas properties in the turbine

| Turbine at 1000°C, 10 bar | | *Air* | *$CO_2$* | *High Viscosity* | *Low Viscosity* |
|---|---|---|---|---|---|
| Molar mass (M) | (g/mol) | 28.96 | 44.01 | 44.01 | 44.01 |
| Specific gas constant (R) | (J/kg·K) | 287.11 | 188.92 | 188.92 | 188.92 |
| Density ($\rho$) | (kg/m$^3$) | 2.71 | 4.15 | 4.15 | 4.15 |
| Speed of sound (a) | (m/s) | 697 | 532 | 532 | 532 |
| Specific Heat ($c_p$) | (kJ/kg·K) | 1.186 | 1.295 | 1.295 | 1.295 |
| Isentropic coefficient ($\gamma$) | (-) | 1.320 | 1.172 | 1.172 | 1.172 |
| Dynamic viscosity ($\mu$) | ($\mu$Pa·s) | 50.56 | 48.66 | 100.0 | 0.01 |

To assess the influence on the total profile loss in a turbomachine conducting the same total work with either air or $CO_2$ as working medium, the change in the physical component area facing the working medium (wet area) should be considered. This wet area is important as the total profile loss is directly proportional to this change. The wet area can be considered as proportional to the cross section area facing the working medium, hence used in the investigation.

## THE LOSS MECHANISM

This section gives a brief summary of the basic theory behind the loss mechanisms in the flow field. A common way to define efficiency, or rather its opposite, that is the loss, is to consider the entropy generation due to irreversible processes.

The entropy generation is always positive (or zero) when considering the whole system involved. A justifiable assumption is that a turbomachine can be considered to be an adiabatic process, i.e. the entropy generation can be simplified to depend only on the internal irreversible heat generation from kinetic energy dissipation by viscous shear, (Eq. 1) [15]. This mechanism is behind the more general processes concerned in turbomachinery flow, namely, viscous dissipation, mixing, heat transfer and shock waves.

Entropy generation per unit area in an adiabatic boundary layer

$$\dot{S} = \frac{d}{dx}\int_0^{\delta}\left(\rho V_x \cdot \left(s - s_{\delta}\right)\right)dy = \int_0^{\delta}\left(\frac{\tau_{y,x}}{T}\right)dV_x \qquad \text{Eq. 1}$$

The loss generation in the boundary layers of a turbulent flow occurs mainly in the inner BL region and to a minor extent in the outer BL region. That is because the velocity gradient and associated shear stress is considerably higher close to the wall ($0 \le y^+ \le 250$) and thus of great importance to the losses [15].

Denton [12] (1993) showed that a boundary layer dissipation coefficient ($C_d$) can be defined as shown in Eq. 2. Denton further proposed that $C_d$ is proportional to $Re_{\theta}^{-1/6}$ in turbulent flows and in the order of 0.002. This enables the entropy generation and the associated loss to be calculated for a known velocity profile.

Dimensionless boundary layer dissipation coefficient per unit area

$$C_d = \frac{T \cdot S_{irrev}}{\rho \cdot U_{\infty}^3} \qquad \text{Eq. 2}$$

The entropy generation results can be summed into a total pressure loss, which historically is what has been measured in experiments. The pressure-based profile loss is defined according to Eq. 3-4, depending on whether a compressor or turbine cascade is considered. The reference frame is relative to

the component considered, e.g. in the stationary frame for a stator and the relative frame for a rotor.

Pressure loss coefficient, compressor

$$Y_p \equiv \frac{p_{0in} - p_{0out}}{p_{0in} - p_{in}} = \frac{p_{0in} - p_{0out}}{\frac{1}{2} \cdot p_{in} \cdot \gamma \cdot M_{in}^2} \qquad \text{Eq. 3}$$

Pressure loss coefficient, turbine

$$Y_p \equiv \frac{p_{0in} - p_{0out}}{p_{0out} - p_{out}} = \frac{p_{0in} - p_{0out}}{\frac{1}{2} \cdot p_{out} \cdot \gamma \cdot M_{out}^2} \qquad \text{Eq. 4}$$

It is interesting to note that the denominator scales directly against both Mach number squared and the isentropic coefficient. One can thus expect that for an isentropic Mach number profile, the lower isentropic coefficient for $CO_2$ will lead to a higher pressure loss coefficient ($Y_p$).

## METHOD

***Geometry:*** The approach in this study was to design typical mid-span sections for both a compressor and a turbine airfoil by using in-house 2D blade-to-blade generation programs. These 2D sections were designed carefully to obtain aerodynamic profiles of high quality that were representative for respective turbomachinery component.

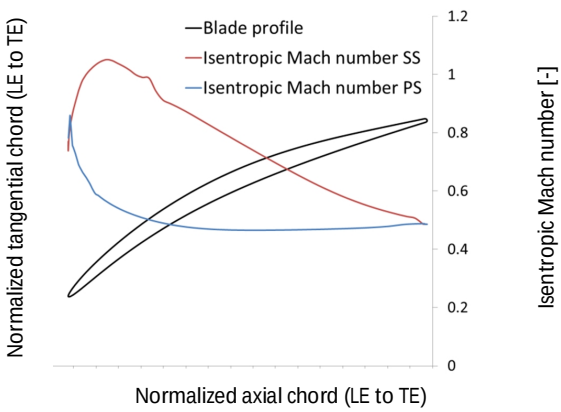


Figure 1: A typical section for a compressor cascade and its corresponding isentropic Mach number obtained from a Mises solver (red suction-side, blue pressure-side). Air as working medium

The compressor was designed to represent a typical second stage compressor vane with consequently a relatively high inlet Mach number (0.75- 0.80). The relatively high inlet Mach number makes it appropriate to design the blade with a weak shock close to the blade leading edge, in order to leave space for the controlled diffusion process towards the trailing edge. The cross section of the 2D compressor section is seen in Fig. 1 together with its isentropic Mach number profile. A 2D plot over the isentropic Mach number is seen in Fig. 2. This 2D plot of the compressor is obtained from a Mises solver which is a 2D blade-to-blade solver developed by Mark Drela, at MIT [16]. The small velocity discontinuity is due to the shock.

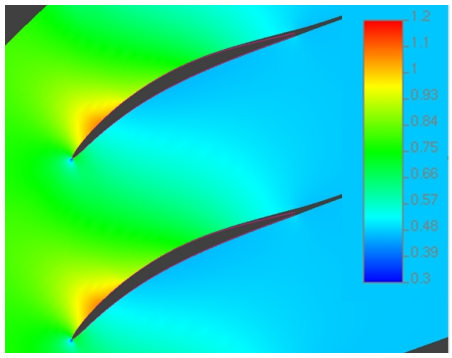


Figure 2: 2D Mach number profile of the compressor operating with air obtained from a Mises solver

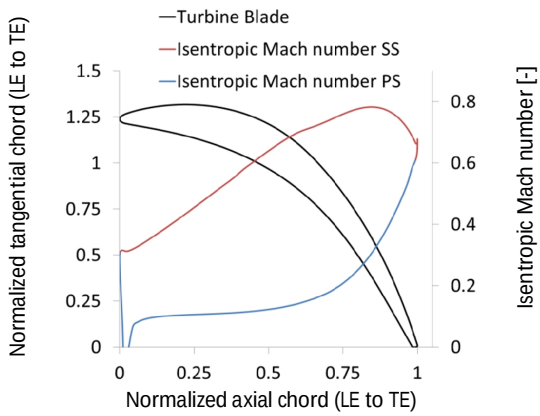


Figure 3: A typical section for a turbine cascade and the corresponding isentropic Mach number obtained from a Navier-Stokes´ solver (red suction-side, blue pressure-side). Flue gas as working medium

A typical LP turbine section can be seen in Fig. 3, 4 where the isentropic Mach number for conventional flue gas is shown. This 2D plot of the turbine is obtained from a 2D blade-to-

blade Navier-Stokes' solver. This subsonic turbine cascade, with a moderate inlet temperature (1000℃) and pressure (10 bar(a)), represents a typical low pressure or power turbine inlet guide vane. These sections were then extruded to straight 3D cascades in order to simulate a traditional linear test cascade where the flow is primarily two-dimensional.

***Mesh:*** The cascades were imported and meshed in Turbogrid™ version 14.5 [17]. The focus was to generate a high-fidelity mesh ($y^+$ on the order of unity) in the 2D blade-to-blade plane as the studied flow phenomena occur in this x-θ-plane. The mesh was a structured mesh of quadrilaterals/ hexahedral cells (Fig. 4 and 5).

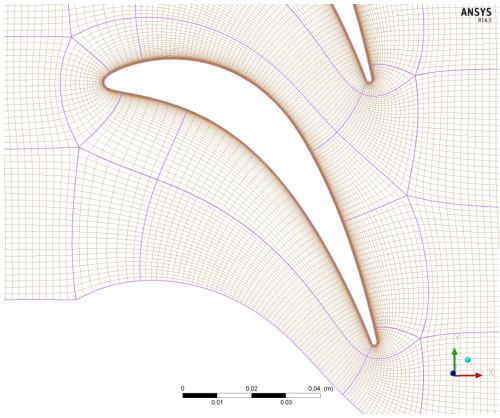


Figure 4: 2D mesh of the turbine cascade

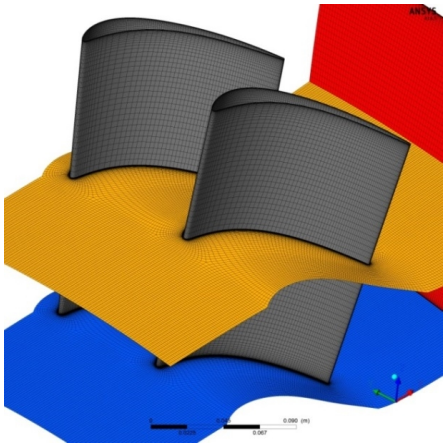

Figure 5: 3D mesh of the turbine cascade

The major part of the differences between the working medium was expected to be the viscous shear loss occurring in the inner boundary layers close to the blade. In order to capture this effect, no boundary layer equations (or wall functions) were used. Instead, the boundary layer was resolved down to the viscous sublayer by refining the mesh down to a $y^+$ on the order of unity along the blade (Fig. 6, 7), and from there applying a gradual expansion ratio of the mesh.

The mesh in the radial span-wise direction (r-axis) was coarser and the boundary layer at the end-walls (hub and casing) was not quite as finely resolved as these regions were excluded in this study.

In Figure 6-7, the mid-span variation in $y^+$ over the blades is shown for the different gases. The figures show that the boundary layer was sufficiently resolved for air, $CO_2$ and the high-viscosity case ($y^+$ read at left y-axis). This means that for the same mesh, the fictive low-viscosity case has $y^+$ values about a factor of 100 to 1000 larger (see $y^+$ at the right y-axis in figure 6, 7).

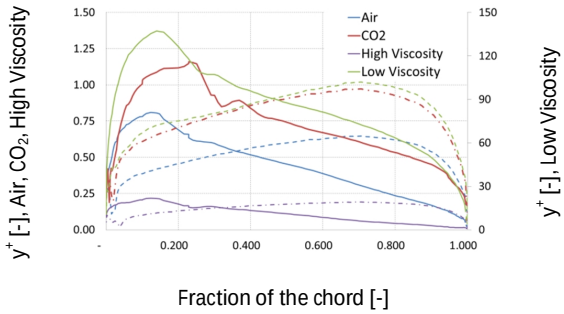


Figure 6: Variation in $y^+$ over the blade mid-span for the compressor obtained from CFX solver. Solid line suction-side, dotted line pressure-side.

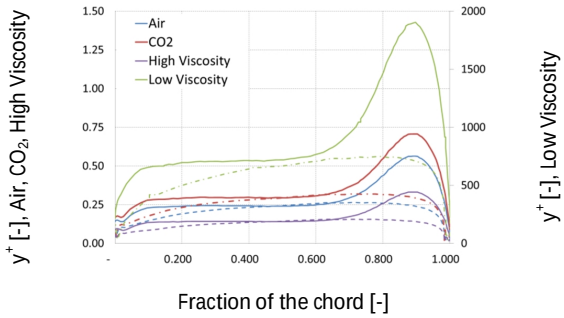


Figure 7: Variation in $y^+$ over the blade mid-span for the turbine obtained from CFX solver. Solid line suction-side, dotted line pressure-side.

The reason for this is that $y^+$ is defined as the ratio of friction velocity times the distance to the wall over the kinematic viscosity, and is therefore inversely proportional to the viscosity according to Eq. 5.

The friction viscosity is defined as the square root of the ratio of the wall shear stress ( $\tau_{wall}$ ) to density ( $\rho$ ), Eq. 6. This implies that when the viscosity approaches small numbers (close to zero), an impracticable fine mesh would be required to achieve $y^+$ in the order of unity. At these very low values of the viscosity, the flow is approaching an inviscid flow with infinitely thin boundary layers and an associated minimal viscous loss.

Non-dimensional wall distance $y^+$

$$y^+ \equiv \frac{u_* \cdot y}{\mu / \rho} \qquad \text{Eq. 5}$$

Friction velocity u*

$$u_* \equiv \sqrt{\frac{\tau_{wall}}{\rho_{wall}}} \qquad \text{Eq. 6}$$

***Pre-processor and flow solver setup:*** The pre-processor and flow solver used was CFX 14.5 [17], and the gas properties were from NIST REFPROP [18] using their standard recommended set of equations. The setup of the boundary conditions was consistent with the design condition used for creating the profile of the 2D sections. The total pressure, total temperature and turbulence intensity etc., were kept constant for all cases.

The blade surface was simulated as a smooth adiabatic no-slip surface while the end-walls were simulated as smooth adiabatic free-slip surfaces. The reason for the free-slip condition was to avoid disturbing the 2D flow field neither with secondary flow effects nor with corner stall.

In order to keep the same flow field (e.g. isentropic Mach number), the inlet- and exit-Mach numbers were held constant for the compressor and turbine, respectively. The rationale behind this approach was to be able to compare with the loss models. One could argue that this is only one part of the issue and that one could instead consider keeping the Reynolds number constant. The Mach number approach, however, is more like a real design case. Most organizations have design recommendations and it is quite common to e.g. favor turbine designs at relative exit Mach numbers close to 0.9. The loss coefficient itself will typically have the minimum loss at a relative exit Mach number slightly less that unity. The influence (such as row entropy rise) is a function of the Mach number squared, and it is therefore beneficial to design for the mentioned level. A lower value will result in a lower loss level at the expense of an expensive turbine with increased stage count.

***Post-processing:*** The data were post-processed in CFX-post 14.5 [17]. The results of particular interest are the pressure-based loss coefficients ($Y_p$). One question, however, was then how to calculate the loss in an accurate and comparable manner. The chosen approach was to create a tangentially narrow section at the mid-span of a cascade, far away from interfering secondary- and clearance-flows. The properties (e.g. pressure, Mach number) were mass-average weighted over these sections.

One can argue against this method, simply due to the fact that the streamlines skew radially from the inlet to outlet. Hence, not exactly the same streamlines were passing through both sections. As the streamline skew between the suction- and pressure side was moderate, and as this method is similar to the traditional method that was used in a set of experiments, has led to use of this method.

***Cross section flow area:*** The influence from the working medium on the cross section area was investigated through a theoretical approach. The approach was to derive an equation describing how the effective cross section flow area has to changes to obtain the same change in mass flow times total enthalpy drop ( $m \cdot \Delta h_0$). This equation considers both the change in mass flow for a constant cross section area and the change in potential enthalpy drop with pressure ratio. The derivation was based on isentropic flow relations and conducted for constant values of Mach number, and finally evaluated for with typical low pressure turbine values.

## RESULTS

***Pressure loss coefficient:*** The variations in dynamic viscosity for air and $CO_2$ with respect to the temperature are shown in Fig. 8. The two graphs follow each other fairly well so that the absolute difference (2.1- to 3.6- $10^{-6}$ Pa·s) is quite constant over the entire temperature range.

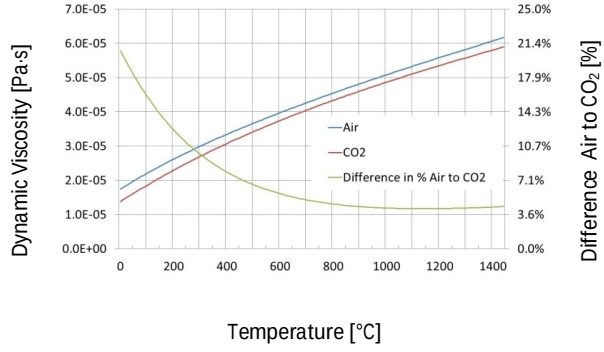


Figure 8: Variation in dynamic viscosity ($\mu$) for $CO_2$ and air with temperature at 10 bar(a)

This relatively constant absolute difference leads, on the other hand, to the relative difference varying more and increasing at the lower temperature range. As an example, the variation in relative difference ranges from 20% at 0°C down to 4% at temperatures above 1000°C.

This leads one to expect to see a greater impact on the profile loss operating at low temperatures, as present naturally in a compressor compared to a turbine.

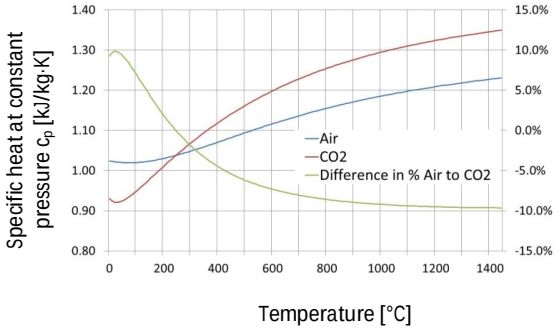


Figure 9: Variation in specific heat ($c_p$) for $CO_2$ and air with temperature at 10 bar(a)

The variation in specific heat ($c_p$) as a function of temperature at 10 bar(a) is shown in Fig. 9 for air and $CO_2$, respectively. The specific heat temperature dependency was quite different compared to the viscosity. The specific heat ($c_p$) values showed a rather large variation, and the lines even intersected at approximately 300°C.

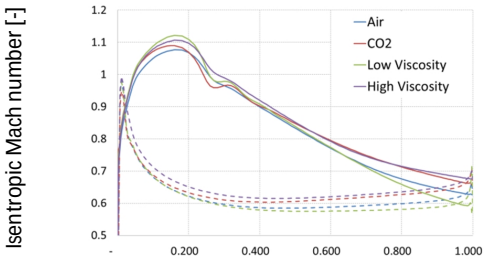


Figure 10: Isentropic Mach number at compressor blade mid-span for the four different cases, air, $CO_2$ high viscosity and low viscosity obtained from CFX solver. Solid line suction-side, dotted line pressure-side.

The isentropic Mach number over the compressor blade is shown in Fig. 10. The intention here was to maintain the same inlet Mach number and hence the velocity profile for all gases. The velocity profiles are similar but some minute spread can be seen, e.g. a slight variation in peak Mach number at the throat. Theses variations are primarily due to the minor differences in how much the boundary layer is growing due to the gas properties, which affects the effective flow area. The main parameters for the compressor cascade are summarized in Table 3 where, e.g., the profile loss for the different gases is seen.

Table 3: Summary of the main result parameters for the four gases at mid-span, compressor cascade obtained from CFX solver

| Compressor Results | | *Air* | *CO2* | *High Viscosity* | *Low Viscosity* |
|---|---|---|---|---|---|
| Inlet Mach number (Ma) | (-) | 0.77 | 0.78 | 0.79 | 0.79 |
| Outlet Mach number (Ma) | (-) | 0.49 | 0.51 | 0.52 | 0.49 |
| Mass flow per unit area | (kg/s·m$^2$) | 367.7 | 446.3 | 373.3 | 363.2 |
| $Re_{chord}$ $10^6$ | (-) | 2.14 | 3.08 | 0.485 | 485 |
| Profile loss coefficient (Yp) | (-) | 1.35 | 1.01 | 2.31 | 0.68 |
| Average blade wall shear | (Pa) | 111.7 | 103.3 | 153.5 | 45.9 |

The isentropic Mach number profile for the turbine vane was kept constant for all the gases by varying the static pressure downstream. The isentropic Mach number profile is typical for a common aft-loaded low-pressure turbine or power-turbine vane design with pure axial inlet flow. The aft-loaded profile, shown in Fig. 11, begins with a steady continuous acceleration from the front back to about 85% of the chord where the Mach number is approximately 0.85.

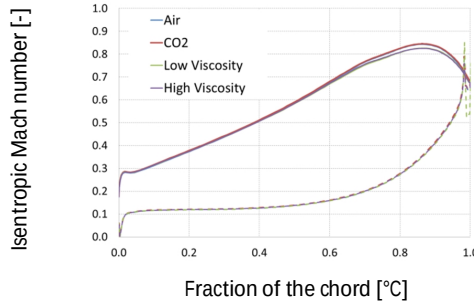


Figure 11: Isentropic Mach number at turbine blade mid-span for the four different cases, air, $CO_2$ high viscosity and low viscosity obtained from CFX solver. Solid line suction-side, dotted line pressure-side.

Thereafter follows a shorter deceleration to the trailing edge where the outlet Mach number is about 0.73. Just as the compressor showed a spread in isentropic Mach number profile, the same is seen for the turbine cascade, but for the turbine this spreads is less. The reason for this minor spread

here is that the boundary layer are less pronounced to grow in the concurrent accelerating flow on the front part of the blade, hence less variation in effective flow area.

A relationship between increasing viscosity and increasing pressure loss can be seen in Table 4, where the main results are provided for the blade at mid-span.

Table 4: Summary of the main result parameters for the four gases at mid-span, turbine cascade obtained from CFX solver

| Turbine Results | | *Air* | *CO2* | *High Viscosity* | *Low Viscosity* |
|---|---|---|---|---|---|
| Inlet Mach number (Ma) | (-) | 0.17 | 0.17 | 0.17 | 0.17 |
| Outlet Mach number (Ma) | (-) | 0.73 | 0.73 | 0.72 | 0.72 |
| Mass flow per unit area | ($kg/s \cdot m^2$) | 527.5 | 622.5 | 617.1 | 617.5 |
| $Re_{chord}$ $10^6$ | (-) | 3.84 | 4.65 | 1.98 | 20000 |
| Profile loss coefficient (Yp | (-) | 2.67 | 2.51 | 2.87 | 1.09 |
| Average blade wall shear | (Pa) | 599.7 | 540.3 | 617.8 | 168.7 |

The profile losses for the compressor cascade predicted using the loss model from Wright & Miller are shown in Table 5, together with the calculated figures. For the turbine cascade, the corresponding figures for the loss correlations from Ainly & Mathieson et.al. and Traupel are given in Table 6. It can be seen that there is a certain spread and that the evolution of the AMDC loss model to the AMDCKO resulted, in line with the aero design, to a lower loss level.

The blade wall shear stress, last row in Table 3 and 4, enhances the indication that there is a correlation between gas viscosity, pressure loss and the blade wall shear stress

Table 5: Summary of the predicted losses by conventional loss models, compressor

| Predicted profile loss either from losses correlation or calculations | | Profile Loss Air | Profile Loss $CO_2$ |
|---|---|---|---|
| Wrigth, P & Miller, D | (%) | 2.10 | 2.10 |
| Calculated with CFX | (%) | 1.35 | 1.01 |

Table 6: Summary of the predicted losses by conventional loss models, turbine

| Predicted profile loss either from losses correlation or calculations | | Profile Loss Air | Profile Loss $CO_2$ |
|---|---|---|---|
| AM Dunham & Came (AMDC) | (%) | 2.34 | 2.25 |
| AMDC Kacker & Okapuu (AMDCKO) | (%) | 1.87 | 1.80 |
| Traupel | (%) | 2.75 | 2.75 |
| Calculated with CFX | (%) | 2.67 | 2.51 |

***Cross section flow area:*** The specific work capacity per area unit ($w_{s,Area}$) is an indirect measurement of the area required for a given work (mass flow times total enthalpy drop ( $m \cdot \Delta h_0$) ). That is because e.g. if the specific work per unit area decreases with a given amount it means that the area must be increased with the same number to compensate for it. The ratio between $w_{s,Area}$ for $CO_2$ and air is given by Equation 7 and the full derivation is seen in Appendix 1.

***Ratio of specific work capacity per area unit***

$$\frac{w_{s,Area,CO2}}{w_{s,Area,Air}} = \frac{\left(\sqrt{\gamma \cdot M} \cdot \left(\frac{p_2}{p_1}^{\left(\frac{\gamma-1}{\gamma}\right)} - 1\right) \cdot \frac{R \cdot \gamma}{(\gamma - 1)}\right)_{CO2}}{\left(\sqrt{\gamma \cdot M} \cdot \left(\frac{p_2}{p_1}^{\left(\frac{\gamma-1}{\gamma}\right)} - 1\right) \cdot \frac{R \cdot \gamma}{(\gamma - 1)}\right)_{Air}} \quad \text{Eq. 7}$$

Evaluating the specific work capacity per unit area through Eq. 7 with typical low-pressure turbine values according to Table 7, indicated a reduction in the specific work capacity per unit area of slightly more than 20 percent for $CO_2$ compared to air.

Table 7: Typical values for the calculation of specific work capacity in a turbine at 1000°C, 10 bar(a)

| Turbine at 1000 °C 10 bar | Molar mass (M) (g/mole) | Specific heat ($c_p$) (kJ/kg·K) | Isentropic coefficient ($\gamma$) (-) | Pressure Ratio ($p_1/p_2$) (-) |
|---|---|---|---|---|
| $CO_2$ | 44.01 | 1.29 | 1.17 | 1.5 |
| Air | 28.96 | 1.19 | 1.32 | 1.5 |

## DISCUSSION

The hypothesis underlying the approach used in the current paper was that the profile loss depends, amongst other things, on the viscosity of the working medium and will hence be slightly reduced when changing the working medium from air to $CO_2$. That is because the lower viscosity in $CO_2$ reduces the shear force in primarily the boundary layer and to some minor extent in the free stream.

This trend was confirmed from the results, e.g. when changing from air to $CO_2$, the profile loss coefficient ($Y_p$) for the compressor was reduced from 1.35% to 1.01%, and for the turbine, from 2.67% to 2.51% for air and $CO_2$, respectively.

This reduction in loss for $CO_2$ compared to air is in line with what Sjolander et.al. [5] found in their compressor experiments and calculations, and there suggested equation for predicting the efficiency change using the isentropic coefficient. Their hypothesis was that it was mainly the lower Mach number downstream seen for $CO_2$, with its associated reduction on the loss, which caused this. This is likely a part of the explanation for the quite large difference in efficiency they obtained. Other causes for this could be that in the test

compressor, the operation point was allowed to change with the gas, which hence affects the efficiency as well.

Jackson et.al. found also an increase in polytrophic turbine efficiency of 2.3% when changing working medium from air to $CO_2$ on their turbine [8]. From this study, however, it was not possible to separate the part of the gain caused by the change in working medium from that caused by the reduction in stage load that accord from this gas change.

The fact that the loss coefficient varied with the viscosity even for the same isentropic Mach number distributions, indicates that the viscosity per se are important. The loss coefficient figures in Table 3 and 4 show that there is a weak relation between the increments in pressure loss with viscosity between air and $CO_2$. The behavior was repeated for the more unrealistic cases with either very low or high viscosity. For the turbine, the doubling in the viscosity between $CO_2$ to the high viscosity gas exhibited an increase of the loss that increased from 2.51% to 2.87%, or a 14% relative increment. For the compressor, the corresponding figures were more pronounced as they increased from 1.01% to 2.31%, which corresponded to a relative increment of 130%. The explanation here was probably a combination of the boundary layer growing more firmly in the adverse pressure gradient and the higher viscosity ratio.

One can also see that when approaching the excessive point where the viscosity approached zero, a pressure loss of 0.68% and 1.09% still remained for the compressor and turbine, respectively. These remaining losses are caused by mixing of the quantities; mass, momentum and energy, which may be considered as the inviscid loss.

The loss coefficient is also affected by the downstream wake mixing and hence a function of the actual point where the loss is evaluated. A real engine would typically have a row spacing of approximately 25-30% of the upstream chord, which reduces the loss by guiding the flow to a more structured flow field.

The predicted profile loss coefficient ($Y_p$) from some typical prominent loss correlations are summarized in Table 5 and 6 for a compressor and turbine cascade, respectively. It can there be seen that the spread between the individual loss models are larger than the impact from changing the working medium.

However, generally the loss model is not chosen arbitrarily. Instead is it often a familiar loss model that is used and then even minor difference between air and $CO_2$ will be important since one specific loss model has a considerably smaller individual spread. This implies that for someone used to designing conventional gas turbines using a specific loss model should be aware that a certain deviation is to be expected when the same model is applied to $CO_2$.

It has hence been shown that the profile loss for a similar blade geometry and isentropic Mach number profile will be some 5-25% lower for $CO_2$ then for air. Performing the study in this manner examines the loss models in the same way and with the same inputs as they are being used in the design phase. The finding that $CO_2$ provides a lower loss, as described above, can easily lead one to conclude that the overall profile loss is surely lower for an entire $CO_2$ compressor and/or turbine, respectively.

This is, however, not as clear, since when considering whole turbomachinery components, i.e. a compressor or turbine, there are also other aspects to consider.

Such an aspect is how the cross section area has to change when designing for either $CO_2$ or air to conduct the same total work. The finding that the specific work capacity per unit area was some 20% less for $CO_2$ relative air indicates a contrary effect on the total profile loss.

This lower specific work per unit area for $CO_2$ is a result of two counteracting effects. The first is the increase in mass flow through a given cross section area and Mach number for $CO_2$. The second, and the reason for the decrease in specific work capacity per area unit, is the significantly lower enthalpy drop for $CO_2$ at the same pressure ratio.

This indicates that the physical size of the turbomachinery in the $CO_2$ cycle will need to be somewhat larger for similar gas state. This larger surface area for a $CO_2$ engine may in turn imply a greater total loss. A part of this is compensated for by the fact that significant parts of the $CO_2$ machinery operate at higher pressure. This is to obtain the same overall temperature drop in the gas turbine - which in turn partially reduces the physical area.

## CONCLUSION

The main conclusions from these viscous 3D calculations are that the gas composition, and primarily the viscosity, influenced the pressure-based profile loss coefficient ($Y_p$) if the isentropic Mach number is maintained constant.

There was a slight reduction seen in the profile loss for an individual cascade operating with a working medium of pure $CO_2$ instead of air.

Theoretically this difference leads to an increased mismatch of the stages downstream even at the design point and hence, increased losses and stability. However, the difference in profile loss is relatively small at the design point and thus the authors' opinion is that the practical effect will be quite small. Thus, it is considered alright to use profile loss correlations derived with air for design point calculations even when the working fluid is $CO_2$.

This work has only focused on the design profile loss at lightly loaded cases. Hence, there is a risk that the current loss models are significantly deficient in predicting the limits for more offensive high-loaded designs, or when approaching operation at off-design conditions as the boundary layers then are at risk to behave differently.

The results show that the physical size of a $CO_2$ engine will be some 20% larger than an air-breathing engine conducting the same work ($m \cdot \Delta h_0$). Thus this tends to increase the total profile loss of the engine as a whole.

## ACKNOWLEDGMENTS

The authors would like to acknowledge Siemens Industrial Turbomachinery AB, Finspong, Sweden, for the permission to publish this paper. Additionally the authors acknowledge all Siemens employees involved in the project.

## REFERENCES

[1] P. J. Cook, "Demonstration and deployment of carbon dioxide capture and storage in Australia," *Energy Procedia*, vol. 1, pp. 3859-3866, 2009.

[2] L. Strömberg, G. Lindgren, J. Jacoby, R. Giering, M. Anheden, U. Burchhardt, *et al.*, "Update on Vattenfall's 30 MWth oxyfuel pilot plant in Schwarze Pumpe," *Energy Procedia*, vol. 1, pp. 581-589, 2009.

[3] M. Sammak, M. Genrup, E. Thorbergsson, and T. Grönstedt, "Conceptual Mean-line Design of Single and Twin-shaft Oxy-fuel Gas turbine in a Semi-closed Oxy-fuel Combustion Combined Cycle," in *Proceedings of ASME Turbo Expo 2012: Power for Land, Sea and Air. June 11-15, 2012, Copenhagen, Denmark*, 2012, pp. 289-297.

[4] W. Sanz, H. Jericha, B. Bauer, and E. Gottlich, "Qualitative and quantitative comparison of two promising oxy-fuel power cycles for CO2 capture," *Transactions-asme journal of engineering for gas turbines and power*, vol. 130, p. 031702, 2008.

[5] S. K. Roberts and S. A. Sjolander, "Effect of the specific heat ratio on the aerodynamic performance of turbomachinery," *Journal of engineering for gas turbines and power*, vol. 127, pp. 773-780, 2005.

[6] V. E. Kyritsis and P. Pilidis, "An analytical approach for gas turbine parameter corrections GT2008-50716," in *ASME Turbo Expo 2008: Power for Land, Sea, and Air*, 2008.

[7] A. S. Roberto Canepa, "Influence of Working Fluid Composition on the Performance of Turbomachinery in Semi-Closed Gas Turbine Cycles " *ASME Turbo Expo 2012: Turbine Technical Conference and Exposition*, vol. Volume 8: Turbomachinery, Parts A, B, and C, 2012.

[8] A. Jackson, A. C. Neto, M. Whellens, and H. Audus, "Gas turbine performance using carbon dioxide as working fluid in closed cycle operation," *ASME paper*, p. 153, 2000.

[9] J. Dunham and P. M. Came, "Improvements to the Ainley-Mathieson Method of Turbine Performance Prediction," *Journal for Engineering for Power*, vol. 92, pp. 252-256, 1970.

[10] S. C. Kacker and U. Okapuu, "A Mean Line Prediction Method for Axial Flow Turbine Efficiency," *Journal for Engineering for Power*, vol. 104, pp. 111-119, 1982.

[11] H. Craig and H. Cox, "Performance estimation of axial flow turbines," *Proceedings of the Institution of Mechanical Engineers*, vol. 185, pp. 407-424, 1970.

[12] J. Denton, "1993,'Loss Mechanisms in Turbomachines,' ASME Paper No. 93-GT-435."

[13] B. Mamaev and A. Klebanov, "Profile Losse In A Turbine Cascade," *Kuibyshev Motor Works, UDC*, vol. 621, pp. 55-60, 1970.

[14] P. Wright and D. Miller, *An improved compressor performance prediction model*: Rolls-Royce plc, 1991.

[15] E. M. Greitzer, C. S. Tan, and M. B. Graf, *Internal Flow: Concepts and Applications*: Cambridge University Press, 2004.

[16] M. Drela, "Two-dimensional transonic aerodynamic design and analysis using the Euler equations," Massachusetts Institute of Technology, 1985.

[17] "ANSYS® Academic Research, Release 14.5.0."

[18] "NIST REFPROP Databas 23, Version 8.0 ".

 

## APPENDIX

The mass flow through a fixed geometry is a function of the axial cross section area (A), axial Mach number (Ma), speed of sound (a) and the density (ρ)

$$m = A \cdot Ma \cdot a \cdot \rho \qquad \text{Eq. A.1}$$

For an ideal gas the density can be expressed as

$$\rho = \frac{M \cdot p}{R_u \cdot T} \qquad \text{Eq. A.2}$$

and the speed of sound

$$a = \sqrt{\gamma \cdot \frac{R_u}{M} \cdot T} \qquad \text{Eq. A.3}$$

(A.2) and (A.3) in (A.1)

$$m = A \cdot Ma \cdot \sqrt{\gamma \cdot \frac{R_u}{M} \cdot T} \cdot \frac{M \cdot p}{R_u \cdot T} = A \cdot Ma \cdot p \cdot \sqrt{\frac{\gamma \cdot M}{T \cdot R_u}} \qquad \text{Eq. A.4}$$

The change in specific enthalpy (dh) is a function of the temperature drop (dT) and specific heat ($c_p$)

$$dh = dT \cdot c_p \qquad \text{Eq. A.5}$$

The temperature ratio (TR) is a function of the pressure ratio (PR) and the isentropic coefficient (γ)

$$TR = PR^{\left(\frac{\gamma-1}{\gamma}\right)} \qquad \text{Eq. A.6}$$

Temperature difference $dT_{1\text{-}2}$

$$dT_{1-2} = T_1 - T_2 = T_1 \cdot \left(1 - \frac{p_2}{p_1}^{\left(\frac{\gamma-1}{\gamma}\right)}\right) \qquad \text{Eq. A.7}$$

The specific work capacity per unit area ($w_{s,Area}$)

$$w_{s,Area} = \int_1^2 \frac{m}{A} \cdot dh \qquad \text{Eq. A.8}$$

(A.4), (A.5) and (A.7) in (A.8)

$$w_{s,Area} = p \cdot Ma \cdot \sqrt{\frac{\gamma \cdot M}{T \cdot R_u}} \cdot \left(T_1 \cdot \left(1 - \frac{p_2}{p_1}^{\left(\frac{\gamma-1}{\gamma}\right)}\right)\right) \cdot c_p \qquad \text{Eq. A.9}$$

The ratio in specific work per unit area between two medium, e.g. $CO_2$ and air

$$\frac{w_{s,Area,CO2}}{w_{s,Area,Air}} = \frac{\left(p \cdot Ma \cdot \sqrt{\frac{\gamma \cdot M}{T \cdot R_u}} \cdot \left(T_1 \cdot \left(1 - \frac{p_2}{p_1}^{\left(\frac{\gamma-1}{\gamma}\right)}\right)\right) \cdot \frac{R \cdot \gamma}{(\gamma - 1)}\right)_{CO2}}{\left(p \cdot Ma \cdot \sqrt{\frac{\gamma \cdot M}{T \cdot R_u}} \cdot \left(T_1 \cdot \left(1 - \frac{p_2}{p_1}^{\left(\frac{\gamma-1}{\gamma}\right)}\right)\right) \cdot \frac{R \cdot \gamma}{(\gamma - 1)}\right)_{Air}}$$

For the same properties of Mach number, pressure and temperature

$$\frac{w_{s,Area,CO2}}{w_{s,Area,Air}} = \frac{\left(\sqrt{\gamma \cdot M} \cdot \left(1 - \frac{p_2}{p_1}^{\left(\frac{\gamma-1}{\gamma}\right)}\right) \cdot \frac{R \cdot \gamma}{(\gamma-1)}\right)_{CO2}}{\left(\sqrt{\gamma \cdot M} \cdot \left(1 - \frac{p_2}{p_1}^{\left(\frac{\gamma-1}{\gamma}\right)}\right) \cdot \frac{R \cdot \gamma}{(\gamma-1)}\right)_{Air}} \qquad \text{Eq. A.10}$$

Publication V

# Aerodynamic Gas Turbine Compressor Design for an Oxy-fuel Combined Cycle

**Dahlquist, A.**, Thern, M., Genrup, M.,

ASME Turbo Expo 2015, GT2015-42028

**Proceedings of the ASME Turbo Expo 2015: Power for Land, Sea, and Air**
**June 15-19, 2015, Montreal, Canada**

**GT2015-42028**

# Aerodynamic Gas Turbine Compressor Design for an Oxy-fuel Combined Cycle

**Adrian Dahlquist**

Siemens Industrial
Turbomachinery AB
SE-612 83 Finspong, Sweden
*Corresponding author.*
Adrian.Dahlquist@siemens.com

**Magnus Genrup**

Lund University
SE-221 00 Lund, Sweden

## ABSTRACT

A number of different CCS-technologies are currently being developed to reduce $CO_2$ emissions from thermal power stations. One of these technologies is based on the oxy-fuel combined cycle process, the basics of which have been described in several publications. The key difference in this cycle is the working fluid, which requires further investigation. The working fluid in the topping gas turbine cycle of an OCC mainly consists of $CO_2$ (80-95 wt%) and steam (5-15 wt%), with a few percentage of enriched $N_2$ and Ar. The gas properties of this working fluid differ significantly from those of a conventional air-breathing gas turbine; hence, the gas turbine has to be designed accordingly.

The isentropic exponent is lower, for example, with the result that a higher pressure ratio is required in an oxy-fuel combined cycle gas turbine than in a conventional combined cycle to achieve exhaust gas conditions that fit the design of a conventional bottoming steam cycle. This higher pressure ratio results in additional challenges in the design of the aerodynamic compressor.

The amount of information in the public domain about designing an oxy-fuel gas turbine is sparse and is mainly limited to the cycle design. The main objective of this work is therefore to demonstrate the feasibility of achieving the aerodynamic compression in a single-spool compressor design, suitable for an oxy-fuel combined cycle application, with the aim of bringing the technology closer to commercialization.

The aerodynamic compressor design includes 1D mid-span and 2D through-flow design calculations, and a steady-state 3D analysis calculation for validation.

The compressor's design suits an oxy-fuel combined cycle with a net plant power of 115 $MW_{el}$.

**Keywords:** $CO_2$, oxy-fuel, SCOC-CC, OCC, Compressor, CCS

## NOMENCLATURE

| | | |
|---|---|---|
| a | Speed of sound | [m/s] |
| C | Absolute velocity | [m/s] |
| $c_p$ | Specific heat at constant pressure | [kJ/kg·K] |
| m | Mass flow | [kg/s] |
| Ma | Mach number | [-] |
| p | Pressure | [bar] |
| PR | Pressure ratio | [-] |
| R | Gas constant | [J/kg·K] |
| T | Temperature | [°C / K] |
| W | Relative velocity | [m/s] |

## ABBREVIATIONS

| | |
|---|---|
| 0-, 1-, 2-, 3D | 0-, 1-, 2-, 3-dimensional |
| ASU | Air separation unit |
| CCS | Carbon capture and sequestration |
| EGV | Exit guide vane |
| GT | Gas turbine |
| HP, IP, LP | High pressure, intermediate pressure, low pressure |
| HRSG | Heat recovery steam generator |
| IGV | Inlet guide vane |
| OCC | Oxy-fuel combined cycle |
| RSM | Root mean square |
| SCOC-CC | Semi-closed oxy-fuel combustion combined cycle |
| ST | Steam turbine |
| VGV | Variable guide vane |

## SUBSCRIPT

| | |
|---|---|
| 0 | Total |
| Des | Design case |
| m | Meridional |
| s | Stage |

## GREEK SYMBOLS

| | | |
|---|---|---|
| $\phi$ | Flow coefficient | [-] |
| $\gamma$ | Isentropic exponent | [-] |
| $\eta_p$ | Polytropic efficiency | [%] |
| $\eta_s$ | Isentropic efficiency | [%] |
| $\rho$ | Density | [kg/m$^3$] |
| $\psi$ | Stage load | [-] |

## INTRODUCTION

Future generations are facing a serious challenge from global warming (cf. IPCC [1]). Efforts are required in several areas to mitigate this, for example, through more efficient energy utilization, more renewables, and the use of Carbon Capture and Sequestration (CCS) technologies. A number of CCS technologies are currently being researched and developed to reduce $CO_2$ emissions emitted from thermal power stations, and they may finally be on the cusp of becoming a reality. One competing CCS technology is the oxy-fuel combined cycle (OCC), which has been presented in previous publications [2-7].

The OCC is a power cycle designed for $CO_2$ capture, with similarities to a conventional combined cycle power plant. The topping cycle is a semi-closed Brayton gas turbine cycle, with a fully conventional bottoming Rankine steam cycle. The main working principle behind the oxy-fuel technology is to form a combustion product of nearly pure $CO_2$ and $H_2O$ in the topping cycle by replacing the normal oxidizer of air with almost pure $O_2$. These combustion products act as the working fluid in the gas turbine as the top cycle is semi-closed and recirculated.

The composition of the working fluid depends partially on the temperature in the flue gas condenser after the heat recovery steam generator (HRSG), where a lower cooling temperature provides a lower steam content. The composition of the working fluid is generally within the range of 80-90 wt% $CO_2$, 10-20 wt% $H_2O$, and a small percentage of other enriched gases remaining from the $O_2$ production in the cryogenic Air Separation Unit (ASU; e.g., Ar and $N_2$).

The higher mass fraction of argon in the working fluid compared to air is the result of that argon not being efficiently separated in the cryogenic ASU, and then getting enriched in the semi-closed cycle. This is because the condensation temperatures of argon and oxygen are close; for example, the condensation temperature of argon is 87.2 K and for oxygen it is 77.2 K at standard atmospheric pressure [8].

The working fluid in the OCC has different gas properties from that of a conventional air-breathing gas turbine. Some of the more significant differences in the gas properties are the isentropic exponent ($\gamma$), specific heat at constant pressure ($c_p$), gas constant (R), and speed of sound (a), as shown in Table 1.

These differences affect both the design of the entire power plant setup and the designs of the individual components. The relatively lower isentropic exponent ($\gamma$) results in the need for a higher gas turbine pressure ratio to achieve a temperature drop over the turbine(s) similar to a conventional combined cycle. Gas turbine pressure ratios in a spectrum of 30 to 60 have been proposed for oxy-fuel cycles by different authors, [2, 4, 5, 9-12]. Other aspects are the lower speed of sound (a) and the larger variations in specific heat ($c_p$) with temperature for a $CO_2$/$H_2O$ mixture compared to air or flue gas [7, 13].

These differences all entail additional challenges for the design of the aerodynamic compressor. Thus, there is a need to further investigate the aerodynamic design of the oxy-fuel gas turbine compressor as information relating to such designs is scarce.

The main objective of this paper is to investigate and demonstrate the feasibility of the conceptual aerodynamic design of a single-spool gas turbine compressor, suitable for OCC application, with the aim of bringing the technology closer to commercialization.

**Table 1: Gas properties.**

| | | *OCC*[1] | *Air* | *OCC*[1] | *Air* |
|---|---|---|---|---|---|
| Pressure ($p_0$) | [bar] | 1.013 | 1.013 | 31.500 | 31.500 |
| Temperature ($T_0$) | [°C] | 60.0 | 60.0 | 437.0 | 437.0 |
| Molar mass (M) | [g/mol] | 38.64 | 28.96 | - | - |
| Isentropic exponent ($\gamma$) | [-] | 1.297 | 1.400 | 1.237 | 1.369 |
| Specific heat ($c_p$) | [kJ/kg·K] | 0.952 | 1.008 | 1.206 | 1.084 |
| Gas constant (R) | [J/kg·K] | 215.2 | 287.1 | - | - |
| Speed of sound (a) | [m/s] | 303.7 | 366.0 | 434.2 | 534.8 |
| Density ($\rho_0$) | [kg/m$^3$] | 1.419 | 1.059 | 20.646 | 15.264 |

[1] Mass fraction 85.1% $CO_2$, 8.3% $H_2O$, 2.6% $N_2$, 3.9% Ar, and 0.1% $O_2$.

1D mid-span designs have previously been published demonstrating the plausibility of an OCC design [2, 3, 14], as well as for the Graz cycle. The latter is another type of oxy-fuel cycle with partly similar aerodynamic design challenges [10, 15-17]. This study further investigates the aerodynamic design of the compressor comprising the entire design chain from an OCC heat and mass balance design through a 1D mid-span, 2D through-flow, and a steady-state 3D flow solver. Hence, this work contributes further knowledge in this subject area and provides increased confidence that an oxy-fuel cycle is achievable in general; more specifically, it also shows that the aerodynamic design of the compressor is a feasible design task.

Related important research areas where the working fluid will have an impact are, for example, materials regarding corrosion, crack propagation, carbonization, and coating carbon

 

deposits. The materials issues are outside the scope of this work, but an initial investigation indicates that there are no obvious obstacles to the use of conventional materials, such as IN718 in an OCC environment [18]. Further investigations are required to assess these concerns and to determine the purification requirements of the working fluid.

## CYCLE DESCRIPTION

The overall cycle configuration, different design aspects, potential trade-offs, and so on for the oxy-fuel combined cycle are more comprehensively described and analyzed in a previously published work [5]. Nevertheless, a general description is appropriate as a few minor adjustments have been made.

The investigated OCC concept contains a recirculated topping Brayton cycle and a conventional two-pressure bottoming Rankine steam cycle. The cycle layout is shown in Figure 1. The numbers in brackets "{ }" in this paragraph refer to the steps in this figure.

The topping cycle contains a gas turbine, which has the shaft configuration of a single-spool gas generator with a free power turbine that operates with a working fluid of mainly recirculated $CO_2$ and $H_2O$. The working fluid is compressed to 31.4 bar from atmospheric pressure as it passes through a single-spool compressor {1-2}.

In the combustion chamber {3}, both fuel {4} and oxygen {5} are injected as no oxidizer is present in the working fluid, and thus it has to be provided from an external source.

It is desirable to operate the cycle as close to a stoichiometric condition (oxygen-to-fuel ratio) as possible to avoid the excessive use of either the oxygen or fuel, as they are both expensive as well as undesirable impurities in the final delivery stream of carbon dioxide for some CCS applications, for example, in Enhanced Oil Recovery (EOR). An oxygen excess of 1.0 wt% was used, compared to the oxygen required for stoichiometric combustion. To achieve desirable combustion properties, the recirculated working fluid is used to dilute the oxygen and fuel streams in the combustor, the basic methods of which have been described in [6]. The low oxygen excess entails elevated CO emissions, which would not be acceptable for an open cycle, but in a closed cycle it is a minor problem provided no material issues and that the $CO_2$ bleed stream is purified (e.g., catalytically). Our view is that the combustion is feasible with only 1 wt% excess of oxygen, strengthened by the fact that the oxygen stream can be injected at the precise location needed for combustion and not diluted with the surrounding working fluid.

However, if it turns out that the oxygen excess needs to be raised slightly, it will not change the basis of the OCC being an attractive option for CCS. An increase to, for example, 5 wt% oxygen excess only reduces the total net cycle efficiency by 0.3-0.4 percentage points.

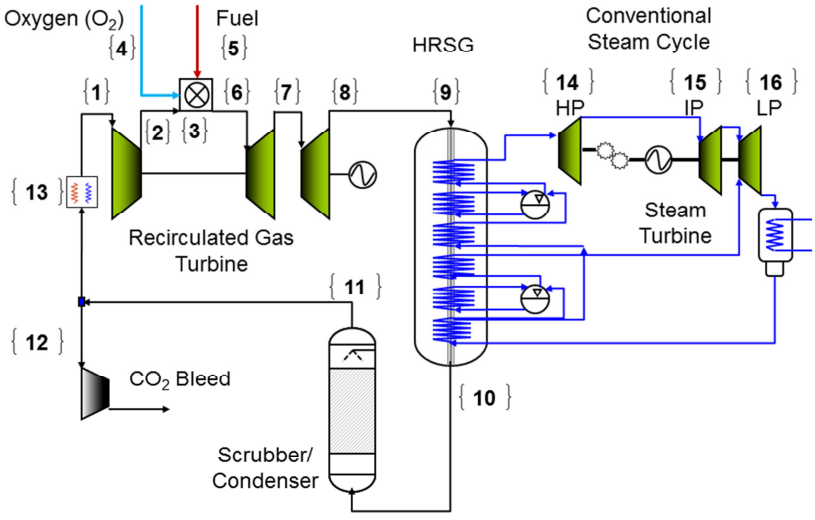


**Figure 1: Illustration of the oxy-fuel combined cycle plant.**

The 1340°C hot combustor outlet flue gas expands through the turbines {6-7-8}, which drives the compressor and generator.

The flue gas leaving the gas turbine diffuser {8} has a temperature of about 610°C and is ducted through the HRSG {9-10} where heat from the gas is transferred to the two-pressure bottoming cycle, which reduces the gas temperature to about 110°C {10}. Before the flue gas is recirculated back to the gas turbine inlet, it is further cooled and purified to remove potential acids, deposits, and soot formations. The main clean-up is accomplishing in a wet spray tower (scrubber/condenser) {11}.

The use of a wet spray tower in combination with a compressor inlet filter provides the desired cooling and purification of the working fluid. The optimum temperature of the recirculated working fluid for cycle efficiency is in the range of 40 to 70°C, and the preferred temperature used herein is 60°C [5].

The flue gas leaving the cooling tower is divided into two separate streams, one minor bleed stream for CCS {12} and a major stream, which is ducted back towards the gas turbine inlet. The mass of the bleed stream is in the range of 6-7% and balances the fuel and oxidizer streams added in the combustor, the moisture absorbed in the cooling tower, and the minor sealing leakage flows in and out of the system. The mass flow balance in the top cycle is maintained through this bleed stream. The $CO_2/H_2O$ bleed stream undergoes a gradual compression, with intermediate cooling, water separation, and possible purification, before it is sequestrated, for example, in enhanced oil recovery or other forms of underground storage.

The main stream, which is ducted back towards the gas turbine, is saturated with steam as it leaves the spray tower {11}. This saturation of the steam in the flow makes it inappropriate to recirculate it directly back to the compressor inlet without further treatments, as there is a severe risk of condensation and the formation of water droplets, which could erode and cause both corrosion in the first compressor stages and inlet filter saturation. To prevent this, the working fluid is passed through a heater {13} in which feed water from the bottoming cycle is utilized to heat the working fluid to a relative humidity of about 80%, which corresponds to a temperature rise of the order of 3-5°C. The flow is passed through an inlet filter before it reenters the compressor to remove any remaining particles and moisture droplets.

A conventional two-pressure HRSG was considered to be the preferred concept for the bottoming cycle, with regard to the efficiency, cost, and complexity of an OCC of this power size. A two-pressure HRSG is consistent with what is common for conventional combined-cycle plants of similar power size. The identified steam turbine for this cycle is a geared high-pressure turbine (HP) {14}, and a directly driven intermediate- and low-pressure turbine (IP, LP) {16}. The simulation results are based on a seawater-cooled condenser operating at 0.0425 bar (15°C inlet, 25°C outlet, and 5°C terminal temperature difference) and with below 15% moisture content at the steam turbine exit.

## METHOD

The approach taken was to continue to develop the previous work published in [5], in which an appropriate power size and technology level was identified as being feasible to bring to the market in the near future. The OCC was simulated in Siemens standard process simulation tool, Krawal-modular. The Krawal tool is an advanced heat and mass balance tool, which utilizes real gas properties (LibHuGas) and a matrix solver.

The performance of the main cycle components is summarized in Table 2. A twin-shaft configuration was chosen for the gas turbine in this study (single-spool gas generator with a free directly driven power turbine). This was in order to investigate the feasibility of managing the relatively high compression ratio of 31 in a single-shaft compressor without sacrificing unnecessary performance.

**Table 2: Cycle component performance.**

| *Aggregates* | *Parameter* | *Unit* | *Value* |
|---|---|---|---|
| ***GT Compressor*** | | | |
| Efficiency | $\eta_s$ | % | 90.3 |
| ***Combustor*** | | | |
| Oxygen excess | | wt% | 1.0 |
| Combustion temp | COT | °C | 1340 |
| ***GT Turbine*** | | | |
| Stage efficiency CT/PT | $\eta_s$ | % | 87.0/92.5 |
| ***Steam Turbine*** | | | |
| HP/IP/LP | $\eta_s$ | % | 90.2/88.9/86.0 |
| HPST | $p_0$ | bar | 100 |
| HPST | $T_0$ | °C | 565 |
| LPST | $p_0$ | bar | 5.00 |
| Condenser | $p_0$ | bar | 0.0425 |
| ***HRSG*** | | | |
| Pressure drop | dp | mbar | 40 |
| Pinch-point evaporator | $T_{pp}$ | °C | 20.0 |
| Approach-point evaporator | $T_{ap}$ | °C | 8.00 |
| ***Auxiliary*** | | | |
| Total recirculation pressure drop* | dp | mbar | 100 |
| Fuel compressor | $\eta_s$ | % | 80.0 |
| $O_2$ compressor | $\eta_s$ | % | 80.0 |
| Pump | $\eta_s$ | % | 75.0 |
| Gear box ST | $\eta$ | % | 98.5 |
| Generator GT/ST | $\eta$ | % | 98.5/98.3 |

* From GT turbine blading outlet to the GT compressor blading inlet.

The turbine cooling and disc-sealing predictions were incorporated using two separate models. The cooling flows were calculated from a developed m-star model [19], which scales the cooling flows with respect to the new gas properties and operation conditions from known gas turbine reference values. The required disc-sealing flows were predicted according Bayley and Owen's method [20, 21].

 

The compressor design is the main topic of this paper, but of course the compressor was designed to be coherent with the aerodynamics of the entire gas turbine in mind. The first step in the design process, after establishing the overall mass and heat balance, was to perform a basic 0D/1D design of the gas turbine to obtain an initial gas path shape and some first numbers for the compressor design.

A basic 1D design of the turbines was made in order to ensure the realistic design of the gas turbine as a unit. The turbine concept was a 2-stage compressor turbine and a 4-stage ungeared power turbine operating at 3000 rpm, with a short turbine intermediate duct in between. The results of the detailed turbine design are outside the scope of this paper and will be addressed in a later publication.

In general, the same fundamental physical laws and design philosophy still dictate the compressor designs, whether it is a conventional air-breathing compressor or a compressor designed for an oxy-fuel application. However, the gas properties of the working fluid and the different requirements for the compressor influence the design trade-offs and dictate what is achievable or not for the compressor.

Thus, this work treats the aerodynamic compressor design no differently from a conventional compressor; however, the differences in gas properties and necessary trade-offs affect the outcome slightly. The question about whether the traditional empirical air-based correlations can still be used or not for the design has been addressed previously [7]. In that study it was concluded that the correlations can be used in the design phase of a modest loaded compressor design, but there is a need for some caution when predicting the behavior at off-design and for more heavily loaded designs.

The aerodynamic design phase of the compressor, after which the global design parameters were specified, can roughly be divided into the following three steps. The first step was to conduct a 1D mid-span design where typical compressor design parameters were determined, such as stage-count, loading ($\psi$), flow coefficient ($\phi$), pressure ratio ($PR_{stage}$), and the shape of the gas path.

With the 1D model results in place, the next step was to create a 2D model for the through-flow program. The through-flow program utilized was HT0300, which originates from Hearsey [22] and has been further developed at Siemens and, for example, includes internal loss and flow deviation models to match the behavior of our house-style compressor blade geometries. This 2D model was tuned until a flow field was attained that met the established requirements of the 1D design as well as our design philosophy for an appropriate radial distribution of the flow and stage parameters.

The initial 1D and 2D design phase appears to be simple, and in fact from a mathematical and computational power perspective it is, which should be seen as one of its strengths. The fact is that it is vital to get these design choices right to enable a successful final design of the compressor. Thus, a significant effort should be involved in making these design choices match the intended compressor performance and overall gas turbine unit design.

Based on the 2D flow field, the third step was to create the 3D blading adapted for the 3D flow solver Multip to optimize and validate the results. The Multip program is a steady-state 3D flow solver, originally developed by Denton at Cambridge University [23]. The program has been further developed at Siemens (e.g., adapted so that it is able to utilize a variable specific heat ($c_p$)).

In reality, the work progress was far from being as straightforward as the description above might at a first glance indicate, and it included more iteration whereby the previous results were adapted based on new findings from the following steps before the appropriate results were eventually obtained.

Finally, the heat and mass balance of the entire oxy-fuel combined cycle was adapted, based on the new performance figures for the compressor.

## RESULTS & DISCUSSION

The global design parameters for the compressor, which were set by the heat and mass balance simulation and the initial 0D/1D design, are summarized in Table 3. The required mass flow for the turbine cooling and disc-sealing is extracted from two intermediate compressor stages and at the compressor outlet. These bleeds are located after compressor stages 7 and 11 at pressures of 8.5 and 16.9 bar, respectively (Table 3).

It should be noted that the temperature ratio is kept at the modest level of about 2.1, despite the relatively high pressure ratio of 31.0, assuming an isentropic efficiency of 90%. That corresponds to a modest temperature rise of about 375°C for an inlet temperature of 63.5°C, which does not cause any material concerns in the rear compressor stages. The corresponding temperature ratio for an air-breathing compressor is about 2.65, which, at similar conditions, would result in a temperature rise of about 555°C—well above the material limit for conventional compressor materials.

There are several different design parameters and trade-offs to consider in all compressor designs, and this is no less true for an OCC compressor where, for instance, the volume flow and speed of sound differs significantly. Not all of them can be addressed in this publication, but comments on some of the parameters are relevant, such as the hub-to-tip ratio, axial inlet and outlet Mach numbers, and stage loading.

The choice of hub-to-tip ratio at the compressor inlet depends upon several factors. For a certain mass flow, shaft speed, and axial inlet Mach number, a lower hub-to-tip ratio results in longer blades, which are located at a lower hub radius, and have a lower blade tip speed. Less IGV swirl is thus required for a given relative Mach number. Longer blades can, however, be difficult to tune adequately, and a lower blade speed results in a reduced stage pressure ratio for a constant stage load.

The blade velocity difference between the blade hub and tip section also increases for longer blades. Attaining a work input that is constant over the blade span will, eventually, lead to such a high flow turning in the hub section that a counter

 

rotating swirl is required, which is a design that is likely to penalize the stage's efficiency.

**Table 3: Global design parameters for the compressor.**

| *Parameter* | *Unit* | *Values* | | |
|---|---|---|---|---|
| Temperature in/out | [°C] | 63.5 | 438.5 | |
| Pressure in/out | [bar] | 1.013 | 31.42 | |
| Mass flow in/out | [kg/s] | 219.8 | 197.7/168.4* | |
| Bleed mass flows | [kg/s] | 8.35 | 13.85 | 29.3 |
| Bleed flows pressure | [bar] | 8.5 | 16.9 | 31.4 |
| Shaft speed | [rpm] | | 5700 | |
| Hub-to-tip ratio in/out | [-] | 0.54 | 0.91 | |
| Hub and tip radius R1in/EGV out | [m] | 0.355/0.661 | 0.380/0.416 | |
| Axial Mach number in/out | [-] | 0.63 | 0.27 | |

* Compressor outlet mass flow before and after the final bleed stream.

The first rotors tip section is transonic and thus requires a high solidity (chord-to-pitch ratio), commonly in the range of 1.3-1.7, to control the shock wave and subsequent diffusion, which is difficult to attain with a low hub-to-tip ratio (long blades) for reasons of mechanical integrity.

A hub-to-tip ratio of 0.54 at rotor 1 inlet was selected for this compressor design. The choice of the outlet radius was a trade-off between keeping both the blade speed and the blade height at a sufficiently high level at the compressor outlet to attain a smooth gas path. For this design, a hub radius of 0.38 m was considered preferable, corresponding to a hub-to-tip ratio of 0.91 at the exit guide vane (EGV) outlet. The length of the compressor from the IGV inlet to the EGV outlet was 2.62 m, and the geometric shape of the gas path is seen in Figure 2 and Figure 3.

**Figure 2: Geometric design of the compressor gas path seen from the side (X-Y view).**

**Figure 3: Geometric design of the compressor gas path seen from the top (radial X-Z view).**

The choice of axial Mach number is important, and a high axial inlet Mach number is appropriate as it reduces the annulus inlet area and increases the work capacity of the stages. An axial Mach number that is too high at the design point risks, however, choking the annulus at off-design operation and severely limiting future engine mass flow upgrades.

By designing the compressor with a relatively lower axial outlet Mach number, the compressor outlet area can be increased, and hence the blade height for a constant root mean square (RMS) radius. The compressor diffusors total pressure drop is also improved by a low exit Mach number design. The axial Mach number cannot, however, be reduced too far as the surge margin then will be decreased. Axial design Mach numbers of 0.63 at the inlet and 0.27 at the outlet are considered appropriate for this compressor design.

Commercial compressor designs with pressure ratios above 30 are usually only common in aero-derivatives, where it is achieved by a twin-spool compressor configuration, with the exception of the GT24/26, which achieves a pressure ratio of 35 in its 22 stage compressor [24]. The trade-off between blade speed and blade height is not as necessary in a twin-spool compressor configuration, where the blade speed in the high-pressure stages, which is located at a lower radius, can be maintained through a higher shaft speed. A twin-spool design would facilitate the aerodynamic design, but at the cost of increasing complexity and likely cost, too. For an industrial gas turbine a single-spool compressor configuration is therefore preferred.

It is common practice to compare different compressor designs through the use of non-dimensional parameters. By comparing the non-dimensional parameters a good understanding of the complexity and design challenge can be obtained.

$$\frac{m \cdot \sqrt{T}}{r^2 \cdot p} \cdot \sqrt{\frac{R}{\gamma}} \qquad \textbf{Eq. 1}$$

$$\frac{N \cdot r}{\sqrt{\gamma \cdot R \cdot T}} \qquad \textbf{Eq. 2}$$

One method is to compare the mass flow that a scaled compressor operating at 3000 rpm would have had if the velocity triangles at the front stage and the geometrical hub-to-tip ratio were kept constant.

A parameter Eq. 3, which relates the shaft speed and mass flow, can be derived through analysis of the non-dimensionless groups for mass flow Eq. 1 and aerodynamic speed Eq. 2 [25]. The equivalent inlet mass flow for the OCC compressor can thereby be corrected to a 3000 rpm air-breathing compressor at ambient ISO condition, through equation Eq. 4 and
Table 4. The corrected 3000 rpm mass flow figure is 951 kg/s
Table 4), which is high but definitely feasible with today's state-of-the-art technology.

The first stage was designed with a higher stage loading compared to the subsequent stages to gain overall compressor efficiency. The stage load of the first stage was 0.386, while the subsequent stages (2-13) were designed with a declining stage

 

load in the range of 0.355 to 0.335. The stage load was further reduced down towards 0.31 for the last three stages to gain extra surge margin at full load (Figure 4, Table 5).

$$\frac{m \cdot N^2}{p \cdot \sqrt{R \cdot T} \cdot \gamma^{3/2}} = \text{Constant} \qquad \textbf{Eq. 3}$$

$$m_{3000} = m_{Des} \cdot \left(\frac{N_{Des}}{N_{ref}}\right)^2 \frac{p_{ref}}{p_{Des}} \cdot \left(\frac{\gamma_{ref}}{\gamma_{Des}}\right)^{3/2} \cdot \sqrt{\frac{T_{ref} \cdot R_{ref}}{T_{Des} \cdot R_{Des}}} \qquad \textbf{Eq. 4}$$

**Table 4: Corrected mass flow at 3000 rpm.**

| *Parameter* | *Unit* | *Design (OCC)* | *Ref (Air)* |
|---|---|---|---|
| Shaft speed (N) | [rpm] | 5700 | 3000 |
| Pressure ($p_0$) | [bar] | 1.013 | 1.013 |
| Temperature ($T_0$) | [°C] | 63.5 | 15.0 |
| | [K] | 336.65 | 288.15 |
| Isentropic exponent ($\gamma$) | [-] | 1.297 | 1.400 |
| Gas constant (R) | [J/kg·K] | 215.2 | 287.2 |
| Mass flow (m) | [kg/s] | 219.8 | 951.0 |

By reducing the stage load towards the back of the compressor the surge margin of the entire compressor as a unit is improved (Figure 4). This is because the aft part of the compressor is more affected by a rising pressure ratio, and thus tends to surge first at full load. The design stage pressure ratio for the first stage was 1.57 and it declines towards the last stage pressure ratio of 1.11 (Figure 5 and Table 5).

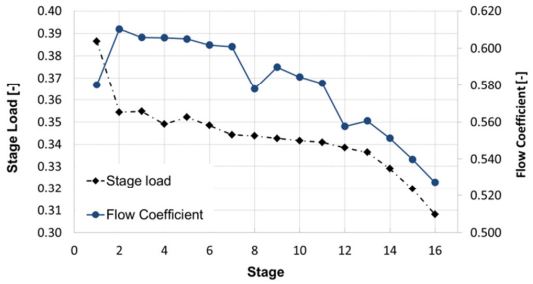


**Figure 4: Stage parameters, stage load (ψ), and flow coefficient (ϕ) for the rotors and stators at the mid-span section.**

The rather high first stage pressure ratio results in the need for a high diffusion across the rotor. A common parameter for examining this diffusion load is the deHaller coefficient [26], which describes the velocity ratio across a blade row ($W_{in}/W_{out}$ or $C_{in}/C_{out}$). The general design recommendation in open literature is to keep this velocity ratio at the mid-span above 0.70-0.72, which corresponds to diffusing about half of the inlet dynamic head into static pressure for an incompressible flow.

The deHaller coefficient considers not the geometrical shape of the gas flow path through the blade row, e.g. the solidity and blade curvature, and for modern controlled diffusion blade geometries it should be possible to undercut the 0.70 limit somewhat. The same holds for a transonic stage, where the compression shock wave generates a significant amount of the pressure rise. Hence, the deHaller coefficient should only be seen as an early stage load indication. The diffusion factor of 0.68 in the first rotor row is thus considered adequate.

The hub section of a blade is generally more prone to stall first and the hub sections were thus designed with a slightly higher velocity and total pressure to mitigate this, and thus gain stall margin.

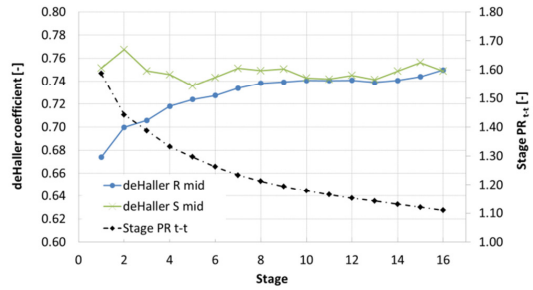


**Figure 5: Total stage pressure ratios and deHaller coefficient for the rotors and stators at the mid-span section.**

The radial distribution of the axial velocity component of the rotor and stator rows is shown in Figure 6 and Figure 7, normalized with the average axial exit velocity from rotor 1. It is noticeable that the velocities are higher at the hub section, and that the axial velocity declines quite smoothly from the inlet throughout the compressor.

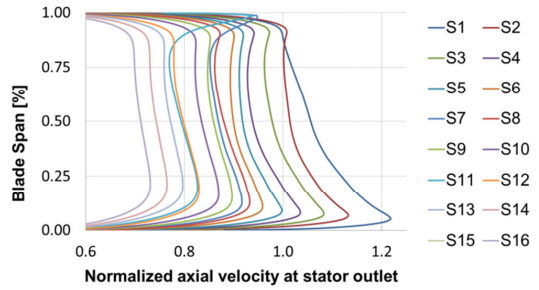


**Figure 6: Normalized axial velocity component out of the stator rows, normalized with the span height.**

The two velocity peaks seen at the casing after stators 7 and 11 are the result of the cooling air bleed after these rows (Figure 6).

Weak local velocity peaks can also be seen at the tip section for the front stages as a result of a slightly higher rotor work input at this radius. This could be avoided by reducing the camber at the rotor tip slightly.

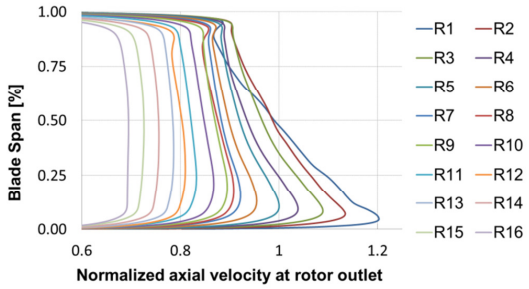


**Figure 7: Normalized axial velocity component out of the rotor rows, normalized with the span height.**

The axial Mach number decreases smoothly from an inlet Mach number of 0.63 down to an exit Mach number of 0.27. Despite this, the flow coefficient does not show the same smooth declining trend that one is accustomed to see. That is because of the slightly larger relative reduction in tangential blade-speed (U) compared to what is normally seen in a constant mid- or hub-radius design, which is, as mentioned above, to keep up the blade height in the rear stages through reducing its RMS radius. The result of a larger reduction of the RMS radius is that the blade speeds are reduced more than common towards the back of the compressor, which keeps up the $C_m/U$ ratio (flow coefficient ($\phi$)). The meridional velocity component ($C_m$) at the rotor inlets is shown in Table 5, normalized by $C_m$ at rotor 1 inlet. The compressor bleed flows after stages 7 and 11 cause a local reduction in the meridional velocity for the subsequent stages 8 and 12, hence for the flow coefficient too (Figure 4, Table 5).

The design philosophy was to aim for a smooth distribution of all the stage parameters throughout the compressor to enhance the match between subsequent stages and provide better overall performance and stability.

Both 15-stage and 16-stage compressor designs were investigated and both seemed feasible for the design point, but the ability to facilitate the design requirements for each individual stage led to a final compressor design with 16 stages. The first two rotor tip sections are transonic, and the Mach numbers at each of these leading edge tip sections are 1.29 and 1.11, respectively. The third rotor is just below unity at the design point and the stage is therefore subsonic.

The calculated surge margin for the compressor was 25.5% (or to occur at a pressure ratio of 38.9 at the compressor design speed of 5700 rpm), which is considered sufficient.

The methods of handling the startup, the off-design and transient operation of the compressor are important for the final gas turbine design. To design these control mechanisms the matching and part load control between the compressors, combustor, turbine(s), and ambient must be known and can, thus, be done first after the preliminary design of the entire gas turbine is completed.

These aspects are not primarily covered in this work partly because the turbine design was not yet completed. A couple of aspects have, however, been considered in the design process to enhance the operability, as discussed previously. Some examples are the choice of a 16-stage design to reduce the overall stage load, reducing the stage loading of the last stages, and having a higher meridional velocity at the hub section.

Another aspect of the compressor that facilitates its operation is the fact that the topping-cycle is recirculated. This means that the temperature of the working fluid at the compressor inlet is controllable despite changes in ambient conditions. The choice of the design temperature of 60°C ensures the controllability of the compressor inlet temperature over a broad ambient range by changing the amount of cooling in the scrubber/condenser ({12} in Figure 1).

The aerodynamic speed (Eq. 2) can thus be controlled to achieve desirable movements in the compressor characteristics to reduce the requirement for compressor operation far away from its design point during continuous and off-design operation.

The startup of the cycle and rapid transients requires, in any case, that the compressor has an appropriate surge margin as these operation points and the required time response will be outside what is controllable by changing the compressor inlet temperature. To manage these operating conditions, a variable inlet guide vane (IGV) and variable guide vanes (VGV) will be used in the front stages. The number of VGVs and their scheduling were not addressed in this work, but for part load operation the expected requirement is 3-4 VGV. This may seem abundant for an industrial single-spool compressor, but one should bear in mind both the working media and the rather high pressure ratio. Further studies are required before a firm number of VSVs can be determined.

During low speed operation, such as during start-up and low load operation, the front stages tend to stall because of a too high stage pressure ratio and low flow coefficient, while the rear stages tend to choke. A complementary control method is then to use compressor intermediate bleed(s) to reduce the loading of the front stages and reduce the volume flow in the rear stages. A bleed control method has a negative effect on the cycle performance and should not be used in continuous operation, and is thus only considered for startup and rapid transients.

An initial study of the control method for an oxy-fuel cycle through IGV and VGV in a twin-spool gas turbine has been investigated by Ulizar et al. [27]. Their work covered the

startup of the cycle on air, the change of working fluid to $CO_2$ at idle, and then the ramping up to full load. They concluded that the control would not pose any obstacle beyond the current level of technology.

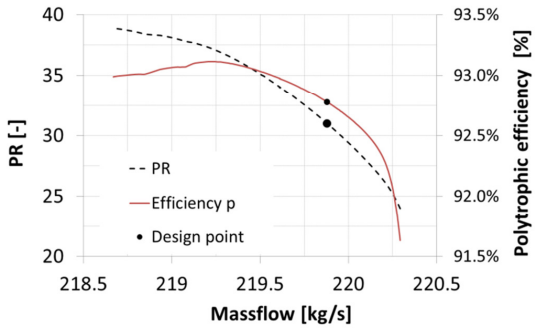


**Figure 8: Compressor characteristics, for example showing a calculated surge margin of 25.5% at the design speed of 5700 rpm.**

The total to total efficiency of the compressor was calculated to be 90.1% and 92.8% isentropic ($\eta_s$) and polytropic ($\eta_p$), respectively. The compressor surge margin and efficiency are shown in Figure 8, and a summary of some performance parameters are shown in Table 5 and Figure 4 and Figure 5.

The 2D through-flow and steady-state 3D solvers showed in general that the results have a good and consistent agreement. The relative Mach number contours for the three first rows from the 3D solver are shown in Figure 9, Figure 10, and Figure 11. One observation is that the shock in rotor 1 is located somewhat close to the trailing edge and a redesign of the camber distribution should be considered for a new design.

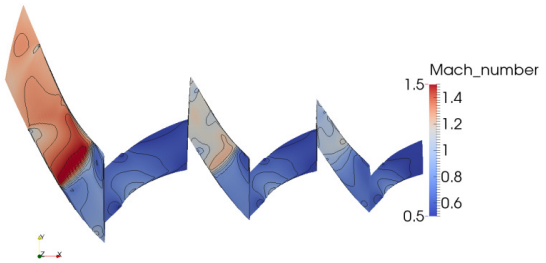


**Figure 9: Mach number contours for the three first stages, in the x-y plane, at the tip span section (95% span).**

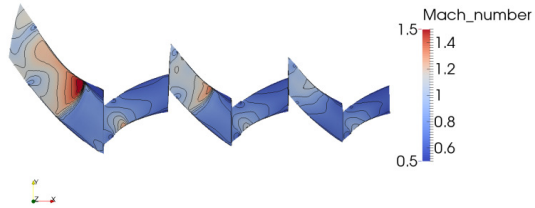


**Figure 10: Mach number contours for the three first stages, in the x-y plane, at the mid-span section (50% span).**

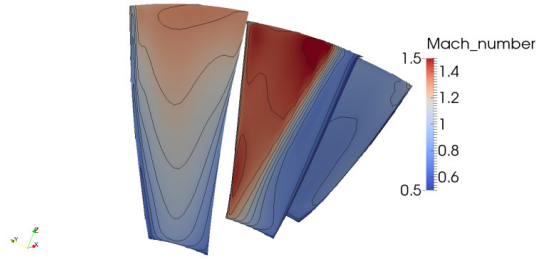


**Figure 11: Mach number contours, in the x-z plane, for the first rotor stages at the inlet, throat, and outlet.**

The oxy-fuel combined cycle has an overall net electrical efficiency of 47.2% and a net electrical power of 115.9 MW. The gross plant power is 149.1 MW, out of which 96.1 MW is from the gas turbine and 53.0 MW is from the steam turbine. The cost of the oxygen production and compression is 26.2 MW, which penalizes the efficiency by -10.7%-points. This energy cost was based on a cryogenic ASU technology with an energy consumption of 735 kW/kg $_{95\%wt}O_2$. There are, however, other promising ASU technologies coming, such as the Ionic Transport Membrane [28], which could potentially significantly reduce the penalty of the cycle efficiency.

The corresponding figures for the compression of the $CO_2$ stream to 140 bar is 6.4 MW, which penalizes the efficiency by -2.6%-points. The amounts of the cooling and sealing flows are 51.6 kg/s or 23.5% of the compressor inlet mass flow of 219.8 kg/s.

**Table 5: Average stage parameters.**

| | $T_0$ [°C] | $p_0$ [bar] | PRs [-] | Stage load [$\psi$] | Flow coefficient [$\phi$] | $C_m^*$ [-] |
|---|---|---|---|---|---|---|
| R1 in | 63.5 | 1.01 | 1.569 | 0.386 | 0.580 | 1.000 |
| R2 in | 102.6 | 1.59 | 1.444 | 0.354 | 0.610 | 1.027 |
| R3 in | 136.0 | 2.29 | 1.386 | 0.355 | 0.606 | 0.998 |
| R4 in | 167.2 | 3.18 | 1.333 | 0.349 | 0.606 | 0.975 |
| R5 in | 196.0 | 4.24 | 1.296 | 0.352 | 0.605 | 0.952 |
| R6 in | 223.2 | 5.49 | 1.263 | 0.348 | 0.602 | 0.926 |
| R7 in | 248.3 | 6.94 | 1.234 | 0.344 | 0.601 | 0.905 |
| R8 in | 271.9 | 8.56 | 1.212 | 0.344 | 0.578 | 0.853 |
| R9 in | 294.3 | 10.37 | 1.194 | 0.343 | 0.590 | 0.856 |
| R10 in | 315.6 | 12.38 | 1.178 | 0.342 | 0.585 | 0.832 |
| R11 in | 335.6 | 14.58 | 1.164 | 0.341 | 0.581 | 0.813 |
| R12 in | 354.9 | 16.97 | 1.152 | 0.338 | 0.558 | 0.768 |
| R13 in | 373.3 | 19.56 | 1.142 | 0.336 | 0.561 | 0.763 |
| R14 in | 391.1 | 22.33 | 1.130 | 0.329 | 0.551 | 0.740 |
| R15 in | 407.9 | 25.24 | 1.120 | 0.320 | 0.540 | 0.716 |
| R16 in | 423.7 | 28.27 | 1.112 | 0.308 | 0.527 | 0.693 |
| EGV in | 438.6 | 31.42 | 31.04** | | | |

* $C_m$ normalized by $C_m$ at Rotor 1 inlet; ** total compressor pressure ratio.

## CONCLUSION

This work demonstrates that the achievement of the higher pressure ratio required in an oxy-fuel cycle compared to a conventional combined cycle power plant from an aerodynamic point is eminently feasible in a single-spool compressor with today's state-of-the-art technology. The aerodynamic design and evaluation was done through 1D mid-span, 2D through flow, and steady state 3D calculations.

A conclusion is that reducing the overall gas turbine pressure ratio slightly below the optimum for the oxy-fuel cycle efficiency [5] is a sensible trade-off to facilitate a single-spool compressor design, as the $CO_2$ and steam-rich working fluid entails additional design challenges. The lower speed of sound of the working fluid at the compressor inlet is one example which limits the design range in terms of blade speed, and thus the possibility of a high stage work input.

Commercial compressor designs with a pressure ratio above 30 are usually only common in aero-derivatives, where it is achieved by a twin-spool compressor configuration. However, for an industrial gas turbine a single-spool compressor configuration is preferred as the cost and complexity is less. A high pressure ratio is harder to achieve in single-spool compressor design as the rear stages will have a lower blade speed. The lower blade speed is a result of the need to maintain the blade height at a reasonable level for efficiency reasons, which forces the design of the rear stages towards a lower RMS radius than at the compressor inlet. This reduces the achievable stage pressure ratio in the rear stages further, hence the need for extra stages.

The final design is a single spool 16-stage compressor with a design mass flow, speed, and pressure ratio of 219.8 kg/s, 5700 rpm, and 31.0, respectively. The performance figures achieved a satisfying efficiency of 90.1% and 92.8% isentropic ($\eta_s$), and polytropic ($\eta_p$), respectively, whilst maintaining a surge margin of 25.5.

The overall performance for the oxy-fuel combined cycle is 47.25% net efficiency, including $CO_2$ compression and $O_2$ production, which should thus be considered an attractive CCS technology with potential for further cycle efficiency improvements through reduced $O_2$ cost.

## PERMISSION FOR USE STATEMENT:



## ACKNOWLEDGMENTS

The authors would like to acknowledge Siemens Industrial Turbomachinery AB, Finspong, Sweden, for permission to publish this paper.

## REFERENCES

[1] T. Stocker, D. Qin, G. Plattner, M. Tignor, S. Allen, J. Boschung*, et al.*, "IPCC, 2013: climate change 2013: the physical science basis. Contribution of working group I to the fifth assessment report of the intergovernmental panel on climate change," 2013.

[2] M. Sammak, M. Genrup, E. Thorbergsson, and T. Grönstedt, "Conceptual mean-line design of single and twin-shaft oxy-fuel gas turbine in a semi-closed oxy-fuel combustion combined cycle," in *Proceedings of ASME Turbo Expo 2012: Power for Land, Sea and Air. June 11-15, 2012, Copenhagen, Denmark*, 2012, pp. 289-297.

[3] E. Thorbergsson, T. Grönstedt, M. Sammak, and M. Genrup, "A comparative analysis of two competing mid-size oxy-fuel combustion cycles," in *ASME Turbo Expo 2012: Turbine Technical Conference and Exposition*, 2012, pp. 375-383.

[4] H. Yang, D. Kang, J. Ahn, and T. Kim, "Evaluation of design performance of the semi-closed oxy-fuel combustion combined cycle," *Journal of Engineering for Gas Turbines and Power,* vol. 134, p. 111702 (10p), 2012.

[5] A. Dahlquist, M. Genrup, M. Sjoedin, and K. Jonshagen, "Optimization of an oxyfuel combined cycle regarding performance and complexity level," in *ASME Turbo Expo*

 

*2013: Turbine Technical Conference and Exposition*, 2013, pp. V002T07A011-V002T07A011.

[6] S. G. Sundkvist, A. Dahlquist, J. Janczewski, M. Sjödin, M. Bysveen, M. Ditaranto*, et al.*, "Concept for a combustion system in oxyfuel gas turbine combined cycles," in *ASME Turbo Expo 2013: Turbine Technical Conference and Exposition*, 2013, pp. V002T07A005-V002T07A005.

[7] A. Dahlquist, M. Thern, and M. Genrup, "The influence from the working medium on the profile loss in compressor and turbine airfoils," in *ASME Turbo Expo 2014: Turbine Technical Conference and Exposition*, 2014.

[8] E. W. Lemmon, M. L. Huber, and M. O. McLinden, *"NIST REFPROP (reference fluid thermodynamic and transport properties), NIST standard reference datasbas 23, Version 8.0 "*.

[9] F. Franco, T. Mina, G. Woolatt, M. Rost, and O. Bolland, "Characteristics of cycle components for CO2 capture," in *Proceedings of 8th International Conference on Greenhouse Gas Control Technologies, Trondheim, Norway*, 2006.

[10] W. Sanz, H. Jericha, B. Bauer, and E. Göttlich, "Qualitative and quantitative comparison of two promising oxy-fuel power cycles for CO2 capture," *Journal of Engineering for Gas Turbines and Power,* vol. 130, p. 031702, 2008.

[11] O. Bolland and P. Mathieu, "Comparison of two CO2 removal options in combined cycle power plants," *Energy Conversion and Management,* vol. 39, pp. 1653-1663, 1998.

[12] I. Ulizar and P. Pilidis, "A semiclosed-cycle gas turbine with carbon dioxide–argon as working fluid," *Journal of engineering for gas turbines and power,* vol. 119, pp. 612-616, 1997.

[13] R. Canepa and A. Satta, "Influence of working fluid composition on the performance of turbomachinery in semi-closed gas turbine cycles," in *ASME Turbo Expo 2012: Turbine Technical Conference and Exposition*, 2012, pp. 399-406.

[14] G. Woollatt and F. Franco, "Natural gas oxy-fuel cycles—part 1: conceptual aerodynamic design of turbo-machinery components," *Energy Procedia,* vol. 1, pp. 573-580, 2009.

[15] W. Sanz, H. Jericha, F. Luckel, E. Göttlich, and F. Heitmeir, "A further step towards a Graz cycle power plant for CO2 capture," in *ASME Turbo Expo 2005: Power for Land, Sea, and Air*, Reno, Nevada, USA, June 6–9, 2005, 2005, pp. 181-190.

[16] H. Jericha, W. Sanz, and E. Göttlich, "Design concept for large output Graz cycle gas turbines," *J. Eng. Gas Turbines Power 130(1), 011701 (2007) (10 pages);* , 2006.

[17] H. Jericha, W. Sanz, E. Göttlich, and F. Neumayer, "Design details of a 600 MW graz cycle thermal power plant for CO2 capture," in *ASME Turbo Expo 2008: Power for Land, Sea, and Air*, 2008, pp. 507-516.

[18] SINTEF Energi AS, Siemens AS Norway, Siemens Industrial Turbomachinery AB, Nebb Engineering AS, Lund University, CLIMIT (2014). *OxyGT final technical report, CLIMIT-programmet 212784*. Available: http://www.climit.no/no/Documents/OXYGT_FINAL_TECHNICAL_REPORT.pdf

[19] H. Grieb, *Projektierung von Turboflugtriebwerken*, 2004.

[20] F. J. Bayley and J. Owen, "The fluid dynamics of a shrouded disk system with a radial outflow of coolant," *Journal of Engineering for Gas Turbines and Power,* vol. 92, pp. 335-341, 1970.

[21] U. Phadke and J. Owen, "Aerodynamic aspects of the sealing of gas-turbine rotor-stator systems: part 1: the behavior of simple shrouded rotating-disk systems in a quiescent environment," *International journal of heat and fluid flow,* vol. 9, pp. 98-105, 1988.

[22] R. Hearsey, "Program HT0300 NASA 1994 version," *Doc. No. D6-81569TN, Volumes,* vol. 1, 1994.

[23] J. Denton, "Multistage turbomachinery flow calculation program-MULTIP," *Whittle Laboratory, University of Cambridge, UK,* 1999.

[24] *Gas Turbine World 2014 performance specs 30th Edition* vol. 44, 2014.

[25] P. P. Walsh and P. Fletcher, *Gas turbine performance*: John Wiley & Sons, Blackwell Publishing, 2004. ISBN: 0-632-06434-X

[26] P. De Haller, "Das verhalten von tragflügelgittern in axialverdichtern und im windkanal," *Brennst.-Waerme-Kraft,* vol. 5, pp. 333-337, 1953.

[27] I. Ulizar and P. Pilidis, "Handling of a semiclosed cycle gas turbine with a carbon dioxide-argon working fluid,"

 

*Journal of engineering for gas turbines and power,* vol. 122, pp. 437-441, 2000.

[28] J. M. Repasky, L. L. Anderson, V. E. Stein, P. A. Armstrong, and E. P. T. Foster, "ITM oxygen technology: scale-up toward clean energy applications," in *International Pittsburgh Coal Conference, Pittsburgh, Pa., USA*, 2012, pp. 15-18.

 

Publication VI

# Aerodynamic Turbine Design for an Oxy-fuel Combined Cycle

**Dahlquist, A.**, Genrup, M.,

ASME Turbo Expo 2016, GT2016-56439

**Proceedings of the ASME Turbo Expo 2016: Power for Land, Sea, and Air**
**June 13- 17, 2016, Seoul, South Korea**

**GT2016-56439**

# Aerodynamic Turbine Design for an Oxy-fuel Combined Cycle

**Adrian Dahlquist**

Siemens Industrial
Turbomachinery AB
SE-612 83 Finspong, Sweden
*Corresponding author.*
adrian.dahlquist@siemens.com

**Magnus Genrup**

Energy Sciences
Lund University
SE-221 00 Lund, Sweden

## ABSTRACT

The oxy-fuel combined cycle (OCC) is one of several carbon capture and sequestration (CCS) technologies being developed to reduce $CO_2$ emissions from thermal power plants. The OCC consists of a semi-closed topping Bryton cycle, and a traditional bottoming Rankine cycle. The topping cycle operates with a working medium mixture of mainly $CO_2$ and $H_2O$. This $CO_2$-rich working fluid has significantly different gas properties compared to a conventional open gas turbine cycle, which thereby affects the aerodynamic turbine design for the gas turbine units. The aerodynamic turbine design for oxy-fuel gas turbines is an unexplored research field. The topic of this study was therefore to investigate the aerodynamic turbine design of turbines operating with a $CO_2$-rich working fluid. The investigation was performed through a typical turbine aero-design loop, which covered the 1D mid-span, 2D through-flow, 3D blade profiling design and the steady-state 3D analysis. The design was performed through the use of conventional design methods and criteria in order to investigate if any significant departures from conventional turbine design methods were required.

The survey revealed some minor deviations in design considerations, yet it showed that the design is feasible with today's state-of-the-art technology by using conventional design practice and methods.

The performance of the oxy-fuel combined cycle was revised based on the performance figures from the components design. The expected total performance figures for the oxy-fuel combined cycle were calculated to be a net electrical power of 119.9 MW and a net thermal efficiency of 48.2%. These figures include the parasitic consumption for the oxygen production required for the combustion and the $CO_2$ compression of the $CO_2$ bleed stream.

## NOMENCLATURE

| | | |
|---|---|---|
| $c_p$ | Specific heat at constant pressure | [kJ/kg·K] |
| h | Enthalpy | [kJ/kg] |
| m | Mass flow | [kg/s] |
| Ma | Mach number | [-] |
| p | Pressure | [bar] |
| R | Gas constant | [J/kg·K] |
| T | Temperature | [°C/ K] |

## ABBREVIATIONS

| | |
|---|---|
| 0-, 1-, 2-, 3D | 0-, 1-, 2-, 3-dimensional |
| ASU | Air separation unit |
| CCS | Carbon capture and sequestration |
| CT | Compressor turbine |
| CCPP | Combined cycle power plant |
| HRSG | Heat recovery steam generator |
| OCC | Oxy-fuel combined cycle |
| PT | Power turbine |
| SCOC-CC | Semi-closed oxy-fuel combustion combined cycle |
| TID | Turbine intermediate duct |

## SUBSCRIPT

| | |
|---|---|
| in | Inlet |
| out | Outlet |
| s | Static |

## GREEK SYMBOLS

| | | |
|---|---|---|
| $\phi$ | Flow coefficient | [-] |
| $\gamma$ | Isentropic exponent | [-] |
| $\eta_s$ | Isentropic efficiency | [%] |
| $\rho$ | Density | [kg/m$^3$] |
| $\psi$ | Stage loading | [-] |

## INTRODUCTION

Global warming is a serious challenge today (IPCC [1]) which calls for efforts in several areas to mitigate the emission of carbon dioxide ($CO_2$), for example through: more efficient energy utilization, more renewables and the use of carbon capture and sequestration (CCS) technologies. CCS refers to the group of technologies where the $CO_2$ formed through combustion of a carbon-containing fuel is separated to prevent it from being emitted to the atmosphere. A number of CCS technologies are currently being investigated and developed to reduce $CO_2$ emissions emitted from thermal power plants. They may finally be on the brink of becoming a reality once either the carbon emission fees reach a certain level or they are called for by legislation. The oxy-fuel combined cycle (OCC) is one promising CCS technology, which has been presented in previous publications [2-7].

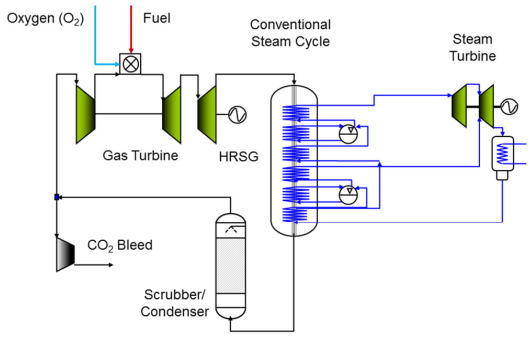


**Figure 1: Schematic sketch of the oxy-fuel combined cycle plant layout**

The oxy-fuel combined cycle is a power cycle designed for $CO_2$ capture, with several similarities to a conventional combined cycle power plant (CCPP). The OCC consists of a topping cycle and a bottoming cycle and a schematic sketch of the OCC is seen in Figure 1. The topping cycle is a recirculated semi-closed gas turbine and the bottoming cycle is a conventional steam cycle. The fundamental key principle of the oxy-fuel technology is to form a combustion product of virtually pure $CO_2$ and $H_2O$ in the gas turbine cycle, which is then separated into its basic components. This is achieved by replacing the conventional oxidizer stream of air with an externally provided stream of almost pure oxygen ($O_2$). The combustion products of $CO_2$ and $H_2O$ act also as the working medium in the gas turbine, as the topping cycle is semi-closed and recirculated. It should be noted that the $CO_2$ part of the working medium remains in gas phase throughout the cycle and that only the $H_2O$ is partially condensed; hence the OCC is not a supercritical $CO_2$ cycle. The ratio of $CO_2$ to $H_2O$ in the working medium depends mainly on the temperature in the flue gas condenser after the heat recovery steam generator (HRSG). A lower cooling temperature increases the amount of $H_2O$ condensation, which reduces the steam content in the working medium. The composition of the working medium falls generally within the range of 80–90 wt.-% $CO_2$, 10–20 wt.-% $H_2O$ and a few percentage points of enriched argon (Ar) and nitrogen ($N_2$) gases. The mentioned non-reactants originate from slippage in the cryogenic Air Separation Unit (ASU) and as argon is not being efficiently separated in the cryogenic ASU it instead becomes enriched in the semi-closed cycle. The mass fraction of argon is therefore higher in the $CO_2$-rich working medium than in atmospheric air. The reason for this is that the condensation temperatures of argon and oxygen are close, i.e. the condensation temperature of argon is 87.2 K and of oxygen is 77.2 K at standard atmospheric pressure [8].

**Table 1: Gas properties at the inlet to the oxy-fuel turbines and the gas properties for air at similar gas states**

| | | *CT* | | *PT* | |
|---|---|---|---|---|---|
| | | *OCC*[1] | *Air* | *OCC*[2] | *Air* |
| Pressure (p) | [bar] | 30.150 | 30.150 | 7.200 | 7.200 |
| Temperature (T) | [°C] | 1,340.0 | 1,340.0 | 930.0 | 930.0 |
| Molar mass (M) | [g/mol] | 36.33 | 28.96 | 36.68 | 28.96 |
| Isentropic exponent ($\gamma$) | [-] | 1.184 | 1.308 | 1.195 | 1.324 |
| Specific heat ($c_p$) | [kJ/kg K] | 1.488 | 1.223 | 1.396 | 1.176 |
| Gas constant (R) | [J/kg K] | 228.9 | 287.1 | 226.7 | 287.1 |
| Speed of sound (a) | [m/s] | 665.0 | 783.5 | 571.6 | 677.6 |
| Density ($\rho$) | [kg/m$^3$] | 8.118 | 6.466 | 2.637 | 2.080 |

1) Mass fraction 80.3% $CO_2$, 13.4% $H_2O$, 2.5% $N_2$, 3.7%Ar, 0.1% $O_2$

2) Mass fraction 81.1% $CO_2$, 12.6% $H_2O$, 2.5% $N_2$, 3.7%Ar, 0.1% $O_2$

As previously discussed, the working medium in the oxy-fuel combined cycle has, indeed, different gas properties compared to a conventional air-breathing gas turbine. The differences in gas properties between the two gases that have the greatest influence on the turbine design are the isentropic exponent ($\gamma$), specific heat at constant pressure ($c_p$), gas constant (R) and speed of sound (a) (Table 1). These differences affect both the design of the entire OCC and the design of the gas turbine unit and its subcomponents, i.e. the compressor, combustor and turbines. The lower isentropic exponent ($\gamma$) calls for a higher gas turbine pressure ratio to achieve a gas temperature drop across the turbine(s) that is similar to a conventional gas turbine. For a high overall

efficiency of the OCC, the exhaust gas temperature (EGT) from the gas turbine must suit the steam turbine design, i.e. the temperature level of the high pressure steam with a low- to modest pinch-point in the super-heater. Gas turbine pressure ratios ranging from 30 to 60 have been proposed for oxy-fuel combined cycles by different authors [2, 4, 6, 9-12]. Other aspects that needed to be considered especially for the OCC were the lower speed of sound (a) and the larger variations in specific heat ($c_p$) with respect to temperature for the $CO_2$-rich medium compared to air or flue gas [5, 13]. These differences lead to further challenges for the aerodynamic design of the gas turbine.

This work was part of a larger survey in which both low-technology readiness level optimization of the overall oxy-fuel combined cycle and more detailed high-technology readiness level aerodynamic design studies of the gas turbine units' compressor, turbines and a preliminary combustor concept were investigated and tested. A cycle design for the OCC was investigated in previous publications [3, 6] in which different cycle design aspects were considered. The outcome from these two studies was a proposed cycle design of an OCC. This cycle design then formed the foundation for the subsequent more detailed investigations of the conceptual aerodynamic design of the gas turbine unit. The combustor concept was also investigated as a part of the work [3, 6]. To make it possible to proceed with the conceptual aerodynamic design of the compressor and turbines, the effect on the aerodynamic losses from the working medium was investigated [5]. The aerodynamic design of the compressor was addressed and proved, theoretically, to be feasible to achieve in a single-spool compressor with today's state-of-the-art technology [7]. It was also shown that the compressor design could be performed by using conventional design methods and while remaining within current practice for conventional design [14]. The missing piece for demonstrating the complete aerodynamic design of a gas turbine unit was the conceptual aerodynamic design of the compressor- and power turbine, which was addressed in this work.

This publication is divided into two parts. The main part addresses the aerodynamic design of the compressor- and power turbine. The second part revises the performance figures of the entire OCC. This was done by updating the process simulation of the OCC with the performance figures from the conceptual aerodynamic designs of the compressor performed in [7] and the compressor- and power turbine performed in this work.

The main objectives of this work were to numerically investigate and demonstrate the feasibility of achieving the aerodynamic design of the turbines for a gas turbine unit in an oxy-fuel combined cycle. The resulting design parameters were also compared against traditional design guidance (rules) for conventional air-breathing turbines. The purpose of that was to investigate whether the turbine design could be performed within traditional design recommendations for an air-breathing state-of-the-art turbine design; that is, aiming to strengthen the confidence of its feasibility and to find out if any fundamental design deviations appear necessary.

## METHOD

The design of the OCC previously investigated in [6] was used as a platform for the present turbine design. The simulation of the entire oxy-fuel combined cycle was performed in the Siemens in-house standard process simulation tool, Krawal-modular, which is a flexible advanced heat and mass balance tool, which utilizes real gas properties (LibHuGas). The shaft configuration and basic design of the gas turbine unit were investigated in a previous work [14]. The different shaft configurations considered were a single-shaft, a single-shaft gas generator with free power turbine, a twin-spool gas generator unit where the low pressure turbine also serves as the power turbine, and a twin-spool gas generator with a free power turbine. The design choice for a conventional combined cycle gas turbine would (most likely) be a single-shaft design. A single-shaft design has the advantage of being a simpler design with improved performance at both base load and part load. It should, however, be noted that gas turbines designed mainly for a conventional combined cycle application generally have a pressure ratio in the range of 18–22. That is because they are typically designed to have an exhaust temperature into the HRSG in the range of 580–650 °C to suit the steam cycle. Exceptions to this are seen for aero-derivatives that, because of their heritage, have a higher pressure ratio, which is usually achieved through a twin-spool compressor configuration. When given the opportunity to design a new gas turbine, a simple and robust design was sought. However, considering that the oxy-fuel gas turbine needs a pressure ratio above 30 and that the electrical generator was decided to be direct-driven [7] it was found that a single-spool gas generator with a free power turbine was a favorable design. A detailed aerodynamic design of a single-shaft compressor was performed in [14].

The approach for the turbines design was to use previous findings and results as the base for the design of the turbines, although the design was performed partly in parallel with each other in an iterative process. The turbine cooling and disc-sealing predictions were incorporated using two different correlation-based models. The cooling flows were calculated from a m-star model [15] with some further developments, which scales the cooling flows with respect to the gas properties, turbine geometry and its operation conditions based on operational gas turbine reference values [6]. The disc-sealing flows were predicted according to the well-established method by Bayley and Owen [16, 17].

This pre-design work of the entire gas turbine unit formed the basis for specifying the boundary conditions and performance parameters that the compressor- and power turbine had to be designed to meet (Table 2, Table 3). The gas states at the compressor turbine inlet and at the power turbine outlet and restrictions on the gas path geometry and its hade angles are examples of parameters set by the pre-design loop. The shaft speed and required shaft power for the compressor turbine were

specified by the compressor design to be 5,700 rpm and 86.5 MW, respectively. The power turbine generator was direct driven at 3,000 rpm (50 Hz) to avoid the extra cost, installation complexity and losses associated with a gearbox of this size. The design target for the power turbine was simply to seek a high shaft power and operability through a high efficiency and favourable inlet conditions to the turbine diffusor, based on the gas state that the compressor turbine delivers.

**Table 2: Constrained design parameters for the compressor turbine**

| *Parameter* | *Unit* | *Values* | |
|---|---|---|---|
| Shaft power | [MW] | 86.5 | |
| Temperature in/out | [°C] | 1,340 | 930* |
| Pressure in/out | [bar] | 31.1 | 7.2* |
| Mass flow in/out | [kg/s] | 193.1 | 236.1* |
| Cooling flow | [kg/s] | 43.0 | |
| Shaft speed | [rpm] | 5,700 | |

* set by the power demand and the compressor turbine efficiency

**Table 3: Constrained design parameters for the power turbine**

| *Parameter* | *Unit* | *Values* | |
|---|---|---|---|
| Temperature in/out | [°C] | 930* | 612 |
| Pressure in/out | [bar] | 7.2* | 1.11 |
| Mass flow in/out | [kg/s] | 236.2* | 244.4 |
| Cooling flow | [kg/s] | 8.2 | |
| Shaft speed | [rpm] | 3,000 | |

* set by the compressor turbine outlet, see Table 2

## Aerodynamic design

The same aerodynamically fundamental physical laws and design philosophy generally determine the aerodynamic turbine design, whether it is a conventional air-breathing turbine or a turbine designed for an oxy-fuel application. The method used for the turbine design was therefore treated as a conventional turbine design, unless otherwise required for obvious reasons. For example, the gas properties of the working medium and the different design requirements for the turbines affect the design trade-offs and dictated what was achievable or not for the turbine.

Current practice is to design the turbine with 1D and 2D aero-tools that primarily rely on loss models derived for conventional turbines. The utilization of these air-based loss models for the oxy-fuel turbine design raised the question of their applicability, which was addressed previously [5]. In that study it was concluded that the correlations can be used in the design phase of, at least, lightly to modestly loaded airfoils. Some caution is advised for predicting the behaviour at off-design and for more heavily loaded designs because of the uncertainty in the boundary layer separation limit. The conviction of the correlations' applicability was strengthened by the consistent agreement between the correlation-based 2D through-flow and Navier–Stokes based 3D steady-state calculations of the compressor [14].

The aerodynamic design phase of the turbine, given that the global design parameters were specified for the turbine, can be roughly divided into three steps. The first step was to conduct a 1D mid-span design where typical turbine design parameters were determined, e.g. stage count, solidity, stage loading ($\psi$), flow coefficient ($\phi$), reaction ($\Lambda$), pressure ratio across each turbine stage, total turbine pressure ratio and an indicative geometrical shape of the gas path. The 1D mid-span design determines most of the design features – hence, a major part of the final design and its achievable performance. The importance of the 1D phase cannot be overstated.

The next step was to perform the 2D through-flow design to obtain the radial span-wise variation of the flow field that satisfies the intended 1D design. Special attention was given to the flow at the end-walls to ensure positive hub reaction (row acceleration) and to avoid too high exit Mach numbers.

Blade stacking features such as twist, lean and sweep can be applied too to improve the reaction, losses and Mach number, particularly in the hub- and tip sections. The stacking strategy was applied in the 2D design, but due to its 3D nature the effect was mainly captured first in the 3D analysis. Inverse twisting of the stator vanes was applied by opening up the stator outlet flow angle towards the tip section, i.e. a more axial flow angle in the tip section. The benefit of this is a more uniform span-wise relative inlet flow angle to the following rotor, which provides less twisted rotor blades and increased flow turning in the rotor tip section. The former is important for cooled blades because it is beneficial for the casting of the cooling system.

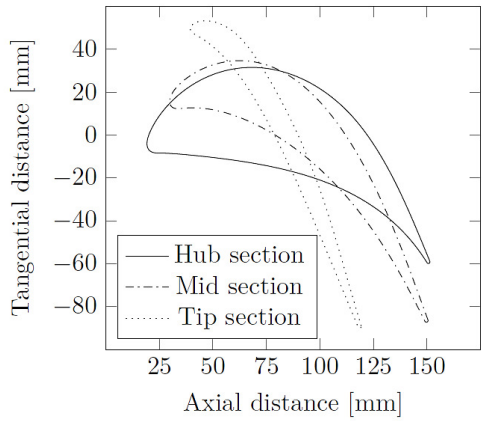


**Figure 2: The 2D cross-section profiles at the hub-, mid- and tip section for rotor 3 in the power turbine**

The mechanical integrity of the turbines was evaluated through basic 1D assessments that included the blades, vanes, blade shrouds, blade (foot) attachments and the blade discs.

This early perception of the design was used to verify that it was also realistic to achieve a mechanical design for the intended aerodynamic turbine design.

When the desired flow field was determined the next step was to profile the 3D-shaped airfoils to achieve this flow field with a sound balance between a low aerodynamic loss and operation range. Each airfoil (either stator or rotor) was generated by stacking a number of 2D blade cross-sections to create the desired 3D blade profiles. The number of 2D cross-sections used was 3 to 5 with an interpolated geometry in between. That is a sufficient approach for the conceptual design. The final airfoil design would, however, benefit from a denser radial profiling stacking and especially the more 3D-shaped blades. The profiling and stacking of the 2D cross-sections were performed with the 2D profiling and 3D stacking program Cato (Siemens in-house program). The 2D cross-sections at the hub-, mid- and tip section for the third rotor in the power turbine are seen in Figure 2. The corresponding calculated 2D velocity profile for the mid-span section is seen in Figure 3 in the form of the Laval number. The Laval number is defined as the ratio between the velocity (V) and the speed of sound at a local Mach number of unity (c*), i.e. the Laval number is defined as V/c* [18]. The 3D design will, in general, not substantially improve the design, but it risks degrading the performance if not carried out carefully.

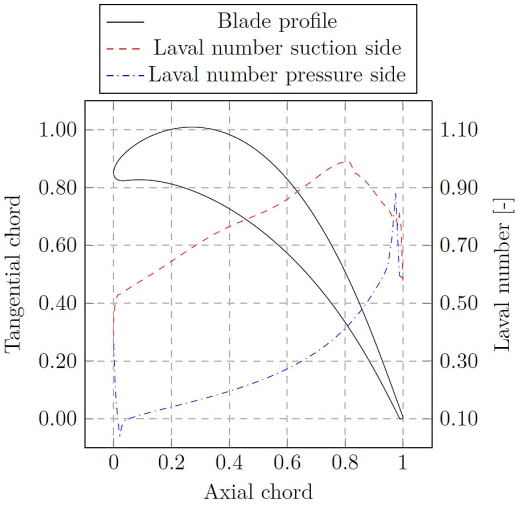


**Figure 3: The 2D cross-section profile and the Laval number distribution for rotor 3 in the power turbine**

Minor improvements can nevertheless be seen from the effect of the 3D blade stacking features and end-wall profiling. These 3D stacking schemes aim mainly to improve the reaction and exit Mach number in regions near the hub and casing by altering the radial pressure profile through creating a favourable radial flow-field curvature (i.e. pressure gradient). 3D stacking can also be used to off-load the end-walls to reduce end-wall losses.

To fine-tune the design and validate the results the 3D flow solver Multall was used. Multall is a steady-state 3D flow solver, originally developed by Denton at the Whittle Lab in Cambridge [19, 20]. Multall uses a simple mixing length turbulence model and a wall function for obtaining the turbulence and the wall shear stresses in combination with the mixing plane. This implies that a quite coarse grid can be used, which greatly reduces the computational time compared to a more advanced 3D flow solver. Multall is therefore appropriate for conceptual studies and to obtain a first prediction of how the 3D flow field ought to be. The grid is a standard H-grid with the recommendation of using a cusp on the leading and trailing edges. The grid used for each blade row consisted of 170 meridional cells, 55 span-wise cells and 55 tangential cells. The number of cells between the airfoil's leading edge and the upstream mixing plane and the trailing edge and the downstream mixing plane was 20 in each case. Exceptions to this were the inlet and the outlet of the turbines, for which about 100 cells were used.

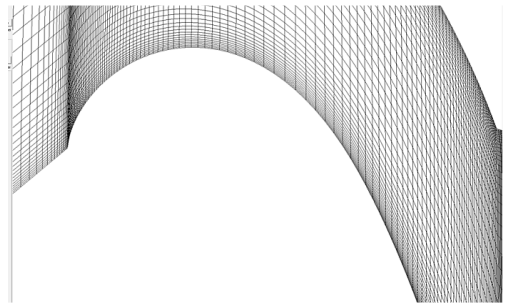

**Figure 4: Section of the grid seen in the tangential vs. meridional plane for rotor 2 in the compressor turbine (170 x 55 x 55 cells in each row)**

A 2D cross-section of the grid in the meridional vs. tangential plane for rotor 2 in the compressor turbine is seen in Figure 4. For a plain blade tip the tip leakage flow was modelled through a pinched tip, by reducing the blade tip thickness towards zero over the last 2–3 cells. Denton also recommends reducing the tip clearance to about 60% of the physical gap to compensate for the contraction effect in the real leakage jet, which was followed (Figure 5). The physical plain tip clearance used for the compressor turbine was 1 mm. The power turbine was modelled with shrouds with two seals in stage 1 and 2 and one seal in stage 3 and 4 with a tip clearance in the range of 1.6–2.6 mm. The turbine cooling and the disc purge flow between the stages were modelled through flow ejection patches. For each patch the mass flow, pressure, temperature, Mach number and entrance flow angle were specified. The Multall version used for this study has also been

further developed, in Siemens, to enable a variable specific heat ($c_p$) to be utilized.

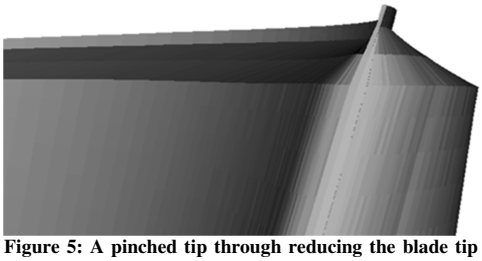

**Figure 5: A pinched tip through reducing the blade tip thickness to zero over the last 2–3 cells (exemplified by Rotor 2 in the compressor turbine)**

The intention with this investigation was to show that the aerodynamic turbine design for the oxy-fuel gas turbine is feasible with today's state-of-the-art technology using conventional design methods, and not to describe the precise design. The exact design philosophies, rules and design parameters could not be presented because of the inherent proprietary nature. This will, however, not affect the purpose of this work. The turbine design herein is not claimed to be either optimal or final. It should instead be seen as an extended conceptual design and proper starting point for the final design.

**Cycle performance**

When the conceptual designs of the two turbines were completed performance maps for the turbines were created. A compressor map was created in the previous work [7]. To revise the steady-state performance of the entire oxy-fuel combined cycle, these three characteristics were used in a new process simulation. The figures for the oxy-fuel combined cycle design are presented in the second part of this paper.

## RESULTS & DISCUSSION

The main boundary conditions and specific design criteria for the compressor- and power turbine were determined by the process simulation. The global design requirements for the compressor- and power turbine are summarized in Table 2 and Table 3. The parameters between the two turbines were determined through an iterative process and are not strictly speaking either any boundary conditions or design criteria. These parameters are marked by an asterisk (*) in Table 2 and Table 3. The gas state in between the two turbines is an example of this. Initially, these figures were set by the previous design steps and progressed to an iterative design process between the two turbines. The figures in Table 2 and Table 3 are the final design values.

The design of the turbines geometry and how they influence and interact with each other and the compressor are vital for a successful gas turbine design (i.e. by avoiding sub-optimization). Therefore, great emphasis was put on the decision of the gas path radius for the compressor turbine, the power turbine and the turbine intermediate duct (TID) between the two turbines (Figure 6).

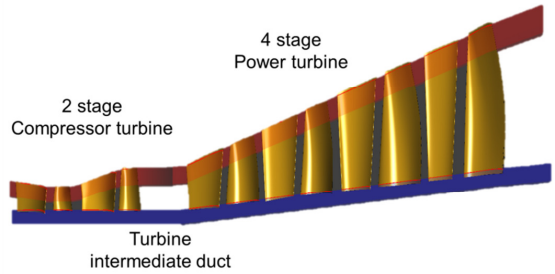


**Figure 6: Gas path shape of the compressor turbine and the power turbine connected through a short intermediate duct**

**Turbine intermediate duct**

The gas temperature after the compressor turbine can become an issue when designing twin-shaft gas turbines as the temperature tends to exceed the material limit for conventional uncooled materials, especially with the drive towards both increasingly higher combustion outlet temperatures (COT) and gas turbine exhaust temperature. This problem becomes more severe in the design of an oxy-fuel gas turbine because of the gas properties. The difference is the variation in specific heat at constant pressure ($c_p$) against temperature for the $CO_2$-rich working medium compared to a conventional flue gas. The variation in specific heat is illustrated in Figure 7 for air and $CO_2$.

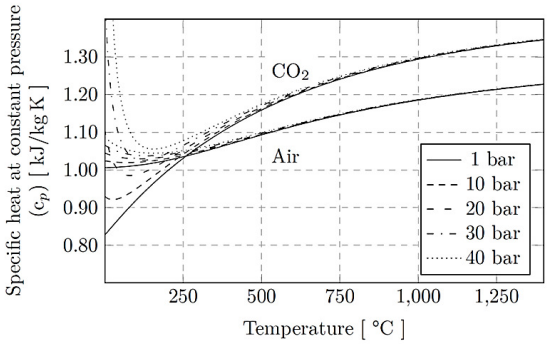


**Figure 7: Variation in specific heat at constant pressure with temperature for air and $CO_2$**

It is seen that the specific heat for $CO_2$ is about 7–10% higher than for air in the temperature range from 600 to 1,400°C, where the turbines operate. In the temperature range

from 0 to 500°C where the compressor operates, the ratio is very different and at temperatures below about 260°C the specific heat for $CO_2$ is actually less than for air. This has the result that the specific compression work is less energy-consuming for a $CO_2$ compressor at low temperature.

The specific heat ratio is the opposite for the turbines in the high temperature range. In a $CO_2$ turbine the specific work extracted for a certain temperature drop is thereby higher compared to a conventional turbine. For a specific COT and sufficient turbine cooling, these differences in the gas properties of the working medium result in a higher gas temperature after the compressor turbine in an oxy-fuel gas turbine. The magnitude of this temperature difference depends on several design parameters such as the gas turbine pressure ratio, component efficiencies, COT, turbine cooling and the steam content in the working medium. Approximately, the duct temperature is expected to be 25–55°C higher in the case of an oxy-fuel gas turbine, compared to a conventional air-breathing twin-shaft gas turbine unit. The trend is that the difference declines with rising COT (1,000–1,500°C) because of the decreasing difference in specific heat in the compressor. That is because the need for higher total gas turbine pressure ratios increases with the COT, for a certain EGT.

Another outcome is that the specific power for the oxy-fuel gas turbine is higher than for a conventional gas turbine because more energy is available for the power turbine. The precise increase in specific power is dependent on the same design parameters as discussed above, but an increase in the specific power of about 20–40% can be expected for a combustor outlet temperature variation from 1,500°C to 1,000°C. The specific power for the OCC, based on the exhaust gas mass flow, is 410 kW/kg.

The process simulation of the oxy-fuel cycle design showed that the gas temperature between the two turbines would be about 930°C at the design point. A turbine intermediate duct (TID) at this elevated temperature has to be cooled, which would increase the cooling medium consumption and thereby decrease the total efficiency. Future engine upgrades through raising the combustor outlet temperature would also be aggravated by a TID. The TID should therefore be kept as small as possible or preferably avoided completely if possible. The length of the TID also becomes significant if any substantial change in the mean diameter between the CT outlet and the PT inlet is to be achieved. That is because, to avoid flow separation along the outer end-wall, its hade angle cannot be too severe. A recommendation for the preliminary design is to keep the hade angle below 25°. At the inlet to the TID the inlet swirl and the inlet Mach number should also be kept modest (< 35° and < 0.55) to keep down the end-wall losses [21]. A TID tends also to have a conical shape and the guidance is to keep the equivalent conical divergence angle below 25° and the area ratio between the CT outlet and PT inlet below 1.3 [21] to avoid flow separation. The two turbines were therefore designed to fit together geometrically with only a small straight TID connecting the two turbines. The design intentions of the turbines were to: achieve suitable blade speeds in both turbines, a proper exhaust flow area from the power turbine, avoid too severe end-wall hade angles and to have a geometrical fit between the turbines. Some of these intentions conflict and required trade-offs.

The shaft speed for the gas generator is most critical for the flow field into the compressor and therefore the velocity triangles and geometry of the first compressor rotor determine (more or less) its shaft speed. The gas generator shaft speed was thereby set by the compressor design performed previously [7] to be 5,700 rpm at the design point. The mean blade diameter for the compressor turbine is then virtually set by the maximum acceptable blade speed. The compressor turbine inlet cannot be allocated at a too high diameter as the blade height then tends to be too short for an adequate aerodynamic design (i.e. hub to tip ratio).

The power turbine generator was determined to be direct driven, which for a two-pole 50 Hz generator determines the shaft speed as 3,000 rpm. The corresponding figure for a two-pole 60 Hz generator is 3,600 rpm. This work focused on the 3,000 rpm design case, since it is most challenging from an aerodynamic point of view. This is because, if the aerodynamic design is satisfied at 3,000 rpm, then it is most likely not an issue to achieve an aerodynamic design for 3,600 rpm by redesigning the airfoils. Then positioning the turbines on similar diameters to keep the TID short with the shaft speeds of both turbines determined resulted in a compromise for the design of the power turbine. The result of this compromise is evident as the blade speed in the power turbine becomes lower than the aerodynamic optima, which results in additional stages if the stage loading is to be kept at the same level. This design trade-off was, however, not obvious and an alternative was to increase the blade speed by positioning the power turbine at a larger diameter. That could have reduced the stage count in the power turbine down to 3 stages from the current 4-stage design, but it would have required a large cooled TID in order to accommodate the radial shift. This trade-off between a 3-stage and 4-stage design is discussed more in the following section "Power turbine". A schematic view of the compressor turbine, power turbine and the turbine intermediate duct is seen in Figure 6.

**Compressor turbine**

The compressor turbine design is a 2-stage turbine with a constant hub radius throughout the turbine to enhance the disc design. The two rotor blades are shroudless to avoid extra weight and cooling as the blades in the compressor turbine are highly stressed both thermally and mechanically. Both rotor blade tips are cylindrical to reduce the tip clearances' sensitivity to axial movements during transients. The entire change in the axial flow area is achieved in the second stator vane, which results in a rather steep but acceptable hade angle at the outer end-wall (21°). The compressor turbine hub radius is 620 mm, the length is 410 mm and the height of the first rotor is 75 mm. The stage loadings for the 2-stage compressor turbine are considered as conservative. That was partly because of the lower compressor work resulting from the variation in

specific heat, as seen in Figure 7 and discussed in the previous section. It was therefore tempting to design the compressor turbine as a 1-stage turbine. When the 1-stage design was investigated, it showed that a couple of significant compromises were required, as both the stage load and blade velocity had to be increased substantially. This would result in a design with very short blade heights if the axial velocity (Ca) was to be kept constant or even more if the flow coefficient ($\phi = Ca/U$) was kept with an increased higher blade velocity. The velocity triangles would also become too skewed and the blade- and disc stresses increased to unacceptable levels in the 1-stage design. This alternative 1-stage design was not shown to be more favourable and was rejected in favour of the 2-stage design. The isentropic total-to-total efficiency for the 2-stage compressor turbine was calculated to be 86.7% and its main stage parameters are summarized in Table 4.

**Table 4: Stage parameters for the compressor turbine**

| *Parameter* | *Unit* | *Stage 1* | Stage 2 |
|---|---|---|---|
| Blade velocity | [m/s] | 394 | 411 |
| $PR_s$ / $PR_t$ | [-] | 2.06/ 1.98 | 2.25/ 2.13 |
| Stage loading ($\psi$) | [-] | 1.32 | 1.21 |
| Reaction hub/ tip ($\Lambda$) | [-] | 0.53/ 0.57 | 0.44/ 0.52 |
| Absolute exit flow angle | [°] | - | 11.2 |
| Isentropic exit Mach number Stator/ Rotor | [-] | 0.74/ 0.87 | 0.85/ 0.87 |

## Power turbine

The power turbine is a 4-stage design with straight conical inner and outer end-walls. The radii at the power turbine inlet are 622 mm and 740 mm and at the outlet the radii are 766 mm and 1,195 mm. The overall length is 980 mm, hence the end-wall hade angles are 7° and 24° degrees at the inner and outer end-walls, respectively. The exit Mach number and stage load are on the low side and thus a 3-stage power turbine was also considered. This alternative was, however, rejected for the following reasons.

First it should be clarified that the stage loading of the last stage cannot be significantly increased without initiating an unfavourable and penalizing flow field into the diffuser. Therefore, for a specific blade speed (U), the stage work in the last stage is almost constant. It was not possible to maintain the geometrical fit between the CT and stator 1 in the PT and then only increase the blade speed in the two rear PT stages by increasing their mean diameter. The reason for this is that the hade angle along the tip casing in the PT then tends to get too severe (> 25°). The mean diameter for the last stage could therefore not be substantially increased without also increasing the mean diameter for the first stage in the power turbine, which would require a TID between the CT and PT. In a 3-stage design it therefore becomes necessary to extract the work in just two stages, instead of in three as in the 4-stage design. This implies that either the stage load ($\psi$) or the blade velocities (U) or both have to be increased considerably. The design study showed that a 3-stage design, where only the stage load was increased, was not feasible without major losses in the turbine efficiency.

**Table 5: Stage parameters for the power turbine**

| *Parameter* | *Unit* | *Stage 1* | Stage 2 | Stage 3 | *Stage 4* |
|---|---|---|---|---|---|
| Blade velocity | [m/s] | 234 | 256 | 283 | 307 |
| $PR_s$ / $PR_t$ | [-] | 1.48/ 1.41 | 1.65/ 1.57 | 1.86/ 1.74 | 1.82/ 1.70 |
| Stage load ($\psi$) | [-] | 1.52 | 1.57 | 1.44 | 1.08 |
| Reaction hub/tip ($\Lambda$) | [-] | 0.45/ 0.54 | 0.47/ 0.55 | 0.45/ 0.56 | 0.34/ 0.54 |
| Absolute exit flow angle | [°] | - | - | - | 4.9 |
| Exit Mach number Stator/Rotor | [-] | 0.59/ 0.65 | 0.66/ 0.72 | 0.73/ 0.80 | 0.75/ 0.76 |

The other alternative would be to increase the stage load ($\psi$) and the blade velocity (U) for all stages in the PT by increasing the mean blade diameter. This would be an attractive aerodynamic design, but it would obviously require a TID and its related issues with an increased cooling medium consumption, as discussed previously.

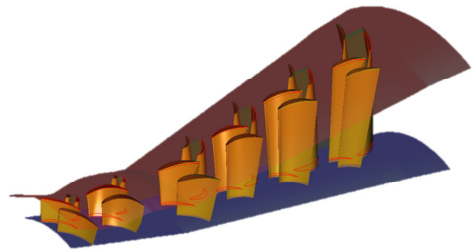

**Figure 8: The 3D geometry design of the turbines**

Adding an extra power turbine stage instead of a turbine intermediate duct is justified against the background that the TID has to be cooled, whilst an additional fourth turbine stage virtually does not increase the cooling. The 3-stage design was thereby not found to be advantageous over the 4-stage power turbine, which was considered as the preferred design choice.

The total and static pressures at the diffuser inlet are 1.108 and 1.035 bar(a), respectively. The isentropic total-to-total efficiency for the power turbine was calculated to be 92.6% and some of the main stage parameters are summarized in Table 5.

When comparing the stage parameters of the turbines design, for the oxy-fuel combined cycle given in Table 4 and Table 5, with typical figures for a conventional turbine design is it seen that the figures do not deviate significantly. The same is true when examining the velocity profile for the airfoils, which shows a very typical distribution, as was witnessed by rotor 3 in the power turbine (Figure 3). This indicates that the design of turbines in an oxy-fuel unit can be performed through the use of traditional design methods and rules used for conventional turbine design. The 3D geometry of the 2-stage compressor turbine and the 4-stage power turbine is seen in Figure 8.

## OXY-FUEL COMBINED CYCLE

The performance figures for the entire oxy-fuel combined cycle are presented in this section. The cycle design layout was presented previously [7], in which only minor modifications have been made to the design since the original design proposed in 2013 [6]. The schematic cycle is shown in Figure 1 and the details are presented in the earlier publications [6, 7]. Performance characteristics for the compressor and turbine were generated from the aerodynamic design of the compressor [7] and the turbines design in this work.

The performance of the entire oxy-fuel cycle was predicted by running the process simulation using these characteristics in order to analyse the steady-state operation. The OCC were, after been revised, calculated to have a gross and net electrical power of 153.7 MW and 119.9 MW respectively with a net efficiency of 48.2%. These figures include the parasitic energy consumption for the oxygen production and $CO_2$ compression, which reduces the total efficiency by 10.6% and 2.6%, respectively.

## CONCLUSION

This work, together with the present authors' previous publications [3, 5-7], provides a conceptual design of an oxy-fuel combined cycle plant and a conceptual aerodynamic design of the gas turbines compressor and turbines.

The design demonstrates the ability to achieve the aerodynamic turbine design for a gas turbine in an oxy-fuel cycle application with today's state-of-the-art technology, using conventional design methods and by remaining within our design expertise. This is despite the different working medium and changed operation condition compared to the gas turbine in a conventional combined cycle power plant, e.g. the increased gas turbine pressure ratio. The aerodynamic turbine design and analysis loop were made through 1D mid-span, 2D through-flow, and steady-state 3D calculation.

The different variation in the specific heat with respect to temperature for the $CO_2$-rich working medium in the oxy-fuel combined cycle, compared to a conventional combined cycle, results in a higher gas temperature after the compressor turbine. Because of this higher temperature it is not desirable to have a turbine intermediate duct, as this would need to be cooled. The compressor- and power turbines were therefore designed to fit each other geometrically, without any turbine intermediate duct. The turbine design was a 2-stage compressor turbine and a 4-stage power turbine. The isentropic total-to-total efficiency for the compressor- and power turbine were calculated to be 86.7% and 92.6%, respectively.

The overall net efficiency of the oxy-fuel combined cycle is 48.2%, including $CO_2$ compression and $O_2$ production. The oxy-fuel combined cycle should therefore be considered as an attractive and competitive CCS technology.

## ACKNOWLEDGMENTS

The authors would like to acknowledge Siemens Industrial Turbomachinery AB, Finspong, Sweden, for permission to publish this paper.

## PERMISSION FOR USE STATEMENT



## REFERENCES

[1] Stocker, T., Qin, D., Plattner, G., Tignor, M., Allen, S., Boschung, J., Nauels, A., Xia, Y., Bex, B., and Midgley, B., 2013, "IPCC, 2013: climate change 2013: the physical science basis. Contribution of working group I to the fifth assessment report of the intergovernmental panel on climate change."

[2] Yang, H., Kang, D., Ahn, J., and Kim, T., 2012, "Evaluation of design performance of the semi-closed oxy-fuel combustion combined cycle," Journal of Engineering for Gas Turbines and Power, 134(11), p. 111702 (111710p).

[3] Sundkvist, S. G., Dahlquist, A., Janczewski, J., Sjödin, M., Bysveen, M., Ditaranto, M., Langørgen, Ø., Seljeskog, M., and Siljan, M., "Concept for a combustion system in oxyfuel gas turbine combined cycles," Proc. ASME Turbo Expo 2013: Turbine Technical Conference and Exposition, American Society of Mechanical Engineers, pp. V002T007A005-V002T007A005.

[4] Sammak, M., Genrup, M., Thorbergsson, E., and Grönstedt, T., "Conceptual mean-line design of single and twin-shaft oxy-fuel gas turbine in a semi-closed oxy-fuel combustion combined cycle," Proc. Proceedings of ASME Turbo Expo 2012: Power for Land, Sea and Air. June 11-15, 2012, Copenhagen, Denmark, pp. 289-297.

[5] Dahlquist, A., Thern, M., and Genrup, M., "The influence from the working medium on the profile loss in compressor and turbine airfoils," Proc. ASME Turbo Expo 2014: Turbine

Technical Conference and Exposition, American Society of Mechanical Engineers.

[6] Dahlquist, A., Genrup, M., Sjoedin, M., and Jonshagen, K., "Optimization of an oxyfuel combined cycle regarding performance and complexity level," Proc. ASME Turbo Expo 2013: Turbine Technical Conference and Exposition, American Society of Mechanical Engineers, pp. V002T007A011-V002T007A011.

[7] Dahlquist, A., and Genrup, M., "Aerodynamic Gas Turbine Compressor Design for an Oxy-fuel Combined Cycle," Proc. ASME Turbo Expo 2015: Turbine Technical Conference and Exposition, American Society of Mechanical Engineers.

[8] Lemmon, E. W., Huber, M. L., and McLinden, M. O., "NIST REFPROP (reference fluid thermodynamic and transport properties), standard reference datasbas 23, Version 8.0 ".

[9] Franco, F., Mina, T., Woolatt, G., Rost, M., and Bolland, O., "Characteristics of cycle components for CO2 capture," Proc. Proceedings of 8th International Conference on Greenhouse Gas Control Technologies, Trondheim, Norway.

[10] Sanz, W., Jericha, H., Bauer, B., and Göttlich, E., 2008, "Qualitative and quantitative comparison of two promising oxy-fuel power cycles for CO2 capture," Journal of Engineering for Gas Turbines and Power, 130(3), p. 031702.

[11] Bolland, O., and Mathieu, P., 1998, "Comparison of two CO2 removal options in combined cycle power plants," Energy Conversion and Management, 39(16), pp. 1653-1663.

[12] Ulizar, I., and Pilidis, P., 1997, "A semiclosed-cycle gas turbine with carbon dioxide–argon as working fluid," Journal of engineering for gas turbines and power, 119(3), pp. 612-616.

[13] Canepa, R., and Satta, A., "Influence of working fluid composition on the performance of turbomachinery in semi-closed gas turbine cycles," Proc. ASME Turbo Expo 2012: Turbine Technical Conference and Exposition, American Society of Mechanical Engineers, pp. 399-406.

[14] van der Merwe, J. W., 2012, "Environmental and Material Influences on the Stress-Corrosion Cracking of Steel in H2O-CO-CO2 Solutions," International Journal of Corrosion, 2012, p. 13.

[15] Grieb, H., 2004, Projektierung von Turboflugtriebwerken.

[16] Bayley, F. J., and Owen, J., 1970, "The fluid dynamics of a shrouded disk system with a radial outflow of coolant," Journal of Engineering for Gas Turbines and Power, 92(3), pp. 335-341.

[17] Phadke, U., and Owen, J., 1988, "Aerodynamic aspects of the sealing of gas-turbine rotor-stator systems: part 1: the behavior of simple shrouded rotating-disk systems in a quiescent environment," International journal of heat and fluid flow, 9(2), pp. 98-105.

[18] Shapiro, A. H., 1953, "The dynamics and thermodynamics of compressible fluid flow," New York: Ronald Press, Card Number 53-8869, 1, p. 81.

[19] Denton, J., 1999, "Multistage turbomachinery flow calculation program-MULTIP," Whittle Laboratory, University of Cambridge, UK.

[20] Denton, J., and Dawes, W., 1998, "Computational fluid dynamics for turbomachinery design," Proceedings of the Institution of Mechanical Engineers, Part C: Journal of Mechanical Engineering Science, 213(2), pp. 107-124.

[21] Moustapha, H., Zelesky, M. F., Baines, N. C., and Japikse, D., 2003, Axial and radial turbines, Concepts NREC White River Junction, Vt, USA.